Reconfigurable Photonic Antennas

A dissertation submitted in fulfilment of
the requirements for the degree of
Doctor of Philosophy

by

Elias R. Lopez Lara
Bachelor of Communication Engineering (Hons)

School of Electrical and Computer Engineering
College of Science, Engineering and Health
RMIT University
August 2009

Declaration

I certify that except where due acknowledgement has been made, the work is that of the author alone; the work has not been submitted previously, in whole or in part, to qualify for any other academic award; the content of the thesis is the result of work which has been carried out since the official commencement date of the approved research program; and, any editorial work, paid or unpaid, carried out by a third party is acknowledged.

Elias R. Lopez Lara
August 2009

Acknowledgements

There so many people that I would like to mention here; relatives, friends, academics and colleagues whom I have shared this chapter of my life.

Firstly, I would like to thank my supervisor, Arnan Mitchell, for giving me the opportunity to undertake this research and for always being looking after my academic, professional and personal development. For sharing not only his outstanding research and professional experience but also for sharing his personal teachings, I want to say thanks. I am in debt with you and I only hope to become living proof of your excellent guidance and teaching skills.

I would also take the opportunity to thank Wayne S. T. Rowe, Kamran Ghorbani and Wei Fu for collaborating always towards the success of this research and the completion of our projects.

I would like to acknowledge BAE System Australia and the Australian Research Council for their financial support and guidance through this project.

Finally, I would like to thank everyone of my colleagues, both academics an fellow post-graduates who created an excellent research environment at RMIT, sharing knowledge, experience and priceless moments with me.

I also would like to share this achievement with all of you that ever got the opportunity to hear my ideas and gave me some advice, help and guidance.

To my dear angel Nancy, whose memories helped me to overcome adversity.

To my flatmates, Los Latinos. Andres, Rafita and San Guicho; mil gracias por todo.

To my family here, and back in Mexico, who always encouraged me to continue my studies and showed me constant support and love.

To all, thank you.

Abstract

Sharing the electromagnetic spectrum and the physical space for multiple wireless applications in commercial and military applications has resulted in large and complex integrated solutions. Traditional microwave approaches required to look for other alternatives to overcome the aerodynamics limits of front-end devices, particularly in airborne platforms. The implementation of Microwave Photonics techniques to remote microwave antennas is increasingly finding more and more application in airborne Electromagnetic Support applications. This is not only because optical fibres are excellent substitutes of bulky transmission lines (e.g., coaxial and rectangular waveguide) but also because traditional microwave signal processing techniques can also be implemented using photonic techniques.

The aim of this dissertation is to investigate the use of Microwave Photonic technologies and photonic signal processing techniques as a means of improving front-end receivers for wireless platforms, particularly for airborne Electronic Warfare applications. This work focuses in specific on the development of a single shared aperture sensor for Electromagnetic Support applications such as early detection radar and direction finding. The use of photonic signal processing techniques such as polarisation diversity, multiplexing and transversal techniques is proposed to control the radiation characteristics of multifunctional broadband antennas.

Major contributions made by this work include the derivation of a flexible and broadband receiving "wireless kiosk" suitable for current and future integrated multiple antenna systems. The design and development of an orthogonal mode transformer that enables the multi-mode operational characteristics of broadband frequency independent two-arm spiral antennas. The implementation of a Photonic 180° hybrid coupler that controls the radiation modes of a multi-mode two-arm spiral antenna. The implementation of a microwave photonic mode transformer using photonic signal processing techniques that substitutes complex and bulky microwave mode transformers such as a microwave Butler matrix. In specific, photonic transversal techniques were used to implement photonic quadrature hybrid couplers that, combined with 180° photonic hybrid couplers, controlled the radiation patterns and polarisation characteristics of a multi-functional four- arms sinuous antenna.

Contents

List of Figures

List of Tables

Chapter 1

Introduction

Future trends in wireless communications systems place greater demands on antenna design, antenna interfaces and signal processing techniques for commercial and military applications. From mobile phones [1], Global Positioning Satellite (GPS) [2, 3] and wireless WLANs [4], to Direction Finding (DF) [5], Countermeasures (CM) tactics [6, 7], and decoy deployment for Electronic Warfare (EW) applications [8, 9], more and more applications emerge everyday requiring specialised front-end devices and complex signal processing units which are able to transmit and receive on multiple bands and multiple diversity schemes. This constant development of new wireless technologies is driving RF boundaries to their limit, particularly at Electronic Warfare for airborne applications, where massive front-end conglomerate solutions cannot be allocated [10].

The development of applications for Electronic Warfare (EW) has been considerably increasing since the Russian-Japanese war in 1904-1905 when radio interference was first time used for military purposes [11]. From Ballistic Missile surveillance [12] and early detection Radars [13] up to applications such as Night Vision and Infrared Guided Weapons [14], its evolution has been motivated by the critical need to rapidly extract essential information from the Electromagnetic (EM) environment in order to achieve a competitive advantage and military supremacy over adversary systems.

Sharing effectively the electromagnetic spectrum and the physical space for military platforms is continuously pushing EW research and development groups to secure integrated solutions that represent a competitive advantage. Such is the case of the integrated mast naval sensor and communications suite for anti-air and surface warfare, currently developed by Thales for the Netherlands navy [15]; or the Advanced Multifunction Radio Frequency Concept (AMRFC) [16], currently supported by the U.S Office of Naval Research, where common phased-array antennas simultaneously service EW, radar, and communications functions. These modern integral approaches have been able to integrate multiple sensors into single platform addressing compatibility and interference issues regarding locating multiple sensors in close proximity. However, most of these integral solutions have resulted in large single surveillance platforms leaving besides aerodynamic and spatial requirements for airborne platforms.

In airborne EW applications, even locating frequency converters close to multiple sensors is not always possible due the aerodynamic specifications of jetfighters [9]. These spatial and aerodynamic requirements often force EW designers to compromise RF per-

formance, size, weight and power requirements, in order to achieve the best balance between the aerodynamics of the aircraft and the performance of EW systems, whilst aiming for fuel optimisation and the extension of mission profiles [9]. EW technology platforms, particularly airborne EW, would find advantageous to develop a new type of front-end receivers that can integrate individual frequency bands from multiple applications using a "single, shared aperture antenna". So, these applications can work collectively without deploying single electromagnetic sensors for each application, whilst reducing their overall spatial requirements.

In the field of communication systems, it has proposed that ultra-broadband frequency antenna [17] and multifunctional single aperture antennas [18] can be used to create a "communication kiosk" [19, 20] that can share a single receiver for multiple applications. This "kiosk" concept has been demonstrated in different forms; for example, multiple band coverage techniques for wireless local area networks [4], and frequency range enhancement techniques for Ultra-WideBand communications [21, 22]. These investigations have even proposed to make this platform so flexible that enable to include future applications as they emerge, only by changing communication protocols [23, 24, 25].

In order to facilitate flexible and efficient deployment, maintenance, revision, upgrade and retirement of EW applications, it would be advantageous to use this "communication kiosk" concept to develop a sophisticated single front-end device for several applications. This front-end device should be able to receive arbitrary combinations of frequencies bands as well as multiple antenna diversity schemes, be significantly flexible so it can adapt to future scenarios without deploying expensive hardware modifications and, be compact, light weight and cost effective so it can be used in airborne EW platforms.

1.1 Thesis overview

This dissertation aims to investigate different electromagnetic sensors (antennas), as well as Microwave Photonics techniques in order to develop a front-end receiver that eases the current shortcomings of integral solutions for airborne electronic warfare applications. This dissertation is organised in 6 main Chapters that introduce the different electromagnetic sensors and Microwave Photonic techniques explored in order to progressively achieve a sophisticated front-end receiver.

Chapter 2 investigates a simple Microwave Photonic combination technique in order to familiarise readers with the basic concepts used through this dissertation. This demonstration investigates frequency bandwidth combination techniques that uses single optical fibre links and simple photonic polarisation diversity scheme to combine the adjacent bandwidths of multiple stacked patch antennas. This demonstration attempts to replace a complex diplexer presented in [21]. Filtering techniques are intentionally avoided in order to investigate the overall interaction of the antennas using photonic techniques, particularly at the overlapping zones of their adjacent bandwidths. It also attempts to confirm that this Microwave Photonic technique does not disturb the performance of the antenna, that this technique can be used efficiently to combine two identical wavelength optical carriers orthogonally without coherence interference effects. Additionally, it investigates the interaction of the antennas at the overlapping zones.

Chapter 3 investigates how to expand the frequency bandwidth combination concept shown in Chapter 2, using Array Waveguide Gratings for optical wavelength multiplexing purposes. It investigates how to combine multiple antennas with adjacent frequency bandwidths into a "single, shared aperture antenna" with a relatively flat gain response and uniform radiation patterns characteristics. It is predicted that the broadband impedance of the electro-optic modulators, which isolates the impedance of every antenna element, eases considerably the design procedures for microwave filters. Thus, the compact integration of the antenna, its filter and its dedicated modulator can be conducted, and the electromagnetic interaction between the antennas in close proximity, investigated. Radiation pattern and gain response of a series of experiments with different spatial arrangements for three stacked patch antennas will be investigated.

Chapter 4 investigates beam forming techniques for single broadband frequency independent antennas using Microwave Photonics. It attempts to modify the traditional feeding structure of a commercial two-arm spiral antenna in order to enable its multimode operation characteristics. It is predicted that replacing the traditional balanced to unbalanced (Balun) transformers with an orthogonal mode customised transformer with double input, can control an arbitrary superimposition of the multiple radiation modes of this spiral antenna. The beam patterns generated by this customised single aperture spiral antenna, will be controlled by using the Microwave Photonic concept of polarisation diversity combination, demonstrated in Chapter 2. The results should demonstrate that the ratio of each radiation mode of the spiral antenna can be continuously adjusted through rotation of an optical carrier polarisation controller in order to generate multiple beam patterns, not only the fundamental and second radiation modes of this customised spiral antenna. This is practically impossible on the RF domain.

Chapter 5 investigates how to expand the beam forming techniques introduced in Chapter 4 in order to control a multifunctional broadband independent frequency sinuous antenna with polarisation diversity and multiple beam forming characteristics. It attempts to modify a four-arm sinuous antenna to enable the individual access of each one of its radiating elements, using a coaxial transmission bundle. Then, the multiple beam patterns, different radiation modes and polarisation schemes that can be achieved with this antenna will be controlled using a Microwave Photonic implementation based on photonic transversal techniques. Substituting complex and bulky microwave Butler matrixes, which are traditionally used to control the characteristics of multiple-arm logarithmic independent antennas using this Microwave Photonics will demonstrate the potential of developing a flexible, light weight, compact, and highly sophisticated front-end device suitable for current and future airborne Electronic Warfare applications.

Chapter 6 summarises all the findings from previous chapters and outlines some ground for future investigations, particularly at the micro-scale integration level of the Microwave Photonic implementations presented through this dissertation.

Appendix A.1 explains the design parameters, radiation properties and multifunctional characteristics of a Four-arm Sinuous Self-complementary Antenna.

Appendix B.1 explains the properties of the Hilbert Transformation used to implement photonic transversal techniques in the proposed Microwave Photonic configuration of Chapter 5.

Chapter 2

Electromagnetic Sensors Photonically Remoted using Microwave Photonics

2.1 Introduction

The key component of emerging broadband wireless technologies, particularly in Electronic Warfare for airborne applications, is to have a light weight, compact and multifunctional front-end receiver that can intercept and categorise timely multiple signals over a large range of frequency. A front-end receiver normally has specialised electromagnetic sensors (antennas) with radiation characteristics that defines their capabilities (e.g., gain and frequency bandwidth, radiation pattern response, and polarisation).

Front-end antenna elements are commonly designed to cover only desired bandwidths for specific applications, resulting in mobile wireless solutions with numerous specialised antennas with customised characteristics, each one of them designed and manufactured for different applications [15]. As mentioned in Chapter 1, it would be very efficient if a single radiating element could cover these multiple radiation modes and polarisation characteristics uniformly across a large frequency bandwidth. Such an element could enable multiple wireless protocols to share the same front-end receiver [25]. Broadband antennas and multiple antenna systems are currently being investigated in attempt to provide an ultra-broadband and flexible wireless front-end interface. The aim of these investigations is to enable wireless systems to have a generic front-end receiver that can be used for multiple applications simultaneously without needing hardware tuning with every emerging wireless technology [26].

Broadband antennas are able to cover a large range of frequencies of the order of one octave with a single component [27, 28], but to achieve this they can compromise the gain response and radiation patterns uniformity across its nominal frequency bandwidth. Multiple antenna systems exhibiting uniform radiation characteristics have been demonstrated [21, 29, 30]; this is achieved, however, at the expense of increasing the complexity of the feeding network. This feeding network can become prohibitively complex as the number of combined elements increases.

Choosing between an antenna with broadband characteristics that does not retain its uniform characteristic across its entire operational bandwidth, or a multiple antenna sys-

tem with uniform radiation patterns but with complex feeding networks, it is determined according to the specific requirements of any application; for example, Ultra WideBand technologies where flat gain and uniform group delay characteristics are required [31, 32]. However, as the number of antenna elements increases, these feeding networks become complex and pushes traditional RF boundaries to the limit. This is particularly true for airborne applications, where complex feeding networks such as the Butler matrix demonstrated in [33] represents a tradeoff between the antenna diversity capabilities of an Electromagnetic Support front-end and the aircraft aerodynamical performance. Microwave Photonics has already been investigated as a feasible alternative for Electromagnetic Support Sensor development.

Microwave Photonics has become very attractive for Electromagnetic Support Sensor applications, not only because it can isolate the response of the antennas from electromagnetic interference but also because multiple microwave signal processing techniques could also be implemented using photonic signal processing techniques (e.g. multiplexing, beam-steering, null steering or channelisation) [34, 35]. These photonic signal processing techniques could enable front-end receivers to achieve ultra-broadband frequency ranges with uniform characteristics by combining the individual response of specialised antennas into an integrated sensor solution; or simplify the control of multifunctional single aperture antennas by switching between multiple receiving modes.

This chapter reviews the ultra-broadband patch antenna developed in [21], where two broadband aperture stacked patch antennas were multiplexed into a single radiating element using a microwave diplexer. Then, it explains basic components of Microwave Photonic links, reviews a variety of photonic multiplexing techniques, and demonstrates a simple Microwave Photonic multiplexing technique that combines the response of two broadband antennas with adjacent bandwidths into a single ultra-broadband receiver. This configuration is proposed to replace the traditional RF diplexer of [21].

2.2 Review of RF Multiple Patch Antenna Systems

Aperture Stacked Patch (ASP) antennas are excellent candidates for investigating the interaction between broadband antennas working in a multiple antenna systems. They exhibit desirable properties including broad radiation patterns, low cross-polarisation, high front-to-back ratio (around 10 dB) and high gain levels (around 8 dBi) [36]. The excellent uniformity of these characteristics across its nominal bandwidth makes these antennas easy to compare.

A previous investigation has explored the combination of two ASP elements, each with an octave bandwidth to form a single radiating element with nearly two octaves of bandwidth [21]. Figure 2.1 shows the reported ultra-broadband element. It shows the diplexer was used to combine the two ASP antennas while maintaining impedance matching across two octaves. According to [21], this diplexer was very difficult to realise and required careful design and hand trimming of most of its components in order to successfully combine signals from the two antennas with adjacent bandwidths. This section reviews the results of this previous investigation for further reference in this chapter.

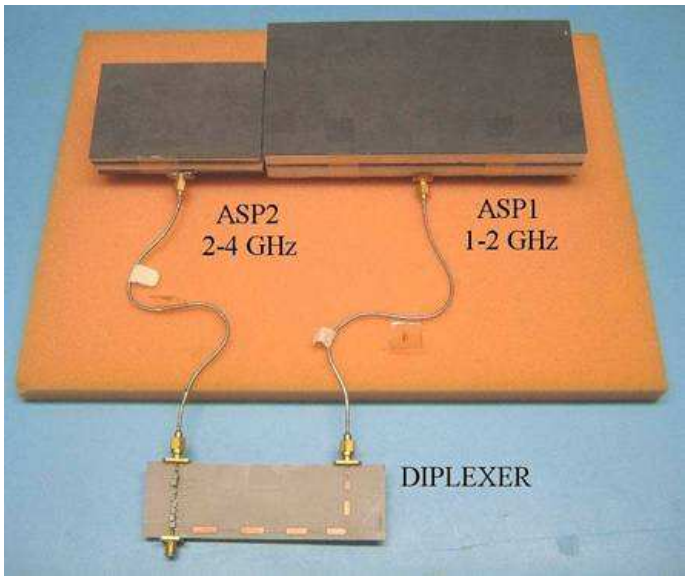

Figure 2.1: Microwave Diplexer Antenna Remoting Application Developed in [21] to Combine the Frequency Bandwidths of Two Aperture Stacked Patch Antennas into a Single Aperture with Almost Two Octave Bandwidth.

2.2.1 Aperture Stacked Patch Gain Response

Characterising the individual radiation performance of the antennas involved in a multiple antenna system is important because it defines the extent of interference that could occur when attempting to combine them together.

Two ASP antennas were available to conduct this investigation. These antennas were the same antennas used for the Ultra-broadband antenna shown in Figure 2.1. Its gain characterisation has been already provided in [21] and will only be reintroduced in this section as a reference.

Figures 2.2 and 2.3 show the individual gain characterisation response of ASP1 and ASP2. It shows that ASP1 and ASP2 exhibit an average gain of approximately 8 dBi from 1.2–2.1 GHz and 1.8–3.8 GHz, respectively. This gain decreases outside of these bandwidths with a slope of approximately 50 dB/ GHz. The gain response provided for both ASP1 and ASP2 across their nominal bandwidth vary by approximately $\pm$ 1 dB. Both gain responses rise considerably at the upper edge of its nominal bandwidth by approximately almost 2 dB. These results are in good agreement with the expected radiation characteristics of Aperture Stacked Patch antennas [21, 36].

It can be clearly observed from Figures 2.2 and 2.3 that the nominal bandwidth of the antennas overlap around 2 GHz. Trying to combine the response of these two antennas without filtering and multiplexing techniques will cause them to interfere coherently creating a poor balanced phase array antenna.

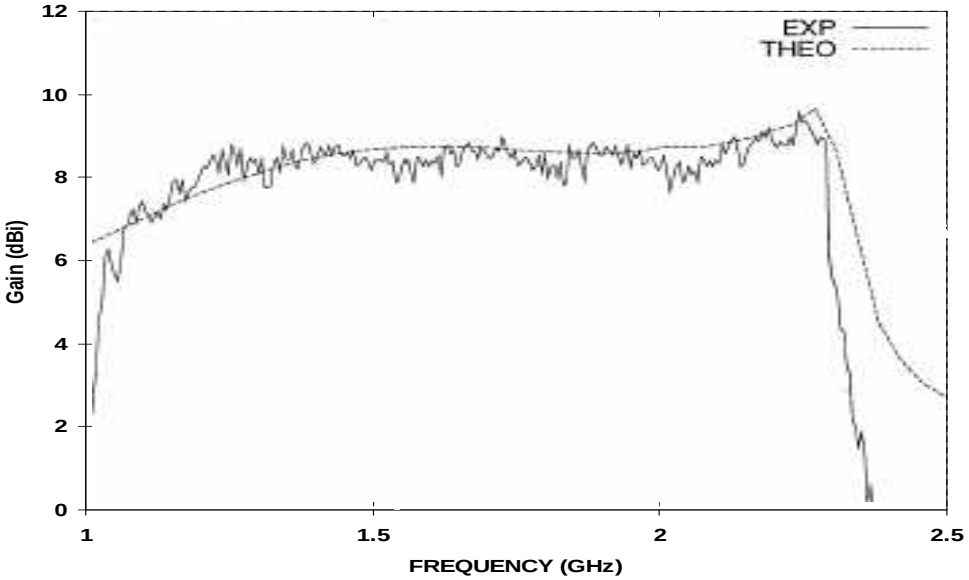

Figure 2.2: ASP1 Gain Characterisation Presented in [21]

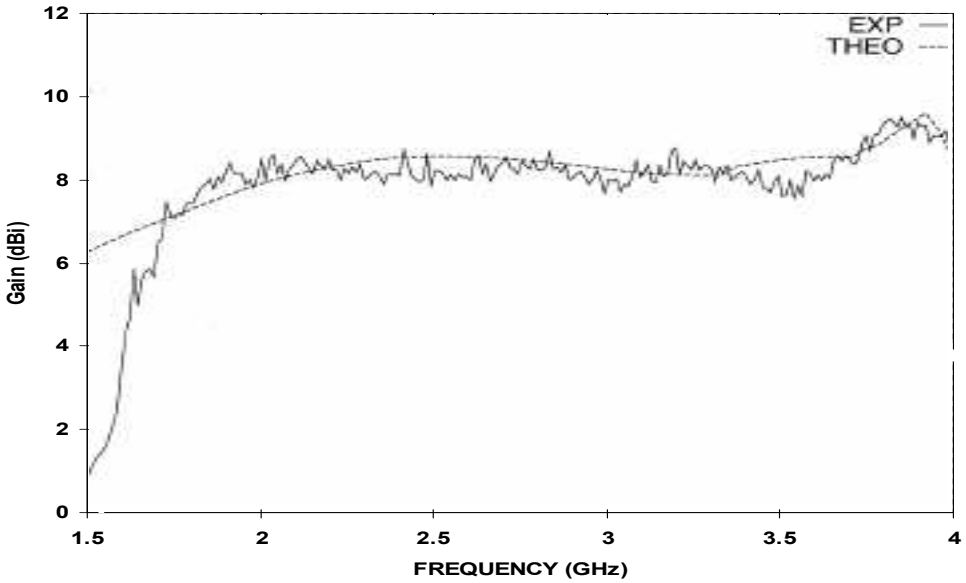

Figure 2.3: ASP2 Gain Characterisation Presented in [21]

2.2.2 Combination of ASP1 and ASP2 using a Microwave Diplexer

When antennas radiate, they offer a load impedance close to $50\,\Omega$. However, when they operate outside of its nominal band, this impedance can be very different from $50\,\Omega$. When combining the two ASP elements it is important that only the intended radiating element is impedance matched to the source but that the non-radiating element is isolated. The microwave diplexer demonstrated in [21] provides this function.

Figure 2.4 shows the gain response of the Ultra-Broadband element shown in Figure 2.1. This response exhibits a flat gain response across the entire operational bandwidth (1–3.8 GHz) with an amplitude variation of approximately 1.5 dB. This variation was considered to be environmental noise and was attributed to the outdoors antenna testing facility used in [21]. Figure 2.4 shows that the gain bandwidth of ASP1 and ASP2 shown in Figures 2.2 and 2.3 are effectively combined into a single Ultra-Broadband element with almost two octaves of bandwidth using the microwave diplexer shown in Figure 2.1.

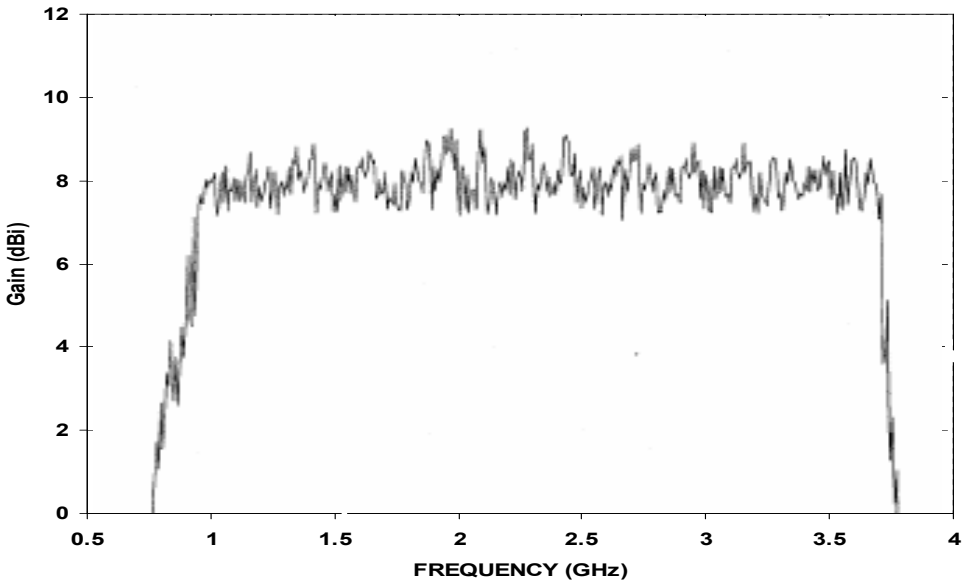

Figure 2.4: Bandwidth Response of the Ultra-Broadband Antenna Presented in [21]

The individual and combined results of the two ASP antennas reviewed in this section showed that the adjacent bandwidth of these two ASP antennas can be effectively combined into a single bandwidth with flat gain radiation characteristics. This response has been achieved using the filtering properties of the RF diplexer shown in Figure 2.1, which was made of a low-pass and a high pass filter carefully designed to be impedance matched at the intersection frequency of 2 GHz. These antennas will be employed through this chapter in order to demonstrate a relatively simple Microwave Photonic multiplexing technique that can substitute the complex RF diplexer.

2.3 Microwave Photonics For RF Signal Combination

Converting RF signals into an optical output for transmission through a fibre-optic cable avoids the bandwidth and loss limitations of coaxial cables or waveguides and reduces weight and volume. By transferring RF signals to the optical domain, Microwave Photonics has enabled traditional Electronic Warfare applications such as antenna remoting to become more flexible [35], while reducing bulky and lossy metallic links [9].

Microwave Photonics is very attractive for antenna remoting applications not only because of the bandwidth advantages of using fibre optics transmission but also because many signal processing functions, that are difficult in the RF domain, can be implemented with relative ease in the optical domain while maintaining broadband operation. One such example is broadband splitting or summation of RF signals.

This section aims to use Microwave Photonics to ensure that the same two radiating elements shown in Figure 2.1 can be combined into a single radiating element while remaining electrically isolated and avoiding impedance loading effects. Before embarking onto Microwave Photonic combination systems, it will be necessary to review Microwave Photonic links and photonic multiplexing techniques.

2.3.1 Microwave Photonics Links

This section introduces fundamental Microwave Photonic link configurations for antenna remoting systems. It explains how the signals received from the antennas can be combined using photonic multiplexing techniques into a single optic-fibre system.

Figure 2.5 shows the basic configuration used to characterise a photonically remote antenna system using a Microwave Photonic link. A continuous wave laser diode (LD) is connected to an electro-optic intensity modulator for external modulation [37, 38]. The RF signal applied to the electrodes of the modulator, modulates the intensity of optical carrier, converting the RF signal into the optical domain. This electro-optic modulated signal is transmitted through optic-fibre links and is converted back into the electrical domain using a high sensitivity Photo Detector (PD).

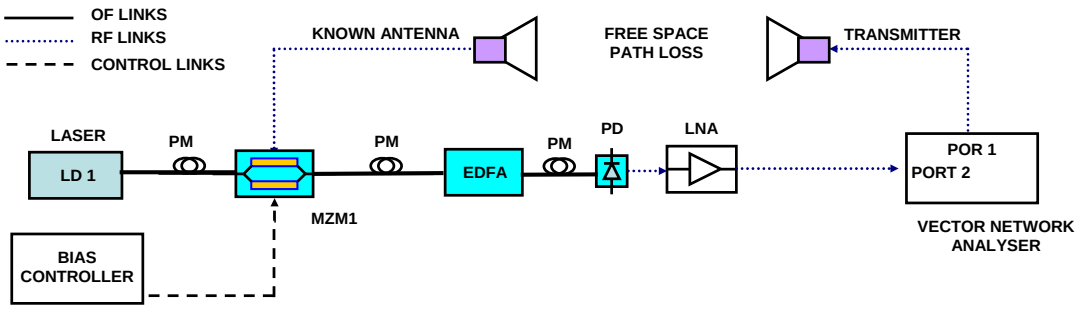

Figure 2.5: Microwave Photonic Link Configuration for Antenna Remoting

Polarisation maintaining optical fibres (PM) and coaxial cables are employed to interconnect the components and conversion stages of the Microwave Photonic link. The PM fibres ensure that the polarisation of the optical carrier complies with the polarisation

requirements of the electro-optic modulator. Mach-Zehnder modulators (MZMs) have a sinusoidal response that can be biased at different points of its transfer function in order to generate different modulation results. One possibility is to bias at a null where the carrier is suppressed and the modulation occurs in the second harmonic [39]. However, MZMs are normally biased at quadrature, where they are more linear, in order to provide maximum gain and minimal harmonic distortion [38].

The link gain of a Microwave Photonic link is defined as the ratio of the detected RF output power at the photo detector to the input RF power [40]. For a Microwave Photonic link using a MZM and without amplification, the link gain is given by

$$G = \frac{S_{MD}^2 \, S_D^2 \, R_D}{R_{MD}} \tag{2.1}$$

where S_{MD} is the slope efficiency of the modulator, S_D is the slope efficiency of the photo detector (also know as responsivity), R_D is the load impedance of the photo detector and R_{MD} is the modulator impedance [38]. The slope frequency of the modulator can also be defined by

$$S_{MD} = \frac{t_{ff} \, P_L \, \pi \, R_{IN}}{2 \, V_\pi} \tag{2.2}$$

where t_{ff} is the fibre to fibre optical transmission losses of the modulator plus any interconnection loss along the optical link, P_L is the CW input optical power of the modulator, R_{IN} the impedance of the RF modulating source and V_π is the switching voltage of the modulator [40]. By replacing Eq. 2.2 into Eq. 2.1 and assuming that the impedance of the modulator is matched to the impedance of the RF source ($R_{IN} = R_{MD}$, the Eq. 2.1 can be expressed as

$$G = \left[\frac{t_{ff} \, P_L \, \pi \; R_D}{V_\pi} \right]^2 R_{MD} \, R_D \tag{2.3}$$

The parameters of the microwave photonic link equipment used in this investigation, listed in Table 2.1, can be used in Eq. 2.3 to approximate the total RF attenuation of Microwave Photonic links without amplification. This attenuation is about -40 dB, which it could be considered to be a disadvantage for photonically remote antennas. However, this attenuation can be compensated due to the fact that a photonic system exhibits a Noise Power levels lower than the RF system.

The dominating output noise of the Microwave Photonic link depends on the level of the received power at the photo detector and it is mostly determined by the Thermal Noise, the Shot Noise and Relative Intensive Noise (RIN) of the link [37]. While the Thermal Noise is a constant value defined by Temperature and the Boltzmann's constant [38], the power spectral-density of the Shot (quantum) Noise is defined by $i_{sh}(w)^2 = 2qIp$ where q is the charge of an electron ($1.6\text{x}10^{19} \, C$) and i_P is the average current of the photo detector. The spectral-density of the RIN Noise is defined by $i_{RIN}(w)^2 = RIN \, i_p^2$, where RIN is an intrinsic characteristic of the optical source and it is attributed to the fact that the output of the laser is not perfectly constant. Figure 2.6 shows the relation between the Noise Power levels and the photocurrent generated by the optical power at the input of the photo detector. It can be observed in Figure 2.6, that as the photocurrent increases, the link passes from being Thermal Noise limited to Shot Noise limited and then RIN Noise limited.

Table 2.1: Microwave Photonic Link Parameters

Device	Parameter	Value	Units
50 GHz Photo Detector	S_D @1550nm	0.65	A/W
(U^{2}T, XPDV2120)	$R_M D$	50	Ω
Mach Zehnder Modulator	V_π @1GHz	4.51	V
(CODEON Mach10)	R_{MD}	50	Ω
	S_{21} Bandwidth	10.19	GHz
	Insertion Loss t_{ff}	-4.29	dB
DFB Laser	Output Power	13	dBm
Agilent 8164A	RIN	-140	dBm/Hz
DFB Buttlerfly Laser	Output Power	16	dBm
FITEL FOL15DCWE-A82	RIN	-140	dBm/Hz

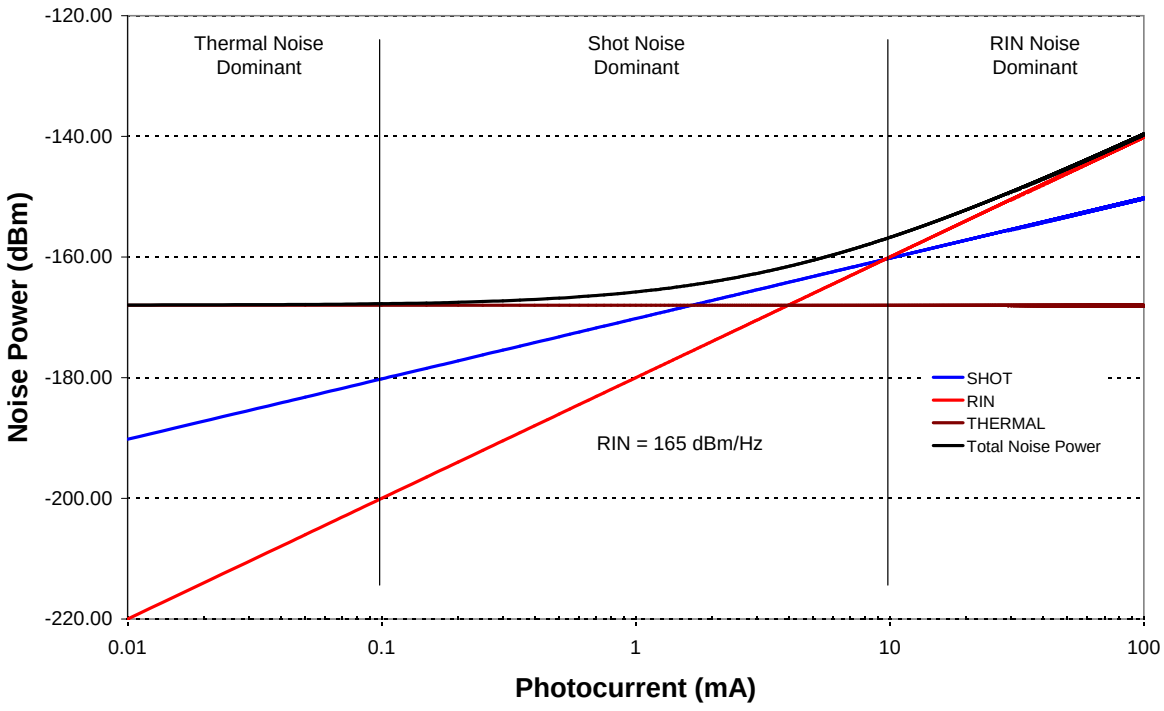

Figure 2.6: Noise power versus photocurrent [37]

The Microwave Photonic links used in this investigation are Shot Noise limited, which according to Figure 2.6 result in Noise Power level below -140 dBm. Therefore, even though converting the RF signal into the optical domain represents about -40 dB loss, good signal to noise ratio can still obtained, allowing further amplification to compensate this loss.

Optical and RF amplifiers are employed to compensate the electro-optic insertion loss of the link and achieve the dynamic range requirements of most advance EW systems. An Erbium Doped Fibre Amplifier (EDFA), which is normally used to amplify optical signals, increases the power of the optical carrier by stimulating emission of photons from dopant Er^{3+} ions incorporated into a fibre [41, 42]. Furthermore, EDFAs are not polarisation dependent, which represents an important feature for multiple signals combination systems where multiple polarisations are employed. A broadband RF amplifier is often used to improve the gain conversion of the photo detector after the optical signal returns to the RF domain.

The Microwave Photonic link configuration shown in Figure 2.5 replaces heavy and lossy coaxial cables used in antenna remoting applications with light weight and low insertion loss optic fibres. The impedance of the electro-optic modulator shown in Figure 2.5 is designed to be a broadband impedance load of approximately $50\,\Omega$. Thus, the antenna element controlled by the modulator can be considered as effectively terminated to $50\,\Omega$ for all frequencies. This characteristic will be crucial when trying to combine multiple antennas that isolate antennas from each other and avoid impedance loading effects.

2.3.2 Photonic Multiplexing Techniques

Combining the RF signal of two antennas can be attempted by using two different photonic remote links. The signals received from the two antennas can be combined by using different multiplexing techniques once they are in the optical domain. Each of these multiplexing techniques represents advantages and disadvantages. This section introduces some photonic multiplexing techniques that can be used to combine two RF signals using Microwave Photonic links.

Figure 2.7 shows a conceptual configuration of two RF signals combined using two individual Microwave Photonic links. This configuration includes two of every single component of the photonic link described in Section 2.3.1. Repeated components represent cost, weight and volume and should be avoided if possible. The number of repeated components shown in Figure 2.7 can be reduced by using photonic multiplexing techniques, which exploit parallelism.

One photonic multiplexing technique that can be implemented uses a 3 dB optical coupler. This optical coupler combines two optical carriers into a single optic-fibre or split one single carrier into two identical carriers. Figure 2.8 shows that locating a 3 dB coupler before or after the modulators can reduced the number of repeated elements shown in Figure 2.7. Placed before the modulators, the 3 dB coupler can be used to split a single laser source into two carriers, reducing the number of laser sources. However, this alternative incurs a 3 dB optical loss for each channel due to the characteristics of the

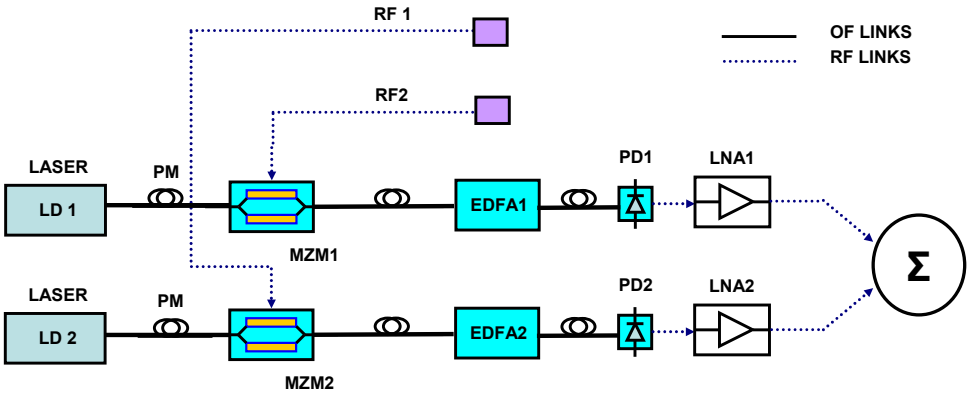

Figure 2.7: Double Microwave Photonic Antenna Remoting System

optical fibre coupler [43, 44], and still requires the used of a microwave combiner at the end of the links to combine the RF signals once they are converted back into the optical domain.

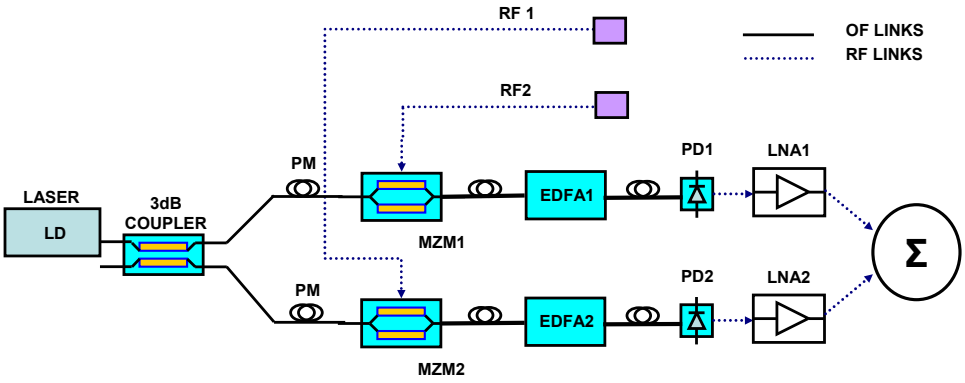

Figure 2.8: Double Microwave Photonic Link Combination Using a 3 dB Optical Coupler Before Modulation

Figure 2.9 shows that placed after the modulators, the 3 dB coupler can be used as an optical combiner that substitutes the microwave 3 dB combiner in the optical domain. This alternative reduces the number of fibres used after the modulators, uses only one EDFA, one photo detector and one RF amplifier.

2.3.3 Coherent Interference in Microwave Photonics Systems

Comparing Figure 2.7 and Figure 2.8, one might think that using a 3 dB coupler before and after the modulators simultaneously could be the next approach. However, having two identical carriers converging into a single optical link generates coherent interference problems [22].

Figure 2.9 shows that one 3 dB optical coupler divides the single optical carriers into two independent optical carrier whose polarisation propagation modes needs to be adjusted to optimise the transfer function of the electro-optic modulators. This is done by using the polarisation controllers (PCs). If the second 3 dB coupler were used to combine these two carriers into a single optic fibre, these carriers will interfere each other

coherently. Any small change in the phase of either arm relative to the other will cause an amplitude change at the output, compromising the stability of the system.

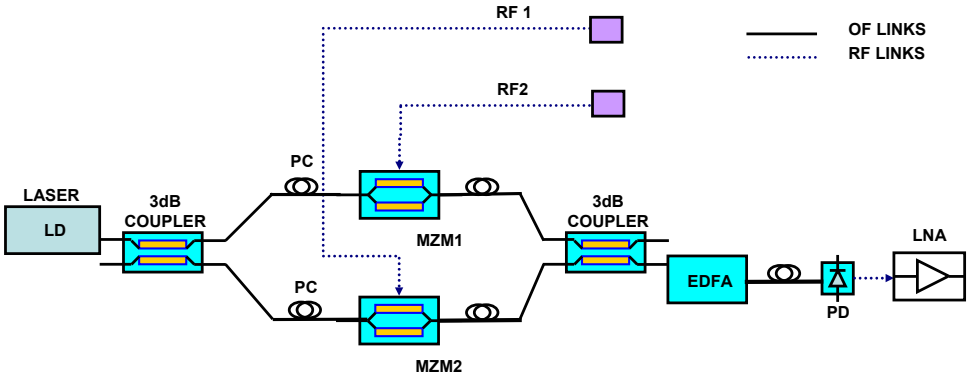

Figure 2.9: Double Microwave Photonic Link Combination Using Two Optical Couplers

Environmental factors such as temperature and vibrations can still disturb each link indistinctively making the single optic fibre link unstable.

An integrated version of the configuration shown in Figure 2.9 could represent a suitable alternative where environmental factor affects equally each link of the configuration. However, a more elegant macro-scale solution can be used to avoid coherent interference effects without integration concerns.

Coherent interference is a problem that can be solved by using polarisation controlling techniques. However, extra components such as the polarisation controllers need to be included into the configuration and are not always an attractive alternative. A more efficient alternative is using a polarisation beam splitter and polarisation diversity concept in order to avoid coherent interference [22, 45].

A polarisation beam splitter (PBS) is a photonic device that can combine two identical optical carriers (modulated with different RF signals) into a single optic-fibre link by combining them orthogonally. PBS devices are often packaged with polarisation maintaining optical fibres, such that TE polarisation at the input of the PBS is routed to the TE polarisation output of Port 1, while TM polarisation at the input is routed to TE polarisation at the output of Port 2. This avoids the need for extra polarisation controlling components.

Figure 2.10, shows the configuration required to combine two RF modulated optical carriers into a single optic-fibre link. It shows that a single laser diode is equally split into two identical carriers using PBS1 with TE polarisation. These carriers are modulated using the electro-optic modulators before being combined again into a single optic-fibre link by the second polarisation beam splitter (PBS2). PBS2 receives the two TE polarised modes and combines orthogonally by rotating one of the TE polarised mode propagating through its TM arm (Refer to Figure 2.10).

Since both carriers are propagating through different polarisation modes in the optical fibre, the signals do not interfere coherently, transmitting the modulated information of both RF signals. The advantages of using PBS instead of ordinary 3 dB optical splitters or combiners in Figure 2.10 is not only to avoid coherent interference effects but also to achieve the full optical power transmission from Port 1 and Port 2 to the TE/TM Port

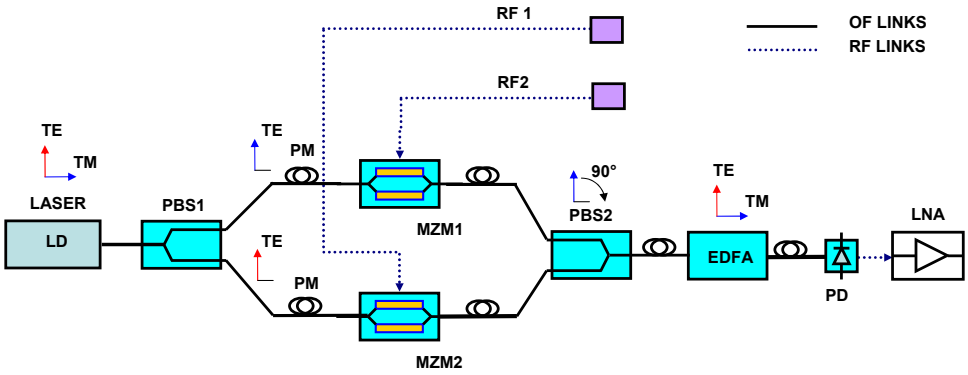

Figure 2.10: Double Microwave Photonic Link Combination Using a Polarisation Beam Splitter

of the PBS. Ordinary optical couplers have a 3 dB power penalty which is not present at polarisation beam splitters [46, 47]. Furthermore, polarisation beam splitters could also be useful when the two optical links attached to the PBS require to be equalised. Placing a Polarisation Controller (PC) before PBS1 could control the amount of optical power directed into each one of the optical links. Unfortunately, trying to combine more than two elements with this technique will require of more sophisticated alternatives such a Wavelength Division Multiplexing(WDM) or a combination of the polarisation beam splitter alternative and multiple lasers solution [48].

The microwave diplexer demonstrated in [21] combines the signal of two ASP antennas. Thus, since only the signals of two ASP antennas are involved in this investigation, the photonic multiplexing alternative that uses the polarisation beam splitter shown in Figure 2.10 and incorporates a Polarisation Controller before PBS1, will be implemented and demonstrated in the following section.

2.4 Microwave Photonic Diplexer Using a PBS

As discussed in Section 2.3.3 a PBS can be employed to combine two modulated RF signals with identical optical carriers into a single optic-fibre link without coherent interference while requiring only a single laser diode, EDFA and photo detector.

This photonic multiplexing technique will be employed in this section to combine the signal received by the two ASP antennas reviewed in Section 2.2 in order to form a single ultra-broadband antenna with similar bandwidth response to the microwave diplexer shown in Figure 2.1.

Figure 2.11 shows the Microwave Photonic configuration proposed to combine the signals received by the two ASP antennas. The parameters and equipment specifications for this implementation can be found in Table 2.1. A single optical source is equally divided into two channels using a polarisation controller and a polarisation beam splitter (PBS1). These optical carriers were directed through Polarisation Maintaining fibres (PM) into Mach-Zehnder Modulators (MZM1 and MZM2), which modulated the optical carrier with the electrical signal received from ASP1 and ASP2, respectively, as described in Section 2.3.1. Once converted into the optical domain, the signals of the antennas

were transmitted using polarisation maintaining fibres up to a second polarisation beam splitter (PBS2). PBS2 combined these two optical carriers into a single optic-fibre link which transmitted the information on both carriers propagating in orthogonally polarised modes (ASP1, TE mode; ASP2 TM mode). Both optical carriers were amplified using an Erbium-Doped Fibre Amplifier (EDFA) before being converted by a Photo Detector (PD) back into the electrical domain. A broadband RF amplifier was employed to increase the photonic link gain at the PD. ASP1 and ASP2 were connected to broadband Mach-Zehnder modulators (MZM1 and MZM2) via microwave phase shifters (MPS1 and MPS2). The microwave phase shifters were used to trim the absolute path length feeding of ASP1 and ASP2.

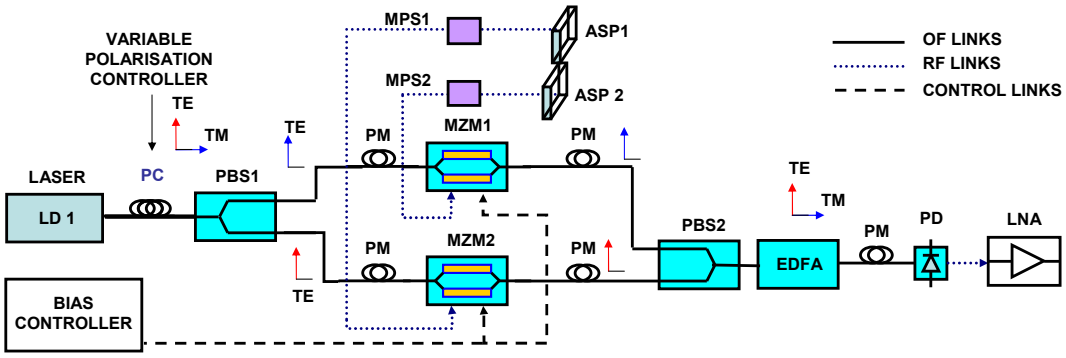

Figure 2.11: Microwave Photonic Diplexer Configuration

It is important to notice that the splitting ratio of the optical power directed to each optical link can be adjusted by physically rotating the polarisation controller (PC) shown in Figure 2.11. Using PBS1 as a splitting device enables an optical wavelength to be divided into two single carriers with complementary optical power and polarisation. The angle "α" which is defined here as the amount of rotation in degrees that the polarisation vector of an optical carrier exhibits related to TM mode orientation of PBS1, determines the splitting ratio of the PC-PBS combination. Thus, adjusting the angle α to $45\,^{\circ}$ will equally split the power of the optical source, enabling both, the MZM1 and MZM2 links. At $\alpha = 90\,^{\circ}$ only MZM1 link will received the whole optical power, and at $\alpha = 0\,^{\circ}$, only MZM2 will received it. The polarisation controller can rotate continuously, so does the polarisation vector. This enables to control the splitting ratio of the optical source which can be further employed to equalise the gain of both links. The following sections presents the individual gain characterisation of ASP1 and ASP2, as well as their combination response using the configuration shown in Figure 2.11.

2.4.1 Gain Characterisation of ASP1 and ASP2 using the Microwave Photonic Diplexer

Having described in Section 2.4 the Microwave Photonic configuration proposed to combine the signals received from the ASP1 and ASP2, this configuration can now be implemented and characterised, using an indoor antenna test facility and IEEE antenna testing standards for antenna characterisation techniques.

Figure 2.12 shows part of the Microwave Photonic implementation setup that was placed inside of an anechoic chamber used for antenna characterisation purposes. This anechoic chamber is lined with pyramidal foam absorber Eccosorb® CV-NRL. A double-ridged waveguide pyramidal horn (model 3115 manufactured by ETS-Lingren) was used as a transmitter and a rotating platform held the Device Under Test (DUT) inside of the anechoic chamber. The ASP antennas, (ASP1, ASP2) were characterised using a 40 GHz Vector Network Analyser (model 37347C Anritsu) connected to the transmitting antenna through a 10 meter coaxial cable at Port 1 (output), and connected to the photo detector shown in Figure 2.11 using a 50 centimeter coaxial cable at Port 2 (input).

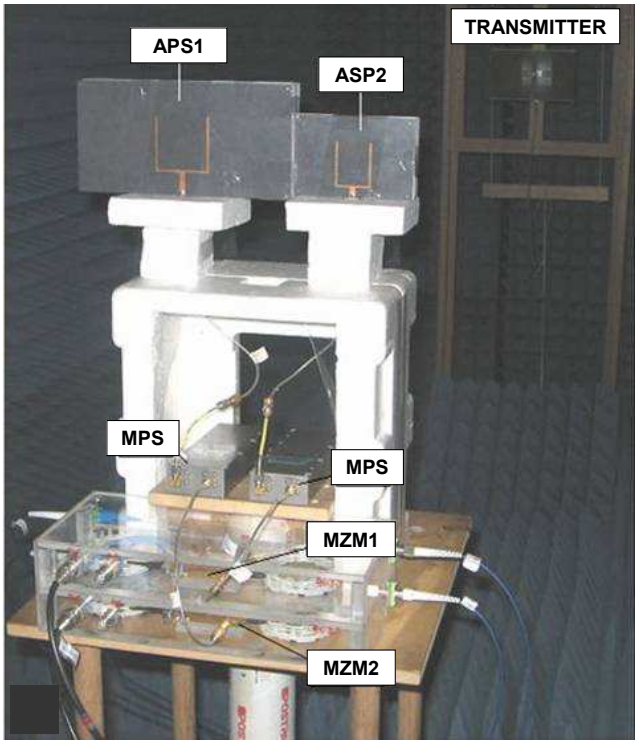

Figure 2.12: Anechoic Chamber and Microwave Photonic Setup

Figure 2.12 shows that large microwave phase trimmers were used in this demonstration to equalised the path length of each link. These large MPS are unnecessary if the absolute path length of ASP1 and ASP2 were determined by cleaving the optical fibres to the desired length, and the antennas were connected directly to the RF input of the modulators. Nevertheless, it is worth noting that having them in the setup could allow the investigation of the response of the system versus the difference between the path length of the links.

Figure 2.12 also shows that each modulator was enclosed in a large Perspex box. This enclosure aims to protect the modulators from accidental damage and becomes also unnecessary in applications with size and weight restrictions. These enclosures can be avoided by integrating the modulators to the antennas and using them as a carrier, which could make the final front-end antenna more compact and light.

Laser diode, EDFA, photodector, polarisation controller and polarisation beam splitters, as well as the individual power suppliers used to control the bias of the modulator,

are not shown in the Figure 2.12 because they were located outside of the anechoic chamber. It is worth noting that having all these components outside of the anechoic chamber demonstrates that using Microwave Photonics reduces the number of components required close to the antenna; making Microwave Photonics more attractive for placing the antenna in places such as the mast of a military vessel or the tip of and aircraft where size and weight are critical design parameters.

The characterisation of the ASP antennas and the Microwave Photonic Diplexer was done using the gain transfer method, which compares the received power level of the device under test (DUT) with a known standard antenna [49]. The gain response of a second standard horn antenna with known characteristics using the Microwave Photonic link shown in Figure 2.5 was used as a reference. It is worth mentioning that the antenna aperture size of ASP1 and the reference horn antenna are approximately the same. Therefore, when the horn antenna was used to characterised the gain of the transmission link, the horn antenna was located at a similar position to ASP1 in order to reduce near field variations between the power received by both antennas (horn and ASP1). ASP2 is considerable smaller than ASP1 and the horn, so its location inside of the chamber was selected considering the effects that results from co-locating two antennas in close proximity. The following sections presents the results of the characterisation of ASP1 and ASP2 using the Microwave Photonic implementation in Figure 2.12.

2.4.2 Individual Gain Characterisation of ASP1 and ASP2 using Microwave Photonic Techniques

The response of the ASP1 and ASP2 using the Microwave Photonic implementation was first characterised individually, by directing the full power of the optical source into either MZM1 or MZM2, respectively. This was done by adjusting the polarisation controller of Figure 2.11 to pure TM or pure TE respectively, as describe in Section 2.4.

Figures 2.13 and 2.14 shows the individual gain response of ASP1 and ASP2 using the Microwave Photonic implementation shown in Figure 2.11. It shows that the average gain of each element is approximately 7dBi.

The gain response of the antennas has been normalised using the photonic characterisation of the standard horn antenna. Therefore, small variations found within the individual response using the Microwave Photonic implementation and its RF characterisation can be attributed to the relative positioning of the reference antenna and the variations of the Microwave Photonic system. These variations include modulator bias and polarisation control which were subject to environmental factors such as the vibration of the rotating platform and the indistinctively bending of the fibres.

Comparing Figures 2.13 and 2.14 with Figures 2.2 and 2.3 it is evident that the radiation characteristics of the antennas have changed since they were fabricated. The difference between the characterisations is approximately 1 dB. This difference could be attributed amongst some other factors to the fact that a crude outdoor antenna range facility was employed in [21] or the introduction of the photonic link implementation.

The individual gain response of ASP1 and ASP2 using Microwave Photonics demonstrated that photonically remoting antennas does not disturb the radiation characteristics

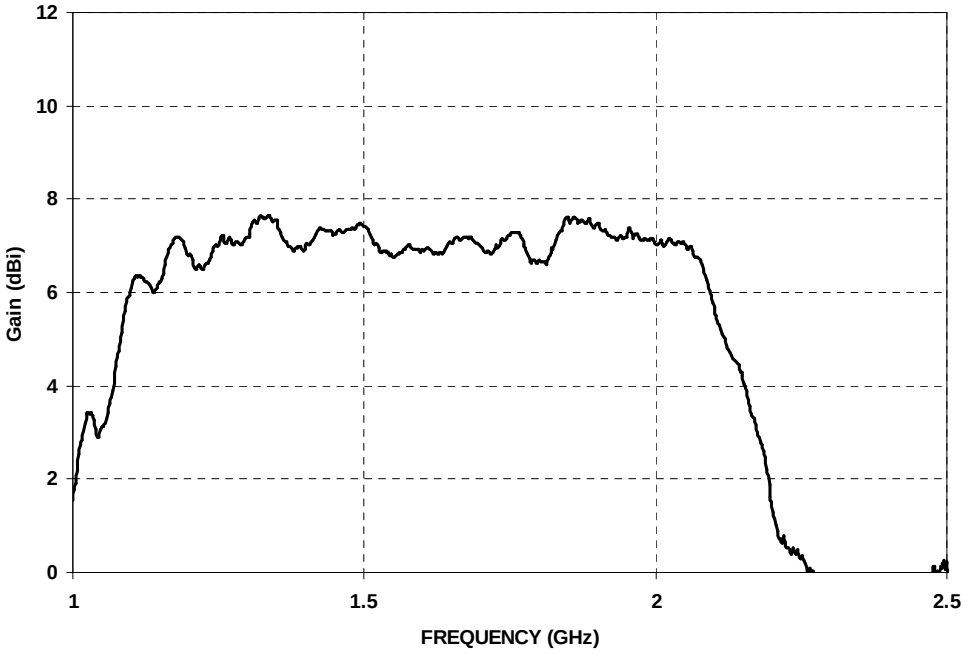

Figure 2.13: Individual Gain Response of ASP1 Using Microwave Photonics

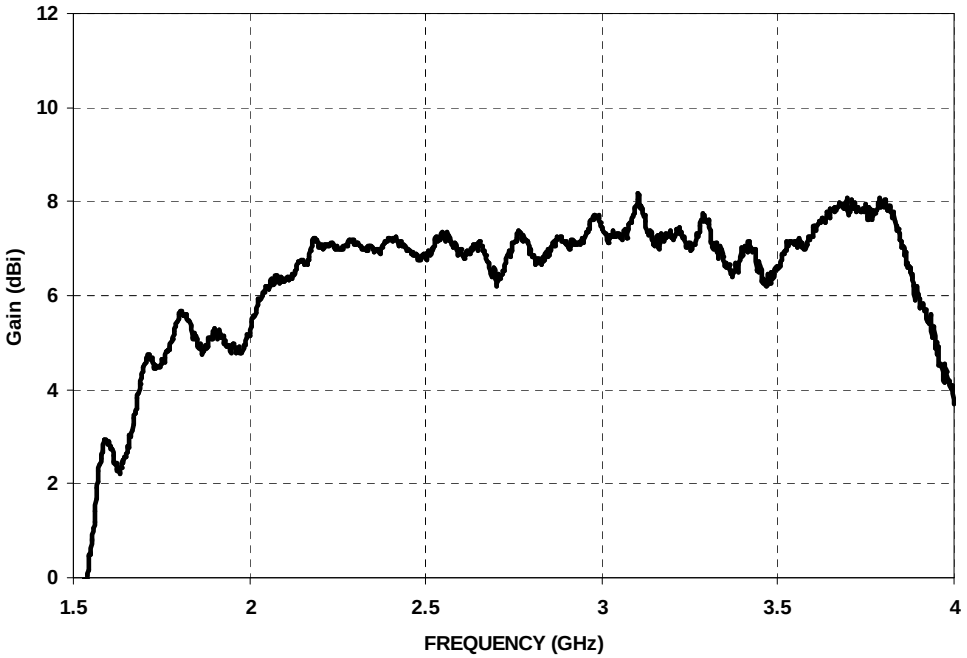

Figure 2.14: Individual Gain Response of ASP2 Using Microwave Photonics

of the antennas. It also demonstrated that the only components required to be close to the antenna are the electro-optic modulators and PM fibres which are lighter than long coaxial cables and RF components.

Combine Gain Characterisation of ASP1 and ASP2

Having characterised the individual response of the antennas, and demonstrating that the Microwave Photonic implementation does not disturb considerably the radiation characteristics of the antennas, the combined response of both antennas operating simultaneously can be characterised.

To characterise the combination of ASP1 and ASP2 it was necessary to equalise the absolute path length of the links, and to adjust the polarisation controller shown in Figure 2.11 such that MZM1 and MZM2 received half of the optical available power ($\alpha = 45\,^{\circ}$), as was explained in Section 2.4.

The absolute path length of the Microwave Photonic links were approximately equalised by selecting optical fibres of similar lengths and fine tuning the microwave phase shifter (MSP1 and MSP2) connected to the antennas (Figure 2.12). This equalisation was achieved by comparing the phase response of each ASP antenna at 2 GHz using a vector network analyser. The frequency point of 2 GHz was selected because it was defined previously as the intersection point where the operational bandwidths of the antenna should intersect [21].

Section 2.4.2 showed that the characterisations of ASP1 and ASP2 were conducted by directing the full power of the laser diode into MZM2 so the individual response of each antenna can be easily normalised. It showed that the link gain characterisation was conducted by connecting a standard horn antenna with known characteristics into MZM2 and directing the full optical power into this link (MZM2). The results for both antennas operating simultaneously were normalised considering that the optical power has been equally divided into MZM1 and MZM2. Since the link gain characterisation of the system has been conducted with the full optical power being directed only to MZM2, a 3 dB optical gain difference between the measurements should be considered; 6 dB RF gain difference [50, 51].

Figure 2.15 shows the combined response obtained with the system when the signals at the intersection frequencies are combined with a $0\,^{\circ}$ phase difference. The response shows that the amplitude of the gain response varies from 6 dBi to 9.5 dBi. The higher point of this variation is situated around the intersection zone at 2 GHz. This variation can be attributed to coherent summation of the operational bandwidths of ASP1 and ASP2. Comparing Figures 2.13 and 2.14 with Figure 2.15 it can be observed that the antennas bandwidth overlap around 2 GHz. The performance of the antennas out of their nominal bandwidths is not defined properly since these antennas were not designed to operate beyond 2 GHz. However, Figures 2.13 and 2.14 demonstrated that ASP1 and ASP2 exhibit considerable gain out of their nominal bandwidths.

Comparing Figure 2.15 with Figure 2.4, it is evident that this implementation has achieved similar response to the microwave diplexer developed in [21]. Considerable differences were found, particular around the intersection zone of 2 GHz, where both

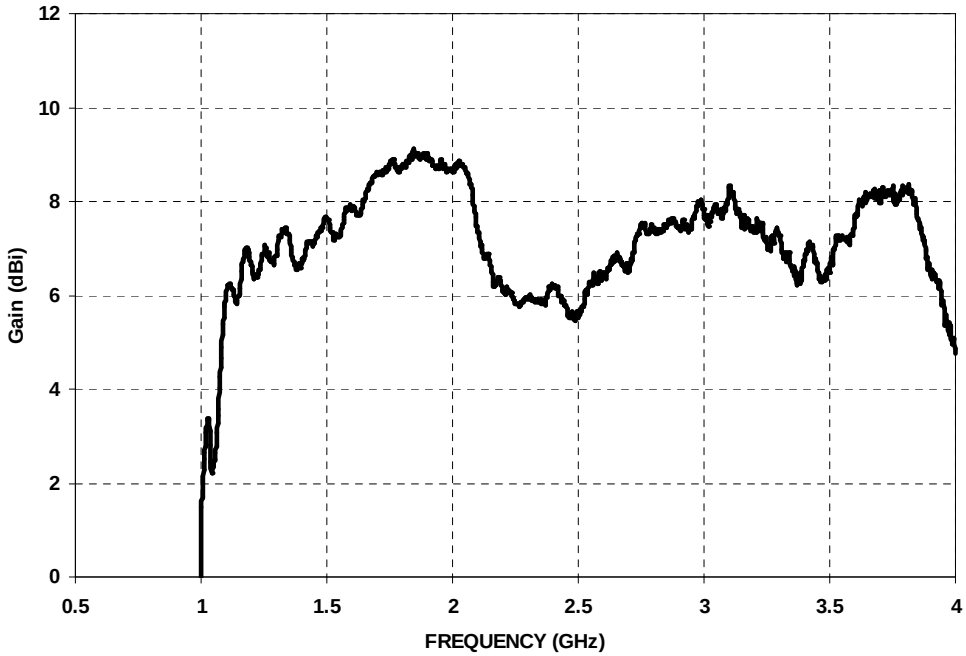

Figure 2.15: Combined Gain Response of ASP1 and ASP2 Using the Microwave Photonic Diplexer

antennas radiate simultaneously with similar radiation levels creating a poorly balanced antenna phased array. This effect is not present in [21] due the filters of the microwave diplexer of Figure 2.1, which shape the radiation response of each antenna. These filters were carefully impedance-matched in order to reduce the gain of each antenna at 2 GHz approximately by -3 dB, so when combined together, ASP1 and APS2 could exhibit a flat gain response across the summation of their operational bandwidths.

Figure 2.16 shows the individual and combined gain response of the antennas using the Microwave Photonic implementation in a single plot, so the interaction zones of the two bandwidths can be clearly observed. A bigger amplitude range has been selected to unveil the full gain characterisation of antennas, particularly for ASP1, which exhibit considerable radiation level out of its nominal bandwidth. Figure 2.16 shows that even a gain difference of approximately 5 dB between the gain response of the antennas can disturb the performance of adjacent antennas. It is worth mentioning that the scale showed in Figure 2.16 was not chosen at the beginning of this chapter to ease the comparison of the results using the Microwave Photonic combination technique demonstrated in this section and the results presented in [21].

From Figure 2.16, it is evident that the Microwave Photonic implementation has indeed enabled a simple coherent summation of ASP1 and ASP2 without using complex microwave diplexer. This has resulted in the expected ultra-broadband gain response from 1.2–3.8 GHz. The 3.5 dB amplitude variation shown in Figure 2.15 is acceptable for this investigation because it was attempted to show the combination of two photonically remote antenna using Microwave Photonic techniques. However, if a flatter gain response is required, for example for UWB applications [32], further signal conditioning steps should be conducted.

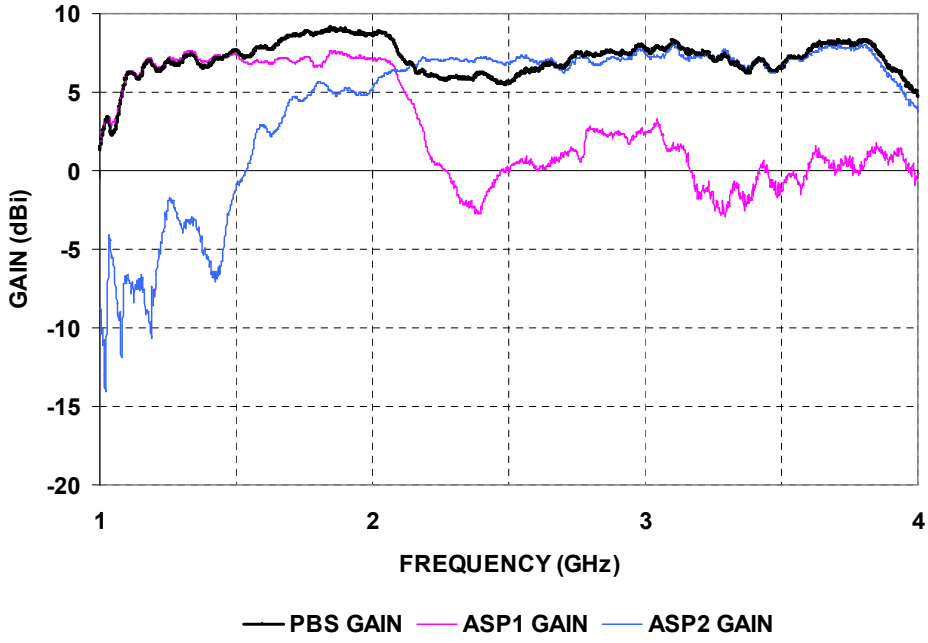

Figure 2.16: Combined Gain Response of ASP1 and ASP2 Using the Microwave Photonic Diplexer (Comparison)

2.5 Summary and Conclusions

In this chapter, a Microwave Photonic diplexer has been proposed and demonstrated. This Microwave Photonic implementation was used to introduce some of the basic photonic remote link concepts and Microwave photonic multiplexing techniques that will be used through this dissertation.

This demonstration replaces a diplexer presented in [21] and demonstrates that complex filtering techniques can be avoided in order to ease the investigation of the overall interaction of the antennas, particularly at the overlapping zones of their adjacent bandwidths. This demonstration showed that the interaction of the antennas at the overlapping zones is stronger compared to the diplexer investigation presented in [21]. However, this Microwave Photonic diplexer solution has demonstrated that converting the RF signal received by two ASP antennas into the optical domain isolated the response of the antennas avoiding impedance loading effects, which can further affect the overall response of the system in the RF domain.

The Microwave Photonic implementation presented in this chapter reduced the elements required for remoting and combining two antenna elements into an ultra-broadband antenna using a single optic fibre link. Thus, this solution could also represent direct volume and weight reduction in antenna remoting systems, particularly if an integrated version of it is developed. This implementation used a polarisation beam splitter and polarisation diversity concept to combine two identical optical carriers with orthogonally polarised propagation modes. Unfortunately, using a polarisation beam splitter limits the system to only two antenna elements, making it not suitable for creating a multiple antenna system with more than two elements.

Other photonic multiplexing techniques may be required if multiple antennas with adjacent bandwidths are employed to create an ultra-broadband antenna element with multiple octaves of operational bandwidth. Techniques for multiplexing multiple broadband photonic channels onto a single optical fibre exist, for example wavelength division multiplexing [48]. Multiplexing techniques for more than two elements along with techniques to address the antenna array effect observed at the intersection points will be explored in the next chapter.

Chapter 3

Multiple Octaves Ultra-broadband Photonic Antenna System

3.1 Introduction

Chapter 2 has shown that multiplexing multiple signals of different antennas with adjacent bandwidths is possible using simple Microwave Photonic techniques but is not something trivial and requires certain considerations. The unstable coherent interference of multiple optical carriers of the same wavelength or the beating effect that occurs when the operational bandwidths of the antennas overlap could result in undesired effects for applications such a Ultra-WideBand technologies (UWB) where wireless hardware should be able to preserve the low power spread pulse standards [31]

This chapter demonstrates an extended version of the photonic multiplexing concept explained in Section 2.4 using a more robust multiplexing technique to combine the responses of three broadband antennas with adjacent bandwidths into a single ultra-broadband receiver. Figure 3.1 shows the conceptual proposed system where multiple antennas are photonically remoted, transferring their electrical responses into the optical domain using electro-optic modulators and photonic multiplexed together into a single optical fiber system.

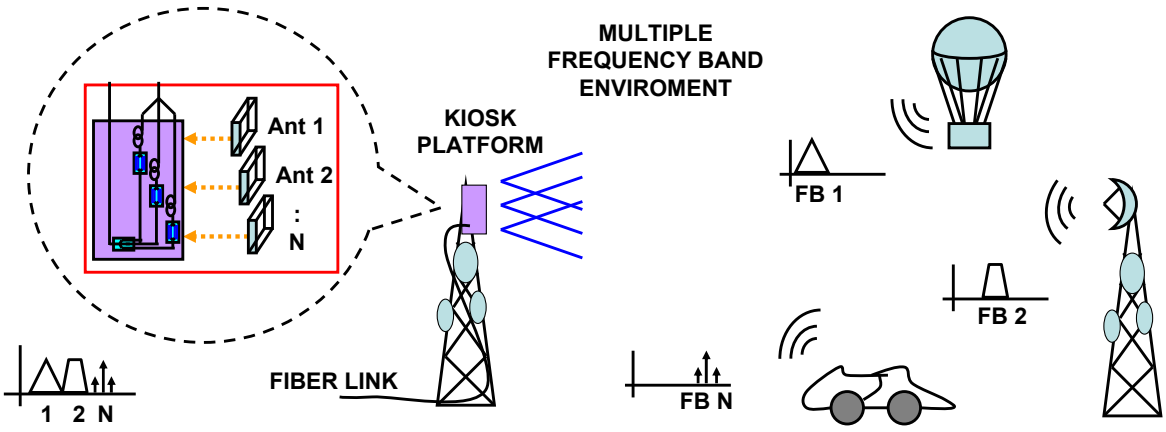

Figure 3.1: Multiple Antenna System

This extended Microwave Photonic implementation addresses the coherent interference and signal beating effects by introducing filtering techniques to shape the gain bandwidth of the antennas. A full electrical characterisation of the combined response of the filters and the antennas will be provided before introducing the Microwave Photonic configuration proposed for combining the antennas into a single ultra-broadband antenna element. Once that the antennas and the system have been introduced, the characterisation of the gain and radiation pattern of the system will be used to highlight the advantages and possible applications of the proposed Microwave Photonic configuration.

3.2 Multiple Patch Antenna System

To effectively combine the response of multiple antennas coherently, a Microwave Photonic configuration not only should be able of isolating the individual RF performance of each antenna into the optical domain but also avoid the response of the antennas to interfere out of their radiation bandwidth. This might only be possible if the gain of the antennas is shaped to an effective bandwidth where the response of the antennas interfere coherently at specific intersection frequencies, and generates balanced arrays with uniform radiation patterns over the entire frequency bandwidth.

This demonstration attempts to verify that multiple Aperture Stacked Patch antennas can be combined into a single ultra-broadband radiating element covering a frequency bandwidth equal to the sum of the individual bandwidth of the antennas.

3.2.1 Antenna Characterisation

As demonstrated in Chapter 2, to implement a flexible Multiple Frequency Band Photonic Receiver such as the one shown in Figure 3.1, it is important to characterise the antenna elements involved in order to define the extent of interference that could occur when attempting to combine multiple antennas together to create a continuous frequency bandwidth.

Three Aperture Stacked Patch (ASP) antennas of adjacent bandwidths have been selected. As mentioned in Section 3.2, ASP antennas are excellent candidates for investigating the interaction between broadband antennas working in a multiple antenna system. Their radiation characteristics make these antennas easy to compare across their radiation bandwidth. ASP antennas however, could also radiate power levels similar to the average power out of their radiation bandwidth and might not preserve uniform radiation characteristics at the upper edge of their radiation bandwidth, as was demonstrated in Chapter 2.

Two ASP antennas corresponding to the radiation bandwidths 1–2 GHz and 2–4 GHz have been already introduced and characterised in Section 2.2.1. Table 3.1 presents the design parameters of the third patch antenna (ASP3 4–8 GHz) which was designed, modelled and optimised using High Frequency Structure Simulator software (HFSS). This third antenna was fabricated using the same techniques used for ASP1 and ASP2 presented in [21], following the parameters presented in Table 3.1. The three ASP antennas were characterised using the gain transfer method, presented in Section 2.2.1.

Table 3.1: ASP3 Antenna Parameters

Feed width, W_f	0.7 mm	Feed thickness, h_f	0.787 mm
Stub length, L_s	7 mm	Layer 1 thickness,	h_1 4 mm
Offset, L_{off}	7.85 mm	Layer 2 thickness, h_2	1.575 mm
Aperture length, L_a	23 mm	Layer 3 thickness, h_3	2.5 mm
Aperture width, W_a	2.5 mm	Layer 4 thickness, h_4	0.787 mm
Patch 1 length, L_1	16 mm	Feed, ϵ_{rf}	2.2
Patch 1 width, W_1	34 mm	Layer 1 ϵ_{r1}	1.07
Patch 2 length, L_2	15 mm	Layer 2 ϵ_{r2}	2.2
Patch 2 width, W_2	33 mm	Layer 3 ϵ_{r3}	1.07
Layer 4 ϵ_{r4}4	2.2		

Figure 3.2 presents the gain responses of the three ASP elements, as well as a numeric sum of the individual response.

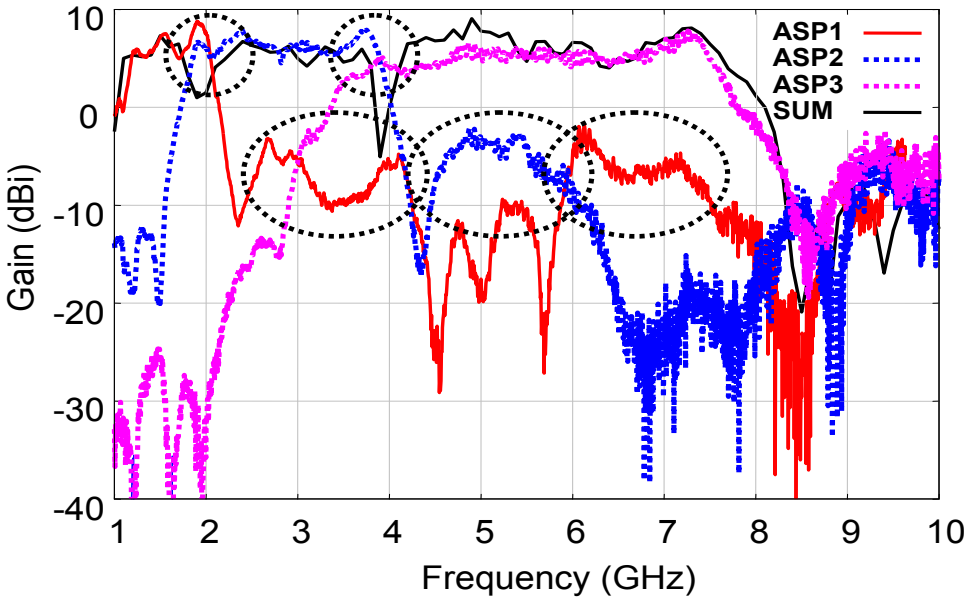

Figure 3.2: Individual ASP Antennas Characterisation

Figure 3.2 shows that ASP1, ASP2 exhibit an average gain of 7 dBi approximately from 1.2–2.1 GHz, and 1.8–3.8 GHz, respectively. This gain decreases outside of these bandwidths with a slope of 50 dB/GHz. ASP3 exhibits an average gain of 6 dBi from 3.5–7.6 GHz and decreases with an approximate 30 dB/GHz slope. Figure 3.2 also demonstrates that the gain response of each antenna exhibits a distinct peak which is about 2 dB above the average gain at the upper edge of the nominal bandwidth before sharply decreasing. The gain response measured of ASP1 across its nominal bandwidth varies by approximately $\pm$ 2 dB, while ASP2 and ASP3 mostly vary at the upper edge of their nominal bandwidth. Figure 3.2 also shows that the power level radiated by ASP1 and ASP2 out of their nominal bandwidths (dotted ellipses) is above -10 dBi from 2.5–4.5 GHz, and 6–7.5 GHz for ASP1, and from 4.5–6 GHz for ASP2. These power levels could

interfere with adjacent antennas. Figure 3.2 also shows that the numeric sum of the individual responses (solid dark line) exhibit two evident intersection frequencies where the response of the antennas interfere stronger than other frequencies, 1.9 GHz and 3.8 GHz.

The distortion exhibited by ASP antennas gain response at the upper edge of their bandwidth is attributed to the aperture of the antenna radiating stronger towards the back than towards the front radiation direction [21]. As shown in Figure 2.15, these distortions could represent detrimental effects not desirable for testing the Microwave Photonic configuration and must be avoided. Although there is not a clear definition for antenna bandwidth among the scientific community, Balanis [52] defines the bandwidth of an antenna as the range of frequencies where its performance, with respect to some characteristics, conforms to a specific standard. In this investigation any gain bandwidth definition must be truncated so the distortions exhibited by the antennas at the upper edge of their bandwidths are not included into the system. The analysis of the gain response of the antennas shown, defines gain bandwidths for the antennas of 1.2–2.1 for ASP1, 1.8–3.8 for ASP2, and 3.5–7.6 GHz ASP3.

These gain bandwidth responses evidently overlap. If these elements were simply combined, they would operate as a poorly balanced array with detrimental consequences to the gain and radiation pattern response at the overlapping frequencies [22]. Figure 3.2 shows a numeric version of adding these responses without extra processing techniques. It shows that the gain performance of the combined response is sensitive to the relative phase and amplitude between the signals received by each antenna at the overlapping zones. Thus, before combining these antennas, we must reduce the overlapping areas and the radiation out of the redefined bandwidths of the antennas using filtering techniques.

3.3 Antenna Gain Bandwidth Shaping Microwave Filtering Techniques

In order to obtain an overall response with the same average power of the individual signals, the field received by each antenna at the overlapping frequencies must intersect each other reduced by 50% or what it is the same, the effective gain exhibited by the antennas must intersect reduced by 6 dB [53]. This defines a new gain bandwidth definition where the antenna must start radiating above a power level 6 dB lower than its average radiated power.

It is possible to use filtering techniques to shape the performances of the antennas so that the radiated power of the antennas out of their nominal bandwidths does not interfere with the power radiated of adjacent antennas. These filtering techniques should also be able to adjust the power radiated by each antenna element at the intersection frequencies so that when combined together constructively with a phase difference of $0\,^{\circ}$, these bandwidths add coherently and constructively, generating a flat gain response over the entire frequency bandwidth of the three antenna elements.

Two design factors were considered for shaping the performance of the antennas using microwave filters. The first factor was to reduce the radiation exhibited by the antennas out of their nominal bandwidth so that the signals received by the antennas do not interfere

destructively with nominal bandwidths of the other antennas. The second factor was to provide clear intersection points for the gain bandwidths so that the combination of the signal at the intersection frequencies can coherently added with a phase difference of $0\,^{\circ}$ and gain levels -6 dB lower than the nominal bandwidth of each antenna.

The numeric analysis of the combination of the individual gain response presented in Section 3.2, provides two frequency points where antennas exhibited the strongest interference. These two points were 1.9 GHz and 3.8 GHz and will be selected as intersection frequencies. At these points the gain response of the antennas should overlap with a power level 6 dB lower than the average radiated power by each antenna.

Figure 3.3 shows a picture of the three reflective filters created to match the desired -6 dB gain bandwidth of each ASP antenna at 1.9 GHz and 3.8 GHz, and to reduce the out of band radiation of the antennas. A low pass stepped impedance filter (F1), a band pass double stub filter (F2), and a band pass double stub filter (F3) were designed to exhibit an insertion loss of -6 dB at the intersection frequencies. 1.9 GHz for F1, 1.9 GHz and 3.8 GHz for F2, and 3.8 GHz and 7.6 GHz for F3. These filters were designed using Agilent's Advanced Design System (ADS) and realised on Rogers RT/Duroid substrates (5880 and 4003C) using Printed Circuit Board fabrication techniques. The Scattering parameters of each filter were analysed using a Vector Network Analyser (VNA).

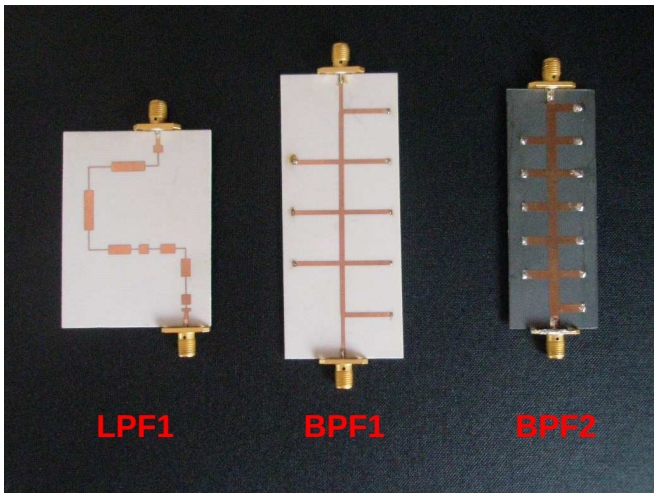

Figure 3.3: Low Pass Filter for ASP1, and Band Pass Filters for ASP2 and ASP3

Figure 3.4 and Figure 3.5 illustrate the simulated and measured results of the reflection coefficient and insertion loss of each filter (LPF, BPF1 and BPF2), respectively. Figure 3.5 shows that the insertion loss exhibited by the filters is less than -0.5 dB with approximately 0.5 dB variation. The roll-off at the stop bands of the filters exhibit a -6 dB insertion loss at the frequency points of 1.9 GHz and 3.8 GHz. Figure 3.4 and Figure 3.5 also illustrate that the LPF exhibited re-entrant modes at 5, 5,5 and 6 GHz.

Comparing the reflection coefficient and insertion loss, simulated and measured results, of the filters for shown in Figure 3.4 and Figure 3.5, is evident that the fabricated filters follow closely the simulated response. The resonances exhibited by the LPF at 4.8, 6.2, 7.4 and 7.8 GHz are re-entrant modes inherent of stepped impedance filters.

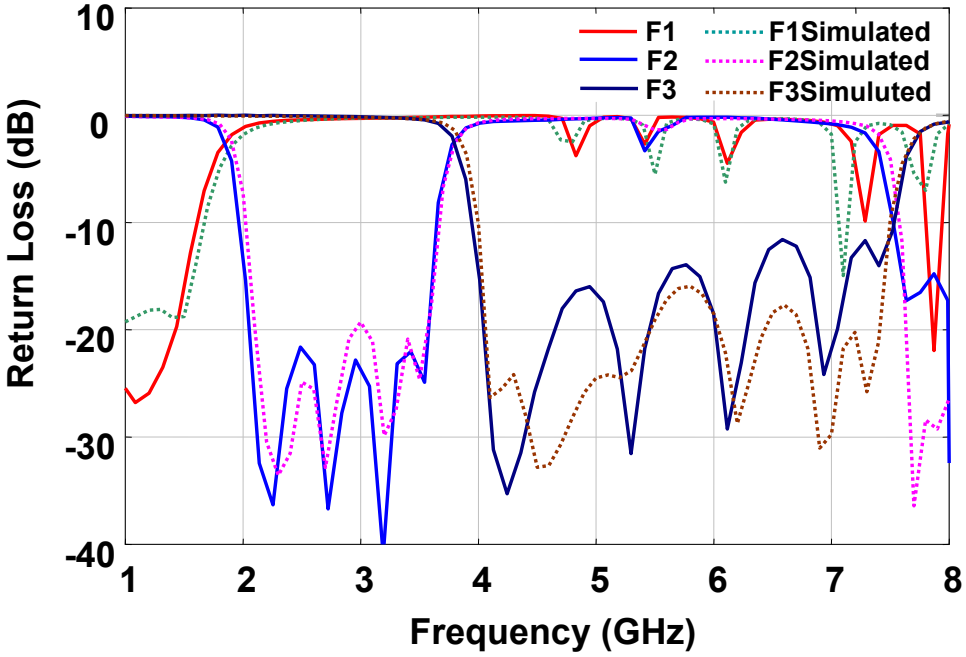

Figure 3.4: Reflection Coefficient Response of Fabricated Filters

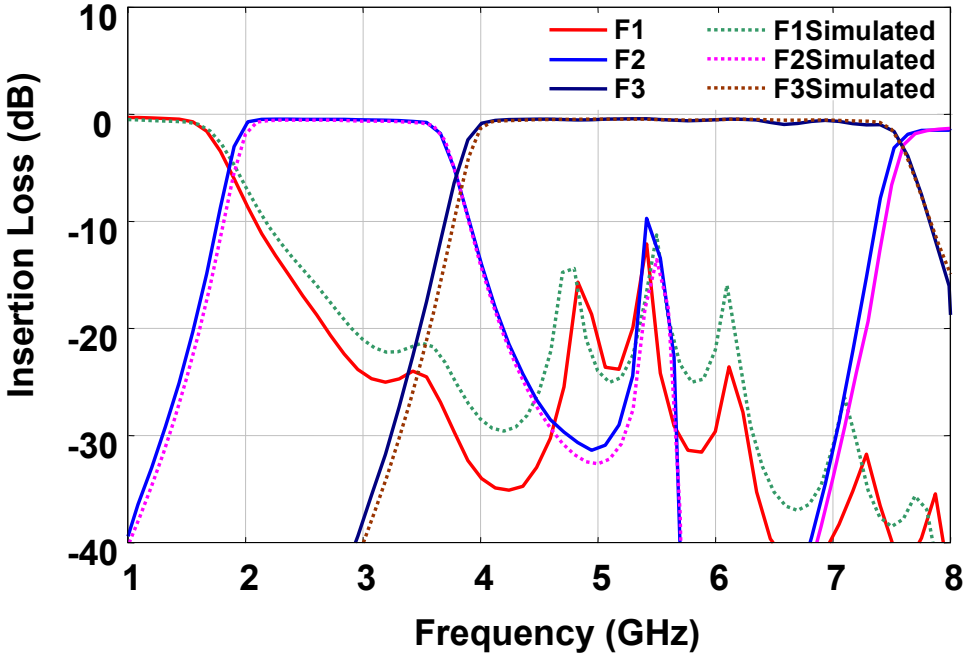

Figure 3.5: Insertion Loss Response of Fabricated Filters

Although F1 and F2 exhibited some re-entrant modes, the overall characteristics of the filters shows that the insertion loss of -6 dB required to combine coherently the gain bandwidth of the antennas at the intersection frequencies has been achieved. These filters should also reduce the power radiated out of the defined gain bandwidths effectively, except for the re-entrant modes.

3.3.1 Filter-Antenna Characterisation

The perfect impedance matching between the antenna and the filters is based on the assumption that the antenna load is purely resistive and terminated by the filter. Any changes on this condition will create a complex impedance termination situation, resulting in reflections along the transmission lines. Impedance mismatches between the antennas and filters can lead to spectral regrowth, inter modulation distortions and other unwanted effects [54]. The fact that the band-pass bandwidth of the filter is narrower than the impedance bandwidth of the antenna and that these components are physically connected through an extra length of transmission line, makes highly probable to exhibit undesirable impedance mismatch effects. This effect must be fully investigated to ensure that the filter-antenna response exhibit an accurate -6 dB gain bandwidth between the intersection frequencies, and reduces the radiation power out of this bandwidth to an acceptable level that does not interfere with adjacent antennas.

The combined filter-antenna elements were characterised using the same methods described in Section 3.2.1. The antennas and the filters have been connected through female-female sma adapters, so their combined performance can be characterised.

Figure 3.6 shows that the reflection coefficient of the filter-antenna elements is below -10 dB from 1.1–1.6 GHz for ASP1, from 2–3.6 GHz for ASP2, and from 4–7.5 GHz for ASP3 except at 4.7, 5.7, 6.6 and 7.2 GHz where the reflection coefficient goes above -10 dB. It also shows that the reflection coefficient of the filter-antenna elements bounce back at the beginning of the roll-offs generating small re-entrant modes. These re-entrant modes are located within the -6 dB expected gain bandwidth and correspond to the frequency region where the stop bands of filters and the impedance bandwidth of the antennas overlap: 1.6 GHz for ASP1, 1.9 GHz and 3.9 GHz for ASP2, and 3.8 for ASP3. It also shows re-entrant modes of approximately -10 dB at 4.8, 6.2, 7.4 and 7.8 GHz for F1-ASP1 and a re-entrant mode around 5.5 GHz of approximately -3 dB for F1-ASP1 and F2-ASP2.

The reflection coefficient values exhibited by the F1-ASP1 element at 4.8, 6.2, 7.4 and 7.8 GHz are combination of the re-entrant modes the filter and the impedance bandwidth of the antenna. The re-entrant modes are inherent harmonics of the filter design parameters and can be appreciated better in Figure 3.4. The only way to reduce these re-entrant modes are either by cascading multiple low pass filters or by choosing another low pass filter design without these inherent harmonics. The bouncing on the reflection coefficient at beginning of the stop bands of the filters are caused by an impedance mismatch between the filters and the antennas [54]. These undesirable effects occur within the expected -6 dB gain bandwidth of the antennas and could make the interference of the received signals from the antennas unpredictable at the intersection frequencies.

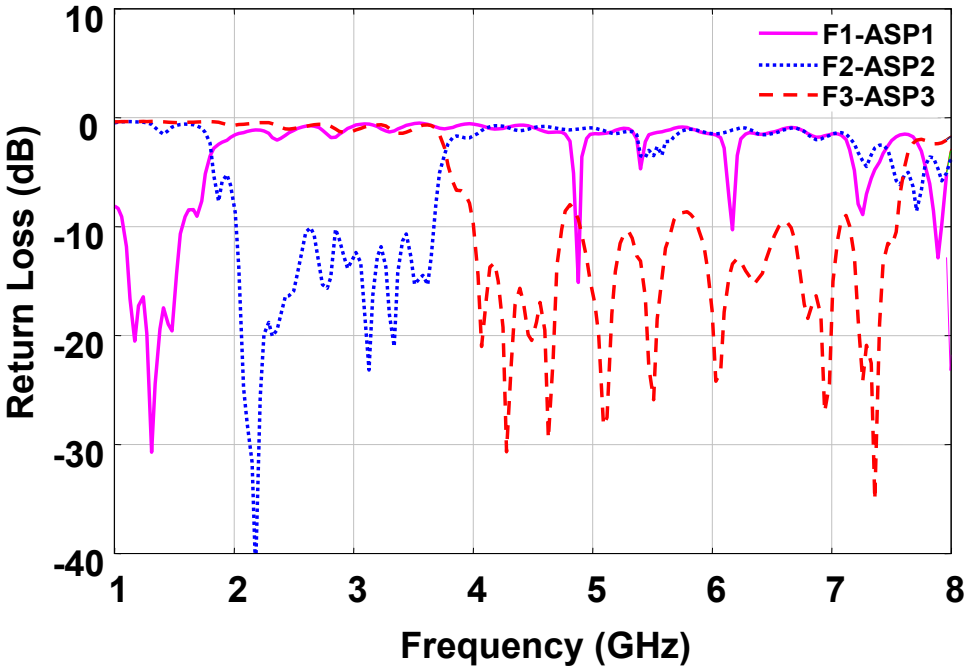

Figure 3.6: Reflection Coefficient Characterisation of the Filter-Antenna Element

Three methods of eliminating these resonances have been identified: the first method is by choosing absorptive filters such as diplexers instead of the reflective filters. The complementary filter of the diplexer can absorb the out of band radiation of the antennas if terminated to a broadband matched load; however, designing the diplexer has proven to be a complex process [21] and it is the intention of this investigation to substitute this microwave component with a Microwave Photonic configuration that simplifies the filter designing process. The second method is by adjusting the widths of the stubs of the filters in order to closely match the impedance response of the antennas and suppress any unwanted reflection; however this process involves considering the antenna parameters making more complex the design of simple filter and can represent to loss control over the required gain bandwidth response. The third method is by using microwave isolators to convert the reflective filters shown in Figure 3.3, into absorptive filters, leaving the current filters intact.

For this investigation it was chosen to use isolators. This simple alternative involves only the interconnection of an extra component between the antennas and the filters, reducing all the complex designing process of adjusting the filters.

3.3.2 Stop Band Mismatch

The whole purpose of the multiple antenna system shown in Figure 3.1 is to provide a simple alternative for combining the responses of multiple antennas together. Using an isolator instead of modifying the filter design to match the load of the antennas should provide the expected response of the Microwave Photonic configuration proposed in this Chapter, highlighting the flexibility of system for receiving any Filter-Isolator-Antenna configuration (FIA element).

The three FIA elements were characterised using the same methods described in Section 3.2.1. Figure 3.7 shows the reflection coefficient characterisation of the FIA elements. Figure 3.7 illustrates that the reflection coefficient exhibited by the FIA element is below -10 dB from 1.25–1.75 GHz for FIA-1; from 1.95–3.55 GHz for ASP2; and from 4–7.5 GHz for FIA-3. It also shows re-entrant modes of approximately -10 dB at 4.8, 6.2, 7.4 and 7.8 GHz for FIA-1, and a re-entrant mode around 5.5 GHz of approximately -3 dB for FIA-1 and FIA-2 elements.

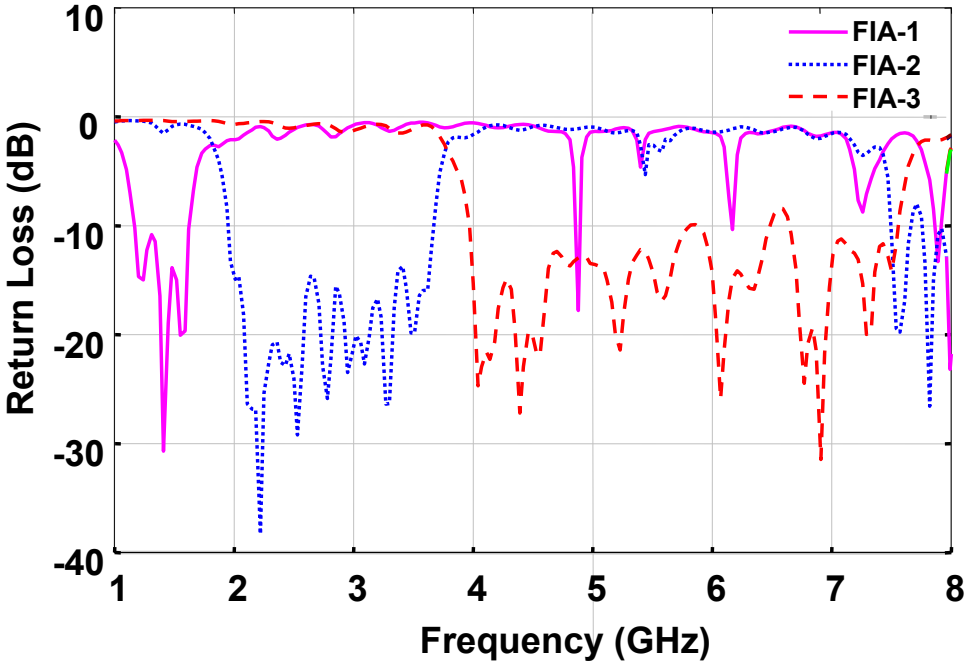

Figure 3.7: The Effect of the Isolator on the Reflection Coefficient of the Filter-Antenna Element

The comparison between the filter-antenna element reflection coefficient response in Figure 3.6 and the reflection coefficient of the FIA elements shown in Figure 3.7, demonstrates that the impedance mismatch effects, caused for the loading of the antennas at the stop bands of the filters, have been considerably reduced. Using isolators to interconnect the antennas to the filters has improved the response of the FIA elements, reducing the reflection coefficient at the active zone. The isolator had minimal effect on reducing the resonances exhibited by FIA-1 at 4.8, 6.2, 7.4 and 7.8 GHz supporting the assumption that these resonances are part of the re-entrant modes of the Low Pass Filter.

The improved reflection coefficient responses of the filter-antenna elements are evidence that simple techniques such as the use of microwave isolator, can be implemented without modifying the design parameters of the filter. The filters should now be able to shape the performance of the antennas so the coherent summation of the bandwidths of the antennas provides a flat response across the entire band.

3.3.3 FIA Elements Characterisation

Having reduced the resonances caused by the interconnection of the antennas and the filters using an isolator, the filters should now effectively suppress the gain radiation out of the nominal bandwidth of the antennas and reduce the gain at the intersection frequencies to -6 dB lower than the average gain of these antennas.

The FIA elements were characterised in order to verify the radiation performance of the antenna elements and to determine the effect that each filter has on the radiation performance of the antennas. The radiation responses of each of the FIA elements were measured using an indoor antenna test facility. Each element was characterised individually without the presence of the other FIA elements so that the effect that the filters have over the antennas can be determined without exhibiting additional interference due antenna coupling effects.

Figure 3.8 presents the results of the gain characterisation for each FIA element. It shows that each FIA element exhibit a mid-band average gain value of approximately 5.5 dBi, with an amplitude variation of ± 2 dB. Figure 3.8 also shows that the gain of ASP2 and ASP3 increases 2 dB above the average value at the upper edge of their gain bandwidth before being suppressed by the filters. The gain responses of the FIA elements at the intersection frequencies (1.9 GHz for ASP1 and ASP2; and 3.8 GHz for ASP2 and ASP3), exhibit a radiation gain level 6 dB lower than the average gain of the antennas.

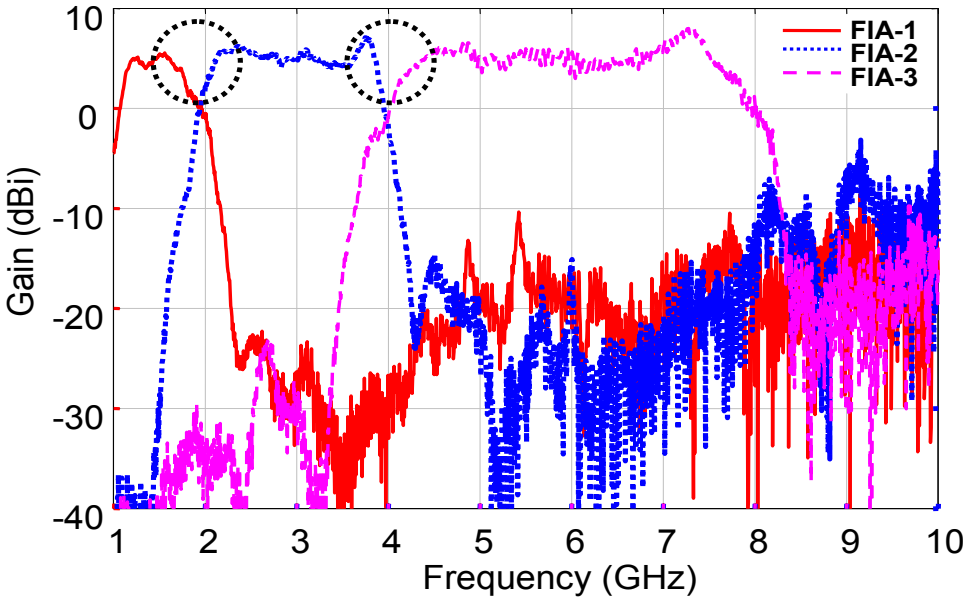

Figure 3.8: Filter-Antenna Elements Gain Characterisation

Comparing Figure 3.8 to Figure 3.2 shows that the filters reduce the gain out of nominal bandwidth of each antenna such that the radiation responses will have less interference on the in-band gain of adjacent antennas. The gain response of Figure 3.8 confirms that the filters do not interfere greatly with the performance of the antennas within their nominal bandwidths.

As shown in Section 3.2.1, the expected performance of the combined filtered antennas can be predicted by coherently summing the individual responses of FIA-1, FIA-2

and FIA-3. The -6 dB adjustment achieved with the filters at the intersection points, 1.9 GHz and 3.8 GHz, should create a flat response provided that the phase difference of the signal at these frequencies is $0\,^{\circ}$. A small delay of the sort that could be achieved with a microwave phase shifter has been included in the total path length for the signal, in order to optimise the coherent summation at the intersection frequencies. Figure 3.9 shows the comparison of the numeric sum of the individual response of the gain bandwidth of the antennas using filtering and phase equalisation techniques (FIA SUM), and the numeric sum of the bandwidths of the same antennas added coherently without any filtering or phase equalisation (SUM), also shown in Figured 3.2. FIA SUM represents the result of adding the three bandwidths of the antennas at the intersection points with a phase difference of $0\,^{\circ}$ and a gain level -6 dB lower than the average in-band gain of each antenna.

Figure 3.9 clearly shows that if the responses of the FIA element can be simply added by a Microwave Photonic configuration that isolates each element from each other, then the desired ultra-broadband gain response from 1.2 GHz to 7.6 GHz could be achieved.

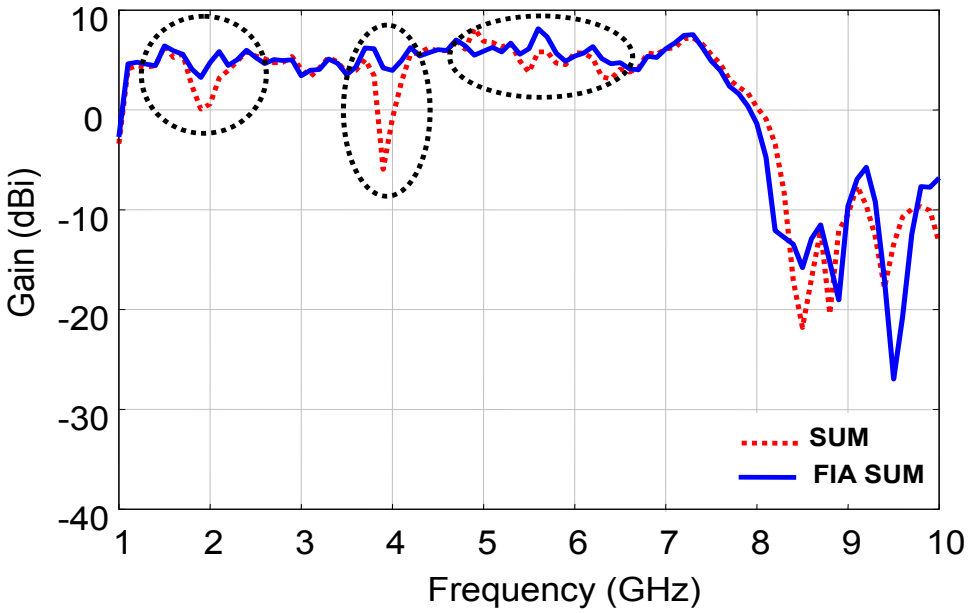

Figure 3.9: Filter-Antenna Elements Gain Characterisation

In conclusion, filtering suppresses the radiation of the antennas out of their nominal bandwidth and modifies the gain response at the intersection frequencies 6 dB below the average gain of the in-band response of each element. The predicted results indicate that it should be possible to combine the adjacent bandwidths of these elements to create a continuous uniform ultra-broadband frequency response, provided that the phase difference of the signals at the intersection frequencies is effectively $0\,^{\circ}$.

3.4 Multiple Frequency Band Photonic Receiver

Having reduced the gain of the antennas radiated out of their nominal frequency bandwidth and created a new -6 dB gain bandwidth definition for each antenna, it is important to demonstrate that the responses of these antennas can be combined into a single optical carrier using the Multiple Frequency Band Photonic Receiver (MFBPR) proposed in this Section.

Figure 3.10 shows the Microwave Photonic configuration proposed to create the MFBPR, together with the antenna measurement network used to characterise it. As shown in Section 3.3.2, an isolator must be placed between each antenna (ASP1, ASP2 and ASP3) and its respective filter to avoid impedance mismatch at the stop bands of the filters. The FIA elements are connected to a broadband Mach-Zehnder Modulators (MZM) via mechanically variable phase shifters in order to optimise the coherent summation of the frequency bandwidths, particularly at the intersection frequencies.

Separate carriers (LD1, LD2 and LD3) of different wavelengths are fed to each modulator which converts the signals received by the antennas into the optical domain. These carriers are combined into a single optical fibre using wavelength division multiplexing using a 100GHz, JDSU® Wideband (Flat Top), Arrayed-Waveguide-Grating (AWG) [55, 56, 57]. The insertion loss of this AWG is approximately 5 dB. The total length of the fibres was cleaved to the same size, ensuring that the path length for all the carriers is approximately the same. Given that the three optical carriers are of different wavelengths, these carriers can be combined into a single Polarisation Maintaining (PM) fibre using an AWG (AWG1) without coherent interference effects [45].

The PM fibre transports the three carriers inside the anechoic chamber, as shown Figure 3.10, where the MZM and the FIA elements are co-located over a rotating platform. Since an AWG can work as a combiner or as a splitter, another AWG (AWG2) splits the carriers back into individual channels so that each carrier can be connected to a distinct MZM and can be modulated by the signal received by its corresponding FIA element. Once modulated, the carriers are combined again by a third AWG (AWG3) into another single PM fibre that transports the combined signal outside the anechoic chamber up to an Erbium-Doped Fibre Amplifier (EDFA), where it is amplified prior to being converted back to the RF domain by a Photo-Detector (PD).

As demonstrated in Section 2.2.1, measuring the antenna response using a vector network analyser in an indoor antenna test facility requires the use of a long coaxial cable to connect it to the transmitting antenna. In order to increase the link gain and improve the quality of the measurement, another alternative must be selected. Figure 3.10 shows that test signals are generated and measured by a Signal Generator (SG) and a Spectrum Analyser (SA), respectively. Since both the SG and the SA were controlled using a GPIB interface and a dedicated program developed on LabVIEW to synchronise the antenna measurement network, the SG could be placed close to the transmitting antenna. This reduced the length of coaxial cable used in the antenna measurement network and improved the total gain of the link.

Several antenna geometric arrangements were attempted. Figure 3.11 shows the final distribution of the FIA elements mounted over the rotating platform inside of the Ane-

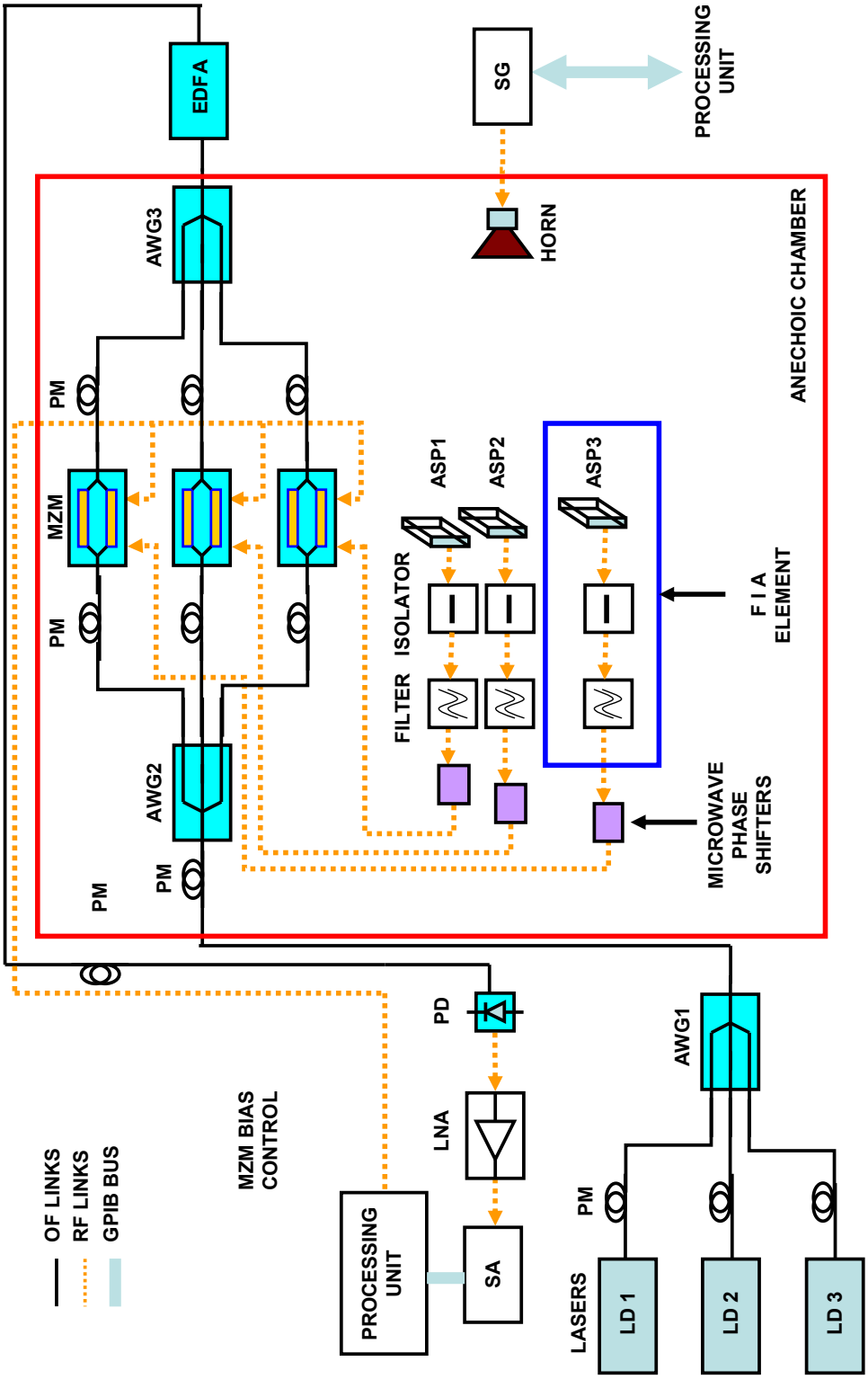

Figure 3.10: Microwave Photonic Band Photonic Receiver Test Setup

choic Chamber. Figure 3.11 shows that FIA-1 and FIA-2 are placed in close proximity in a diagonal configuration, while FIA-2 and FIA-3 are separated approximately 10 cm along the H-plane of the antennas.

Mounting the Microwave Photonic configuration inside the anechoic chamber proved to be a challenging task. The fact that the antennas are fed vertically and that the isolators and filters are attached to the antennas, restricted the number of possible geometric arrangements. The antenna measurement network in Figure 3.10 must be able to photonically remote the three FIA elements adding the individual responses of the antennas coherently.

3.4.1 MFBPR Gain Characterisation

Having assembled the Microwave Photonic configuration in Figure 3.10 and placed the antennas inside the anechoic chamber as shown in Figure 3.11, the FIA elements can now be characterised. This is done as individual elements first, by activating one laser diode at a time; then simultaneously, by activating the three laser diodes at the same time in order to obtain the combined response of the MFBPR.

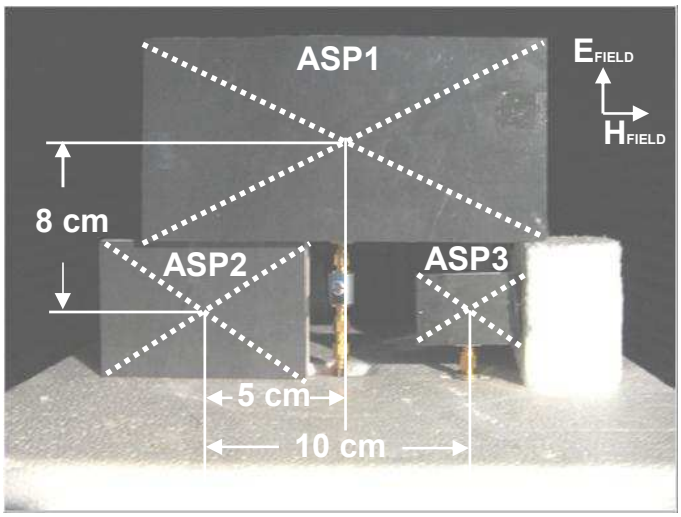

Figure 3.11: Co-location of Filter-Isolator-Antenna Elements Inside The Anechoic Chamber

Section 3.3 showed that in order to operate the three antennas together and obtain the flattest possible gain response across the entire frequency bandwidth of 1.2–7.6 GHz, it is necessary to adjust the phase of the signals received at the intersection frequencies (1.9 GHz and 3.8 GHz) to $0\,^{\circ}$. The link gain for each channel is equalized by adjusting the optical power of the lasers individually, so the MFBPR does not disturb the gain response of the FIA elements. Although the lengths of the optical links were cleaved to be the same length; the relative phase of each FIA needed to be initially adjusted in order to compensate the different electrical path lengths between the different FIA elements. This was achieved using the vector network analyser to measure the phase response of each FIA element at the intersection frequencies and adjusting the length using microwave phase shifters so the phase difference between all the links were equal to $0\,^{\circ}$.

Figure 3.12 shows the gain response of each element and the combined response obtained of the MFBPR when the signals at the intersection frequencies are combined in phase. Figure 3.12 shows that the average gain of each FIA element is around 5.5 dBi and presents a gain variation of $\pm$ 2 dB.

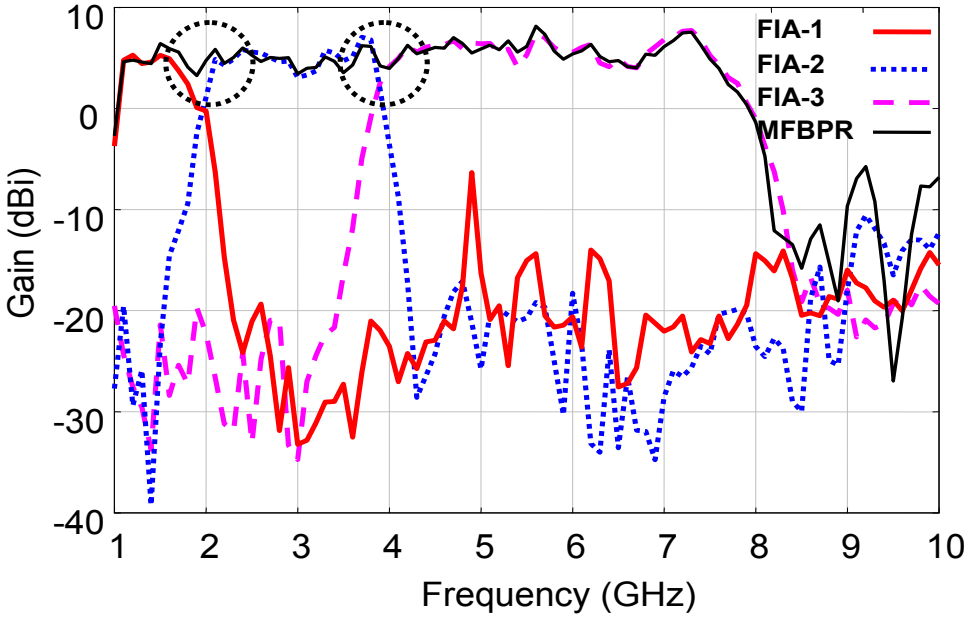

Figure 3.12: Individual And Combined Gain Response Of The MFBPR

From Figure 3.12, it is evident that the MFBPR has indeed enabled a simple coherent RF summation of the FIA elements. This has resulted in the desired ultra-broadband gain response from 1.2–7.6 GHz. Comparing Figure 3.12 with Figure 3.8 it is evident that the MFBPR has not disturbed the individual response of the FIA antennas.

3.4.2 Radiation Pattern Characterisation

The combined gain performance of MFBPR shown in Figure 3.12 represents only the special case where the radiation is measured directly in front of the antenna. To completely characterise the radiation of an antenna, its relative amplitude, relative phase, polarisation, needs to be measured. A representation of any of these radiation properties as a function of space coordinates is defined as a radiation pattern, or antenna pattern, of the test antenna [49].

Analysis of the radiation performance of the Multi Frequency Band Photonic Receiver was conducted in two stages: first, the mid-band radiation performance; and second, the radiation performance at intersection frequencies. The radiation pattern response was recorded following the antenna characterisation standards in [49]. This was done by having the same antenna arrangement shown in Figure 3.11 and rotating the whole MFBPR inside the Anechoic Chamber to measure the gain response of the system, versus azimuth angle at different frequencies and different orientations (H and E planes). The radiation patterns recorded were normalised to 0 dBi, considering as a reference the higher radiation power received by the antennas at the frequency of interest.

MFBPR Mid-band Radiation Performance

The MFBPR, operating at a frequency within the gain bandwidth of ASP1, ASP2 or ASP3, will only exhibit the radiation patterns corresponding to a single element due to the filters introduced in Section 3.3 and the RF isolation resulting from converting the RF signals into the optical domain using the MZM. Therefore, it is anticipated that the radiation performance of the MFBPR within the effective gain bandwidth of each element will be typical of an ASP antenna [21].

The H-plane radiation patterns of the MFBPR at the in-band frequencies of the each of the antennas were obtained by simultaneously activating LD1, LD2 and LD3 and rotating the MFBPR inside the Anechoic Chamber to measure the gain response of the system, versus azimuth angle.

Figure 3.13 a), b) and c) show the radiation patterns of the MFBPR operating at 1.5 GHz, 3 GHz and 7 GHz. These patterns are compared to the individual ASP radiation patterns. The ASP measurements plotted in Figure 3.13 a) exhibit all the standard characteristics of ASP antennas such as broad radiation patterns, low cross polarisation, front to back ratio (around 10 dB) and gain levels (around 8 dBi) [21, 36]. The radiation pattern generated by the MFBPR at 1.5 GHz, exhibits a narrower back radiation beam and a major disruption at around $270\,^{\circ}$. Similar characteristics are exhibited by the radiation patterns at 3 GHz, where the MFBPR exhibits a disruption at around $90\,^{\circ}$ and $270\,^{\circ}$. The MFBPR results at 7 GHz, Figure 3.13 c), exhibit a characteristic ripple at the back radiation response and a similar deformation to ASP1 around $270\,^{\circ}$.

Comparing the MFBPR results with the ASP radiation patterns, the major differences observed are the deformations on the sides of the radiation patterns which can be attributed to the interference created by objects (antennas) sitting in close proximity to the FIA elements. These objects also caused the beam width to broaden, particularly at the back lobe of the radiation patterns.

The in-band radiation characteristics of the system have proved to be close to the radiation performance exhibited by ASP antennas, demonstrating that the individual performance of each antenna remains almost undisturbed by the Microwave Photonic configuration. The isolation of the antennas provided by the filters at the in-band frequencies has worked, eliminating any undesirable unbalanced array effect between the antennas. However, the isolation provided by the filters at the intersection frequencies is reduced due to the roll-off response of the filter.

MFBPR Intersection-Region Radiation Performance

At the intersection frequencies of the MFBPR, 1.9 GHz and 3.8 GHz, the antenna elements conform an antenna array. The effects of this array over the radiation characteristic of the MFBPR at these frequencies will be determined by the relative position of the antennas. Also, as mentioned in Section 3.2.1 this will be determined by the relative phase and power level of the signals received by the antennas. Some atypical radiation patterns are expected because the antennas are operating at the upper and lower edges of their bandwidths. The H-plane and E-plane radiation patterns of the UBPA were characterised at 1.9 GHz and 3.8 GHz in order to investigate the arrangement shown in Figure 3.11.

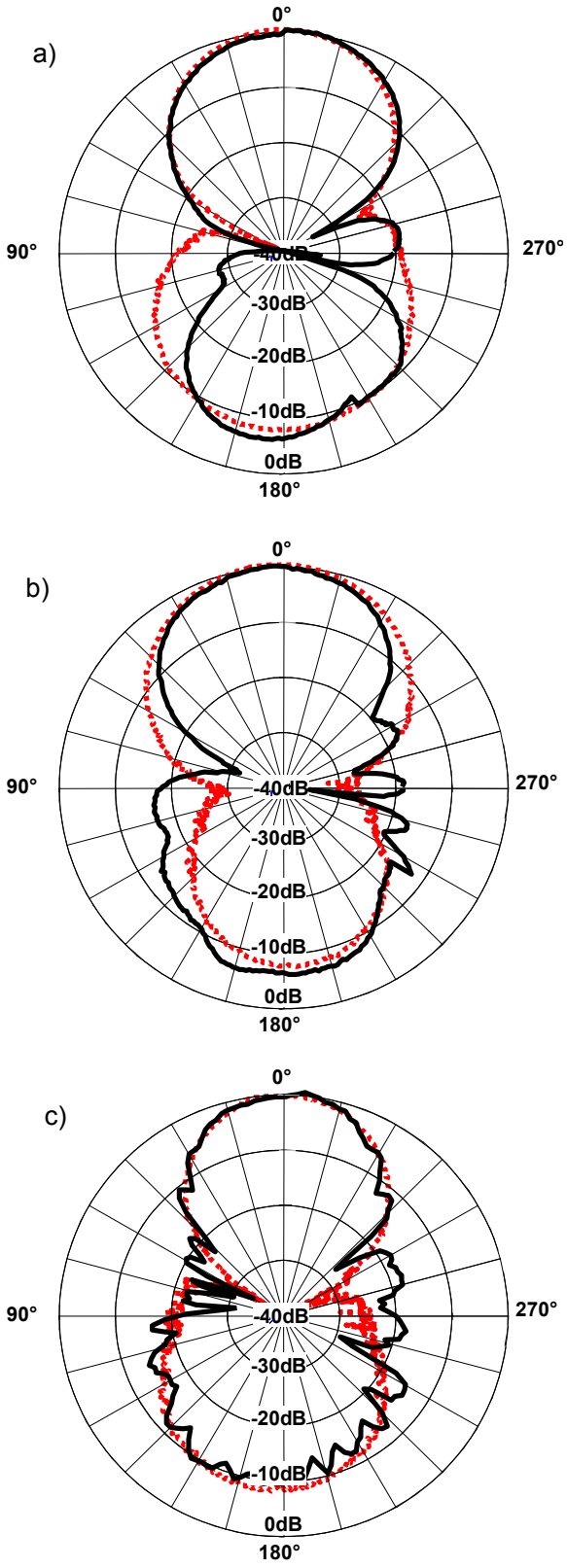

Figure 3.13: H-plane Radiation Patterns. a) @ 1.5 GHz, b) 3 GHz, c) @ 7 GHz. Individual ASP Response (dotted lines), MFBPR Response (solid dark lines)

The H-plane radiation patterns of the MFBPR at the intersection frequencies were obtained by simultaneously activating LD1, LD2 and LD3 and rotating the MFBPR inside the Anechoic Chamber to measure the gain response of the system, versus azimuth angle.

Figure 3.14 a) and b) presents the radiation patterns response of the MFBPR measured on the H-plane at 1.9 GHz at 3.8 GHz, respectively. Figure 3.14 a) shows that the radiation pattern of ASP1 operating at the upper edge of its band, 1.9 GHz, exhibits lower front-to-back ratio and bigger side lobes compared to the in-band radiation characteristics at 1.5 GHz presented in Figure 3.13 a). The combined response of the MFBPR at 1.9 GHz is approximately 6 dB higher than the individual responses, which demonstrates that the two individual responses are coherently added. It presents a front-to-back ratio of 10 dB, a 3 dB beam-width of $30\,^{\circ}$ approximately and side lobes that are less than 10 dB. These radiation characteristics are deemed acceptable for our proposed application, being close to the radiation characteristics of an independent ASP antenna.

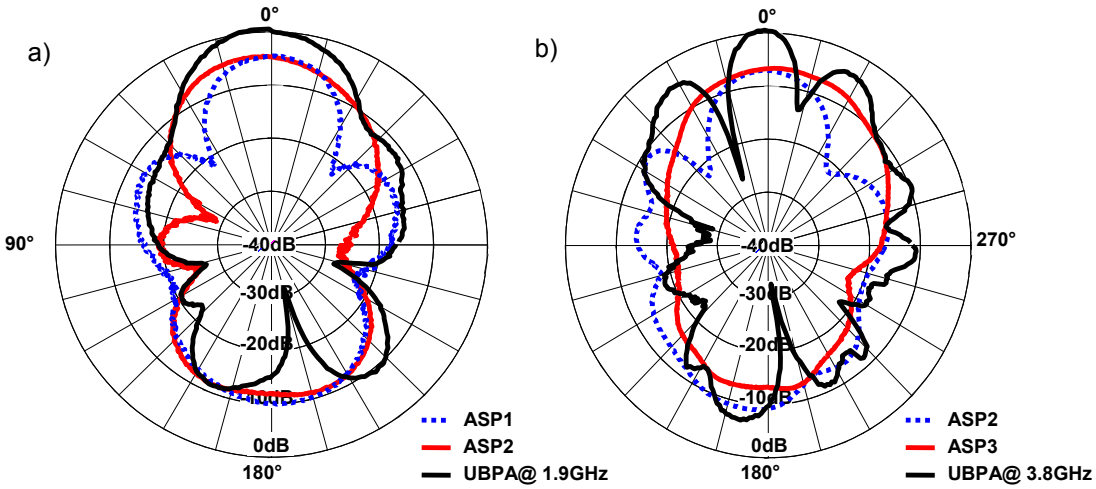

Figure 3.14: H-plane Radiation Pattern Response at the Intersection Frequencies of the MFBPR. a) 1.9 GHz and b) 3.8 GHz. Individual RF and Combined Response

Figure 3.14 b) shows that ASP2 operating at the upper edge of its band, 3.8 GHz, exhibits low front-to-back ratio and sides lobes compared to response of its lower edge (1.9 GHz) shown in Figure 3.14 a). The combined response of the MFBPR at 3.8 GHz is 6 dB higher than the individual responses and presents a front-to-back ratio of almost 7 dB, a 3 dB beam-width of $15\,^{\circ}$ approximately, and side lobes approximately 8 dB lower than the main lobe. These radiation characteristics are considerably degraded when compared to the characteristics at 1.9 GHz in Figure 3.14 a).

The degradation in radiation pattern at the intersection frequencies can be attributed to two causes: the first is the degradation of the radiation patterns of the antenna elements themselves at the intersection frequencies, corresponding to the lower and upper band edges of the gain bandwidth of the antennas; the second cause of degradation is the coherent summation of two elements operating as an unbalanced array, causing beam narrowing and side lobes. These effects occur whenever the separation of the individual elements of an array are equal to or greater than one wavelength.

Figure 3.15 a) and b) presents radiation patterns response of the UBPA measured on the E-plane at 1.9 GHz and 3.8 GHz, respectively. Figure 3.15 a) shows that the com-

bined response of the UBPA at 1.9 GHz presents a front-to-back ratio of 6 dB, a 3 dB beam-width of $45\,^{\circ}$ approximately and a small disruption around $90\,^{\circ}$. These radiation characteristics concur with the radiation characteristic of ASP antennas for the E-plane presented in [21]. Figure 3.15 a) shows that the beam of the combined response is narrower than the individual responses.

Figure 3.15 b) shows that combined response of the UBPA at 3.8 GHz presents a front-to-back ratio of almost 15 dB and a 3 dB beam-width of $70\,^{\circ}$ approximately and a small disruption around $90\,^{\circ}$. Figure 3.15 b) shows that the beam of the combined response is broader than the individual responses.

The antenna configuration of Figure 3.11 attempted to reduce the spacing between the antennas according to [58]. Compared to an in-line geometric configuration along the H-plane between ASP1 and ASP2, used in [59], Figure 3.16, the separation between the ASP1 and ASP2 in this investigation has been reduced on the H-plane but increased in the E-plane (Figure 3.11). This has improved the radiation patterns of the system at 1.9 GHz on the H-plane without disturbing considerably the E-plane response. Comparing the radiation pattern at 3.8 GHz in Figure 3.14 b) with the radiation patterns presented in [59] at 1.9 GHz, it is evident that co-locating the antennas in an in-line arrangement over the H-plane of the antennas generates radiation patterns with higher sides lobes which are proportional to the separation of the antennas. The presence and location of the sides lobes on the H-plane at 3.8 GHz, Figure 3.14 b), corresponds to an array of two antennas separated by approximately 2 wavelengths which matches the current separation (10cm) between ASP2 and ASP3, Figure 3.11. The E-plane measurements, on the other hand, exhibit better radiation characteristics. This is obvious, since the antennas are not overlapping on this plane and the fact that the aperture of the antennas is aligned along its H-plane. The radiation patterns on the E-plane at 1.9 GHz exhibits a narrower beam-width than at 3.8 GHz, demonstrating that the antennas started to overlap.

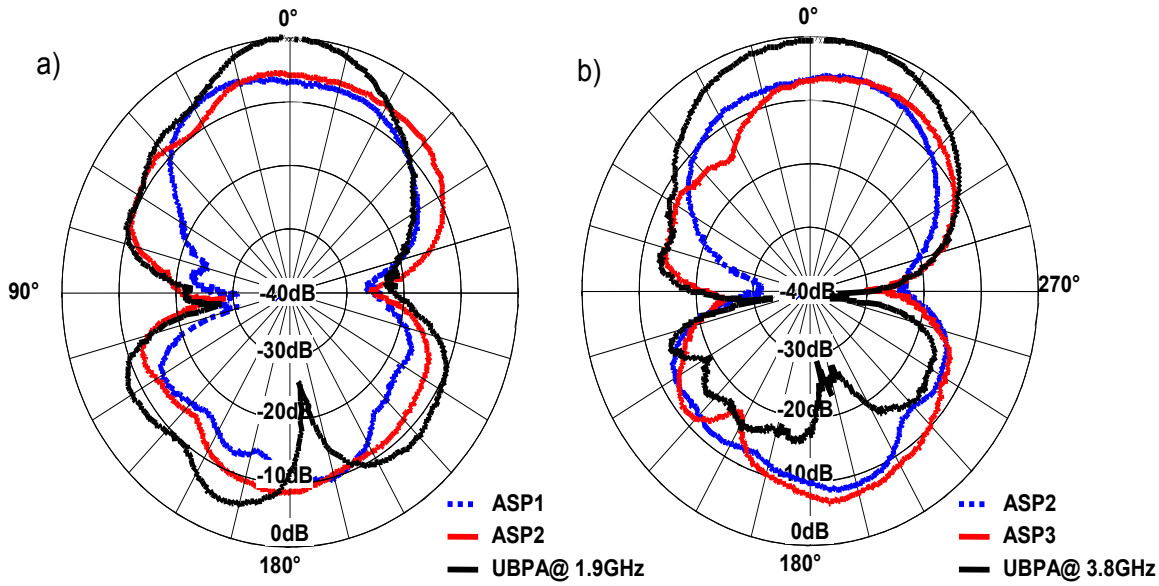

Figure 3.15: E-plane Radiation Pattern Response at the Intersection Frequencies of the MFBPR. a) 1.9 GHz and b) 3.8 GHz. Individual RF and Combined Response

In multiple antenna systems such as the MFBPR, the shape of the radiation patterns is partially defined by the phase and time delay imperfections between the received signals from each of the antennas [30]. These imperfections are present as side lobes which increases according to the distance between the antennas [60, 61, 62]. The frequency ranges of the antennas are related to each other by almost one octave of bandwidth, and are proportional to the size of the antennas. Figure 3.11 shows that the size of ASP3 is almost half of the size of ASP2 and ASP2 is almost half of the size of ASP1. Therefore, provided that ASP2 and ASP3 can be co-located in a similar configuration to ASP1 and ASP2 as in Figure 3.11, the radiation response of the system at 3.8 GHz should exhibit similar results to the ones exhibited by the system at 1.9 GHz, Figure 3.14 a).

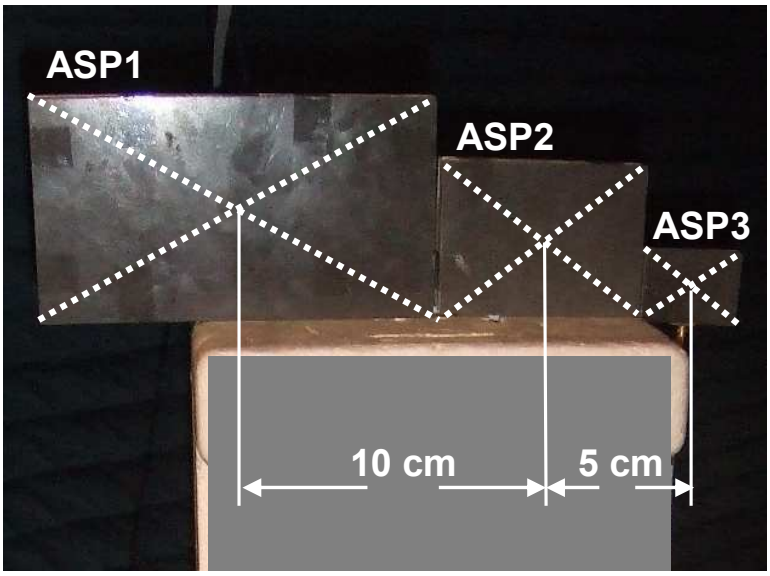

Figure 3.16: In-line Arrangement for MFBPR

3.5 Summary and Conclusions

In this Chapter, a Multiple Frequency Band Photonic Receiver has been proposed and demonstrated. This Microwave Photonic implementation overcomes the complex task of multiplexing more than two antennas with adjacent frequency bandwidths using RF techniques. It demonstrates that it is possible to isolate the response of the antennas into the optical domain, avoiding the impedance loading effect exhibited by the filters of a microwave multiplexer approach.

Simple filtering techniques have been used to shape the gain response of the antennas and control the coherent interference of the signals at the intersection frequencies. This has reduced the interference between the signals received by the antennas, and enabled the proposed system to obtain a relatively flat gain response across the whole bandwidth with radiation patterns characteristic of ASP antennas.

Investigation into the performance of this approach indicates that the placement of the antennas is more critical than the presence of objects surrounding the antennas. This

is particularly the case at the intersection frequencies, where the distance between the pair of antennas working at the same frequency generates an array factor that disturbs the radiation pattern response.

Minimising the separation between the antenna elements with adjacent bandwidths so the antennas can be located as close as possible (a diagonal) proved to reduce the level of side lobes generated on the radiation patterns at the intersection frequencies. As a consequence of using rectangular antenna patches; the H-plane of the antenna is larger than its E-plane. Using the E-plane axis of the antenna for placing adjacent antennas, enable the antennas to be placed in a diagonal distance which compromises the radiation patterns of the system over both planes. In-line placements exhibit unaltered radiation patterns over the orthogonal axis of the system, but create considerable deformations over the patterns on the plane parallel to the alignment axis. Consequently, and since it is not always possible to use the E-plane of the antennas to co-locate adjacent element due the spatial requirements of the feeding network, a diagonal placement of the antennas was found to be a suitable option. The diagonal placement between the antennas adopted in this investigation compromises both radiation planes, minimising the deformation on the H-plane corresponding to the largest side of the antennas.

One possible approach for enabling the reduction of the distance between the antennas involves the integration of the modulators, filters and the antennas into a single module. This approach will no longer require the isolator, and will enable the modulator and the filter to be attached to the antenna in such a way that none of these obstruct the antennas from being placed in close proximity.

In summary, the Multiple Frequency Band Photonic Receiver enables the coherent summation of multiple filtered antenna elements, achieving a uniform and ultra-broadband multiple antenna system with some deformations to the radiation pattern at the intersection frequencies. These deformations are related to the relative placement of the antennas, the relative phase between the signals received by the antennas and the amplitude of these signals.

Chapter 4

Microwave Photonic Mode Controller for a Two-arm Spiral Antenna

4.1 Introduction

Radio direction finding is defined by the National Telecommunications and Information Administration (NTIA) as: “the determination of the position, velocity and/or other characteristics of an object, or the obtaining of information relating to these parameters, by means of the propagation properties of the radio waves,” [63]. The basic configuration for direction finding systems is presented in Figure 4.1 and consists of a configuration of electromagnetic field sensors (antennas) able to capture incoming Radio Frequency (RF) signals, a receiver system that amplifies and filters the signals received by the antenna, some means of processing this amplitude and phase information into an angle of arrival and an intensity indicating the range to the source. This information is then presented on an operator display [64].

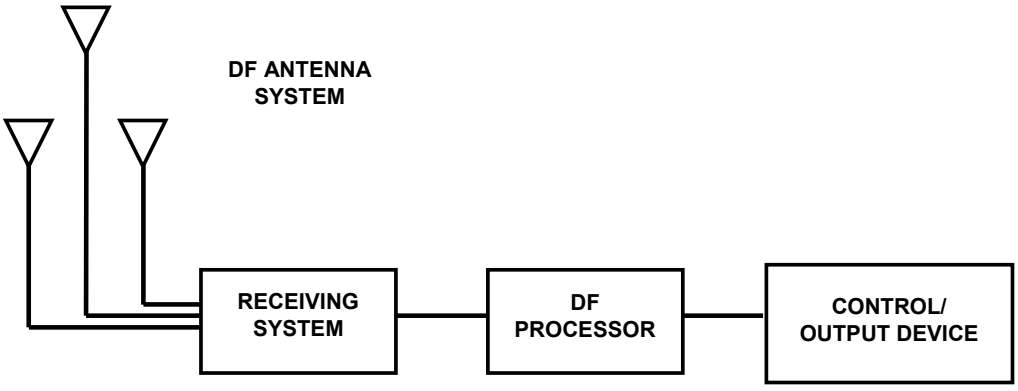

Figure 4.1: Basic Configuration For Direction Finding (DF) Systems

Civilian applications of direction finding systems include: radio navigation and satellite global positioning services for cargo tracking; signal direction finding and location systems for wildlife and sports tracking; radio astronomy; smart antennas for telecommunications and, search and rescue services for disaster response where fast detection of the location of an emitter could represent the difference between finding a person alive

or not in natural disasters [64]. Most of these applications are allocated to specific frequency ranges which enable specialised systems such as phased array antenna, to detect the location of a signal within a metre range or less, as is the case with Global Positioning Systems (GPS) [3]. In order to achieve this precision, a phased array must exhibit high selectivity and directivity. These characteristics, however, are normally obtained at the expense of reduced operational bandwidths, large and complex implementation and low latency response.

Modern direction finding systems often employ phased array antenna systems and triangulation techniques for detecting the location of an incoming signal. However phased array antennas are not sufficient for some military applications, such as Electronic Support Measure (ESM) systems [65].

Reconnaissance for anti-radiation homing and warning systems are among some ESM applications where the rapid response of direction finding and identification systems is critical for detecting hostile radar and homing systems [65]. These applications cannot rely only on highly directional phased array antennas alone, as although very high sensitivity can be achieved in a single direction, these systems are practically blind in all other directions and thus the probability of detecting an incoming threat from an arbitrary direction is low. For this reason it is important to have a coarse receiver that is able to monitor a broadband frequency range and multiple spatial and polarisation modes with reasonable sensitivity to provide an initial warning of a potential threat. This coarse detection system can then be used to direct the more refined resources of the phased array to provide a conclusive identification of the threat.

In many practical implementations, these requirements are covered by crossed Log-Periodic array of dipoles or by broadband spiral antennas. However, the complexity of the feeding interfaces required to control these systems increases with the number of antenna elements, making maintenance, reliability, versatility, cost, size and weight prohibitive factors for some applications, such as airborne applications [9, 66]. It would be desirable that an antenna used as a front-end receiver had a single aperture antenna for which all these radiation modes share a common coincident phase centre and a flexible mode controller network, so all these disadvantages can be minimised.

Multiple-arm frequency independent antennas such as Archimedean and logarithmic spiral antennas are mostly designed to radiate its fundamental mode with impedance matching and beam pattern exhibiting frequency independent characteristics [67]. However, these antennas can also radiate other useful modes for direction finding purposes.

In this chapter a Microwave Photonic multiplexing and photonic weighting techniques are used to realise a continuously variable mode transformer for a customised cavity backed two-arm spiral antenna. This spiral antenna can be reconfigured to operate in both its fundamental and second order radiation modes. The proposed Microwave Photonic system is able to receive the fundamental and second order radiation modes of the antenna, as well as the two normal modes and an arbitrary number of unbalanced modes over a single optical fibre link. This implementation will be introduced, characterised and finally, integrated to the customised antenna for characterisation purposes, so the advantages of this implementation over traditional microwave devices can be validated.

4.2 Frequency Independent Self-complementary Antennas

A frequency independent antenna might not be completely frequency independent. However, for practical purposes, some antennas exhibit radiation characteristics that remain uniform over specific frequency bandwidths.

According to [68], a frequency independent antenna is one where the dimension of the radiating element changes proportionally with the frequency. Spiral [69, 70] and sinuous [71, 72, 73] antennas are a clear example of frequency independent antenna, where design parameters such as angle and grown rate change in order to keep constant the relation between the dimension of the radiating element and the operational frequency of the antenna across a broad range of frequencies.

The radiation modes of these antennas are mostly determined by their feeding interface. The most common way to feed these antennas is using a Balanced to Unbalanced (Balun) transformation which is impedance matched to the fundamental mode of the antennas. The impedance of the balanced mode is normally approximated using the self-scaling and self-complementary principle described in [74]. Multiple-arm frequency independent antennas can be operated in various modes with distinct radiation patterns. However, placing a balun as an interface stops higher order modes from being generated [75]. If higher order radiation modes can be received independently over a large frequency range by broadband mode controllers, this antennas can be used for direction finding implementations by themselves [64, 68, 76].

In the following sections a commercial cavity back spiral antenna is modified to enable the control of multiple radiation modes that can be exhibited by the commercial spiral. The fundamental and second order radiation modes of a customised cavity backed two-arm equiangular spiral antenna, as well as an arbitrary number of unbalanced modes are fully characterised using traditional microwave methods so they can be used as a reference for the Microwave Photonic Mode Controller proposed in this chapter.

4.2.1 Radiation Modes of a Self-complementary Antenna

An analysis of self-complementary structures can be found in [74]. In this study is reasoned that an antenna which is composed of N self-complimentary elements can be analysed by considering that each individual element exhibits a 'normal' radiation mode. Combining these normal modes with determined phase difference achieves a number of useful radiation patterns. This combination of normal modes is defined as an "M mode". For any M mode of a rotationally symmetric antenna, the normal modes are often feed with equal magnitudes and with progressive phases as given by $2\,\pi\,M/N$, where N is the number of arms and M is an integer that defines the desired M mode.

Figure 4.2 shows some of the M modes that can be generated by an N-arm self-complementary antenna using a combination of its normal modes. Only one M mode has a broad single beam radiation pattern (M=1). The other M modes exhibit a null at broadside and can be considered as higher-order modes peaking further from the broadside null as the order of the mode increases.

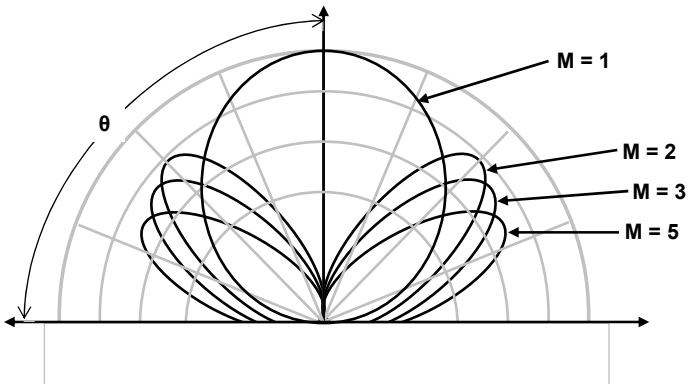

Figure 4.2: M-modes Radiation Patterns of a Multi-arm Self-complementary Antenna

A crude version of direction finding, where M=1 and M=2 radiation modes of a self-complementary frequency independent antenna are constantly compared, can be achieved if both radiation modes are impedance matched to the mode controller implementation.

4.2.2 Characteristic Impedance of the Self-complementary Antenna

Broadband performance of a self-complementary antenna can only be achieved if each of the characteristic input impedance of the antenna for a desired M mode is matched by its feeding interface. Effectively, only one of the M modes shown in Figure 4.2 can be matched at a time by the same feeding interface. However, if the input impedance of the interface is designed to be the average impedance of the desired M modes then, the interface provides acceptable matching for each of them.

The input impedance for a self-complementary N-arm structure in free space is given as

$$Z_M = \frac{\frac{\eta_0}{4}}{sin\left(\frac{M\pi}{N}\right)} \tag{4.1}$$

where $\eta_0 = 120\pi\,\Omega$ is the impedance of the free space and M is the integer that defines the M mode [74]. N is the number of arms on the structure. Table 4.1 shows calculated values corresponding to the input impedance of different multi-arm self-complementary structures for different modes of excitation.

Table 4.1: Input Impedance for Self-Complementary Structures in Free Space

	Self-complementary Modes				
#Arms	1	2	3	4	5
2	94.2				
3	108.8	108.8			
4	133.3	94.2	133.3		
5	160.3	99.1	99.1	160.3	
6	188.5	108.8	94.2	108.8	188.5

According to Table 4.1, the input impedance of a two-arm frequency independent antenna operating in mode M=2 is undefined. Nevertheless, the coupled stripline transmission line connected to the feeding point of the two-arms of the antenna, not the balun itself, could potentially excite two distinct propagation modes of the antenna, corresponding to the differential and common modes transmission modes of a coupled transmission line [77, 78]. These transmission modes fulfill the amplitude and phase requirements to operate a two-arm self-complementary structure in its fundamental and second order modes.

The following sections present the antenna selection criteria for this investigation followed by the design of a double feed orthogonal mode transformer able to excite both the fundamental and second order modes of a two-arm self-complementary antenna with frequency independent characteristics.

4.3 Double Feed Broadband Two-arm Spiral Antenna

The primary requirement for this investigation was a broadband antenna which performance validated the broadband response of the Microwave Photonic implementation proposed to control the multiple radiation modes of a frequency independent antennas such as spiral antennas. A cavity backed two-arm spiral antenna based on [79] was chosen as shown in Figure 4.3. This antenna is a right hand circularly polarised antenna fabricated by RFSpin®, and has a broadband frequency response from 2–24 GHz and axial ratio below 3 dB for the entire frequency range. An absorptive cavity makes this antenna a unidirectional antenna and supports the radiation modes for the lower frequency band of the antenna.

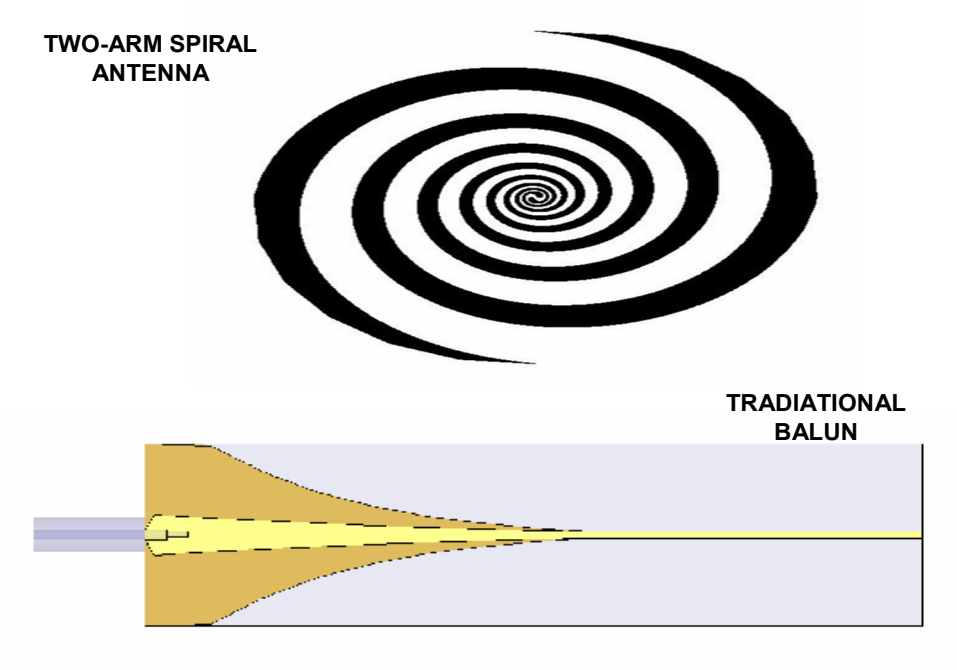

Figure 4.3: Two-arm Spiral Antenna and Original Commercial Balun

The original commercial feeding interface of this antenna is an adiabatic mode transformer, also known as a balun, that converts a single unbalanced microstrip line into a double conductor balanced transmission line which is impedance matched to the fundamental radiation mode of the spiral antenna [80, 81, 82].

This balun only allows control of the fundamental radiation mode (M=1). For direction finding purposes, it is desired to be able to switch between the M=1 and M=2 modes and thus another alternative to the balun must be investigated modifying the antenna to enable control of both radiation modes.

4.3.1 Double Feed Feeding Interface

Frequency independent antennas operating in their fundamental mode can exhibit broadband radiation characteristics; however, operating in higher order modes, this broadband response can be reduced to a fraction of the fundamental bandwidth. This is particularly true for the case where the feeding interface decreases the cutoff frequency of these modes.

The original balun of the two-arm spiral antenna shown in Figure 4.3 was replaced with an alternative mode transformer that enables the spiral antenna to switch between multiple possible radiation modes. This mode transformer was designed based on the principles presented in [17] for orthogonal mode transformers. This alternative mode transformer consists of an adiabatic taper, and converts the balanced double conductor line connected to the spiral patch to two individually connectorised unbalanced striplines.

According to Section 4.2.2 and [70, 74, 78], the characteristic impedance of a two-arm self-complementary structure with a dielectric substrate should be around $100\,\Omega$. This characteristic impedance exhibits a differential mode impedance of approximately $150\,\Omega$ and a common mode impedance of approximately $75\,\Omega$.

The impedance of the unbalanced lines of the orthogonal mode transformer was initially chosen so that the characteristic impedances of each line formed a differential mode impedance similar to the fundamental radiation mode of the spiral antenna, and a common mode impedance, similar to its second order radiation mode to ensure similar impedance match to both radiation modes.

Figure 4.4 shows the orthogonal transformer designed to match the average characteristic impedance of the spiral antenna, operating in its fundamental (M=1) and second order (M=2) modes. Two $50\,\Omega$ unbalanced striplines are adiabatically transformed into two $75\,\Omega$ unbalanced transmission lines whose ground planes are gradually reduced and inner conductors are converged in close proximity to create a coplanar double strip transmission line of $100\,\Omega$ characteristic impedance. This orthogonal mode transformer has been designed and modelled using Ansoft's High Frequency Structure Simulator software (HFSS). An optimisation process was undertaken varying design parameters such as substrate thickness, line width, inner conductor proximity, substrate shape and parallel ground presence.

Figure 4.4 presents that optimised model that will be integrated to a replica of the two-arm spiral antenna presented in [79]. Table 4.2 summarises the final parameters of the proposed orthogonal mode transformer.

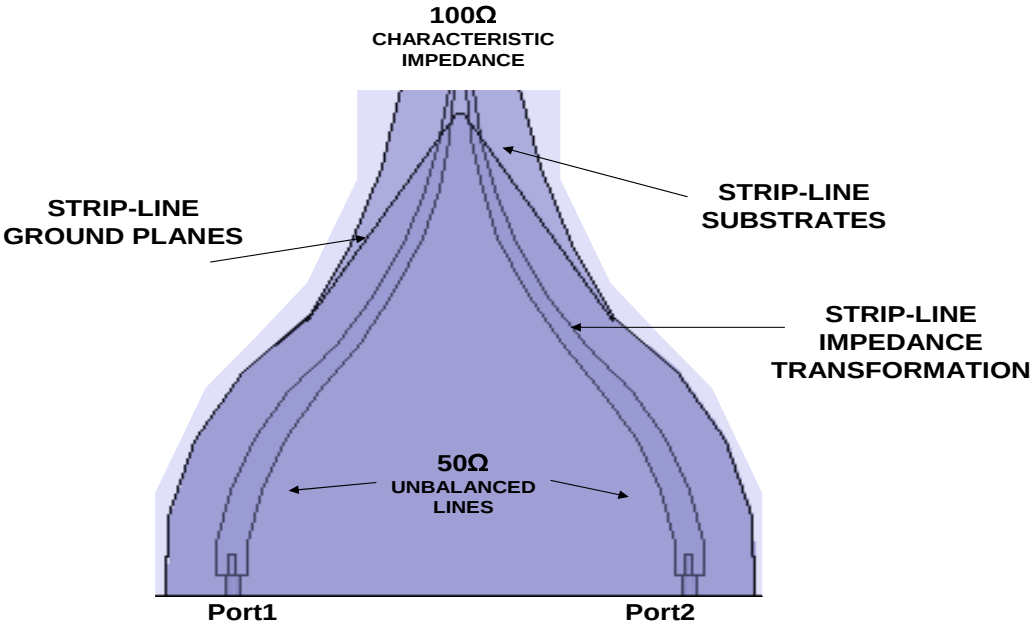

Figure 4.4: Proposed Orthogonal Mode Transformer

Table 4.2: Orthogonal Mode Transformer Parameters

Layer	Substrate Type	Relative (ϵ_r) Permittivity	Loss Tangent	Thickness (d)
1	Copper		0.004	0.8μm
2	Duroid5880®	2.2	0.0009	3.175mm
3	Copper		0.004	0.8μm
4	Duroid5880®	2.2	0.0009	3.175mm
5	Copper		0.004	0.8μm

The parameters presented in Table 4.2 represent a suitable design for a mode transformer which can interface two independent 50 Ω transmission lines to the balanced feeding point of the spiral antenna. To verify that this mode transformer remains impedance match over the bandwidth of the spiral antenna for both M=1 and M=2 modes, a simulation of the entire antenna structure must be performed.

4.4 Double Feed Spiral Antenna Simulation

Previous investigations have demonstrated that two-arm spiral antennas can be operated in other radiation modes than the fundamental mode [18, 83, 84]. These investigations have resulted in narrow operational bandwidth and therefore their applications have been limited. In order to test a variety of broadband mode controllers using the customised spiral antenna shown in Figure 4.5, the orthogonal mode transformer, shown in Figure 4.4, must be able to excite both the fundamental and the second order modes of the antenna over a broad frequency range.

Based on the design parameters presented in [79], a two-arm equiangular spiral antenna and the orthogonal mode transformer shown in Figure 4.4, were designed, modelled and optimised using Ansoft's High Frequency Structure Simulator software (HFSS). The arms of the antenna were designed using the equation editor of HFSS, following the design parameters shown in [79]. The orthogonal mode transformer was designed following the parameters presented in Section 4.3.1.

Figure 4.5 shows the model created in HFSS of the customised spiral antenna. A discrete modal analysis of the model was conducted using an adaptive frequency of 14 GHz and a delta error of 0.02. The transition between the mode transformer and the antenna spiral, the impedance transition length and the cavity size were finally optimised such that the customised spiral antenna approximates the commercial spiral response shown in [79]. The following sections present the S-parameters, as well as the radiation patterns and gain response of the simulation analysis of the integrated model of the antenna and the orthogonal mode transformer (customised spiral antenna).

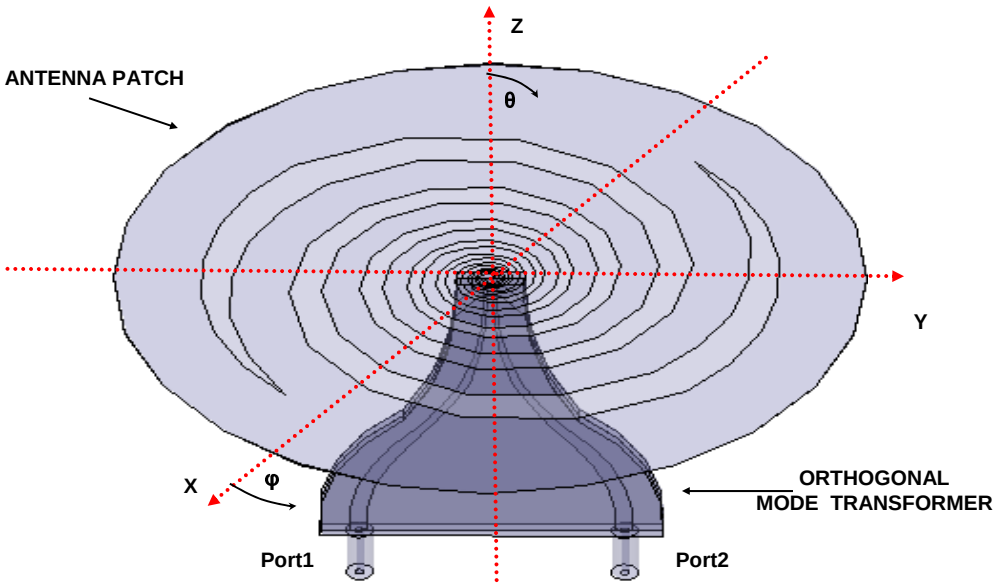

Figure 4.5: HFSS Model of the Customised Spiral Antenna

4.4.1 Spiral Antenna S-parameters Results

Some of the design parameters of the customised spiral antenna such as the characteristics of the microwave absorber, transitions and space between the multiple layers of the orthogonal mode transformer were approximated, therefore the simulation results presented in this section will be used for proof of concept.

Figure 4.6 shows the reflection coefficient of the customised spiral antenna measured at Port 1 and Port 2. It shows that most of the frequency points between 3 GHz and 18 GHz are above 10 dB and that the performance of each port is similar in the lower part of the operational frequency bandwidth of the antenna but exhibits random performance after 8 GHz.

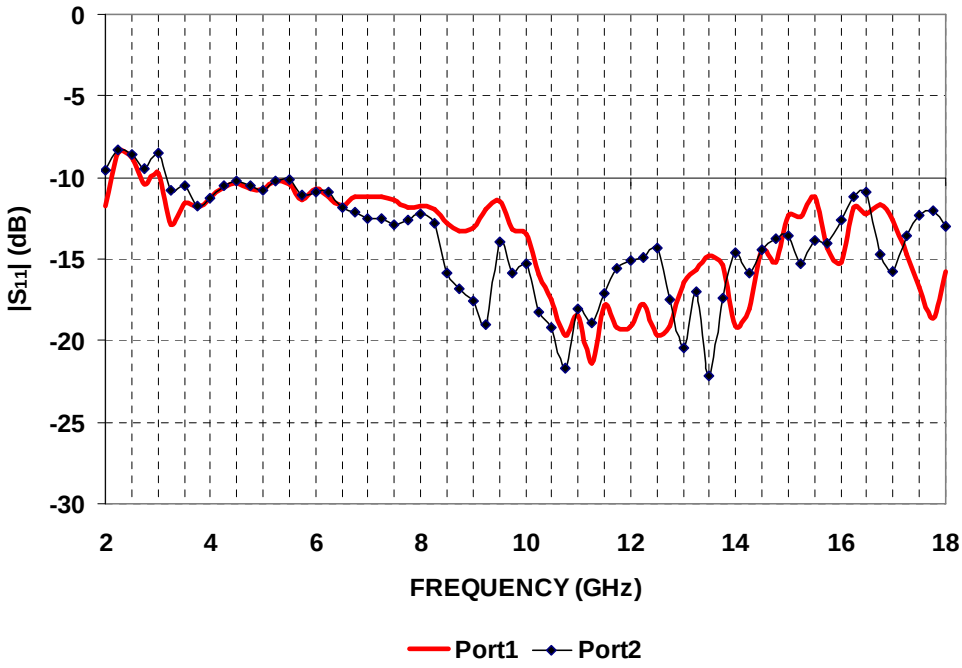

Figure 4.6: Simulated Results of Reflection Coefficient of the Antenna Measured at Port 1 and Port 2

The reflection coefficient results shown in Figure 4.6 confirm that the orthogonal mode transformer and the spiral antenna are impedance matched. Thus, signals fed to the unbalanced ports of the antenna could be transmitted up to the radiating elements (arms) of the spiral antenna with minimum impedance mismatch losses.

4.4.2 Spiral Antenna Radiation Pattern Characterisation

According to [70, 74], each stripline of the orthogonal mode transformer transition shown in Figure 4.4 can be considered as an single unbalanced generator exciting an unbalanced radiation mode of the antenna shown in Figure 4.3. The radiation response of this antenna will be determined by the way that the signals of these two unbalanced generators are combined together.

A $180\,^{\circ}$ phase difference between these unbalanced generators will excite the fundamental radiation mode of the spiral, defined by a broad lobe beam facing in the broadside direction. A $0\,^{\circ}$ phase difference will excite the second order radiation mode defined by a characteristic null in the broadside direction. It is only at these two states that the currents of such a transition will effectively be same amplitude in both conductors [70, 74]. Any amplitude difference between these unbalanced generators will disturb the current distribution of the spiral antenna causing radiation patterns characterised by tilted beams [85].

4.4.3 Preliminary Analysis of the Radiation Patterns of the Customised Spiral Antenna

The radiation patterns of a spiral antenna are not uniform across its entire operational bandwidth. As the operation frequency increases the radiation pattern start to become narrowed and uneven [83]. In order to obtain clear and defined radiation patterns for demonstration purposes, the radiation patterns of the customised cavity backed spiral antenna were investigated at its lower frequency bandwidth.

This was done by exciting the ports of the antenna with different combinations of signals of different amplitude and phase information between 3.75–5.5 GHz. Figures 4.7 and 4.8 show the three-dimensional representation of the first and second radiation modes of the simulated model.

The radiation plots presented in this section correspond to the planes of the three-dimensional radiation patterns of the antenna at $\phi = 90\,^{\circ}$ and $\phi = 0\,^{\circ}$ planes for a particular frequency.

Figure 4.9 shows a discrete number of radiation patterns at the $\phi = 90\,^{\circ}$-plane of the antenna when Port 1 is excited and Port 2 terminated to a broadband $50\,\Omega$ impedance. It shows that the beam shape changes varies from a higher gain tilted beam to a lower gain beam centered at the broadside direction of the antenna across the selected frequency range.

According to [70, 74] the radiation of each port should be defined by a single tilted beam. Although the radiation pattern analysis presented in this section shows a discrete number of frequency points, the results shown in Figure 4.9 suggest that a tilted beam is rotating around the Z axis of the customised spiral antenna. This rotating characteristic makes it complicated to map every frequency against frequency and the spiral antenna orientation. So, a single frequency point that provides enough information for the analysis of the radiation patterns of the customised antenna must be selected before continuing with this investigation.

4.4.4 Polarisation Ellipse of the Customised Spiral Antenna

Finding the polarisation ellipse of the customised antenna ease the selection of the particular frequency point at which all the radiation patterns should be recorded for comparison purposes.

The polarisation of any antenna is defined as the curve traced by the instantaneous electric field radiated by the antenna in a plane perpendicular to its Z axis [52]. This curve defines the polarisation pattern response of the antenna and can be quantified by rotating a linearly polarised antenna while measuring the field received by the antenna under test.

Figure 4.10 shows a selection of polarisation patterns that can be obtained with this technique for different polarised antennas. It also shows the polarisation ellipse corresponding to each polarisation pattern.

The customised two-arm spiral antenna in Figure 4.5 can be considered as a dipole like antenna element, folded around the Z axis of the antenna which polarisation ellipse

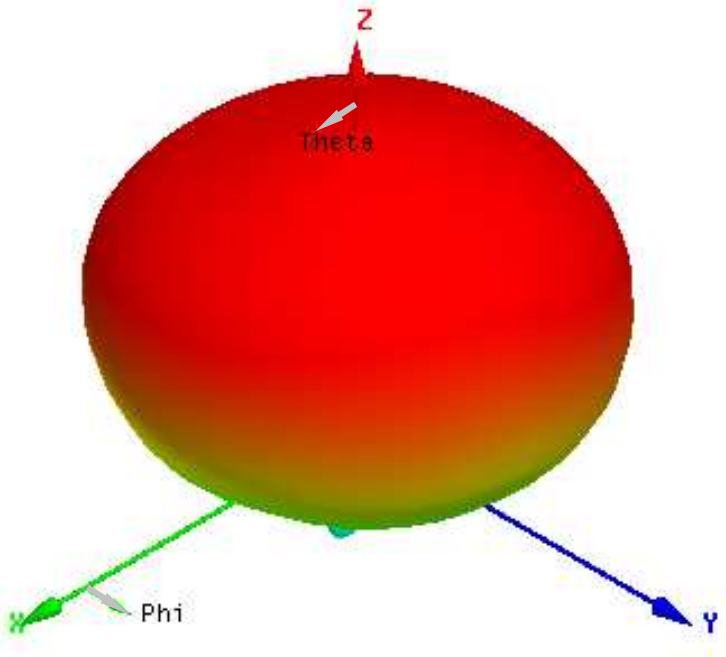

Figure 4.7: Three Dimensional Radiation Pattern of the First Order Radiation Modes

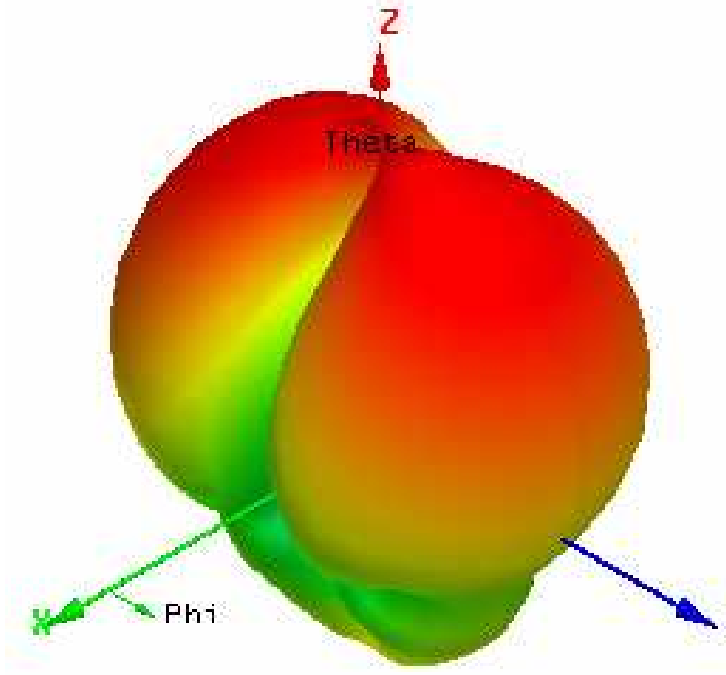

Figure 4.8: Three Dimensional Radiation Pattern of the Second Order Radiation Modes

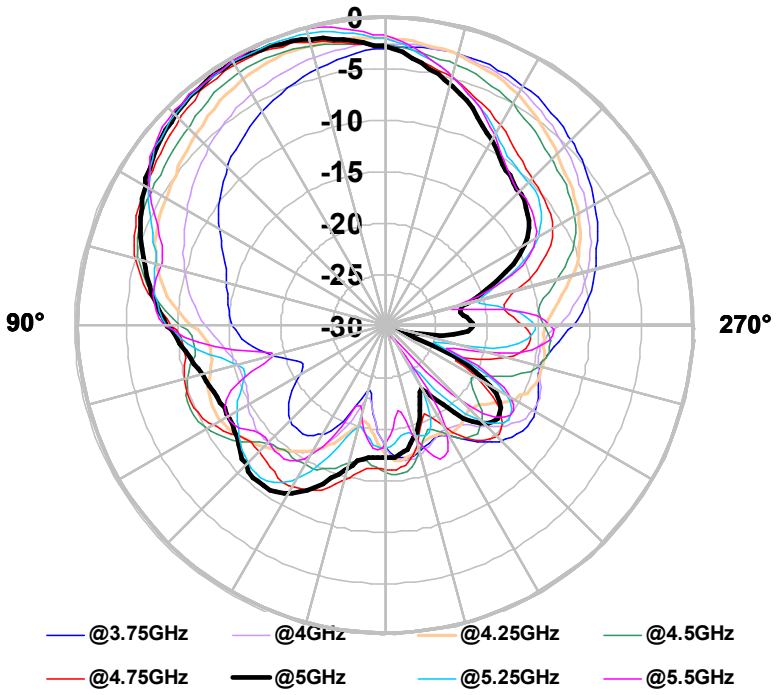

Figure 4.9: Simulated Result of the $\phi = 90\,°$-plane Radiation Pattern Response of the Antenna Measured at Port 1 versus Frequency

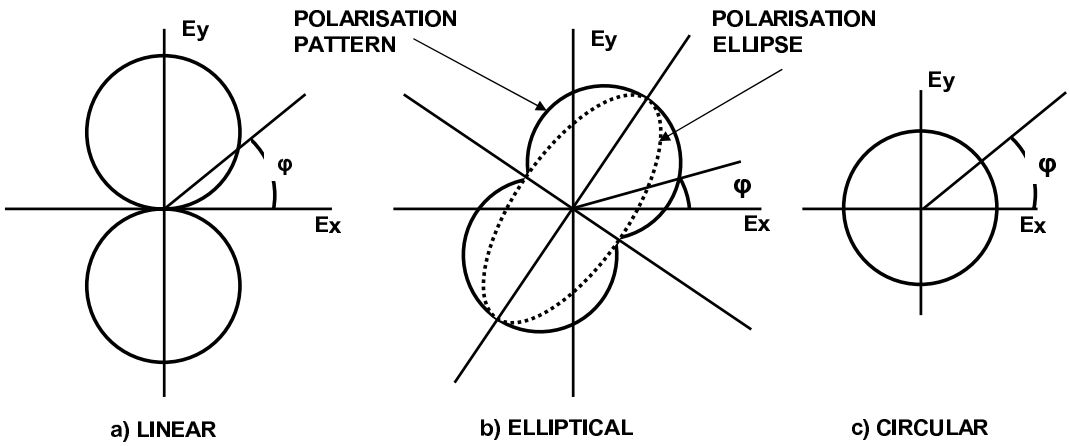

Figure 4.10: Field Components of Various Polarisation Patterns

rotates with frequency, as demonstrated in Section 4.4.3. For a dipole like antenna such as the antenna under investigation, the axes of its polarisation ellipse matches with the axial axes of the radiation beams generated by the antenna [86].

A close analysis of the results presented in Figure 4.9 shows that the radiation pattern obtained at 5 GHz represents the axial cut of a tilted beam. This axial cut corresponds to the major axis of the polarisation ellipse for the customised spiral antenna at this particular frequency.

The following sections present an analysis of the radiation pattern response of the antenna obtained at this particular frequency (5 GHz), so the following radiation response can be compared consistently through all this chapter.

4.4.5 Individual Radiation Pattern Response at 5 GHz

The plane of the antenna at $\phi = 90\,^{\circ}$, selected for the analysis of the geometry of the antenna shown in Figure 4.5, coincides with the major axis of its polarisation ellipse at (5 GHz). In order to simplify the analysis of the radiation patterns of the customised spiral antenna, the orientation of the antenna and this frequency will remain consistent through this chapter.

Figure 4.11 and Figure 4.12 show the individual $\phi = 90\,^{\circ}$ and $\phi = 0\,^{\circ}$ planes radiation patterns measured at Port 1 and Port 2 at 5 GHz . Figure 4.11 shows that each radiation pattern exhibit a single beam tilted in opposite direction to each other. These beams have a 3 dB beam-width of approximately $60\,^{\circ}$, and face at approximately $\pm\,30\,^{\circ}$ off broadside. Figure 4.12 shows two broad beams almost identical centered at broadside with a 3 dB beam-width of approximately $110\,^{\circ}$.

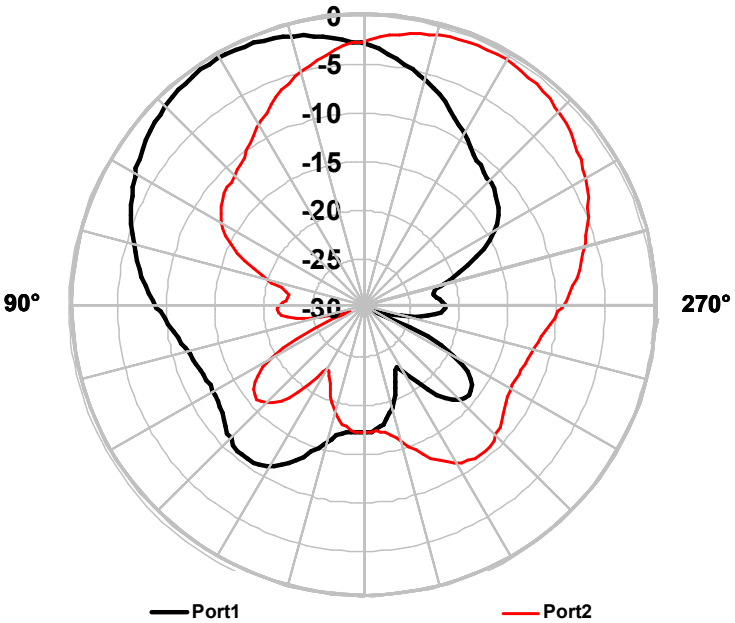

Figure 4.11: Simulated Results of the $\phi = 90\,^{\circ}$-plane Radiation Pattern Response @ 5 GHz, Measured at Port1 and Port2

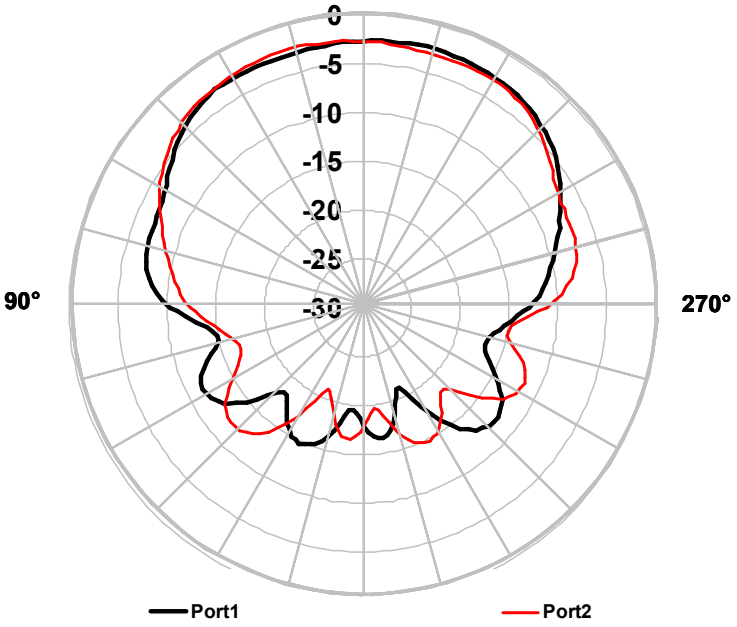

Figure 4.12: Simulated Results of the $\phi = 0^\circ$ Radiation Pattern Response @ 5 GHz, Measured at Port 1 and Port 2

The $\phi = 90^\circ$ and $\phi = 0^\circ$ planes radiation pattern response measured at each port of the antenna are clear evidence that each one of these unbalanced radiation modes are defined by a single radiation lobe tilted off broadside. These beams are oriented according to the radiating area of the antenna. For direction finding applications it is desirable that the radiation pattern of each unbalanced mode remains fixed at a certain angle. Mapping each beam of the spiral antenna against frequency and its relative orientation could be complex but still useful. This is not a component of this investigation. However, the primary focus is the possibility of combining these two unbalanced modes to create the fundamental and second order modes of the antenna, so different mode controllers can be tested.

4.4.6 Fundamental and Second Order Mode Radiation Pattern Results

The fundamental and second order modes of the spiral antenna are considered to be main modes because each port of the antenna is fed with signals with the same amplitude. The phase of these signals varies according to the radiation mode but the currents travelling through the conductors of the spiral antenna are considered to be approximately the same amplitude [87].

The ports of the HFSS model shown in Figure 4.5 were fed simultaneously with same amplitude but different phase scenarios for both the fundamental and second order modes. As explained in Section 4.4.2, a 180° phase difference between the ports of the antenna will excite the fundamental radiation mode of the spiral, defined by a broad lobe beam; this corresponds to the first scenario. A 0° phase difference, will excite the second order radiation mode, which corresponds to the second scenario.

Figure 4.13 shows the $\phi = 90\,^{\circ}$-plane radiation pattern response of the fundamental and second order radiation modes. It shows that exciting the ports of the customised spiral antenna with the same amplitude and opposite phase generates a single beam radiation pattern centered at broadside with approximately a 3 dB beam-width of $60\,^{\circ}$. Exciting these ports with signals with the same phase creates a double beam radiation pattern. Each beam faces at approximately $\pm 30\,^{\circ}$ off broadside and exhibits a 3 dB beam-width of approximately $35\,^{\circ}$.

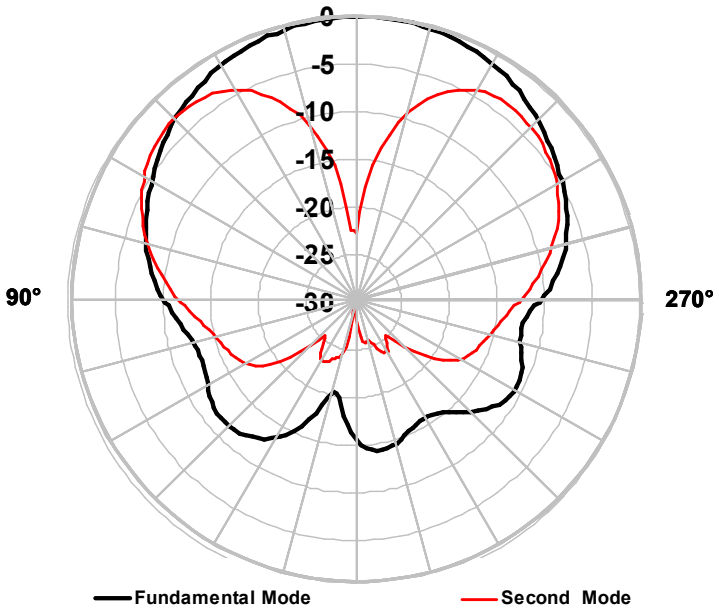

Figure 4.13: $\phi = 90\,^{\circ}$-plane Radiation Pattern Response of the Fundamental and Second Order Modes

From the results shown in Figures 4.11, 4.12 and 4.13 it is evident that the combination of the individual patterns of the antenna interferes constructively at broadside, creating a single beam for the fundamental mode and, destructively for the second order mode, creating a double beam pattern. These results match the axial cuts $\phi = 0\,^{\circ}$ and $\phi = 90\,^{\circ}$ of the three-dimensional representations of the simulated results presented in Figures 4.7 and 4.8.

This customised antenna has only been analysed as a transmitter; however, the same phase scenarios apply for the receiving mode. Thus, it is worth remembering that the signals received through the ports of this antenna will exhibit an intrinsic $180\,^{\circ}$ phase difference.

4.4.7 Simulation Analysis Summary

The radiation pattern analysis shows that the individual response of each port is frequency dependent and rotates around the Z axis of the spiral antenna. Having an antenna that exhibits a radiation pattern that rotates with frequency requires a full characterisation of each radiation pattern response for each frequency so an unfriendly signal can be located over the operational bandwidth of the spiral antennas. This represents a complex imple-

mentation and does not improve traditional systems that use a set of two spiral antenna with opposite polarisation. Nevertheless, the radiation response shown in Section 4.4.6 suggest that the customised cavity backed spiral antenna shown in Figure 4.5 is able to generate the fundamental and second order radiation modes of a customised two-arm spiral antenna.

The broadband characteristics of the chosen spiral antenna operating in its fundamental mode have been previously demonstrated in [79]. The broadband characteristics of the customised spiral antenna with the orthogonal mode transformer will be demonstrated in the following sections, realising a real model of the antenna shown in Figure 4.5.

4.5 Spiral Antenna Realisation and RF Characterisation

Simulation results presented in Section 4.4 have shown that a customised version of the two-arm spiral antenna developed in [79], could provide the broadband response and mode transformation requirements for the investigation of mode controllers in this Chapter. This antenna can now be realised and characterised. This section presents a brief description of the realisation of the customised spiral antenna and its RF analysis.

The spiral antenna and the multi-layer orthogonal mode transformer were developed using printing circuit board and copper etching techniques on a low permittivity substrate. The absorptive cavity was fabricated according to the dimensions specified on the simulated model. A gap of 10mm between the edge of the absorptive cavity and the antenna substrate was chosen to increase the unidirectional characteristics of the customised spiral antenna.

Table 4.3 shows the final parameters selected for the fabrication of the double feed cavity spiral antenna. These parameters were selected as close as possible to the design parameters used in simulation. Particular differences are presented in the selection of the microwave absorber which frequency response was approximated in the simulated model, and the spacing between the layers of the orthogonal mode transformer and its separation from the absorber which was also approximated.

Table 4.3: Double Feed Spiral Antenna Fabrication Parameters

Component	Material	Relative Permittivity (ϵ_r)	Thickness (mm)	Diameter (mm)
Antenna	Duroid5880®	2.2	0.575mm	$\phi = 90mm$
Cavity	Aluminium		100mm	$\phi_i = 90mm$ $\phi_o = 98mm$
Absorber	Eccosorb® CV-NRL	Reflectivity $-20\,dB\,@\,4\,GHz$	90mm	$\phi = 90mm$

Figure 4.14 shows the fabricated version of the modelled spiral antenna from Sec-

tion 4.4. The unbalanced transmission line impedance transformation and coupling areas of the orthogonal mode transformer are in its inner parts and are not noticeable. Thus, only a diagram of this transition is shown in Figure 4.14.

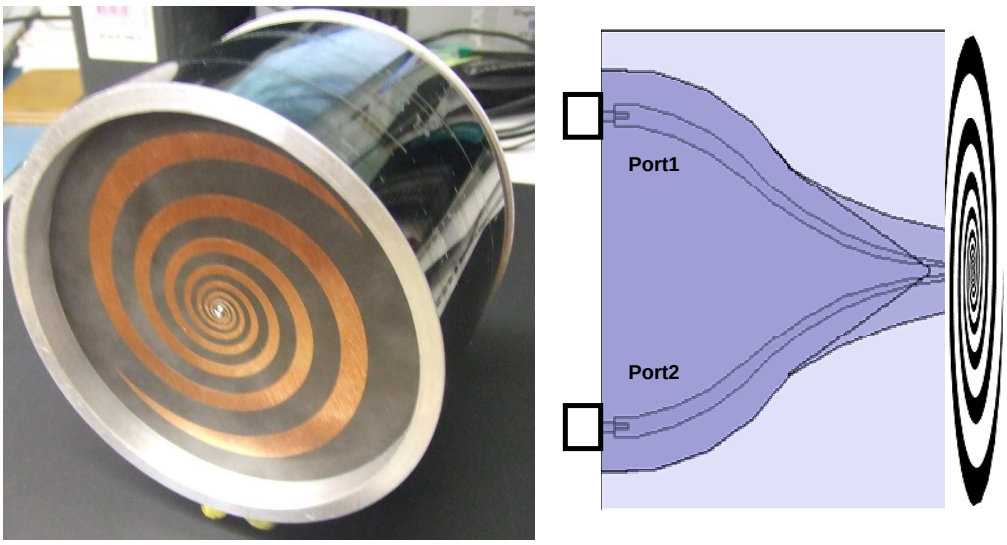

Figure 4.14: Fabricated Double Feed Two-arm Spiral Antenna

Keeping the design parameters of the multi-layer mode transformer close to the simulated model shown in Section 4.4 represented a fabrication challenge, particularly at the interconnection point of the spiral antenna and the mode transformer. Holding the two substrates of the transformer close together without including any extra material was difficult to achieve. Also, the "pins" employed to interconnect the orthogonal mode transformer with the spiral were as short as possible and needed to be carefully soldered in order to achieve a reliable interconnection. The effect of all these fabrication tolerances can be analysed conducting a full RF characterisation of the fabricated model.

4.5.1 Spiral Antenna S-Parameters Characterisation

Having completed the fabrication of the simulated model of the spiral antenna, it was necessary to characterise its RF performance in order to have a comparative response to be used for the Microwave Photonic implementation proposed later on in this Chapter. This section presents a partial scattering parameters characterisation, followed by the radiation pattern response of the fundamental and second order modes of the customised spiral antenna and the gain characterisation of the ports, measured individually and simultaneously.

Figures 4.15 shows the reflection coefficient response of the antenna measured at each one of the ports. It shows that both reflection coefficients responses exhibit similar responses below 11 GHz. The reflection coefficient measured at Port 1 remains above 10 dB approximately from 2 to 12 GHz. Measured at Port 2, this coefficient exhibits a response that is above 10 dB from 2 to 13 GHz.

Comparing Figures 4.6 and 4.15 it is evident that the impedance bandwidth expected from simulation has not been achieved. This can be attributed to the some fabrication tol-

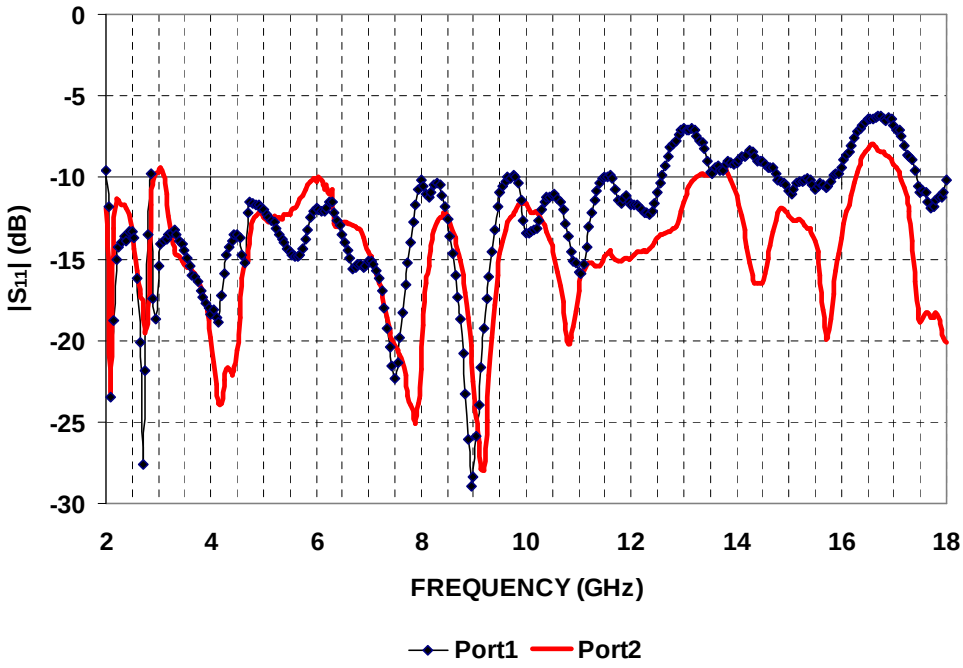

Figure 4.15: Reflection Coefficients of the Antenna Measured at Port 1 and Port 2

erances of the orthogonal mode transformer mentioned previously. Achieving the design parameters of this transformer was a complicated task, particularly at the interconnection point of the spiral and the orthogonal mode transformer. These tolerances resulted in an impedance discontinuity that affects particularly the higher frequency range of the antenna.

The reflection coefficient results demonstrated that the simulation analysis achieved a close approximation of the performance of the antenna, even though the expected impedance bandwidth was not fully achieved. Proceeding with the radiation pattern characterisation of the customised spiral antenna, should confirm if the orthogonal mode transformer enables the control of the fundamental and second order ration modes of the spiral antenna. For this purposes a basic microwave mode controller was selected.

4.5.2 Radiation Mode Controllers

Frequency independent antennas are broadband radiating elements that can radiate multiple patterns useful for direction finding but requires complex microwave mode controllers that normally limit the response of the antenna to a particular radiation mode.

In order for multiple-arm antennas to receive multiple radiation modes over a wide range of frequencies, a complex mode controller is required. These mode controllers are composed of tapered-line magic-T's, phase difference circuits, isolated power dividers and quadrature hybrid couplers [33, 88]. The performance of these controllers is normally limited by the performance of their primary components, which compromises the versatility of the system. Also, in most cases these controllers do not allow control of the main unbalanced radiation modes of the antenna also know as "normal modes" [74].

This definition of normal modes will be adopted in the following sections to differentiate the individual unbalanced modes of the antenna and the unbalanced modes obtained by unbalancing the received power at the ports of the antenna, arbitrarily.

Complex microwave mode transformers can effectively control multiple radiation modes of multi-arm frequency independent antennas. One of them is a Butler matrix mode transformer network [33], which consists of a complex network of pseudo-continuously tapered stripline couplers combining multiple normal modes of the antenna. This transformer can be prohibitive in applications such as navigation systems in military aircraft where weight, volume, instantaneous detection and high latency response are critical design specifications.

A two-arm spiral antenna mode controller does not need to be as complex as the Butler matrix in [33]. A $180\,^{\circ}$ microwave hybrid coupler is able to combine two signals phasing them with a $0\,^{\circ}$ or a $180\,^{\circ}$ phase difference which are the only combinations required to excite the fundamental and second order modes of this antenna.

4.5.3 Spiral Antenna Radiation Pattern Characterisation

The radiation pattern analysis presented in Section 4.4.3 showed that the patterns exhibited by the spiral antenna operating in any normal mode or any other higher order mode that is not the fundamental, are frequency dependent. These patterns rotate around the Z axis of the antenna. Thus, in order to compared the measured radiation response of the second order mode of the antenna, the antenna requires to be positioned along the minor and major axes of its frequency dependent polarisation ellipse, as explained in Section 4.4.4.

The minor and major axes of the polarisation ellipse of the customised antenna at 5 GHz were located by connecting the antenna to a 2–18 GHz $180\,^{\circ}$ microwave hybrid coupler as shown in Figure 4.16 as a receiver and rotating a linearly polarised double ridged pyramidal horn antenna transmitter, model 3115 by ETS-Lindgren®. The sum terminal of the hybrid coupler was connected to Port 2 of a vector network analyser in order to measure and monitor the response of the second order radiation mode of the antenna while the horn transmitter was rotating continuously.

The maximum and minimum readings that the vector network analyser records from the antenna correspond to the major and minor axes of the polarisation ellipse shown in Figure 4.10 a). Once these axes were located on the spiral antenna, the antenna was rotated to align these axes to the horizontal and vertical planes of the antenna measurement facility.

Fundamental and Second Order Modes Radiation Pattern Response

Having aligned the customised spiral antenna with the horizontal and vertical plane of the antenna measurement, characterising the radiation patterns of the fundamental and second order radiation modes should verify if the double feed orthogonal mode transformer shown in Figure 4.4 and the $180\,^{\circ}$ microwave hybrid coupler enable the customised spiral antenna to receive both radiation modes.

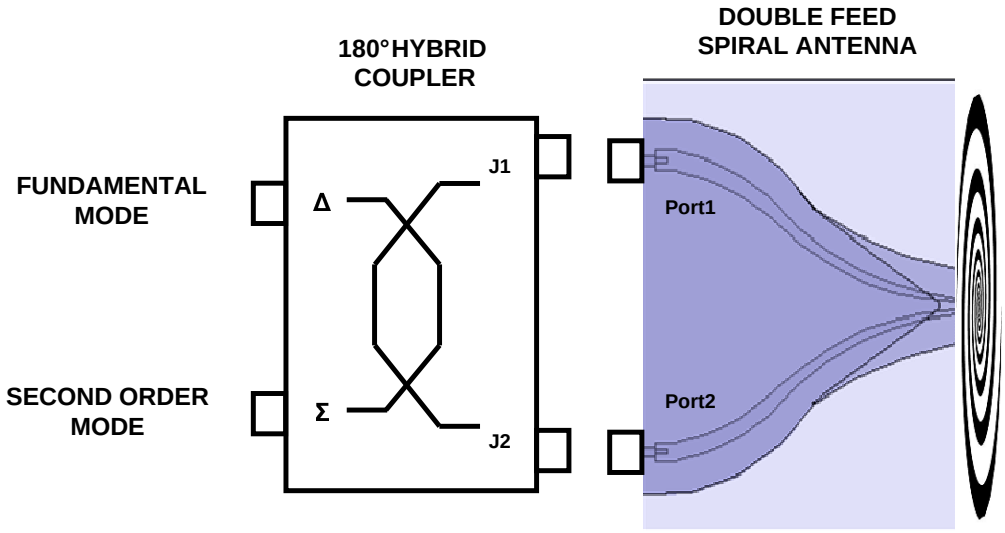

Figure 4.16: $180\,^{\circ}$ Hybrid Coupler Interconnection

The fundamental mode of the antenna was received through the differential terminal of the hybrid coupler, and the second order mode through the sum terminal. The radiation pattern response was normalised to zero considering the maximum radiation power exhibited by the antenna at broadside direction.

Figure 4.17 shows the $\phi = 90\,^{\circ}$-plane radiation pattern response of the fundamental and second order radiation modes. It shows that the fundamental mode exhibits a single beam centered at broadside with a 3 dB beam-width of approximately $65\,^{\circ}$. It also shows that the second order mode exhibits a radiation pattern defined by a null at broadside and two beams facing off broadside at approximately $\pm\,35\,^{\circ}$.

The radiation pattern response of the customised spiral antenna demonstrates that the double feed orthogonal mode transformer and the spiral antenna performs as predicted in simulation. Testing the customised spiral antenna with the $180\,^{\circ}$ microwave hybrid coupler showed how this device can control the individual radiation response of each port of the antenna and combine them with the $0\,^{\circ}$ and $180\,^{\circ}$ phase difference required to measure the fundamental and second order radiation modes of the antenna, the fundamental and second order radiation modes.

This section presented only the radiation pattern response measured at 5 GHz on the $\phi = 90\,^{\circ}$-plane for simplicity. An analysis of the gain response of the ports of the antenna operating individually and simultaneously could provide more information about the operational bandwidth where these radiation modes exhibit uniform characteristics.

4.5.4 Spiral Antenna Gain Characterisation

Having demonstrated that the double feed orthogonal mode transformer is able to reproduce the fundamental and second order radiation patterns of the spiral antenna at a specific frequency. It is important to test the performance of the customised antenna across the entire operational bandwidth. The gain analysis of the antenna should provide more information that confirms if this antenna meets the broadband requirements to test the Microwave Photonic implementation proposed later on in this chapter.

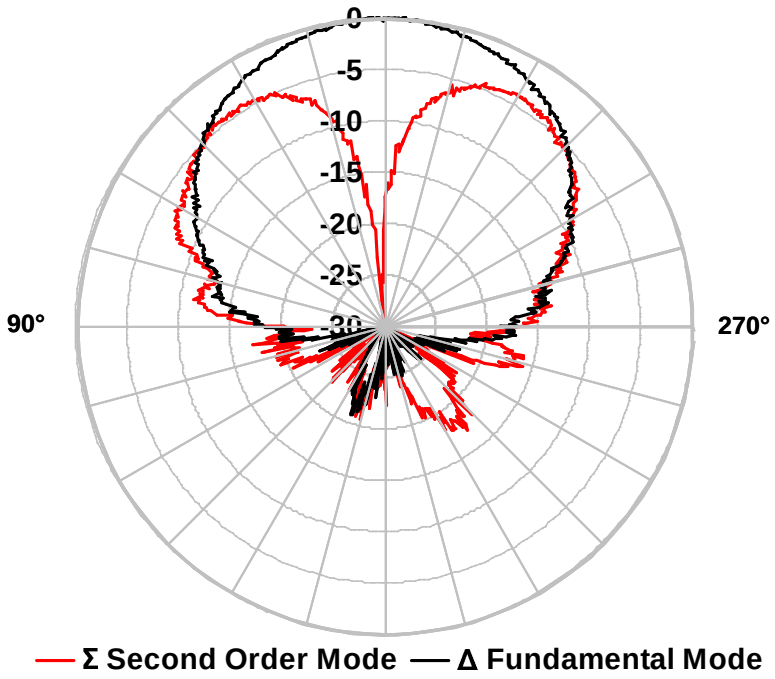

Figure 4.17: $\phi = 90\,^{\circ}$-plane RF Radiation Patterns of the Fundamental and Second Order Mode

The relative gain of antenna is defined as the ratio of the power received by the antenna under test and the power of another antenna of know characteristics in the same direction [52]. It represents another useful measure for describing the performance of the antenna because it also takes into account the efficiency of the antenna, not only the directivity, which is described by radiation patterns.

Section 4.5.3 demonstrated that the customised spiral is frequency dependent. The polarisation axis of this antenna rotates around the Z axis with frequency. Thus, in order to measure the gain response across the frequency range of the hybrid coupler (2–18 GHz) and avoid aligning the customised spiral antenna for every radiation mode at every frequency point, the linearly polarised antennas used in Section 4.5.3 were replaced by two right hand circularly polarised spiral antennas, model LS24 by RFSpinS®. A circularly polarised antenna exhibits two linearly polarised components orthogonally oriented. So, one might think that any misalignment of the polarisation ellipse with one of the components will be compensated by the orthogonal component of the circularly polarised transmitter antenna.

The antenna measurement method used to characterise the gain performance of the spiral antenna is the gain transfer method explained in Section 2.2.1. One of commercial spiral antennas was employed as a transmitter, while the other was used as the reference antenna of known radiation characteristics. The following sections present the relative gain characterisation of each one of the radiation modes of the customised spiral antenna.

Fundamental and Second Order Modes Gain Characterisation

Having demonstrated that the impedance bandwidth response of the ports of the antenna does not perfectly match the simulated impedance bandwidth shown in Section 4.5.1, it is important to investigate if the realised antenna exhibits broadband gain bandwidth while operating in the fundamental and second order radiation modes.

The fundamental and second order radiation modes of the antenna were measured connecting simultaneously the input terminals of the 180° microwave hybrid coupler to the ports of the antenna, as shown in Figure 4.16. The differential and sum terminals of the hybrid coupler were connected to Port 2 of the VNA at a time as shown in Section 4.5.3. $50\,\Omega$ broadband loads were employed to terminate any inactive terminal.

Figure 4.18 shows the gain response of the customised spiral antenna measured through the differential and sum terminals of the microwave hybrid coupler. It shows that the fundamental mode gain response at broadside direction is above the commercial spiral gain response from 2 to 12 GHz. It shows that the relative gain of the fundamental radiation mode it is approximately 6 dB above the relative gain of the commercial spiral around 2 GHz. Then, it decreases until it approximately matches the gain performance of the commercial spiral antenna at higher frequencies.

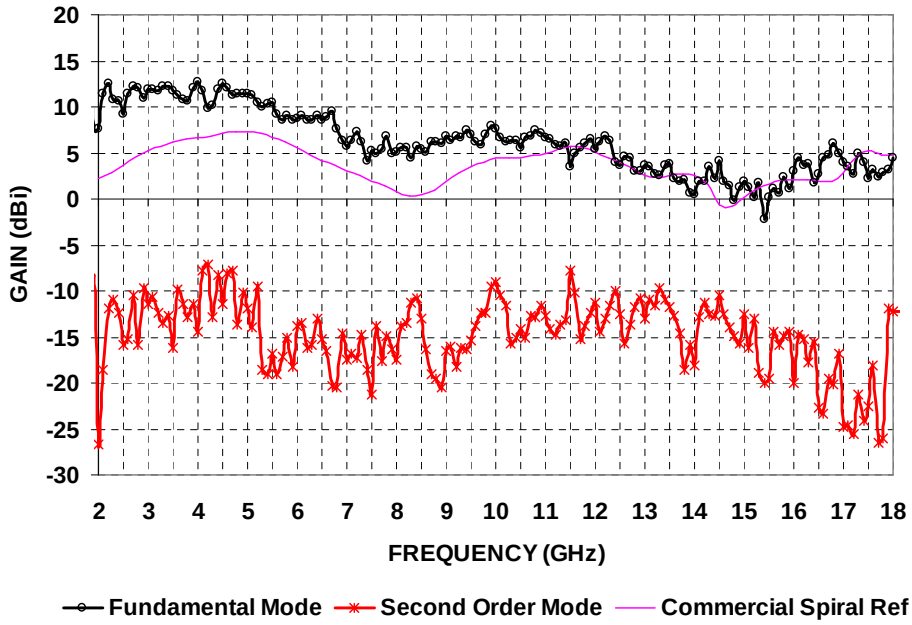

Figure 4.18: Gain Performance of the Fundamental and Second Order Modes

This considerable gain difference between the customised spiral antenna and the commercial spiral antenna can be attributed to the orthogonal transformer shown in Figure 4.4 and some design specification differences between both models. The commercial spiral was optimised to perform from 2–24 GHz and uses a balun to transmit the balanced mode of the antenna into the system. The orthogonal mode transformer can be considered to be receiving this power twice, particularly at the low frequency range. The impedance bandwidth of the customised spiral antenna in Figure 4.15 shows that the performance of the orthogonal mode transformer is only better for the lower frequency range (2–10 GHz).

Figure 4.18 also shows that the gain response of the second order radiation mode, which corresponds to location of the null in the radiation pattern shown in Figure 4.17 exhibits an amplitude variation of approximately 5 dB across the entire bandwidth. This variation shows an erratic performance and it is defined by the level of interference at the broadside direction of the two normal radiation modes of the antenna shown in Figure 4.11 and Figure 4.12.

The difference between the fundamental and the second order modes at broadside direction (Figure 4.18), varies from approximately 20 dB to 10 dB. According to the radiation patterns shown in Figure 4.17, this difference should be higher than this, at least at 5 GHz. Using a circularly polarised antenna as a transmitter instead of a linearly polarised horn antenna to measure the gain response of the antenna represents that the customised spiral antenna is receiving two orthogonal linearly polarised waves instead only one. This definitely has modified the accuracy of the characterisation process, particularly for the second order mode. Thus, differences between the nulls measurements were tolerated.

The gain response of the fundamental mode of the customised spiral antenna has resulted to be higher than the commercial spiral antenna at its lower frequency bandwidth. This demonstrates that the realised orthogonal mode transformer not only reproduces the balanced to unbalanced mode transformation function of the original balun shown in Figure 4.3 but also improves the overall performance of the spiral antenna. The gain performance of the customised antenna over the frequency bandwidth, 2–18 GHz suggests that this antenna can be used to fulfil the primary requirement for this investigation; a broadband antenna response with multi-mode characteristics.

Normal Modes Gain Characterisation

The individual response of the ports of the antenna which corresponds to the normal radiation modes of the antenna were also measured individually considering the insertion loss of the $180\,^{\circ}$ hybrid coupler. In order to provide more information about how the two normal modes contributes towards the formation of the fundamental and second order modes after the $180\,^{\circ}$ hybrid coupler, the following measurements were conducted.

The input terminals (J1 and J2) of the $180\,^{\circ}$ hybrid coupler shown in Figure 4.16 were disconnected of the ports of the antenna one at a time so the response of the port could be measured individually. The differential terminal of the hybrid coupler was connected to Port 2 of the VNA and $50\,\Omega$ broadband loads were employed to terminated the inactive terminals and ports.

Figure 4.19 shows the individual gain response of each port across the frequency bandwidth (2–18 GHz) at broadside direction. It shows that both gain responses follow approximately similar trends starting with an average gain of 5dB, which decreases as the frequency increases. The similarity between these trends matches the response of the impedance bandwidth shown in Figure 4.15, showing smaller differences below 12 GHz, and higher differences above this frequency.

According to Section 4.4.6, the normal mode radiation patterns of the customised antennas can be controlled to form the fundamental and second order radiation mode of the spiral antenna. The individual gain responses presented in this section, provide extra

evidence that confirms this. However in order to prove it, it was necessary to disconnected the ports of the antenna from the 180° hybrid coupler, which in real circumstances is practically impossible.

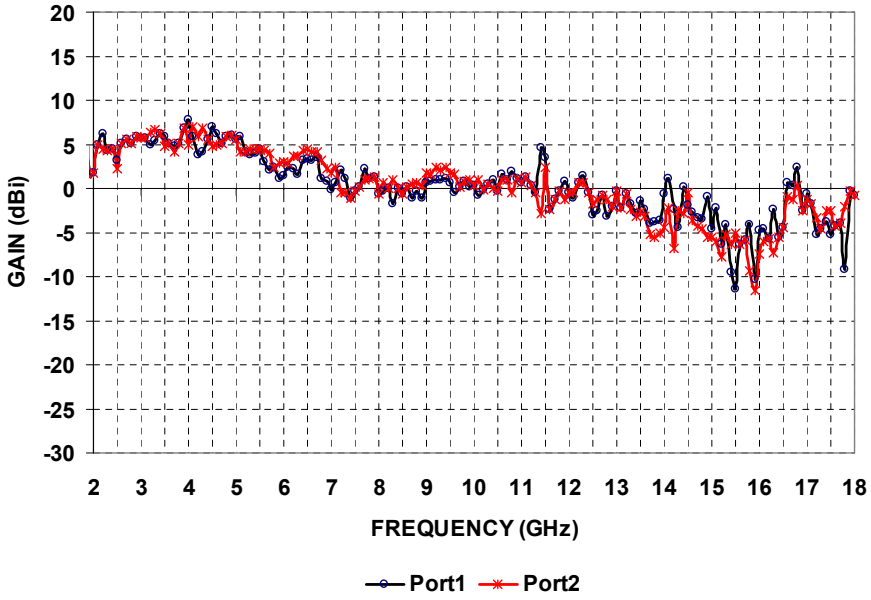

Figure 4.19: Gain Performance of the Port 1 and Port 2 of the Spiral Antenna

4.5.5 Spiral Antenna Characterisation Summary

In summary, this section has demonstrated that the performance of the customised spiral antenna is close to the predicted results shown in Section 4.4. It has also demonstrated that the realised orthogonal mode transformer designed to substitute the original balanced to unbalanced mode transformer of the antenna, could potentially enable controlling the normal radiation modes of the customised spiral antenna to form its fundamental and second order radiation modes.

Employing a traditional 180° microwave hybrid coupler to control the fundamental and second order radiation modes of the spiral antenna highlighted the inherent restriction of the hybrid and similar interfaces. These interfaces do not enable to control the individual normal radiation modes of the antenna. In order to measure these modes, these interfaces must be disconnected from the antenna.

The final impedance bandwidth of the antenna is 2–12 GHz. Although this bandwidth differs from the simulated results for the frequency range above 12 GHz, it was demonstrated that the gain bandwidth of the antenna extends beyond 12 GHz. This is considered an advantage since the operational bandwidth of commercial Microwave Photonic devices currently extends beyond 20 GHz such as 40 GHz electro-optic modulators [89]. Thus, using this antenna as a proof of concept for the Microwave Photonic implementation proposed in following sections will demonstrate how this Microwave Photonic implementation can exceed and improve the performance of traditional microwave mode controllers such as the 180° hybrid coupler employed in this section.

4.6 Microwave Photonic Controls for Antenna Systems

Chapter 3 has demonstrated that, by using Wavelength Division Multiplexing (WDM) and filtering techniques it is possible to combine a number (N) of antenna elements into a single optical fibre system. The basic form of Microwave Photonic multiplexing have been described in Section 2.4 using a polarisation beam splitter and polarisation diversity techniques. This simple Microwave Photonic multiplexing technique demonstrated that two orthogonal modulated optical carriers with the same wavelength can be combined together into a single optical fibre without coherent interference [22, 45] and acceptable signal stability over time. In this section it will be demonstrated that these photonic combination techniques can also be used to control the normal radiation modes of the double feed two-arm spiral antenna presented in Section 4.5, replacing traditional $180\,^{\circ}$ microwave hybrid couplers. It will also demonstrated that an arbitrary number of combination of these normal radiation modes can be achieved, using optical carrier weighting techniques.

4.6.1 Microwave Photonic Phasing Control

Section 4.4.5 has shown that the arms of a two-arm spiral antenna can be controlled as two independent generators and exhibit two characteristic normal radiation modes. Provided that each port of the antenna can be photonically remoted onto individual optical carriers, it should be possible to use Microwave Photonics to superimpose these normal radiation modes to generate the fundamental and second order radiation modes of the spiral antenna. Radiation into the fundamental or second order modes is determined by phasing the signal at the ports of the spiral antenna with a relative phase difference of $180\,^{\circ}$ or $0\,^{\circ}$, respectively.

Microwave Photonic Configuration

Since only two electro-optic modulators are required to photonically remote the two ports of the spiral antenna presented in Section 4.5, a Microwave Photonic Mode Controller (MPMC) to phase these two ports with a relative phase difference of $0\,^{\circ}$ or $180\,^{\circ}$ can be implemented using the photonic multiplexing technique demonstrated in Section 2.4. This multiplexing technique is based on the polarisation diversity concept [22] and combines two identical optical carriers into a single optical fibre without coherent interference.

Figure 4.20 depicts the configuration for the Microwave Photonic mode controller proposed to control the fundamental and second order radiation modes of a double feed two-arm spiral antenna. It shows a single optical source connected to a 3 dB Polarisation Beam Splitter (PBS1) using a polarisation controller in order to split the optical source in two optical channels (TE and TM) with the same polarisation orientation. Each channel is connected to a Mach-Zehnder Modulator (MZM) through a Polarisation Maintaining (PM) fibre. The MZM modulates the optical source using the electrical signal received by the antenna, which is connected to the MZM modulator through a microwave phase shifter in order to compensate any phase difference existing between the two microwave-photonic links. Once modulated, these carriers propagate to a second polarisation beam

splitter (PBS2), where they are combined into a single optical fibre. This combination is incoherent due to the orthogonal polarisation of the optical carriers (see Section 2.3.3). One of these signals will be rotated by $90\,^{\circ}$ due the polarisation rotation characteristics of the polarisation beam splitter, allowing these two signals to travel orthogonally polarised to the processing unit where an Erbium-Doped Fibre Amplifier (EDFA) increases the optical gain of the system before the modulated signals are converted by a Photo Detector (PD) back into the electrical domain. The electro-optic Mach-Zehnder Modulators, were sourced from Micreo Limited, Australia, model number 592-BPH02. The photo detector was manufactured by U^{2}T$^{\textcircled{R}}$, model XPDV2120R.

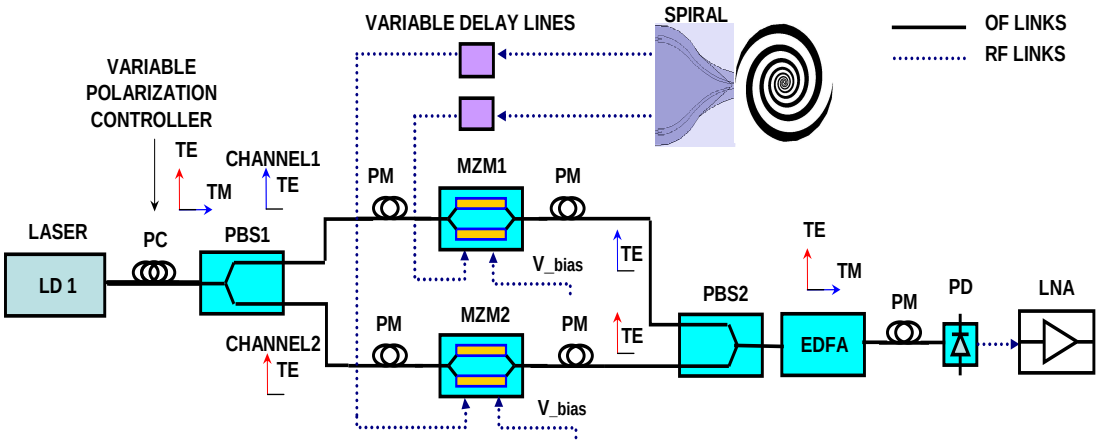

Figure 4.20: Microwave Photonic Configuration for Controlling Antenna Radiation Modes

The phase of the combined signals was controlled using the counter phase modulation characteristic of Mach-Zehnder modulators [90, 91]. To achieve a relative phase difference of $0\,^{\circ}$ between the modulated signals, the modulators are biased at the same quadrature points. To achieve $180\,^{\circ}$ phase difference between the modulated signals, the modulators are biased at opposite quadrature. It is important to notice at this point that the signals received at the ports of the customised antennas exhibit are already a $180\,^{\circ}$ phase difference relative to each other. This fact needs to be considered to avoid confusion between the phase shift generated by the changing of the bias of the modulators, and the phase difference between the ports of the antennas required to generate the fundamental and second order radiation modes.

Path Length Equalisation of the Photonic Links

It is necessary to equalise the path length of both Microwave Photonic links (MZM1 and MZM2) in Figure 4.20 in order to ensure that the signals from each port of the customised spiral antenna receives the same link gain and phase delay, so the combined response of both ports provides either the fundamental or the second order radiation modes.

Path equalisation was achieved by measuring and comparing the forward transmission response of each Microwave Photonic link using a vector network analyser. The link gain difference between the links was made approximately zero by rotating the position of

the polarisation controller so each link received half of the optical power available. The fibres of each link were cleaved to approximately the same length and fine adjustment was achieved using variable microwave phase shifters, so that the relative phase difference between the links was $0\,^\circ$ when the modulators are biased at the same quadrature points.

4.6.2 Microwave Photonic Phasing Control Characterisation

Having equalised the path length and gain of the photonic links it was possible to characterise the complete Microwave Photonic mode controller shown in Figure 4.20. This section aims to confirm the relative phase difference between two RF signals can be changed from $0\,^\circ$ to $180\,^\circ$, by simply changing the bias of the modulators.

The system characterisation was done by measuring the forward transmission response of each Microwave Photonic link in Figure 4.20 using the same vector network analyser. Each link was characterised connecting Port 1 of the VNA, first to the RF input of MZM1 and then to the RF input of MZM2. Port 2 of the VNA was connected to the Photo Detector (PD).

The relative phase and gain difference between the two links shown in Figure 4.20 (MZM1 and MZM2) were measured. First for a relative phase difference of $0\,^\circ$ the quadrature bias voltage of the MZM1 and MZM2 were set to be V_q and V_q, respectively. Then for a relative phase difference of $180\,^\circ$ bias voltage of MZM1 and MZM2 were set to V_q and $V_{q+\pi}$, respectively.

Figure 4.21 presents the gain response of the links for both $0\,^\circ$ and $180\,^\circ$ relative phase difference settings. It is evident that the gain of the two links is fairly similar from 2–8 GHz but exhibits a considerable variation above this range.

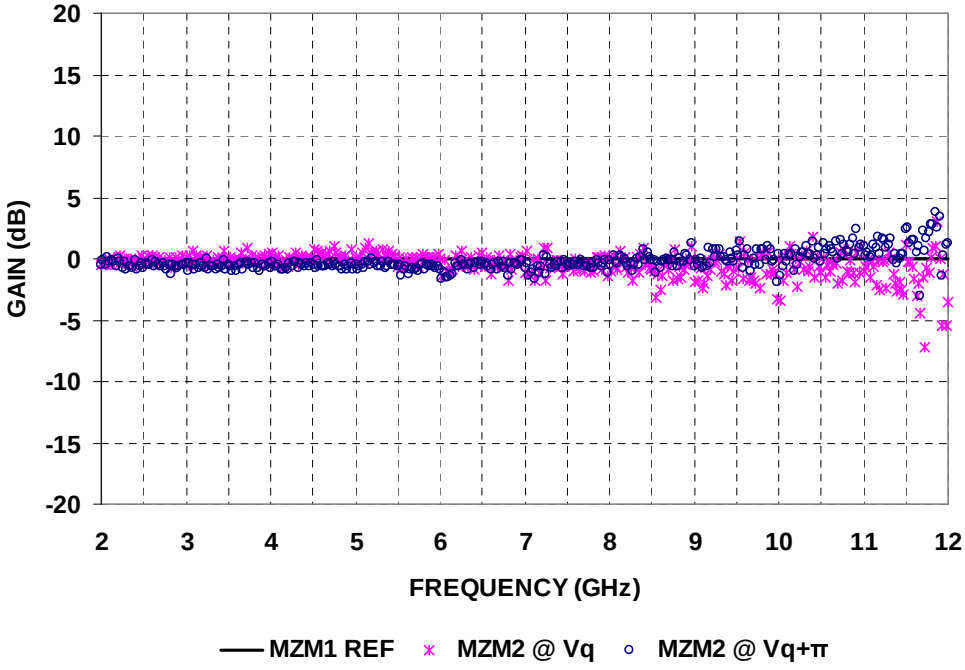

Figure 4.21: Relative Gain Difference of the Links of the MPMC

Figure 4.22 presents the relative phase of the two links with nominal $0\,^\circ$ and $180\,^\circ$ relative phase difference settings. It is clear that relative phase differences close to $0\,^\circ$ and $180\,^\circ$ are achieved.

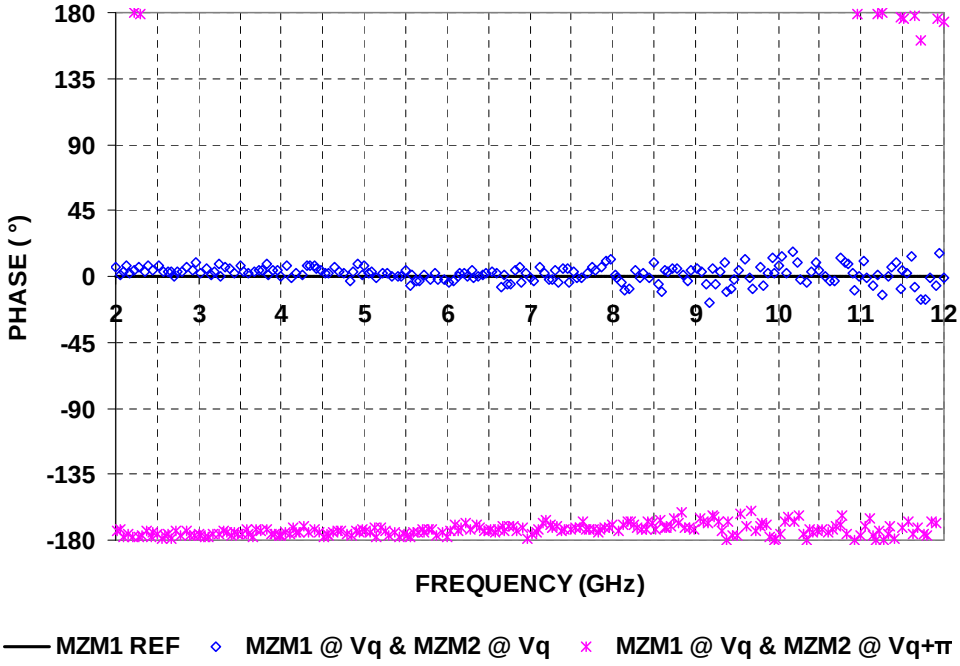

Figure 4.22: Relative Phase Difference of the Links of the MPMC

The results shown in Figure 4.21 and Figure 4.22 demonstrate that the polarisation orientation and bias voltage controls of the Microwave Photonic configuration shown in Figure 4.20 enables the system to phase two microwave signals with a relative phase difference of $0\,^\circ$ or $180\,^\circ$ over a broad frequency range using a single optical carrier.

Having achieved appropriate phase control over a broad bandwidth range, this implementation should be able to generate the radiation response of the fundamental and second order radiation mode of the spiral antenna, substituting the $180\,^\circ$ microwave hybrid coupler used in Section 4.5.

4.7 Spiral Antenna Characterisation - Microwave Photonic Mode Controller

Having demonstrated in Section 4.6 that it is possible to create a Microwave Photonic phase controller using photonic multiplexing techniques and use it as a phasing control for two microwave signals, it is now possible to connect the double feed two-arm spiral antenna presented in Section 4.5 and measure the fundamental and second order modes, as well as an arbitrary number of combination of the normal radiation modes in which the realised spiral antenna can operate.

The radiation pattern characterisation is divided as follows: Section 4.7.1 explains the characterisation procedure adopted in this investigation; Section 4.7.2 presents the indi-

vidual radiation patterns received through Port 1 or Port 2 of the antenna; Section 4.7.3 then presents the radiation patterns received when equal amplitude excitations are received through Port 1 and Port 2, with either $0\,^\circ$ or $180\,^\circ$ phase shift between them; and finally, Section 4.7.4 presents the radiation patterns that can be achieved when unequal amplitude signals are received through Port 1 and Port 2.

4.7.1 Characterisation Procedure

The Microwave Photonic mode controller presented in Section 4.6.1 and the spiral antenna shown in Figure 4.14 were characterised using the same antenna measurement methods used in Section 2.2.1. However, this time the vector network analyser used for the RF characterisation was located closer to the transmitting antenna as shown in Figure 4.23. This adjustment was made in order to increase the power transmitted by the antenna and avoid the transmission losses of long coaxial cables. The platform that hold the antenna rotates around the horizontal plane of the antenna measurement system every $0.5\,^\circ$ around θ.

The first step was to characterise the transmission link by measuring the received power using a standard antenna of known characteristics. This standard antenna was a right hand circularly polarised spiral antenna, model LS24 by RFSpin®. It is worth noting that this standard antenna has an RF balun built into it and thus it has only a single RF connector which excites the fundamental radiation mode.

This standard antenna was connected to the photonic mode controller of Section 4.6.1. The single RF output of the standard antenna was attached to the input of MZM1 and the antenna, modulators and polarisation beam splitters were mounted on the platform inside the anechoic chamber.

Having recorded the gain response of the standard antenna to be used as a reference, the known standard antenna was then replaced by the double feed two-arm spiral antenna of Section 4.5. The dual outputs of this antenna were connected to MZM1 and MZM2 of the Microwave Photonic mode controller from Section 4.6.1.

As demonstrated in Section 4.4.3 the radiation patterns of the normal modes of the spiral antenna rotate around the Z axis of the antenna. These patterns exhibit linear polarisation characteristics. Thus, in order to compare the results obtained in previous section using the $180\,^\circ$ microwave hybrid coupler with the radiation pattern response of the antenna using the Microwave Photonic mode controller, the spiral antenna must be oriented such that the major and minor axes of the polarisation ellipse are aligned to the horizontal and vertical axes of the antenna measurement system as demonstrated in Section 4.5.3. It is worth noting that the following results have been normalised to the power received by the realised spiral antenna, when both ports are simultaneously measured, enabling both optical channels of the Microwave Photonic mode controller. That is, the polarisation controller adjusted at $\alpha = 45\,^\circ$, as was done for the characterisation of the transmission link with the known standard antenna.

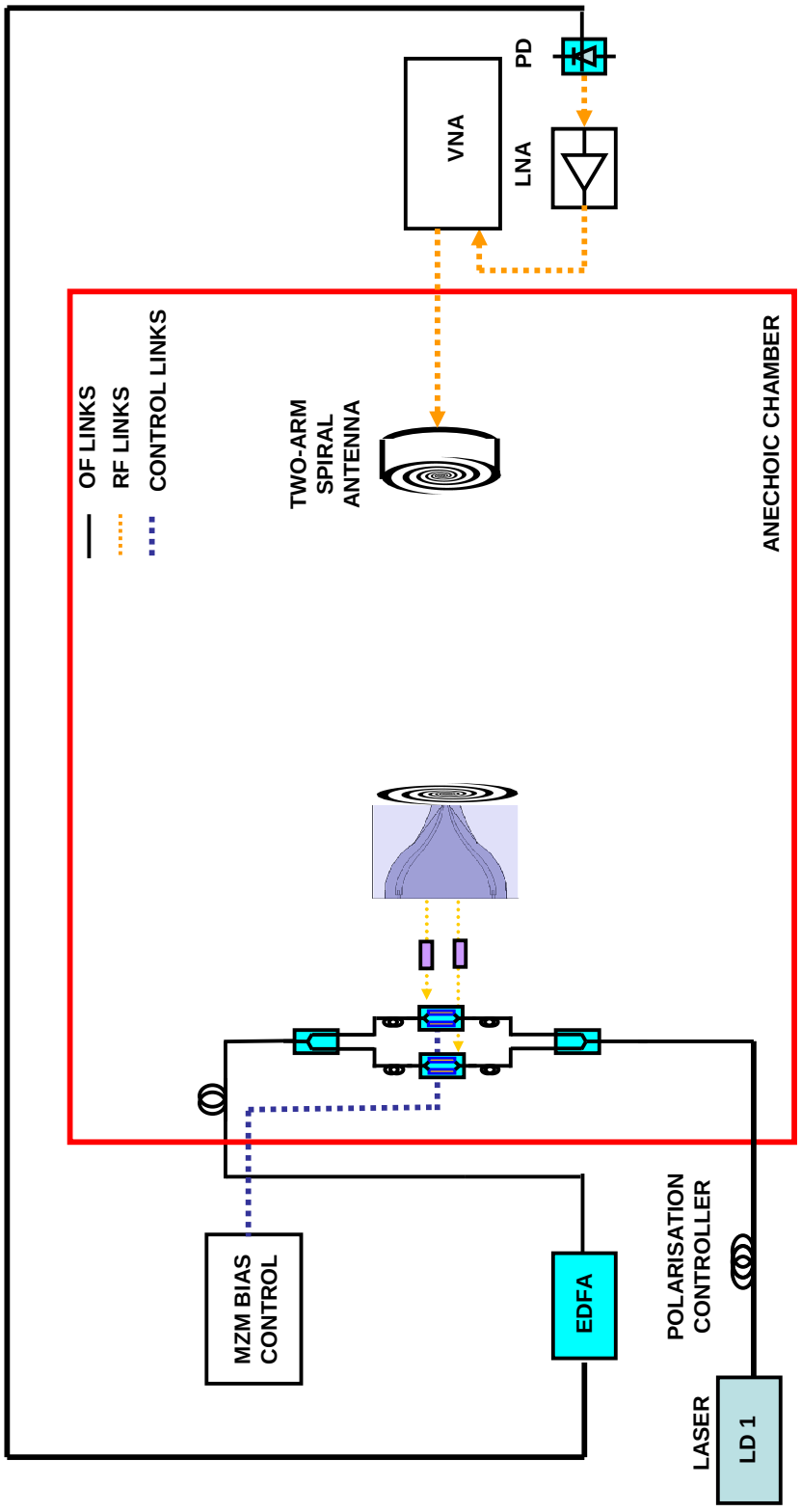

Figure 4.23: Microwave Photonic Mode Controller Test Setup Two-Arm Spiral Antenna

4.7.2 Normal Modes Radiation Pattern Response

According to Section 4.4.5 two normal radiation modes can be received at the ports of the spiral antenna shown in Figure 4.14. This section investigates how effectively these two radiation modes can be measured by the Microwave Photonic mode controller described in Section 4.6.1.

The radiation response of the antenna was measured through each Port 1 and Port 2, adjusting the polarisation controller of Figure 4.20 at $\alpha = 0\,^\circ$ and $\alpha = 90\,^\circ$ respectively, so the full power of the optical carrier could be directed first to MZM1 and then to MZM2.

Figure 4.24 and Figure 4.25 shows the $\phi = 90\,^\circ$ and $\phi = 0\,^\circ$ planes radiation pattern response measure through Port 1 and Port 2, respectively. It is worth noting that directing the full power of the optical carrier into one modulator at a time, will increase the optical power by 3 dB in each link. As a consequence, the overall link gain for each RF signal received through the ports of the antenna will be increased by 6 dB compared to the gain received when the polarisation controller is adjusted at $\alpha = 45\,^\circ$ and the optical power is divided in two. The maximum power reading at broadside direction of normal mode radiation patterns has been normalised to -6 dB in order to simplify the comparison of these results with the following sections. However, it must be remembered that these patterns are actually 6 dB higher than what it is shown in this section using the Microwave Photonic configuration shown in Figure 4.20.

Figure 4.24 shows the $\phi = 90\,^\circ$-plane radiation pattern response of the antenna measured through each port at 5 GHz. The radiation patterns shows two single beams tilted by approximately $\pm\ 20\,^\circ$. These beams exhibited a 3 dB beam-width of $50\,^\circ$, and $45\,^\circ$, respectively.

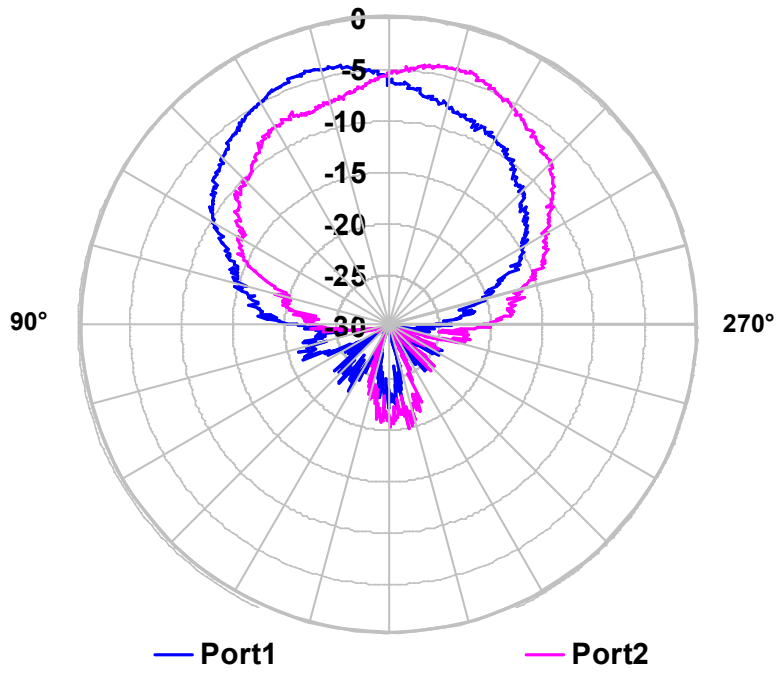

Figure 4.24: $\phi = 90\,^\circ$-plane Radiation Pattern Measured Through Port 1 and Port 2

Figure 4.25 shows the radiation pattern response of each port of the antenna measured in the $\phi = 0\,^{\circ}$-plane at 5 GHz. It shows two single beams slightly tilted by approximately $\pm 5\,^{\circ}$. It shows that Port 1 and Port 2 exhibited a 3 dB beam-width of $45\,^{\circ}$, and $40\,^{\circ}$, respectively.

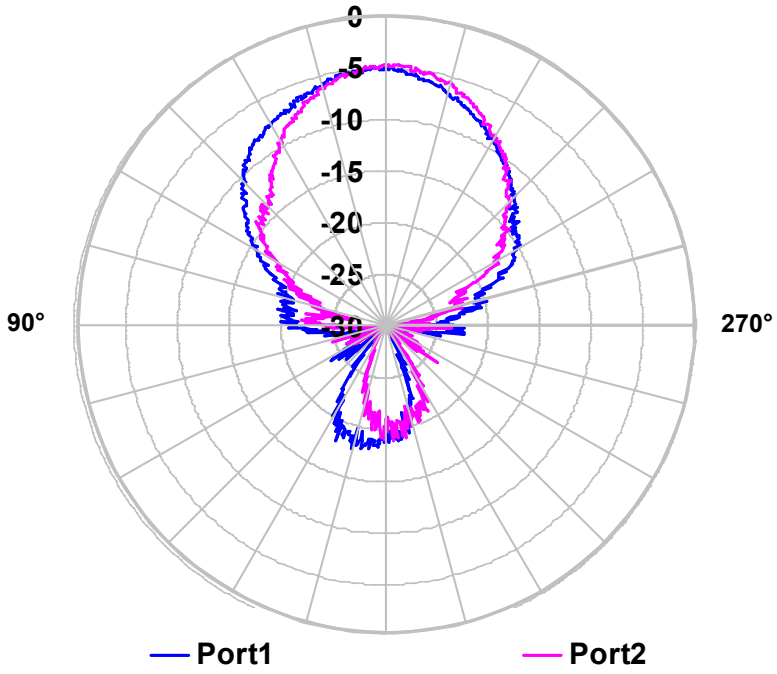

Figure 4.25: $\phi = 0\,^{\circ}$-plane Radiation Pattern Response Measured at Port 1 and Port 2

Comparing the results presented in Figure 4.24 and 4.25 with those shown in Figure 4.11 and 4.12, it is clear that these results are in excellent agreement with the simulated results, except that they have been modified by -6 dB. Nevertheless, the similarity of these results confirms that the Microwave Photonic implementation can receive the two orthogonal modes of the customised spiral antenna that generates its fundamental and second order radiation modes.

The characterisation procedures shown in Section 4.5.4 showed that in order to characterise the normal modes of the spiral antenna, it was necessary to disconnect it from the $180\,^{\circ}$ hybrid coupler. This section has demonstrated that the Microwave Photonic mode controller is able to receive the radiation pattern response of each port of the spiral antenna individually without having to disconnect the spiral antenna.

4.7.3 Fundamental and Second Order Modes Radiation Pattern Response

As discussed in Section 4.4.5, the fundamental and second order radiation modes of a double feed two-arm spiral antenna can be generated by combining the radiation response of the normal mode with a relative phase difference of $180\,^{\circ}$ and $0\,^{\circ}$, respectively. Since these relative phase differences can be achieved using the Microwave Photonic mode

controller as described in Section 4.6.2, it should be possible to control the spiral antenna to receive its fundamental and second order radiation modes.

The measurement of the fundamental and second order radiation modes was done by adjusting the polarisation controller in Figure 4.20 such that $\alpha = 45\,^{\circ}$, so each link received half of the available optical power, making the link gain of both links almost identical. The phase difference between the signals received from Port 1 and Port 2 was initially adjusted to be $0\,^{\circ}$ by biasing both modulators (MZM1 and MZM2) at the same quadrature points (V_q), and then to be $180\,^{\circ}$, by biasing MZM2 at opposite quadrature (($V_{q+\pi}$). It is worth remembering that the RF characterisation of the antenna demonstrated that the phase difference between the signals received from the antenna through its ports is already $180\,^{\circ}$ out of phase (Section 4.4.6). Therefore, biasing the modulator at opposite quadrature should generate the fundamental radiation mode of the antenna, and biasing them at the same quadrature point should provide the radiation response of the second order radiation mode of the spiral.

Figure 4.26 presents the $\phi = 90\,^{\circ}$-plane radiation response of the spiral antenna, when the bias voltage among the modulator is adjusted at with the same quadrature bias points and opposite quadrature bias points.

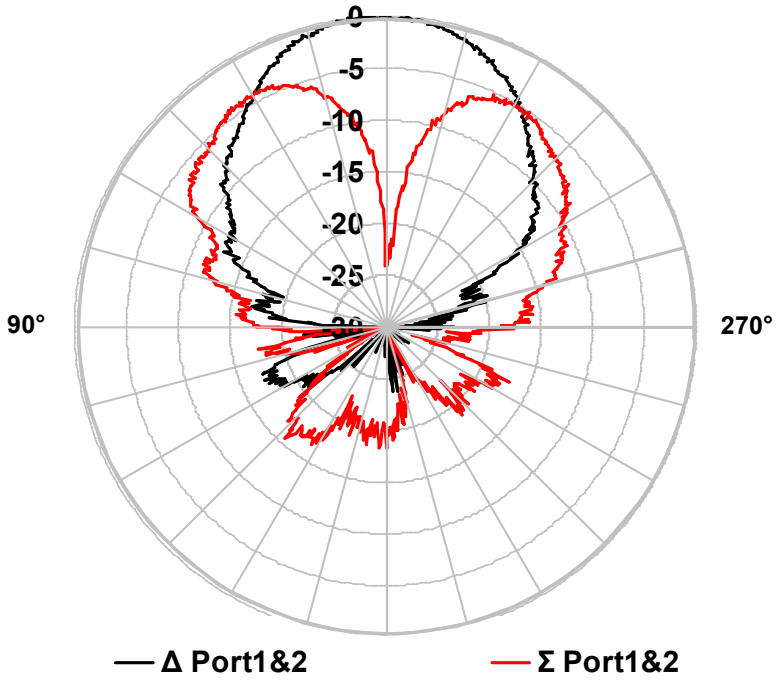

Figure 4.26: $\phi = 90\,^{\circ}$-plane Radiation Pattern Response of the Fundamental and Second Order Modes

Figure 4.26 shows the fundamental and the second order modes response of the spiral antenna measured in the $\phi = 90\,^{\circ}$-plane. It shows that biasing the modulator at opposite quadrature generates a single beam centered at broadside with a 3 dB beam-width of approximately $55\,^{\circ}$ (Δ), corresponding to the fundamental mode. It also shows that biasing the modulators at the same quadrature point generates a radiation pattern corresponding to the second order mode(Σ), defined by a null at broadside and two beams facing around $30\,^{\circ}$ off broadside.

The results confirm the initial $180\,^\circ$ phase difference exhibited between the signal from measured through each port of the antenna. The results are similar to the radiation pattern characterised using $180\,^\circ$ microwave hybrid coupler in Section 4.5.3, except that the null rejection is slightly higher in the RF domain, and that the noise level of the signal has increased. This could be attributed to differences in the alignments of the antenna orientation for both characterisations and difference in the signal amplitude received through the ports of the antenna. Nevertheless, these differences can be reduced by adjusting the modulator biases or the polarisation splitting ratio at the polarisation controller.

The results shown in Figure 4.26 demonstrated that controlling the bias voltage of the modulators generates a relative phase difference among the signals received by the microwave photonic implementation shown in Figure 4.20. This implementation can configure the signal received through the ports of the antenna to exhibit a $0\,^\circ$ and $180\,^\circ$ phase difference, reproducing the performance of the $180\,^\circ$ microwave hybrid coupler used to measure the RF results in Section 4.5.3. Thus, this Microwave Photonic mode controller can be used as a "$180\,^\circ$ Photonic Hybrid Coupler".

4.7.4 Unbalanced Modes Radiation Pattern Response

Diverse mode controllers have been proposed to control the multiple radiation modes of multi-arm spiral antenna, simultaneously [92]. However, these mode controllers normally restrict the control of the normal radiation modes of the antenna that generate the fundamental and second order radiation modes of the spiral antenna explained in Section 4.4. Controlling the radiation modes of each port of the antenna individually using the Microwave Photonic mode controller in Figure 4.20 can represent an extra advantage for direction finding systems. These normal radiation patterns can be combined to generate an arbitrary number of unbalanced modes, by changing the amplitude and phase difference between the signals received through the ports of the antenna.

Using a variable polarisation controller like the one shown in Figure 4.20, will adjust the portion of optical power delivered to MZM1 and MZM2 and this will in turn adjust the proportion of the normal modes associated with Port 1 and Port 2 that contribute to the radiation. The polarisation adjustment provides a continuous and arbitrary control over the power split and thus it should be possible to generate an arbitrary number of combination of the normal radiation modes.

Up to now three different responses of the system have been demonstrated. Section 4.7.3 has shown the response of the system when $\alpha = 45\,^\circ$, and Section 4.7.2 has shown the response of the system when $\alpha = 0\,^\circ$ and $\alpha = 90\,^\circ$. To fully illustrate the flexibility of the configuration of this photonic system, this section will demonstrate intermediate configurations for the polarisation controller. The first configuration will be for $\alpha = 67.5\,^\circ$, which generates a link gain difference between the two channels of the Microwave Photonic implementation corresponding to 3 dB for MZM1 and -3 dB for MZM2. The second configuration will be for $\alpha = 112.5\,^\circ$, which corresponds to -3 dB for MZM1 and 3 dB for MZM2.

Figure 4.27 shows that the combined response of the normal radiation modes of the antenna generates an unbalanced radiation mode with two characteristics beams facing

approximately at $\pm 30\,^{\circ}$. The beam-width of these beams is approximately $45\,^{\circ}$ and $30\,^{\circ}$, respectively. The power difference between these two lobes, at their maximum radiation direction, is approximately 4 dB. This unbalance radiation patterns exhibits a null of approximately -6 dB lower than the maximum reading and it is located at approximately $-3\,^{\circ}$. Figure 4.27 also presents the normal modes of the antenna corresponding to Port 1 and Port 2 weighted by 3 dB and -3 dB respectively.

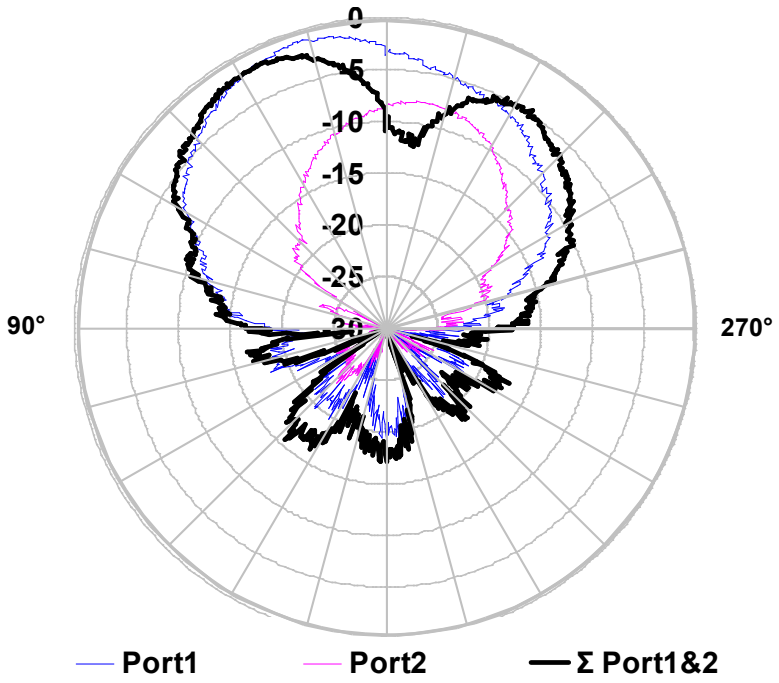

Figure 4.27: $\phi = 90\,^{\circ}$-plane Radiation Pattern Response of an Normal Radiation Mode

Figure 4.28 shows another unbalanced radiation mode with two characteristics beams facing approximately at $30\,^{\circ}$ and $330\,^{\circ}$. The beam-width of these beams is approximately $45\,^{\circ}$ and $30\,^{\circ}$, respectively. The power difference between these two lobes, at their maximum radiation direction, is approximately 2 dB. This unbalance radiation patterns exhibits a null of approximately -6dB lower than the maximum reading and it is located at approximately $3\,^{\circ}$ Figure 4.27 also presents the normal modes of the antenna corresponding to Port 1 and Port 2 weighted by -3 dB and 3 dB respectively

Figure 4.28 shows that an arbitrary combination of the two normal modes of the antenna generates an unbalanced radiation mode with two characteristics beams facing at $25\,^{\circ}$ and $330\,^{\circ}$. The beam-width of these beams is approximately $45\,^{\circ}$ and $30\,^{\circ}$, respectively. The power difference between them, at their maximum radiation direction, is approximately 2 dB.

These results show that the amplitude of the normal radiation modes received through Port 1 and Port 2, can be adjusted such that one radiation pattern response is approximately 6 dB higher than the other. The combination of these patterns generates unbalanced radiation pattern whose null location can be slightly steered. This null steering characteristic might be used to extend the directional finding capabilities of this implementation using the spiral antenna.

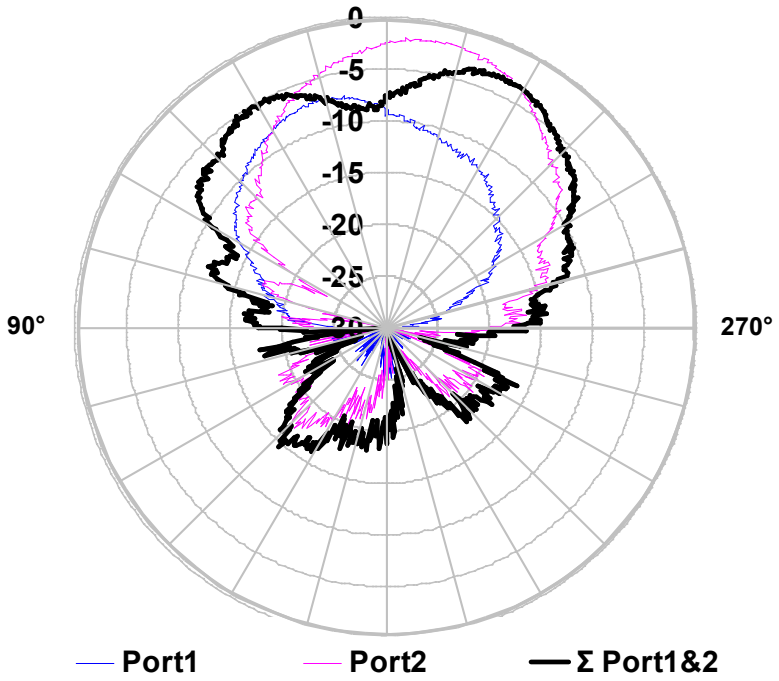

Figure 4.28: $\phi = 90\,^{\circ}$-plane Radiation Pattern Response of an Arbitrary Unbalanced Radiation Mode

This section demonstrates that the Microwave Photonic mode controller not only can measure the radiation characteristics of the spiral antenna through its ports individually but also control them to receive an arbitrary number of unbalanced radiation modes. Achieving this in the RF domain using a $180\,^{\circ}$ microwave hybrid coupler will be extremely difficult.

4.7.5 Photonically Controlled Radiation Pattern Response Summary

The analysis of the radiation pattern response of the double feed two-arm spiral antenna, using the Microwave Photonic mode controller in Figure 4.20, demonstrated that Microwave Photonics can be employed to substitute the function of a $180\,^{\circ}$ microwave hybrid coupler. The Microwave Photonic mode controller demonstrated in this section is able to phase the signal received by the ports of the spiral antenna to exhibit its fundamental or second order radiation modes. Further, this Microwave Photonic mode controller does not interfere considerably with the radiation performance of the spiral antenna and can receive an arbitrary number of unbalance modes by applying photonic weighting functions and polarisation diversity techniques.

4.8 Photonically Controlled Spiral Antenna Gain Response

Having demonstrated that the two normal modes radiation pattern of the realised spiral antenna can be arbitrary combined and controlled using the Microwave Photonic mode

controller for a particular frequency point, an analysis of the gain performance across the operational frequency bandwidth should be conducted.

The gain of each normal radiation mode exhibited by the ports of the antenna is presented in Section 4.8.1. Then, Section 4.8.2 presents the gain of the system when the ports are combined together to receive the fundamental and second order radiation modes of the spiral antenna.

4.8.1 Normal Modes Gain Response

The normal modes of the antenna are defined by two independent tilted radiation patterns and can be characterised by adjusting the angle of the polarisation controller α to $0\,^\circ$ and $90\,^\circ$ as was done in Section 4.7.2. A gain characterisation of the realised spiral antenna using the Microwave Photonic mode controller will confirm the broadband characteristics of this implementation.

The gain performance of the spiral antenna was characterised by comparing the received power of the realised spiral antenna using the Microwave Photonic mode controller with the power received by a commercial right hand circularly polarised spiral antenna, model LS24 by RFSpin®. The characterisation of the transmission link was conducted using two RFSpin® circularly polarised antennas as was done in Section 4.7.1. One of them was used as transmitter and the other one, as the standard antenna of known characteristics.

Figure 4.29 shows the gain performance of the normal modes of the realised spiral antenna measured at broadside direction. The relative gain of each normal mode is above 10 dB from 2–7 GHz and above 8 dB from 8–12 GHz, following similar trends. Beyond 12 GHz each normal mode performs differently. The differences beyond 12 GHz can be attributed to the impedance bandwidth differences shown in Figure 4.6. Although these results are qualitative comparable with the RF characterisation in Section 4.5.4,

Figure 4.29 shows that the relative gain response of these modes is 6 dB higher than the RF results shown in Figure 4.19. This difference corresponds to the 6 dB link gain increment explained in Section 4.7.2, caused by adjusting the polarisation controller in Figure 4.20 to direct the full optical power of the carrier into one link at a time.

The results shown in Figure 4.29 show that the Microwave Photonic mode controller is able to receive both normal radiation modes of the Spiral Antenna over a broad frequency bandwidth without significantly disturbing the radiation characteristics of the antenna.

4.8.2 Fundamental and Second Order Modes Gain Response

As demonstrated in Section 4.7.3 the two normal modes of the antenna can be combined together in order to generate the fundamental and second order modes of the antenna by simply changing the bias voltage of one of the modulators shown in Figure 4.20. This section will investigate the gain response of the fundamental and second order modes of the antenna using the Microwave Photonic mode controller.

The fundamental and second order radiation modes gain characterisation was done by adjusting the polarisation controller at $\alpha = 45\,^\circ$ as was done in Section 4.7.3. The

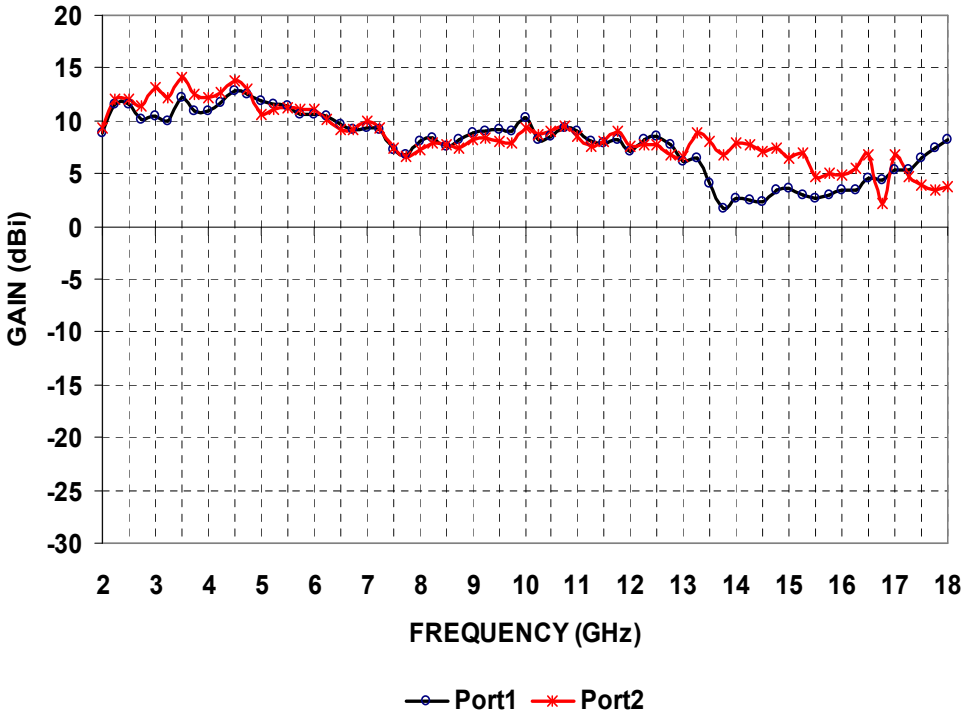

Figure 4.29: Gain Performance of the Port 1 and Port 2 of the Spiral Antenna

response was normalised to the link gain characterisation obtained using the known spiral antenna in Section 4.7.1.

Figure 4.30 shows the gain performance of the fundamental and second order radiation modes of the spiral antenna compared to the standard gain of the known commercial spiral antenna. It shows that the relative gain of the fundamental radiation mode it is approximately 6 dB above the relative gain of the commercial spiral from 2–8 GHz. Then, it decreases until it matches the gain performance of the commercial spiral antenna.

Figure 4.30 also shows the gain characterisation of the spiral antenna operating in its second order mode. This response corresponds to the null rejection response of the antenna at broadside. It shows that relative gain of the antenna remains below -10 dB (approximately -20 dB compared to the fundamental mode) for most of the frequency range.

The fundamental and second order radiation modes gain characterisations shown in Figure 4.30 are in good agreement with the RF results presented in Figure 4.18, demonstrating that the Microwave Photonic mode controller combines the two gain responses of the two normal modes of the antenna reasonably across its entire bandwidth.

It is worth noting that the gain response of the normal modes shown in Figures 4.29 and the gain response of the fundamental mode of the antenna shown in Figure 4.30 have similar average levels. This might seem inconsistent, however, it is important to remember that the gain of the individual normal modes can only be measured by adjusting the polarisation controller of Figure 4.20 to $\alpha = 0\,^\circ$ or $\alpha = 90\,^\circ$. Thus, the link gain of the normal modes is actually 6 dB higher than the link gain that these modes experiment when the polarisation controller is adjusted to $\alpha = 45\,^\circ$.

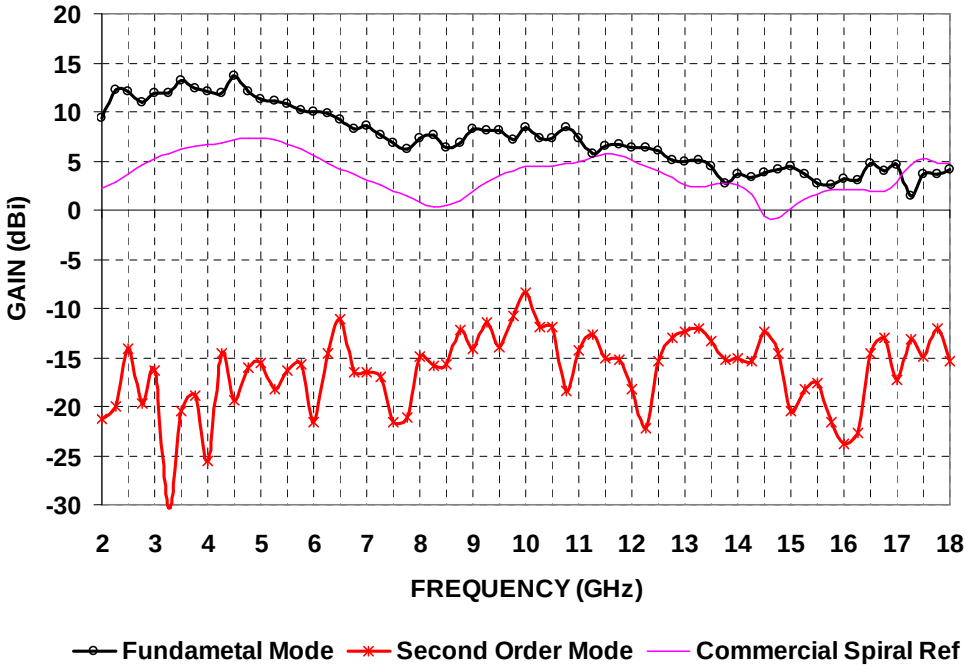

Figure 4.30: Gain Performance of the Fundamental and Second Order Radiation Modes

The fact that the gain measurement of the normal modes (Figure 4.29) and the fundamental radiation mode (Figure 4.30) using the Microwave Photonic mode controller exhibits similar average values could represent an extra advantage for directional finding systems.

4.8.3 Photonically Controlled Spiral Antenna Gain Response Summary

The gain analysis of the spiral antenna using the Microwave Photonic mode controller in Figure 4.20 demonstrated that it is possible to combine the normal modes of the realised spiral antenna over a broad range of frequencies. This Microwave Photonic mode controller is able to generate the required feeding to receive the fundamental mode of a dual feed two-arm spiral antenna and the second order radiation modes. It has also demonstrated that the two normal modes that are combined to generate the fundamental and second order modes of the antenna can be control individually by only adjusting the mode controller of this Microwave Photonic implementation. This is something that cannot be done easily by using traditional microwave techniques such as a balun transformer or a 180° microwave hybrid couplers.

This section demonstrated that the response of a two-arm spiral antenna is defined by the coupling of the two unbalanced transmission lines selected to interface the spiral antenna with the mode controller and the spiral antenna. The Microwave Photonic mode controller does not disturb the performance of the antenna significantly.

It was also demonstrated that all of the available optical carrier power can be arbitrarily redirected to either MZM by simply adjusting the polarisation at the input. This

enables a link gain that can be 6 dB higher than when the optical power is split between the two ports. This is an advantage over traditional RF mode controllers, due to the fact that, measuring the fundamental mode of the antenna and its individual radiation patterns provides similar signal levels at broadside and could also represent an advantage for directional finding systems.

4.9 Summary and Conclusions

A microwave photonic mode controller for a double fed two-arm spiral antenna was implemented and demonstrated. This mode controller enable the reception of the fundamental and second order radiation modes of the spiral antenna by combining the two normal modes of the spiral antenna, and uses a single optical link.

This chapter demonstrated that by biasing two single electro-optic modulators at the same quadrature points or opposite quadrature points, the relative phase difference between two RF modulated signals can be phased to be 0° or 180°, respectively. This Microwave Photonic mode controller proved to reproduce the performance of a 180° Microwave hybrid coupler. This Microwave Photonic mode controller does not disturb the RF performance of the antenna significantly, resulting in an effective "180° photonic hybrid coupler".

It has also shown that the normal modes of the antenna can be arbitrarily controlled to create the multiple unbalanced radiation modes of the two-arm spiral antenna. This will not be possible if the antenna is interconnected to a 180° microwave hybrid coupler.

It also demonstrated that the gain response of the normal modes is 6 dB higher than in a normal system where a microwave hybrid coupler is employed. This characteristic could be an advantage over traditional RF mode controllers and direction finding applications.

This chapter demonstrated that the frequency dependency of the radiation patterns exhibited by a two-arm spiral antenna creates a rotation of the modes of the antenna along its Z axis. Designing a direction finding system based on this antenna, would require extra processing techniques in order to define the angle of arrival for a defined signal. However, this rotational characteristic of the radiation patterns can be avoided if multiple arms frequency independent antennas are used instead of the two-arm spiral antenna. It is anticipated that the current approach could be extended, through the use of other wavelength division multiplexing (WDM) techniques to support three, four or even more arms of a multiple-arm frequency independent antenna.

Chapter 5

Reconfigurable Photonic Sinuous Antenna

5.1 Introduction

As explained in Section 4.1, direction finding applications requires a front-end device capable of receiving multiple radiation modes and multiple polarisations so amplitude or phase comparison methods can determine the angle of arrival of an unfriendly signal. It would be desirable that this front-end device had a single aperture antenna for which all these radiation modes share a common coincident phase centre, such that weight, volume and system complexity can be minimised.

Chapter 4 attempted to make the most of the fundamental and second radiation modes of a two-arm spiral antenna in order to provide an amplitude comparison method using a single aperture antenna. It was demonstrated that the Microwave Photonic Mode Controller implemented in Chapter 4, can control and receive the fundamental, the second mode and an arbitrary number of unbalanced radiation modes of the spiral antenna using a single optical fibre link.

Practical use of this system in determining the angle of arrival of an unfriendly signal for direction finding applications could be problematic for a single two arm spiral antenna. The two arm spiral provided multiple beam patterns along only one axis. It might be imagined that this single axis could be aligned to the horizon to allow direction finding within a quadrant of a single plane; however, since the radiation pattern of the spiral rotates around the central axis of the antenna, even this limited direction finding could be problematic.

To realise a truly practical direction finding system with a single aperture, an antenna with the desirable characteristics of spirals will be required, but with more degrees of freedom to provide two axis scanning and radiation patterns that do not rotate with frequency.

One possible antenna to meet these requirements is the sinuous antenna. Sinuous and Spiral antennas share similar radiation characteristics [87]. Both are considered as balanced radiation elements with broadband frequency characteristics. Both are frequency independent when operating in the fundamental mode. And, both are able to radiate

circular polarisation, which decreases the level of signal degradation and polarisation instability, ensuring a successful signal transmission [93]. Sinuous antennas differ from spiral antennas because sinuous antennas exhibit radiation patterns that are frequency independent even in higher order radiation modes and multiple polarisations [87]. These characteristics make sinuous antennas suitable candidates for compact direction finding systems.

In order to scan over two axes, the sinuous antenna must have at least three arms, and to enable radiation into linear polarisations in vertical and horizontal axes, four arms will be required [87]. In order for this four-arm sinuous antenna to radiate in multiple radiation modes and in both linear and circular polarisations, a sophisticated controlling network must be designed and implemented. The complexity of these Butler matrices increase proportionally to the number of radiating elements (arms) of the antenna. The Butler matrix for a four-arm sinuous antenna will be rather bulky, complex and usually frequency bandwidth restricted [17, 87]. Switching between radiation modes will also be somewhat cumbersome.

This chapter demonstrates that the microwave Butler matrix normally used to control the circular polarisation performance of a four-arm sinuous antenna can be replaced by a Microwave Photonic implementation with a broadband frequency response. This implementation uses photonic transversal techniques, as well as counter phase modulation control of electro-optic modulators. It is demonstrated that both linear and circular polarisations can be received as well as fundamental and higher order modes. Switching between these radiation modes is also straight forward and can be achieved electro-optically.

The multiple radiation modes and polarisation of the sinuous antenna have been widely investigated. However, most of these investigations remain confidential and are not generally available publicly. Using the information available to public domain, this chapter will first provide a comprehensive study of the sinuous antenna, its alternative feeding networks and its design parameters in order to familiarise the reader with this type of antennas. Then, it will present the steps followed to design, simulate and fabricate the four-arm sinuous antenna that will be used in this investigation, as well as its partial RF characterisation, which highlights the limitation of microwave controlling networks. Once that the radiation characteristics of the sinuous antenna have been fully understood, each of the components that form the proposed Microwave Photonic implementation that will replace the traditional microwave Butler matrix will be introduced and characterised. To finalise, the components will be implemented together in the proposed Microwave Photonic Mode Transformer which will be connected to the sinuous antenna for characterisation purposes so it can be demonstrated that this implementation is able to control the multiple radiation modes and multiple polarisations that the four-arm sinuous antenna can receive

5.2 Single Aperture Antenna with Multiple Polarisation and Multiple Radiation Modes

As discussed in Section 4.1, in most civil and military direction finding applications it is highly desirable to have a front-end device able to receive multiple polarisations and multiple radiation modes.

The aim of this section is to illustrate how a multiple arm sinuous antenna with self-complementary structure could meet these requirements. This will be done by creating a sinuous antenna based on a literature review, simulating a model of it using High Frequency Structure Simulator software HFSS, realising it and characterising it using traditional microwave techniques.

5.2.1 Self-complementary Sinuous Antenna

A self-complementary antenna may consist of N-arms and N slots with a rotational symmetry such that a rotation of $360\,°$/N around the perpendicular axis to the surface of the antenna leaves the antenna unchanged for a viewer located at bore-sight direction.

As shown in Figure 5.1, the sinuous antenna geometry is fully defined by an angular span (α) and a rotation angle (δ), as well as the log-periodic growth rate (τ).

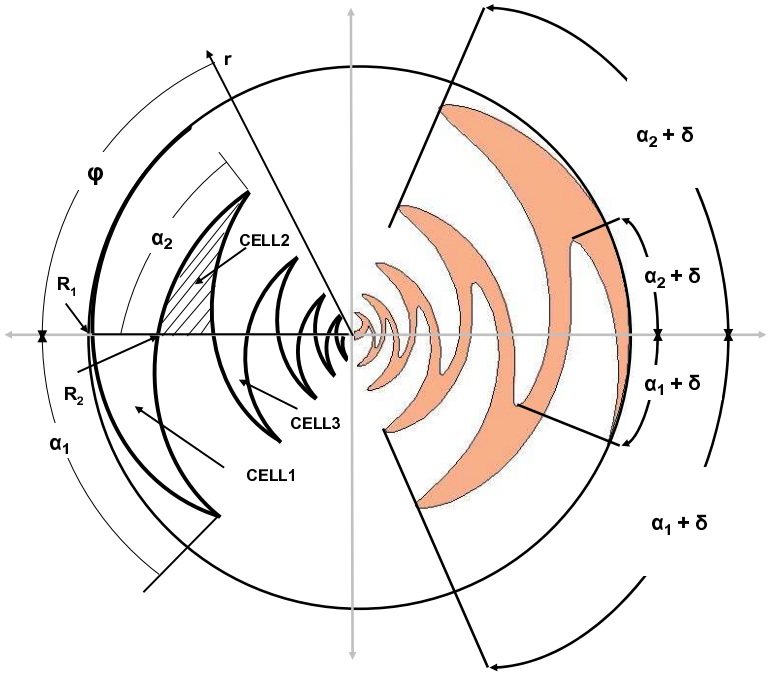

Figure 5.1: Sinuous Arm Parameterisation

The centre locus which defines each arm of the sinuous antenna is a series of cells starting with $cell_1$ at the outer radius R_1. R_p defines the outer radius of the $cell_p$; α, defines its angular width, and τ_p defines the ratio of the inside-to-outside radius for each cell R_p/R_{p-1}. The equation for the p^{th} cell is given by

$$\phi = (-1)^{p}\alpha_{p} sin\left[\frac{180ln(\frac{r}{R_p})}{ln\,\tau_{p}}\right] \qquad R_{p+1} \leq r \leq R_{p} \tag{5.1}$$

where r and ϕ are the polar coordinates of the centre locus.

The radii R_{p} are related by

$$R_{p} = \tau_{p-1} R_{p-1} \tag{5.2}$$

The area of one single arm of the sinuous antenna is formed by sweeping the centre locus of Eq. 5.1 by $\pm\,\delta$ around the origin (ϕ), as shown in Figure 5.1. To complete the sinuous antenna the single arm is duplicated at 360/N degree angular increments to form an N-arm structure, where N is the number of arms. The amount of interleaving between the arms, defined by α_{p} and δ should be adjusted so that $\alpha + \delta \; < \; 70\,^{\circ}$ to ensure good antenna efficiency, as well as a high gain and wide frequency response [85].

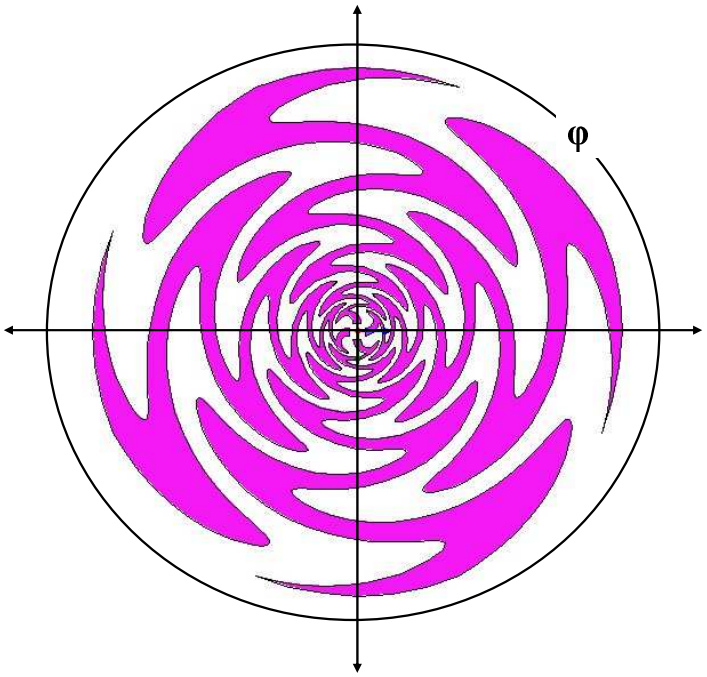

Figure 5.2: Sinuous Antenna

Figure 5.1 also shows that δ defines the self-complementary condition for the N-arm sinuous antenna. It is believed that δ is important in providing the capacitance necessary to tune out the sharp inductive corners of the sinuous antenna. Figure 5.2 shows a picture of a four-arm sinuous antenna created by means of duplicating one single arm three times around the central axis of the antenna every $\phi = 90\,^{\circ}$.

The application for coarse direction finding requires at least access to M=1 (bore-sight) and M=2 (angled beams) for both vertical and horizontal orientations so simultaneous azimuth and elevation measurements can be done. According to Appendix A each arm of the self-complementary sinuous antenna can be considered as a travelling wave monopole antenna. Various modes of radiation can be achieved using this antenna by feeding these monopoles with single transmission lines of a suitable phase. It should be

noted that each of the elements of the antenna load each other and thus that the different radiation M modes will each have a different characteristic impedance. Thus, to maintain broadband radiation characteristics for several of these M modes, the impedance of each desired M mode must be estimated and a feeding point designed to provide an adequate impedance match for each of them over multiple octaves.

5.2.2 Sinuous Antenna Radiation Modes Impedance

Recall that in Chapter 4, it was demonstrated that two unbalanced transmission lines can be driven with a relative phase difference of $0\,^{\circ}$ or $180\,^{\circ}$ in order to generate the M-modes M=1 and M=2 of a two-arm cavity backed spiral antenna, respectively. These two unbalanced transmission lines can be considered as two individual sources feeding each normal mode of a self-complementary structure with an input impedance that compromises the performance of these modes. A sinuous antenna operating over multiple modes needs to balance the performance of the antenna between the input characteristic impedance of these M radiation modes. This can be done by roughly calculating an average input impedance located among all the desired M modes that exhibits similar response for all of them. Multiple modes of the sinuous antenna might be excited with a same feeding interface; however, only its M=1 and M=2 radiation modes will be investigated for direction finding purposes in this Chapter.

Appendix A shows that the input impedance of a four-arm self-complementary structure operating in mode M=1 and M=2 are $Z_0 = 133.3\,\Omega$ and $Z_0 = 94.2\,\Omega$, respectively. Selecting an average input impedance of $112\,\Omega$ as the feeding interface of the four-arm sinuous antenna shown in Figure 5.2 represents an option to control these two modes of the antenna simultaneously. According to [85] this average impedance limits the inherent mismatch of the feeding interface to less than 1.19 for both modes.

Practical implementations of a four-arm sinuous antenna using $140\,\Omega$ balanced feed lines for M=1 radiation mode has resulted in VSWR values on the average of 1.7:1 bandwidths [85]. Similar to this, various investigations [71, 73] have demonstrated that operating a multi-arm sinuous antenna in mode M=1 using balanced transmission lines, whose impedances approximate the values presented in Table A.1, has obtained broadband radiation characteristics. Thus it is expected that designing a sinuous antenna and its feeding interface with an average impedance of $112\,\Omega$ should enable to operate this antenna in both modes simultaneously with similar broadband radiation characteristics.

5.2.3 Sinuous Antenna Summary

In this section a multi-arm self-complementary sinuous antennas has been introduced. Provided that the radiation characteristic of this antenna can be achieved as in theory, this antenna could match all the requirements for testing the Microwave Photonic implementation presented in this Chapter, which main objective is to substitute complex microwave mode controllers implementation such as the Butler Matrix shown in [33] on coarse direction finding applications.

5.3 Sinuous Antenna Design

Section 5.2.1 shows that a sinuous antenna can be considered as multiple broadband travelling wave monopoles that could be used to receive multiple polarisations and multiple radiation modes through a single aperture. It is not, however, simply a matter of designing an appropriate patch as described in Section 5.2.1. A practical sinuous antenna, like a broadband spiral will require several other components including: a proper absorptive cavity that reduces the backward radiation of the patch and supports its lower frequency bandwidth response; a suitable interface to the feeding point of the arms of the sinuous antenna; and a phasing network able to feed each arm of the antenna and provide them with the correct phase in order to obtain the desired radiation mode. This section presents the procedure used to design the four-arm sinuous antenna used for this investigation, including each of these components.

5.3.1 Design of a Four-arm Sinuous Antenna Patch

As described by in [87] and shown in Section 5.2, the radiation characteristics of the sinuous antenna are defined by its designing parameters $\alpha, \tau, \delta,$ R and the number of cells of each radiating element. There are some limits to these values that ensure its good performance t and is R is the most important of them, since it defines the frequency bandwidth of the sinuous antenna.

Based on the design parameters presented in [73], a four-arm sinuous antenna of a frequency bandwidth from 2–18 GHz was designed. A 9-cell (P=9) sinuous antenna was designed using the equation editor of HFSS and the following design parameters: $\alpha = 45\,^{\circ}$, $\delta = 22.5\,^{\circ}$, and $\tau = 0.75$. The values of R_1 and R_p were calculated considering $\lambda_L = 150mm$ and $\lambda_H = 16.66mm$. The calculated values were $R_1 = 31.83mm$ and $R_p = 3.53mm$. Figure 5.2 shows the model created in HFSS of the four-arm sinuous antenna.

A sinuous antenna with sufficient interleaving between its radiating elements has approximately the same frequency limits as a spiral antenna. According to [73] the sinuous antenna patch shown in Figure 5.2 should radiate efficiently from 2–18 GHz. However, there are some real design considerations such as its absorptive cavity and feeding interface that must be considered before simulating a model closer to the final outcome.

5.3.2 Absorptive Cavity Design

Similar to spiral antennas, sinuous antennas radiate bidirectionally. In real application such as most civil and military applications, only forward radiation is desired. One method to avoid backward radiation is by using a conductive cavity filled with microwave absorber [94]. This method can also be applied to the sinuous antenna shown in Figure 5.2 to stop it radiating bidirectionally and to improve its performance at low frequency.

In order to hold the antenna patch and generate unidirectional radiation patterns, the proposed antenna substrate and absorptive cavity presented in [73] were further investigated.

Table 5.1 summarises the materials chosen for the cavity backed model of the four-arm sinuous antenna. It illustrates that a thin antenna substrate has been chosen to hold the printed circuit patch of the sinuous antenna. Foam spacer has been selected to separate the antenna substrate from the absorber and the cavity bottom. The microwave absorber AN74 was manufactured by Emerson and Cuming Microwave Products.

Table 5.1: Sinuous Antenna Components

Layer	Substrate Type	Relative Permittivity (ϵ_r)	Relative Permeability (μ_r)	Los Tangent	Thickness (d)
1	Duroid®	2.2	1	0.0009	0.125mm
2	Foam	1.07	1	0.004	2mm
3	Eccosorb® AN74				10mm
4	Foam	1.07	1		2mm

Thin antenna substrates have demonstrated not to affect the radiation characteristics of the antenna significantly [73]. In this case, a 0.125mm Duroid® substrate should provide enough stability and rigidness to the printed antenna without disturbing its radiating characteristics. Foam spacers were employed to avoid that the energy travelling along the radiating elements of the antenna (arms) being absorbed completely by the microwave absorber. The microwave absorber attenuates most of the energy radiated in the direction of the cavity, stopping the radiated energy for bouncing back at the bottom of the cavity and interfering with the energy radiated in the opposite direction to the cavity (forward direction). The circumference of the cavity has been chosen merely to locate the antenna so the overall size of the antenna does not increase. However, the deepness of the cavity has been selected to be less than a $\frac{\lambda}{4}$ of the lower frequency of its operational bandwidth, in attempt to minimise the volume of the antenna.

It is expected that the microwave absorber AN74 reduces most of the energy radiated backwards by the sinuous antenna. However, a fine tune of the final parameters which considers a feeding interface is still required.

5.3.3 Feeding Interface Design

Having designed the antenna patch and its absorptive cavity, the feeding interface must be selected and designed so that an impedance match to the multiple polarisation and radiation modes can be achieved.

As shown in Section 4.5.2, balanced to unbalanced transformers (Baluns), microwave power dividers and hybrid couplers have been proposed and used to measure some of the radiation modes of the spirals and sinuous antennas [92]. Using a pair of balanced to unbalanced transformers has been successfully demonstrated [17, 73]. However, this approach limits the diverse functionality of the sinuous antenna defined by its four normal

modes. The proposed approach shown in [73] only enable the antenna to receiving two orthogonal polarisations operating in mode M=1, also known as the fundamental mode of the antenna. As discussed in Section 5.1, it is desired that several radiation modes are available for directional finding systems and thus other feeding interfaces must be investigated.

Similar to Section 4.3.1 and based on the principle for independent feeding of self-complementary structure shown in [74], a multiple unbalanced transmission lines interface was investigated. This interface must be able to interconnect the four radiating elements of the sinuous antenna with the phasing network and avoid unbalanced currents that might disturb the radiation performance of the antenna.

Coaxial Feeding Interface

Recall from Section 5.2.2 that in order to operate a sinuous antenna in its fundamental mode (M=1) and in its higher order mode (M=2) simultaneously with similar broadband radiation characteristics, the average value of its input impedance should be $112\,\Omega$.

A bundle of semi-rigid coaxial cables with characteristic impedance $Z_0 = 50\,\Omega$ was realised based on the principle for multiple unbalanced lines mode transformer presented in [17] in order to have independent control of the four radiating elements of the sinuous antenna shown in Figure 5.2.

Table 5.2 summarises the possible coaxial cables commercially available and shows the frequency bandwidth response of available commercial coaxial cables operating in a bundle that can be used to interface a multiple-arm self-complementary structure [92]. The only semi-rigid coaxial cables available at the time of this investigation were 3.881mm and 2.156mm. The 2.156mm coaxial cables were selected.

Table 5.2: Maximum Frequency Performance for Coaxial Bundle Feed (GHz)

#Cables/size(mm)	3.581	2.156	1.016	0.086
2	7	12	22	30
4	6	10	18	25
6	5	8	14	20
8	4	6	12	16

Figure 5.3 shows a detailed drawing of the coaxial bundle. It shows that four coaxial cables, whose external conductor has been stripped, reach the bottom of the cavity and pass through by 2mm inside the cavity. The stripped coaxial connectors are surrounded by an external 2 x 8mm (radius, height) conductive cylinder connected to the cavity and to the external conductor of each coaxial cable. Each one of the stripped coaxial cables fills the external conductive cylinder with its polytetrafluoroethylene (PTFE) dielectric (ϵ_r=2.1). Each inner conductor of the stripped coaxial cables is connected to one radiating element of the sinuous antenna.

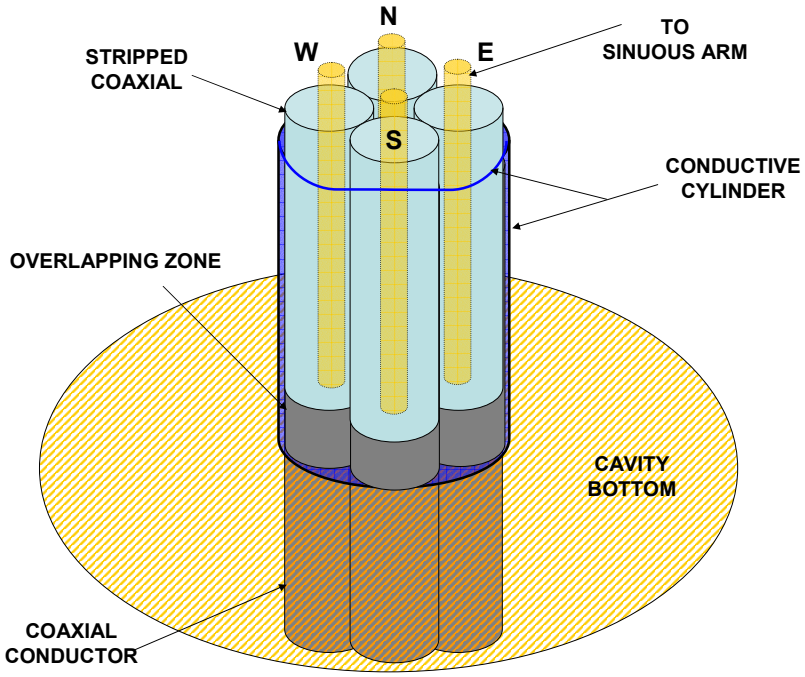

Figure 5.3: Sinuous Antenna. Coaxial Bundle

It should be noted that the 2.156mm coaxial cable becomes multi-mode at 10 GHz and thus this represents an upper limit to the bandwidth of the antenna. A smaller diameter cable could be used to increase this upper frequency limitation. It should be noted as well that the inner conductors of the coaxial bundle are considerably bigger than the feeding point of the sinuous antenna and thus the antenna patch must be modified.

Sinuous Antenna and Coaxial Bundle Integration

In order to interconnect the coaxial bundle shown in Figure 5.3 to the radiating elements of the sinuous antenna and achieve a smooth impedance transition, the feeding point of the antenna needs to be modified for impedance matching purposes and reliable interconnection.

A modification of the feeding point of the antenna was designed. This modification aims to maintain the self-complementary characteristic of the structure, at the same time that it enhances the interconnection of the inner coaxial conductors of the bundle with the radiating elements of the antenna.

Figure 5.4 shows the modification realised to the 9^{th} cell of each radiating element in order to enable interconnecting the sinuous antenna with the coaxial bundle. It shows that size of the “tail” of the cell has been increased, rounded and directed to the centre of the sinuous antenna.

Having a bigger area for interconnecting the inner conductors of the coaxial cables will ensure a reliable interconnection. However, it is expected that this modification might disturb the self-complementary characteristics of the antenna and thus the size of this ’tail’ is one of the parameters that must be optimised when modelling the antenna.

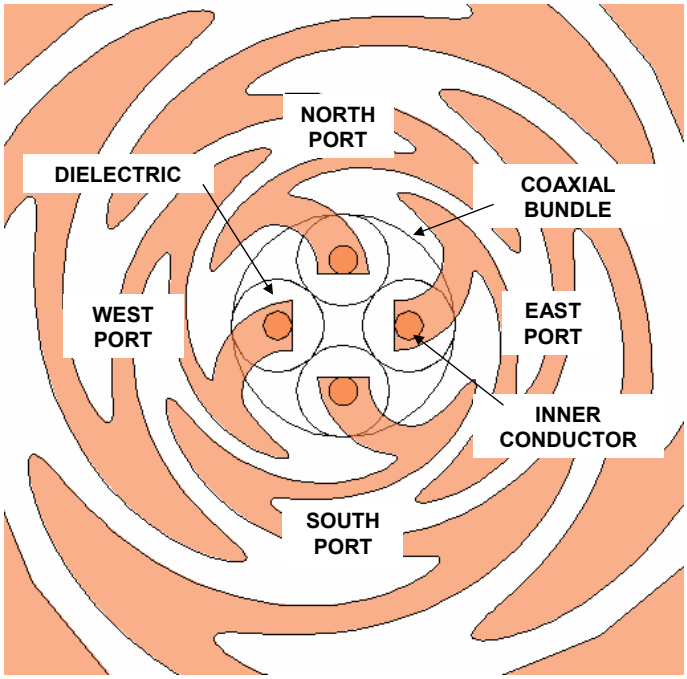

Figure 5.4: Sinuous Antenna. Coaxial Bundle Detail

5.3.4 Antenna Design Summary

Achieving a broadband performance of the sinuous antenna operating in mode M=1 and M=2 simultaneously, will only be possible as long as the coaxial bundle response matches the impedance bandwidth for both modes. As shown in Table 5.2, it is predicted that the frequency bandwidth for which the sinuous antenna was initially designed (2–18 GHz) will be limited by the maximum frequency response of the 2.165mm coaxial cables used to created the coaxial bundle shown in Figure 5.3.

The modification realised to the feeding point of the antenna shown in Figure 5.2 might also affect the overall frequency response, particularly at the upper frequencies of its operational bandwidth. Since each radiating element of the sinuous antenna is accessed by one coaxial cable of the bundle, these feeding points will now be referred as port North, South, East and West (Port N, S, E and W) as shown in Figure 5.4 and Figure 5.3.

5.4 Sinuous Antenna Simulation

Based on the parameters presented in Section 5.3 the four-arm sinuous antenna patch, the absorptive cavity and coaxial bundle interface were assembled into single structure, modelled and optimised using HFSS. This section presents the simulation results of the scattering parameters and radiation patterns received by the ports of the sinuous antenna antenna.

5.4.1 Scattering Parameters Simulated Results

An analysis of the scattering parameters (S-parameters) of the sinuous antenna designed in Section 5.3 should verify its estimated impedance bandwidth response, and find out if the coaxial bundle and the modifications made to the antenna in Section 5.3.3 offer a reliable impedance transition between individual feeding sources and the radiating elements of the sinuous antenna.

A discrete modal analysis of the sinuous antenna was conducted using HFSS. An adaptive frequency of 10 GHz and a delta error of 0.02 were selected to define the mesh size of the model. An optimisation process was undertaken varying design parameters such as feeding point transition, coaxial inner conductor proximity, outer conductor proximity to the substrate. Figure 5.5 shows the optimal final design of the antenna including all its layers and coaxial bundle.

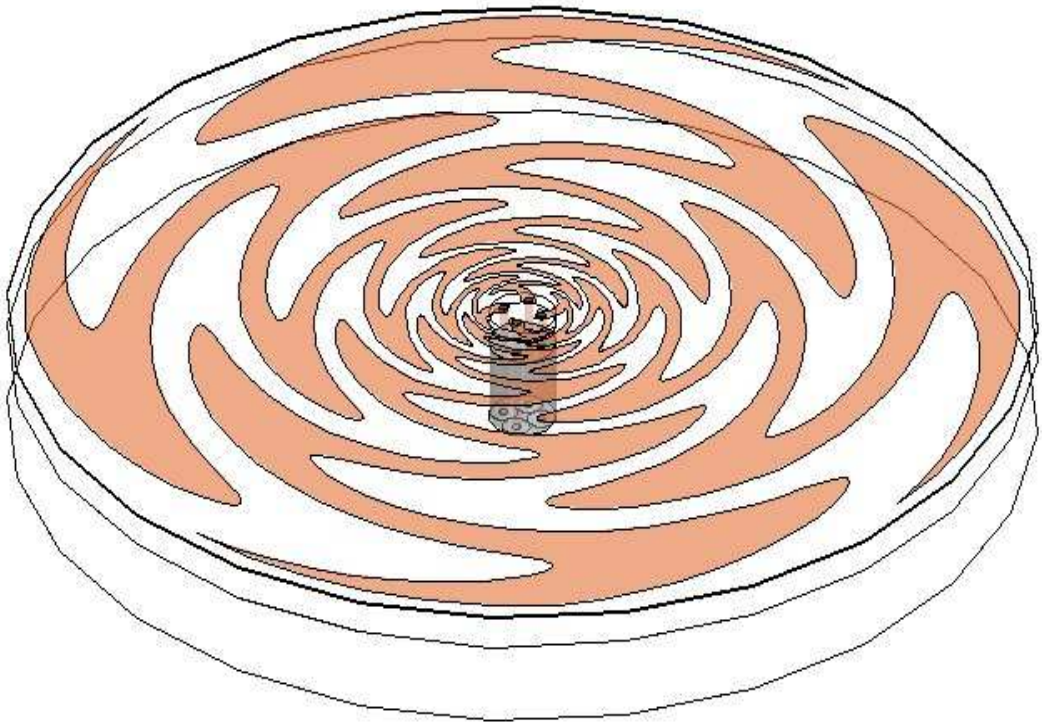

Figure 5.5: Final Sinuous Antenna Design

It was predicted that the symmetry of the self-complementary sinuous antenna shown in Figure 5.5 will exhibit similar radiation performance characteristics through each one of the ports of the bundle. This was confirmed after obtaining similar results from simulation. Only a selection of the S-parameters results is presented in this section for simplicity.

Figure 5.6 shows the reflection coefficient of Port-E, as well as the coupling factor of Port-E and Port-W and Port-E and Port-N. It shows that the reflection coefficient of Port-E remains approximately below -10 dB from 2–12 GHz. Figure 5.6 also shows that the coupling between Port-E and its adjacent port (Port-N) is below -15 dB. It also shown that the coupling between Port-E and its opposite port (Port-W) is below -18 dB across the entire bandwidth analysed.

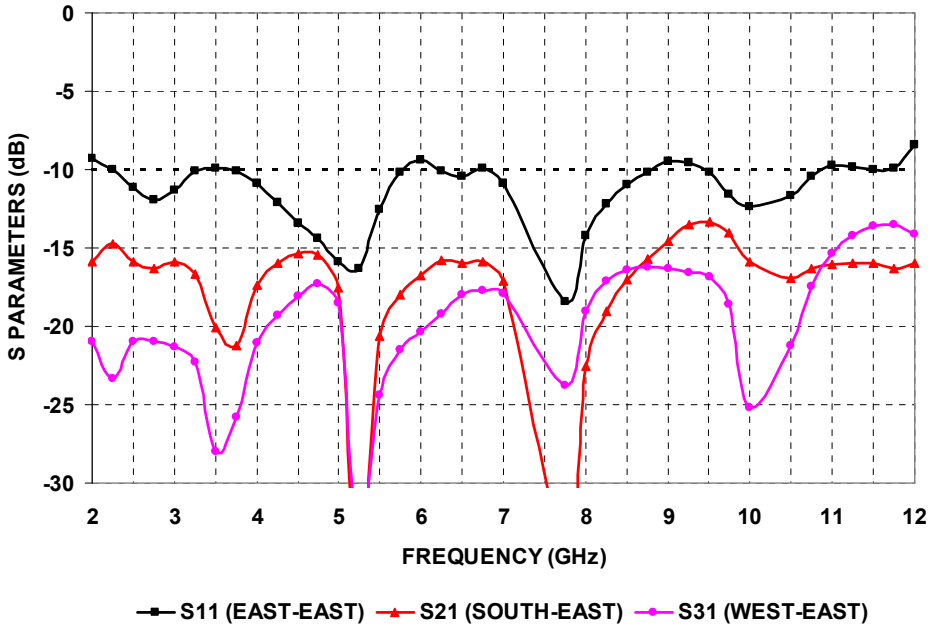

Figure 5.6: Scattering Parametrisation of the Coaxial Bundle. Simulated Results

The selection of scattering simulated results presented in Figure 5.6 apply to each one of the ports of the antenna. These results define the impedance bandwidth of the sinuous antenna as well as the mutual coupling between the interlaced radiating elements of the antenna.

5.4.2 Radiation Pattern Simulation Results

According to [17] if the coaxial bundle is working properly, each port of the coaxial bundle of the self-complementary sinuous antenna should measure a normal mode radiation pattern defined by a single beam tilted off bore-sight. A radiation pattern simulation analysis should confirm this.

Similar to the analysis of the scattering parameter, it is expected that the radiation pattern results measured at each one of the ports of the antenna are the same. Therefore, for brevity, only the H-plane and E-plane radiation patterns of Port-E are presented. Port-W, Port-N and Port-S terminated to $50\,\Omega$ virtual loads.

In Section 4.5.3, the radiation pattern analysis were conducted at 5 GHz in order to ensure the normal and higher order radiation modes aligned with the H-plane and E-plane of an antenna measurement system. In this Section, the same commercial two arm spiral employed in Chapter 4 will be used as the transmit antenna and hence for consistency, the radiation pattern analysis will also be conducted at 5 GHz.

Figure 5.7 shows that the radiation pattern on the E-plane and H-plane for Port-E. It shows that the radiation pattern corresponding to the E-plane a single beam with a 3 dB beam-width of approximately $30\,^{\circ}$. This beam is tilted around $12.5\,^{\circ}$ off bore-sight. It also shows that the H-plane radiation pattern of Port-E exhibits a single broad beam centered along bore-sight with a 3 dB beam-width of approximately $60\,^{\circ}$.

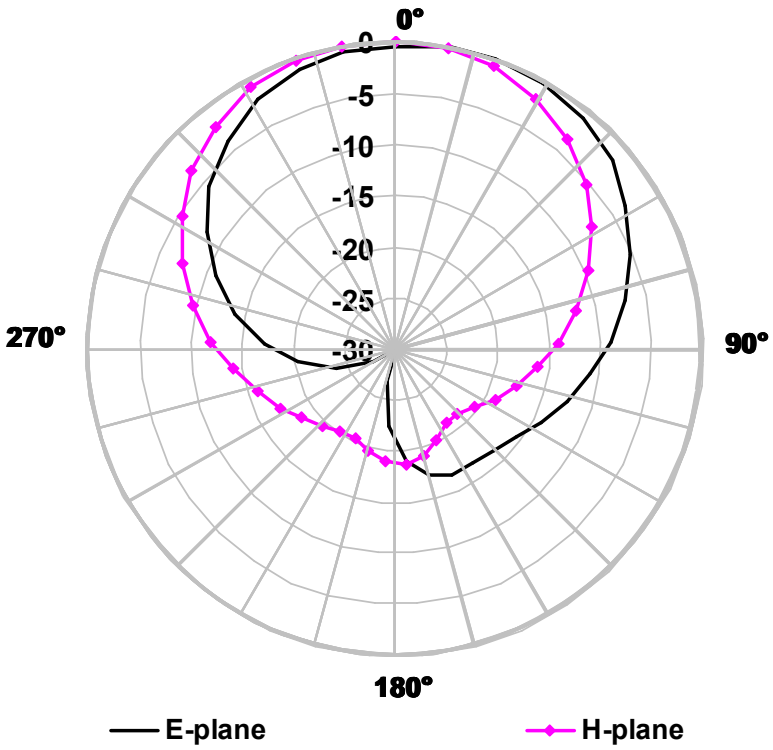

Figure 5.7: E-plane and H-Plane Radiation Patterns for Port-E. Simulated Results

The radiation patterns shown in Figure 5.7 correspond to a broad beam tilted off bore-sight directed in the same direction of the radiating element connected to Port-E. They define the radiation pattern characteristics of one normal mode of the sinuous antenna which can be controlled independently through one port of the coaxial bundle.

These results demonstrate that each radiating element exhibits a tilted beam aligned with the main axes of the antenna when the inactive ports are terminated to broadband $50\,\Omega$ loads. That is, if the Port-E of the antenna is the only port fed, the radiation characteristics of the antenna should exhibit a single beam radiation pattern tilted off bore-sight (θ) in the East direction.

5.4.3 Simulation Analysis Summary

The broadband characteristics of the sinuous antennas have been previously demonstrated with moderate operational bandwidths [72, 73]. A bandwidth from 2–18 GHz might be obtained using traditional balanced feeding networks such as a Balanced to Unbalanced (Balun) transformer.

The simulation analysis of the sinuous antenna interfaced with the coaxial bundle shows that the coaxial bundle narrows the expected frequency bandwidth of the antenna to 2–12 GHz and exhibits an impedance bandwidth of approximately 143%. This frequency bandwidth might be enhanced using coaxial cables with maximum frequency response $\geq$ 18 GHz (e.g. 1.016mm coaxial cables). However, it is not the intention of this dissertation to optimise the broadband performance of the antenna, but rather demonstrate

that a microwave mode transformer network of hybrid coupler traditionally used for controlling the radiation modes of the sinuous antenna can be simplified and improved using Microwave Photonic techniques. Thus, the 143% bandwidth obtained with the available coaxial bundle is considered acceptable as proof of concept and must be verified.

The radiation analysis of the simulation results provide enough evidence to be confident that practically interfacing the sinuous antenna with the proposed coaxial bundle shown in Figure 5.3 will allow the independent control of each one of the four radiating elements of the sinuous antenna. These radiating elements should exhibit four tilted beams aligned with the main axes of the antenna.

Provided that this antenna can be realised and its performance matches the simulated results presented in this Section, these four beams can be combined with different relative phase differences in order to generate the response of four individual monopole antennas, two orthogonal linearly polarised dipole antennas, or a dual circularly polarised antenna using the appropriate control and phasing network.

5.5 Sinuous Antenna Realisation and Characterisation

Section 5.4 presented simulations predicting that the sinuous antenna shown in Figure 5.2 could generate four normal modes independently. This antenna can now be realised and characterised. This section presents a brief description of the realisation of the antenna, an RF analysis of the scattering parameters and characterisation of the radiation patterns and gain performance of the realised sinuous antenna.

The final antenna design was realised according to the parameters presented in Section 5.3. The patch was made on Duroid 5880® of 0.125mm thickness and $\frac{1}{4}$oz electrodeposited copper foil using traditional printed circuit board lithography. The cavity was aluminum based and foam spacers were employed to avoid that the energy travelling along the radiating elements of the antenna (arms) was completely absorbed by the microwave absorber (AN74). The coaxial bundle was manufactured as specified in Section 5.3.3 using 2.156mm coaxial cables. Figure 5.8 shows a picture of the final design of the sinuous antenna, unassembled. It shows that a gap of 5mm radius was included between the coaxial bundle and the microwave absorber in order to isolate the outer conductor of the bundle from the absorber. The upper and lower layers of 2mm of foam are not presented in Figure 5.8 so the location of the coaxial bundle and the microwave absorber can be clearly observed. The semi-rigid coaxial cables were 10cm long and can be observed on the back of the cavity of the antenna.

5.5.1 Scattering Parameters Characterisation

The characterisation of the antenna measuring the reflection coefficient at each port, and the coupling between adjacent and opposite ports will confirm the broadband impedance characteristics of the antenna predicted by HFSS in Figure 5.6.

The scattering parameters analysis was conducted using a 40 GHz Anritsu Vector Network Analyser (VNA) model 33C743. The reflection coefficient was measured con-

Figure 5.8: Unassembled Sinuous Antenna

necting one port of the antenna at a time to Port-1 of the VNA and terminating the other inactive ports of the antenna to broadband $50\,\Omega$ loads. As where it was assumed that the simulated results of each rotationally symmetric radiating element of the antenna would be identical, it is expected that the practically realised antenna will exhibit some variations in the reflection coefficient measured at each port of the antenna due fabrication tolerances. The reflection coefficient response of all the ports was thus measured in order to assess this variation. These reflection coefficient results are presented in this Section.

Figure 5.9 presents the reflection coefficient response of the antenna measured at the four ports of the antenna (Port-N-E-W-S). While all the responses follow similar trends, Figure 5.9 shows observable differences between the reflection coefficient response at each port, particularly around 5 GHz, 6.5 GHz and 8 GHz. Figure 5.9 also shows that the four reflection coefficients remain below -10 dB from 4 GHz up to 10 GHz, except around 5.25 GHz, 8 GHz and 9 GHz, where the these coefficients go just above -10 dB. These results show close agreement with the simulation results of the reflection coefficient presented in Figure 5.6. Differences between the simulated and measured results, particularly at lower frequencies, can be attributed to fabrication tolerances, as well as to the parameters selected for the reduced size cavity and the length of the coaxial cable in the simulated model, whose radiation boundaries might have overlooked the overall response. The upper frequency limit of this bandwidth agreed with the maximum frequency response predicted for the coaxial bundle in Section 5.3.3.

The coupling between the radiating elements of the antenna was measured setting up the VNA in forward transmission mode. Port-1 of the VNA is connected to one port of the sinuous antenna, while adjacent and opposite ports are connected to Port-2 of the VNA at a time to measure the energy received by these ports. The differences between the coupling results obtained of Port-E, Port-N, Port-W and Port-S were not considerable. Thus, only the results using Port-E will be presented to simplify its interpretation. The adjacent port to Port-E (Port-N) and its opposite (Port-W) were connected to Port-2 of the

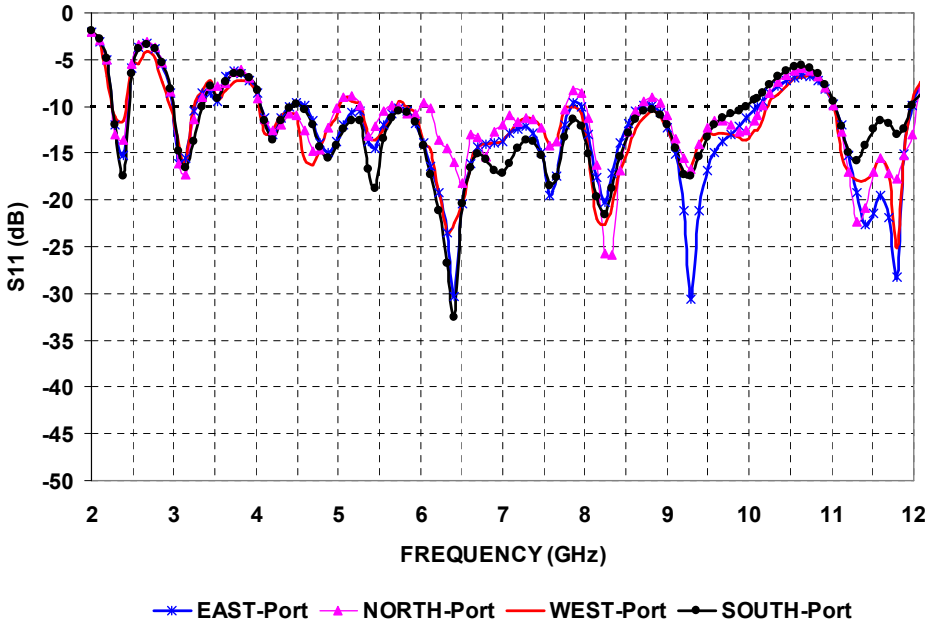

Figure 5.9: Reflection Coefficient Response of the Antenna Measure at the Coaxial Ports

VNA, one at a time to measure the energy received by these radiating elements when Port-E is transmitting. This energy defines the coupling factor between adjacent and opposite radiating elements. The inactive ports of the antenna were terminated to broadband $50\,\Omega$ loads.

Figure 5.10 shows the amount of energy that couples from Port-E to Port-N and Port-W. It shows that the energy coupled from opposite ports (Ports E-W and S-N) is all below -10 dB for the entire operational bandwidth of the antenna (4-10 GHz). It also shows that the energy coupled between adjacent ports (Ports E-N, E-S, W-N and W-S) is mostly below -10 dB except around three particular frequencies (5 GHz, 6.5 GHz and 8.25 GHz). These results provided similar coupling factors among the radiating elements of the antenna as observed in the simulated results shown in Figure 5.6.

Comparing Figures 5.9, 5.10 and 5.6 is clear that the designed bandwidth from 2–12 GHz of the sinuous antenna shown in Section 5.4 has been reduced with the realised antenna to 4–10 GHz, resulting in an impedance bandwidth of approximately 85%. As it was expected, the amount of energy coupled between ports was stronger between adjacent ports than opposite ports. Small differences between the reflection coefficient response at each port were present. These differences can be mostly attributed to impedance mismatched between the stripped coaxial cable of the bundle interface and the radiating elements of the antenna. These differences should not significantly modify the symmetry of the antenna.

5.5.2 RF Radiation Patterns Characterisation

Section 5.4 has shown that each radiating element of the sinuous antenna can be considered as an independent unbalanced generator feeding one normal mode of the sinuous antenna independently. These modes are characterised by a single beam radiation pattern

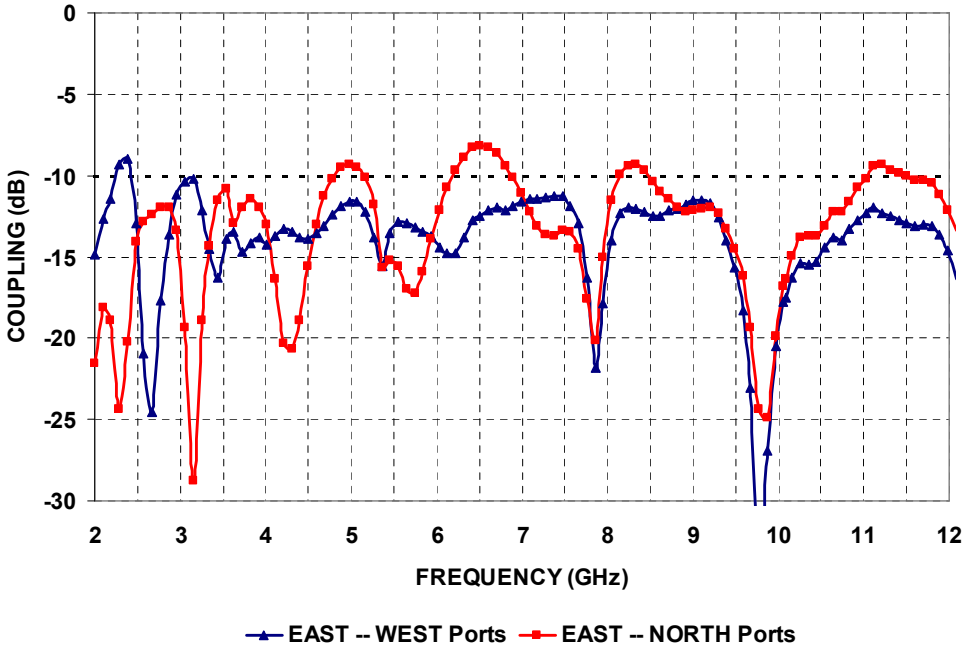

Figure 5.10: Coupling Factor Among Opposite and Adjacent Ports

which is tilted off bore-sight, in the same direction of the radiating element. Provided that the simulation results are correct and that the symmetry of the antenna has not been affected by the coaxial bundle, the radiation patterns response measured at the ports of the antenna should exhibit similar performances.

Monopole Radiation Patterns

Section 5.4 has shown that it is possible to obtained four symmetrical beams corresponding to each one of the four radiating elements of the antenna. In order to verify the simulation patterns and the symmetry response of the antenna, the radiation pattern performance of Port-E and Port-W of the realised antenna was individually characterised measuring the received power of Port-E and Port-W one at a time while the inactive ports were terminated to broadband $50\,\Omega$ loads.

The radiation pattern performance of the ports of the antenna were measured using a double ridged linearly polarised pyramidal horn antenna by ETS-Lindgren® as a transmitting source while the sinuous antenna was rotated around its azimuth axis (θ). The radiation pattern response was normalised to zero considering the maximum radiation power exhibited by the antenna at bore-sight direction.

Figure 5.11 shows the E-plane and H-plane radiation patterns exhibited by Port-E at 5 GHz. It shows that the antenna exhibits a single radiation beam facing at approximately $-22.5\,^\circ$ off bore-sight in the E-plane. This beam exhibits a $50\,^\circ$ 3 dB beam-width and a front-to-back ratio of approximately 15 dB. Figure 5.11 also shows that the radiation pattern on the H-plane exhibits a single beam pattern almost centered along the central axis of the antenna (bore-sight). This beam presents a 3 dB beam-width of approximately $60\,^\circ$ and front-to-back ratio of approximately 15 dB.

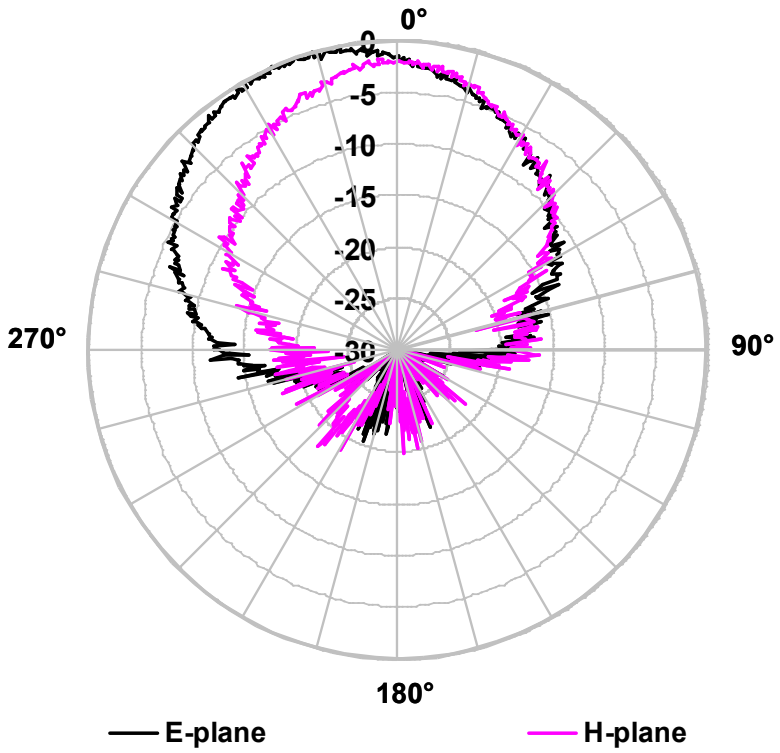

Figure 5.11: Port-E, E-plane and H-plane Radiation Pattern Response @ 5 GHz

Figure 5.12 shows the E-plane and H-plane radiation patterns exhibited by Port-W at 5 GHz. It shows that the antenna exhibits a single radiation beam facing at approximately $+22.5\,^{\circ}$ off bore-sight in the E-plane. This beam exhibits a $50\,^{\circ}$ 3 dB beam-width and a front-to-back ratio of approximately 15 dB. Figure 5.12 also shows that the radiation pattern on the H-plane exhibits a single beam pattern almost centered along the central axis of the antenna (bore-sight). This beam presents a 3 dB beam-width of approximately $60\,^{\circ}$ and front-to-back ratio of approximately 15 dB.

Although the H-plane radiation pattern response of both ports showed that the beams were slightly tilted, this tilting of the beam can be attributed to misalignment between the transmitting antenna and the plane of the antenna parallel to the surface of the sinuous antenna ($\theta = 90\,^{\circ}$).

The radiation pattern analysis of Port-E and Port-W confirms the simulation results presented in Section 5.4, providing considerable evidence that each port can be considered as an independent unbalanced source exciting one of the four normal radiation modes of the antenna. It is evident that four almost identical beams are exhibited by the radiating elements of the antenna, which are excited by the individual ports of the coaxial bundle. These results also confirms the symmetry of the sinuous antenna around its main axes.

Monopole Radiation Patterns Frequency Stability

Spiral and sinuous antennas share a fundamental fabrication characteristic, they can be considered as an array of multiple monopoles, folded in different geometries. As shown

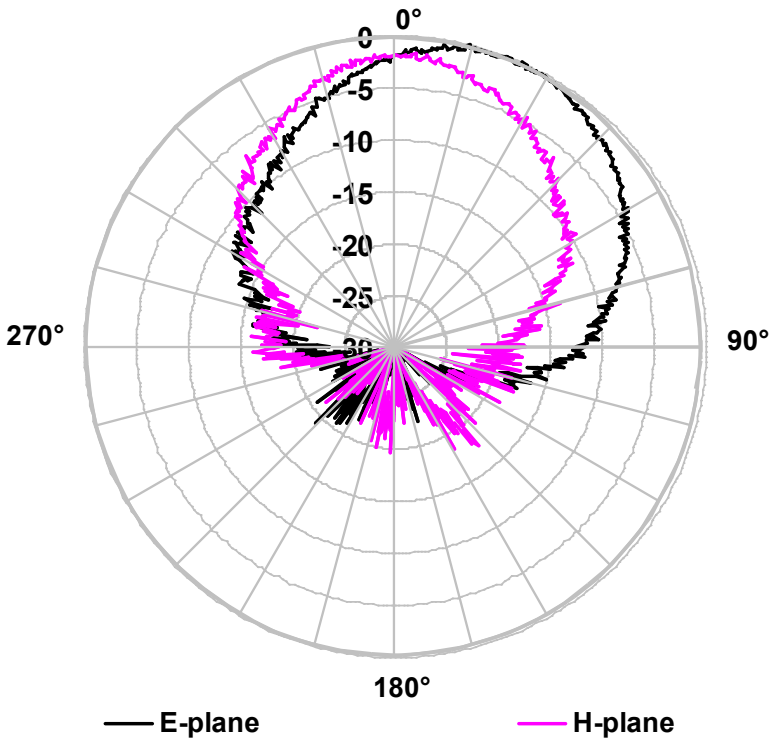

Figure 5.12: Port-W, E-plane and H-plane Radiation Pattern Response @ 5 GHz

in Section 4.4.3, the radiation patterns of a spiral antenna rotate progressively with the frequency as the effective radiation aperture travel along the spiral. This should not be the case for a sinuous antenna. In the sinuous antenna case, the alternating clockwise and counter-clockwise wrapping senses in each radiating element of the antenna might affect significantly the radiation pattern performance, making it wobble around the main polarisation axes of the antenna but will stop it from rotating around its central axis.

Previous investigation of sinuous antennas have shown that the vector orientation of the radiation modes exhibited by the sinuous antenna wobbles with frequency by only $\pm 4^\circ$ [68, 85]. A frequency sweep investigation attempted to find out whether the realised antenna also provides similar stability of the radiation characteristics of the antenna over its operational bandwidth. This was done measuring the H-plane radiation pattern response of single radiating element of the sinuous antenna (Port-E), as was done for the monopole response, at different discrete frequency points.

Figure 5.13 shows the E-plane radiation patterns of Port-E, measured at 5, 6, 7, 8 and 9 GHz. It shows that the radiation beam exhibited by Port-E remains facing at around 22.5° off bore-sight, demonstrating that the rotation of the radiation patterns of the normal modes of the sinuous antenna with the frequency can be considered negligible.

5.5.3 Monopole Radiation Patterns Summary

In summary, the radiation pattern characterisation of the sinuous antenna provides sufficient evidence to believe that each one of its radiating elements can be controlled in-

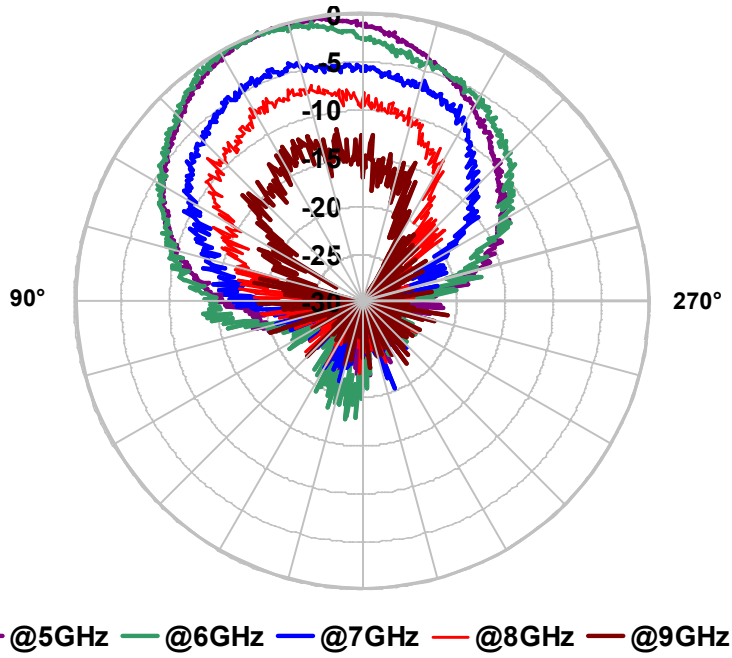

Figure 5.13: Radiation Patterns Stability. E-plane Frequency Sweep of Port-E

dependently. These radiation characteristics are effectively symmetric around the central axis of the antenna. The normal radiation modes of the sinuous antenna were proven to be more stable across its frequency bandwidth than rotating radiation patterns of the spiral antenna. This property is highly desirable for direction finding systems, where having an antenna whose directionality is frequency independent can provide information about the angle of arrival of a hostile signal across a broad frequency range. In this case the four normal modes of the sinuous antenna define four possible quadrants for detection.

5.5.4 Sinuous Antenna Radiation Modes Configuration

A multiple-arm sinuous antenna with an even number of radiating elements can be considered as an antenna with multiple dipoles antennas oriented around a common axis. Opposite radiating elements of the antenna form these dipoles, which can be employed to excite or receive multiple linear polarisations if phased correctly using a mode transformer. These mode transformers are traditionally balance to unbalance transitions (Baluns), microwave power dividers or microwave hybrid couplers networks that combine and transform the unbalanced normal modes of each radiating element into a balanced radiation mode that can be transmitted over traditional balanced transmission lines.

A relative phase difference of $180\,^{\circ}$ between the opposite ports of the sinuous antenna will generate a radiation mode corresponding to the 1^{st} order mode of a dipole. This mode is defined by a broad single beam radiation pattern with linear polarisation properties, facing at bore-sight direction [18].

This section presents the radiation characteristic of the antenna operating the ports in pairs and with a relative phase difference of $180\,^{\circ}$ to verify that the realised antenna presented in Section 5.5 could be operated as two orthogonal dipoles.

Dipole Radiation Pattern Response

Having demonstrated that each port of the realised sinuous antenna can be controlled independently to excite the normal mode of each one of the radiating elements of the antenna (Section 5.5.2), and that these modes are symmetric around the central axis of the antenna, this symmetry allows opposite ports of the antenna to be phased in pairs and operate as a dipole antenna.

As explained in Section 4.5.3, a dipole antenna presents a characteristic response to the polarisation pattern. Figure 4.10 a) shows the characteristic polarisation pattern of a dipole antenna and its polarisation ellipse. The minor and major axes of this polarisation ellipse will be used to define the electrical co-polar and cross-polar axes of the dipole.

The two dipoles of the sinuous antennas can be easily identified (North-South and East-West) by physically inspecting the structure of the antenna in Figure 5.5. These two orthogonal dipoles must be aligned with the H-plane and E-plane of the antenna test facility in order to be correctly characterised. Any misalignment of the axes will generate a decrement on the received power equal to $R\sin(\theta)$, where "R" is the maximum possible receiving power by the dipole and θ presents the angle difference between the axes of the polarisation ellipse of the antenna and the H-plane and E-plane of the antenna test facility [49].

Aligning the main axis of the dipoles was done by manually rotating the sinuous antenna around its central axis, while a linearly polarised horn antenna, aligned along the E-plane, transmitted a continuous wave signal at 5 GHz. The signal received by the sinuous antenna was measured using a $180\,^{\circ}$ microwave hybrid coupler. First, Port-E and Port-W were connected to the hybrid , allowing them to operate as a dipole, while Port-N and Port-S of the antenna were terminated to broadband $50\,\Omega$ loads. Then Port-N and Port-S were connected to the hybrid and Port-E and Port-W, terminated to broadband $50\,\Omega$ loads.

Once the axes corresponding to the polarisation ellipse are located along the H-plane and E-plane, the two dipoles of the sinuous antenna can be characterised. The sinuous antenna was characterised using the same technique used for measuring its four normal radiation modes presented in Section 5.5.2.

Figure 5.14 shows the 1^{st} mode radiation pattern of the dipole form by Port-E and Port-W. It shows that measuring the response of both ports through the differential output (Δ) of the hybrid coupler exhibits in a single broadside beam radiation pattern facing bore-sight with a 3 dB beam-width of approximately $80\,^{\circ}$. Figure 5.14 also shows the cross-polarisation response of this dipole, which is approximately 25 dB lower than the co-polarisation response of Port-E and Port-W of the sinuous antenna operating as a dipole.

Figure 5.15 shows the 1^{st} mode radiation pattern of the dipole form by Port-N and Port-S. It shows that measuring the response of both ports through the differential output (Δ) of the hybrid coupler exhibits in a single broadside beam radiation pattern facing bore-sight with a 3 dB beam-width of approximately $80\,^{\circ}$. Figure 5.15 also shows the cross-polarisation response of this dipole, which is approximately 20 dB lower than the co-polarisation response of Port-N and Port-S of the sinuous antenna operating as a Dipole antenna.

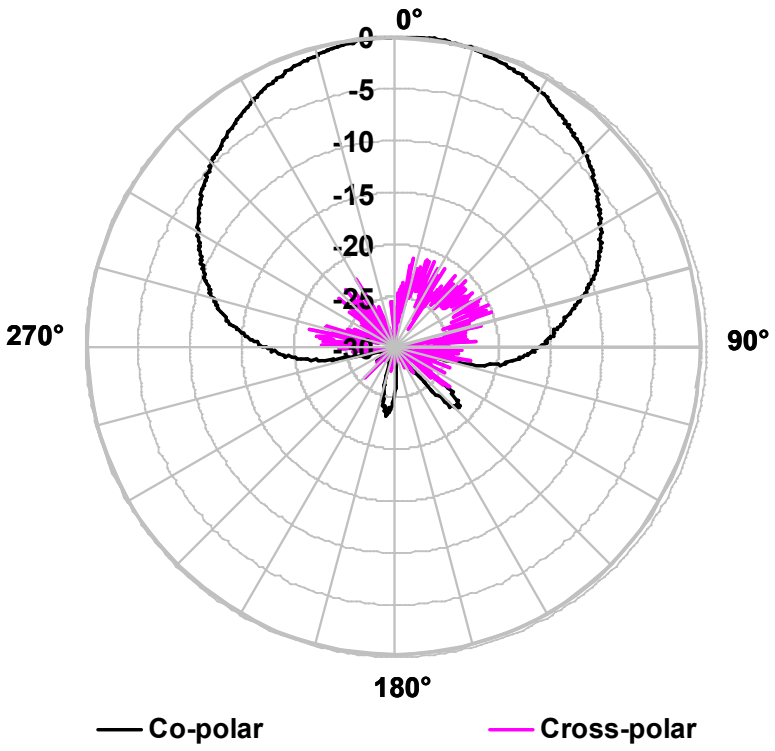

Figure 5.14: 1 st mode radiation pattern of Port-E and Port-W operating as a dipole

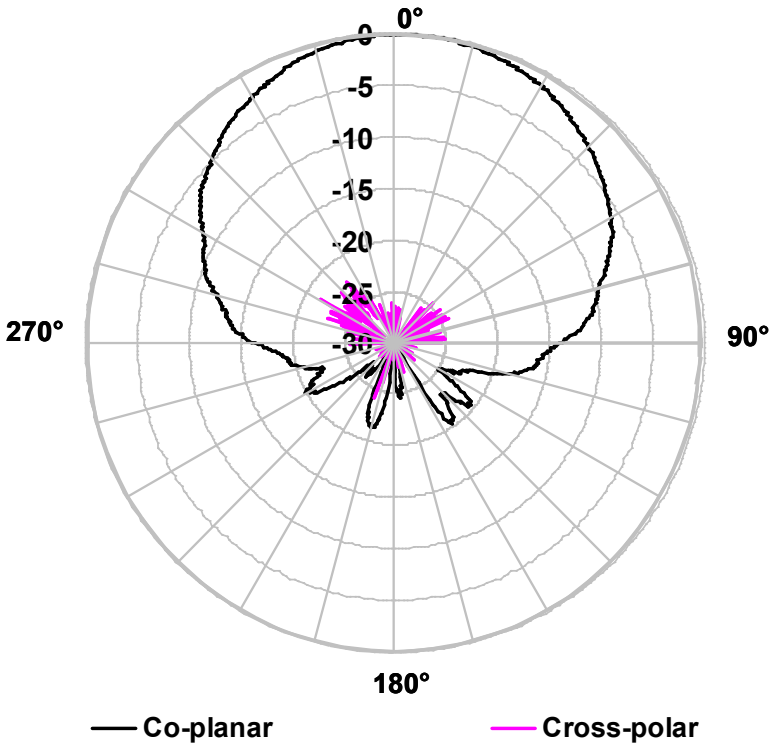

Figure 5.15: 1 st mode radiation patterns of Port-N and Port-S operating as a dipole

The radiation patterns shown in Figure 5.14 and Figure 5.15, correspond with the major and minor axes of the polarisation ellipse of both dipoles. These radiation patterns demonstrate that two linear polarisations can be effectively received by the sinuous antenna when two opposite radiating elements of the antenna are operating as a dipole antenna.

Dipole Higher Order Mode Radiation Patterns

Section 5.5.2 demonstrated that each radiating elements of the antenna can be operated independently. The relative phase among these elements can be controlled to generate the 2^{nd} order mode of a dipole antenna. Opposite radiating elements can be operated simultaneously and phased with a 0° phase difference to do this. This higher order mode is defined by a characteristic null at bore-sight direction and two opposite beams tilted off bore-sight. This section presents the 2^{nd} order mode radiation characteristics of the antenna.

The 2^{nd} order mode of the dipole formed by Port-E and Port-W and the dipole formed by Port-N and Port-S were measured by connecting them to the 180° microwave hybrid coupler as was done previously in this section for the 1^{st} order mode but this time the sum output of hybrid (Σ) was measured.

Figure 5.16 and Figure 5.17 shows the radiation patterns corresponding to the 1^{st} and 2^{nd} order modes of the two orthogonal dipoles of the sinuous antenna. The radiation patterns of the 2^{nd} order mode exhibit a null located at bore-sight, approximately 25 dB lower than their response in the 1^{st} order mode. These patterns show two beams facing at $\pm 22.5^\circ$ which exhibit a 3 dB beam-width of approximately 30°.

The comparison of the radiation patterns of the 1^{st} and 2^{nd} order modes of both dipoles demonstrate that the individual response of each port can be added coherently to form a single beam radiation patterns or two tilted beams facing at opposite directions.

5.5.5 Sinuous Antenna Circular Polarisation Configuration

The optimum function of the sinuous antenna is to operate as a dual circularly polarised antenna. Section 5.5.4 demonstrated that the sinuous antenna is able to receive two orthogonal linear polarisations. These orthogonal polarisations can be used to generate circularly polarised signals. A relative phase difference of 90° between two orthogonal linear polarisations generates a right hand circularly polarised signal, while -90°, generates a left hand circularly polarised signal.

Figure 5.18, shows the basic configuration required for measuring dual circularly polarised signals with a four-arm sinuous antenna. At the time of this investigation two 180° microwave hybrid couplers were not available for measuring both dipoles simultaneously. Therefore, the circularly polarised radiation patterns that can be obtained from the antenna, using a microwave mode transformer in Figure 5.18, will not be presented for the full characterisation of the sinuous antenna. Nevertheless, it is expected that these radiation patterns will exhibit similar performance to the individual radiation patterns to the performance of the dipoles presented in Section 5.5.4.

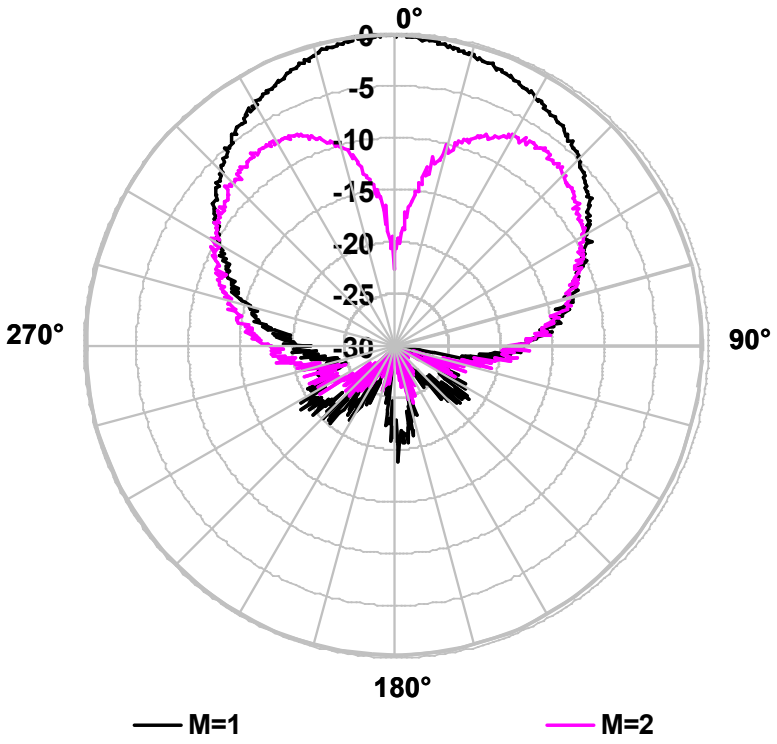

Figure 5.16: 1^{st} and 2^{nd} Order Radiation Patterns. Port-E and Port-W

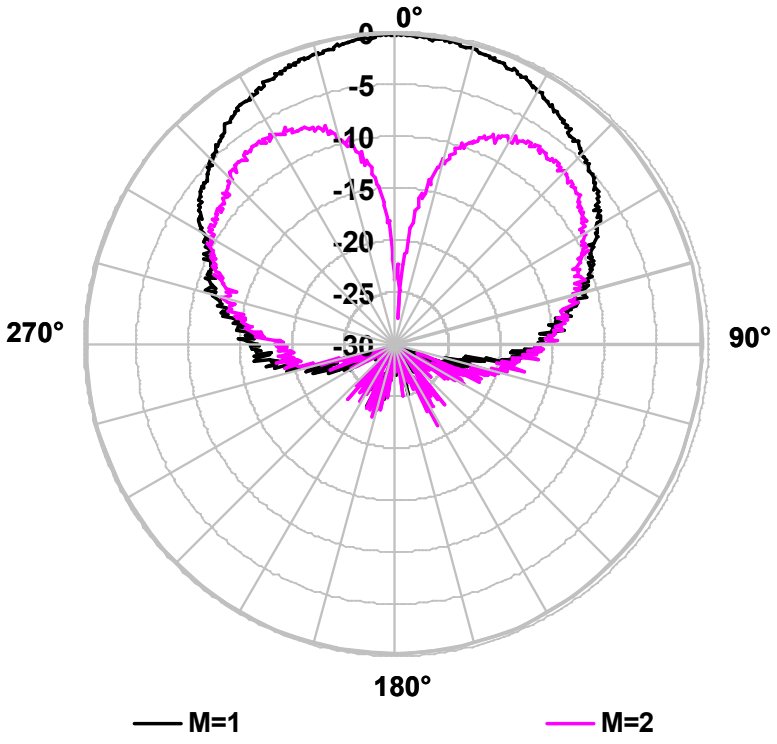

Figure 5.17: 1^{st} and 2^{nd} Order Radiation Patterns. Port-N and Port-S

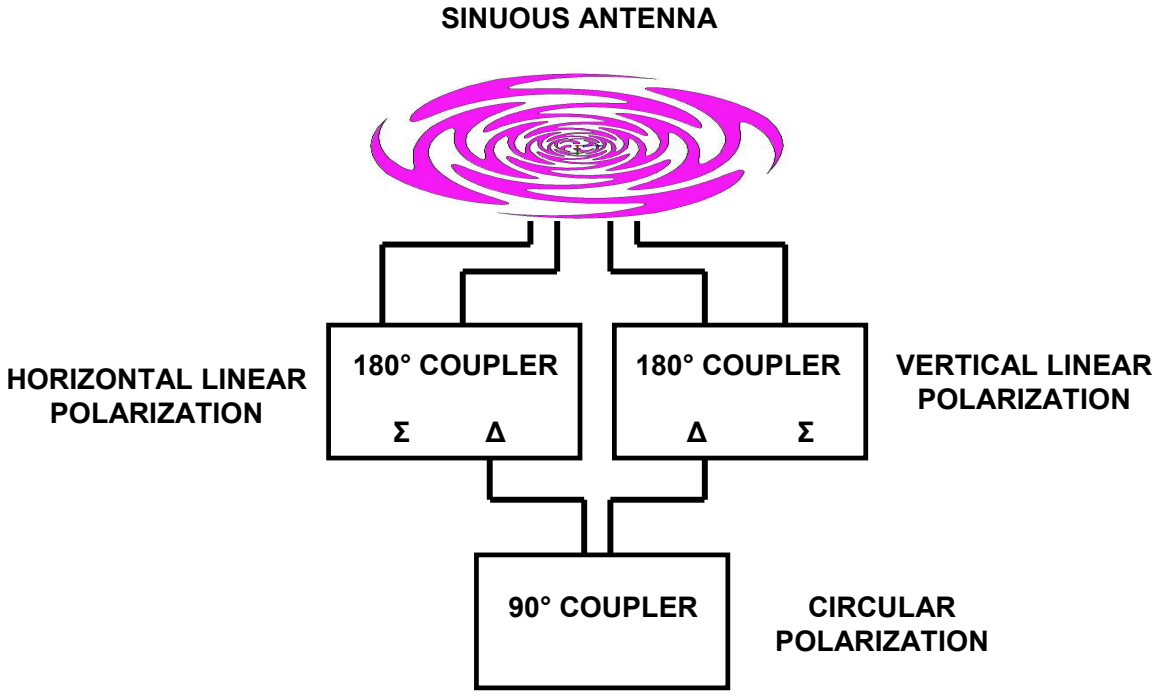

Figure 5.18: Basic Mode Transformer Network For Circular Polarisation Detection

5.5.6 RF Radiation Patterns Summary

The radiation pattern characterisation of the realised sinuous antenna has demonstrated that each one of its ports can be phased and controlled independently. Four normal mode radiation patterns defined by four beams tilted by approximately $22.5\,^{\circ}$ are effectively symmetric around the central axis of the antenna and represent four possible quadrants for signal detection.

This section has also demonstrated that operating these four normal modes in pairs and phasing them with a relative phase difference of $180\,^{\circ}$ or $0\,^{\circ}$ can generate the 1^{st} and 2^{nd} order modes of two orthogonally oriented dipoles.

These two dipoles can be operated simultaneously to generate dual circularly polarised signals by connecting the antenna to a microwave mode transformer formed by two $180\,^{\circ}$ microwave hybrid couplers and $90\,^{\circ}$ microwave hybrid coupler as shown in Figure 5.18. However, connecting the antenna in this way limits the antenna only to two possible circular polarisations. Measuring the individual response of each monopoles or operating the antenna as two dipoles will only be possible by disconnecting and changing from one port of the microwave hybrid couplers to another. This is not suitable for real applications and has shown to compromise the integrity of the antenna, as demonstrated in this Section. Nevertheless, the only way of characterising the RF response on this antenna is by this method and it should be employed again to characterise the radiation gain characteristics of the antenna across the entire operational frequency of the antenna.

5.5.7 RF Gain Characterisation

The relative gain of an antenna is defined as the ratio of the power in a given direction to the power of a reference antenna in its referenced direction. It represents another useful measure for describing the performance of the antenna because it also takes into account the efficiency of the antenna, not only the directivity, which is described by radiation patterns.

According to the gain transfer antenna characterisation method mentioned in Chapter 2 Section 2.2.1, two standard antennas of known characteristics can be employed in order to characterise the link gain of the system and obtain the relative gain of the antenna under test comparing its gain response with the response of the known antenna.

Considering that the self-complementary sinuous antenna exhibits a rotational symmetry around its central axis, and that its four radiating elements can form two dipoles orthogonally oriented, presenting the radiation characteristics of only the two components of the dipole formed by Port-E and Port-W should be considered as sufficient evidence of the overall performance of the antenna.

This section presents the individual and the combined gain characterisation of two opposite ports of the antenna (Port-E and Port-W) in order to investigate the performance of the normal modes of the antenna over the broadband impedance bandwidth (2–12 GHz), demonstrated in Section 5.5.

Monopole Gain Characterisation

Comparing the individual gain performance characterisation of Port-E and Port-W should confirm if the symmetry of the four radiating elements show in Section 5.5.2 remains constant across the entire operational frequency of the sinuous antenna.

The individual gain response of Port-E and Port-W (Horizontal Dipole) was characterised using the antenna gain transfer method. Port-E and Port-W were connected to a $180\,^{\circ}$ microwave hybrid coupler and measured individually by connecting only one port at a time to one input of hybrid coupler, while all the inactive ports of the hybrid coupler and the antenna were terminated to $50\,\Omega$ broadband loads.

Two Double Ridged Pyramidal Horn antenna, model 3115 by ETS-Lindgren® were used to characterised the system link gain and measured the response of the sinuous antenna. One of them, for transmitting a linearly polarised signal inside the anechoic chamber, and the other as the known standard antenna, which was used as a reference for normalising the sinuous antenna response.

Figure 5.19 shows the individual gain response of Port-E and Port-W. It shows that the individual responses follow similar trends, with particular differences around 5.5 GHz and 9.25 GHz. These two gain responses has a 3 dB gain bandwidth from 3.5 GHz to 10.5 GHz and exhibit two characteristic gain increments at the start and the end of their 3 dB gain bandwidths. A difference of approximately 1 dB in present between these two responses. The gain response of Port-E presents a higher amplitude variation than Port-W. This variation can be attributed to some fabrication tolerances at the interconnection between the radiating element of the antenna and the coaxial bundle.

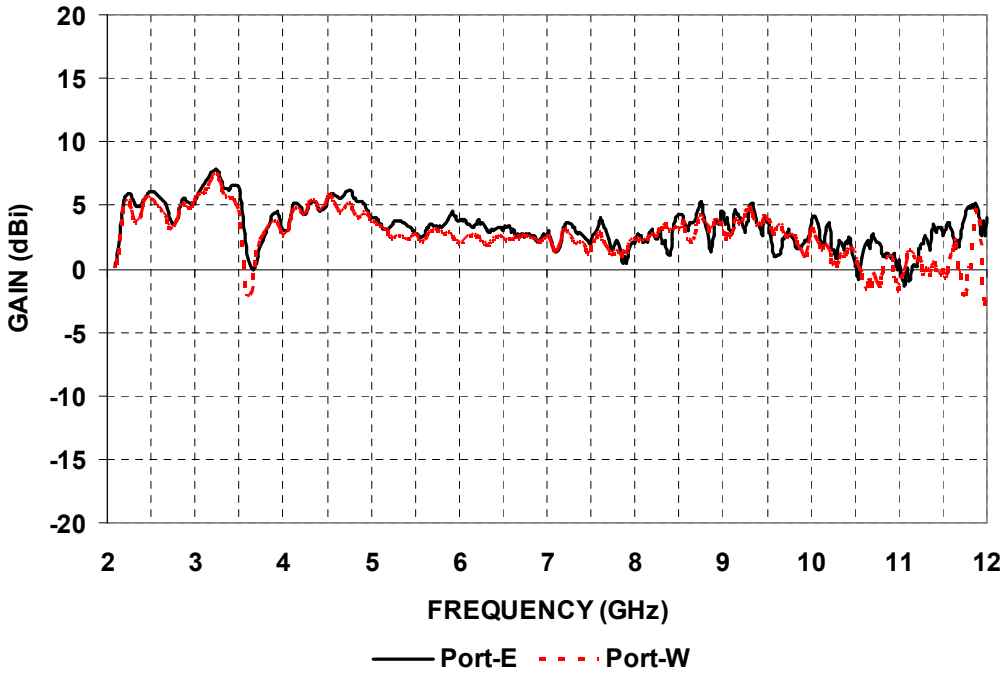

Figure 5.19: Port-E and Port-W. Monopole Gain Characterisation

The similarity between the gain response of the ports shown in Figure 5.19 together with the radiation patterns of each port presented in Section 5.5.2, provide enough evidence to confirm that the four radiating elements of the sinuous antennas are fairly symmetric around the central axis of the antenna across its entire operational bandwidth.

Dipole Gain Characterisation

Although the frequency response of the antenna can be limited by the moderated frequency bandwidth of the $180\,^{\circ}$ microwave hybrid coupler, the combined gain response of the horizontal dipole formed by Port-E and Port-W and the vertical dipole formed by Port-N and Port-S can be investigated.

The gain response of the horizontal dipole was investigated by connecting both ports (Port-E and Port-W) to the $180\,^{\circ}$ microwave hybrid coupler simultaneously and measuring first the differential output (Δ) and then the sum output (Σ) of the hybrid as was done in Section 5.5.4.

Figure 5.20 shows that the combined response of the horizontal dipole operating in its 1^{st} order mode (Δ) and its 2^{nd} order mode (Σ), compared to the individual gain response of Port-E. It shows that the gain response of the 1^{st} order mode of the horizontal dipole exhibits a gain level difference related to the individual response of Port-E of approximately 6 dB along the entire frequency bandwidth, except around 9.5 GHz, where this difference is around 2 dB. The gain response at bore-sight of the horizontal dipole operating in 2^{nd} order mode, corresponds to the location of the null shown in Figure 5.16 and remains below -5 dBi from 2–10 GHz, exhibiting a relative difference with its 1^{st} order mode response of approximately 10 dB.

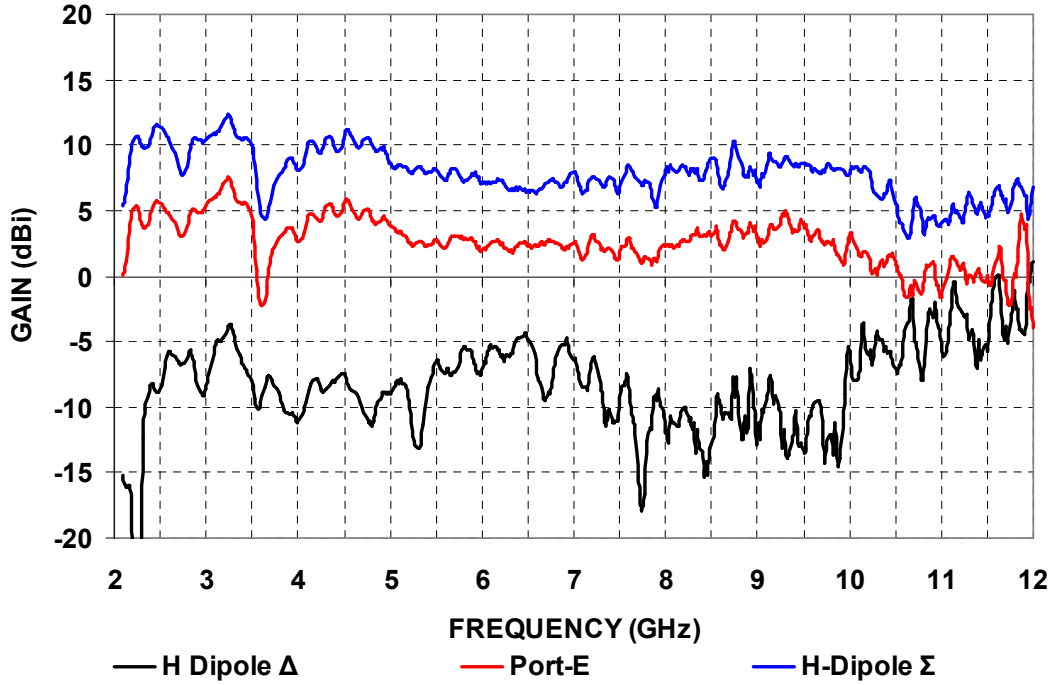

Figure 5.20: Port-E and Port-W. Horizontal Dipole Gain Characterisation

These results complement the radiation patterns characterisation presented in Section 5.5.4 confirming that the four normal modes of the antenna can be combined coherently to generated the 1^{st} and 2^{nd} order modes of two orthogonal dipole antennas. These radiation modes corresponds to the M=1 and M=2 radiation modes of the sinuous antenna described in Figure 4.2.

Dipoles Co-polarisation and Cross-polarisation Performance

Having demonstrated in Section 5.5.2 that the radiation characteristics of the sinuous antenna are symmetric around its central axis, and that the gain response of these modes exhibits similar performance. Investigating the cross-polarisation response should confirm if the performance of the sinuous antenna operating as two orthogonal dipoles is uniform across the entire operational bandwidth of the antenna.

The gain characterisation of the horizontal dipole formed by Port-E and Port-W has been already presented. Therefore, this section will use the gain characterisation of the vertical dipole, formed by Port-N and Port-S, to show the co-polar and cross-polarisation performance response of this dipole. Having demonstrated in Section 5.5.2 that the four port are symmetric around the central axis of the antenna, it is evident that this response will also correspond with the performance of the horizontal dipole.

The vertical dipole form by Port-N and Port-S was aligned with the polarisation of the transmitting horn antenna in order to measure its co-polarisation response as was done previously in this section for the horizontal dipole. Then, the polarisation of both antenna were aligned orthogonally, by rotating the horn antenna 90° around its central axis, in order to measure its cross-polarisation response.

Figure 5.21 shows the comparison of the co-polarisation and cross-polarisation characteristics of the dipole formed by Port-N and Port-S, when added coherently by the microwave 180 ° hybrid coupler to operate in mode M=1. It shows that the cross-polarisation of this dipole exhibits an inverted sinusoid response from 4–10 GHz, which peaks at the centre of the band and ranges between -5 dBi and -20 dB across the band.

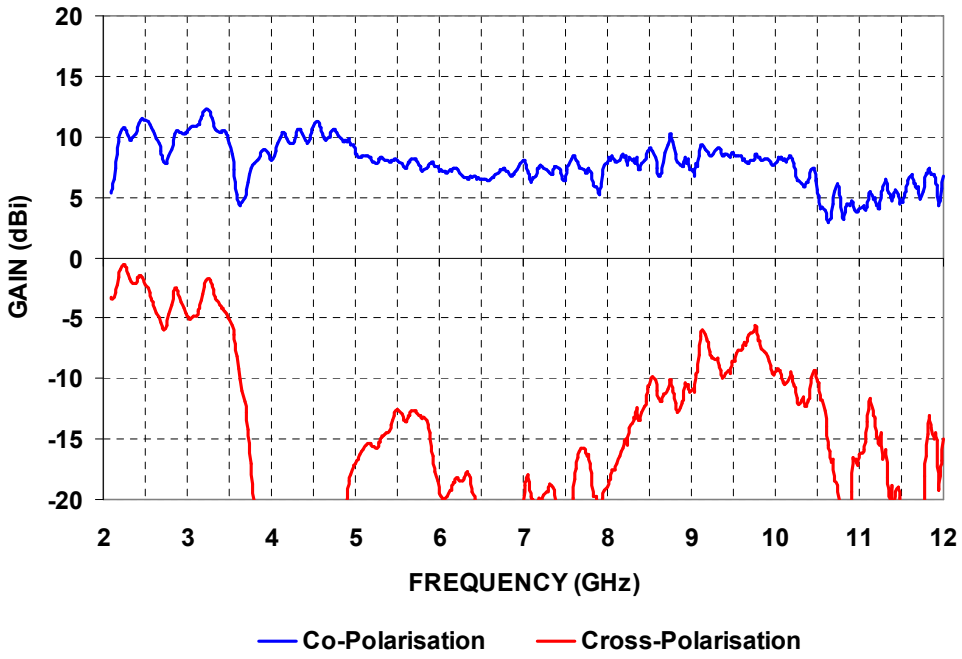

Figure 5.21: Vertical Dipole. Co-polar and Cross-polarisation Gain Characterisation

The co-polar and cross-polarisation gain characterisation presented in Figure 5.21 demonstrates that the performance of the sinuous antenna working as two orthogonal dipoles is acceptable around its centre frequency but might not at the edges of its operational bandwidth. These results clearly shows that the capability of the sinuous antenna to differentiate orthogonal polarisations gets reduced particularly at the upper limits of its operational bandwidth. This can be attributed to the fact that the feeding point of the antenna has been modified to allocate and enable a reliable interconnection between the coaxial bundle and the radiating elements of the antenna, as shown in Figure 5.4.

5.5.8 RF Gain Analysis Summary

In summary, the RF analysis of the sinuous antenna demonstrated that the radiation characteristics of the antenna are limited by the coaxial bundle and the reduced size cavity. It effective operational bandwidth is 4–10 GHz. It also demonstrated that each radiating element of the antenna measured through the ports of the bundle exhibits a characteristic radiation mode facing in the direction of the main axis of the radiating elements of the sinuous structure, and that a 180 ° inherent relative phase difference is present between the signal received by opposite ports. These radiation characteristics remain constant across the entire operational bandwidth of the sinuous antenna, allowing it to be operated as

four individual elements or two orthogonal dipoles. However, the radiation characteristics of each dipole its moderated, exhibiting an optimum performance around the centre and lower frequencies of the operational bandwidth of the sinuous antenna.

5.6 Microwave Photonic Techniques for Controlling Multiple Antenna Radiation Modes

Section 5.2, 5.3, 5.4 and 5.5 have shown that a four-arm sinuous antenna is a single aperture antenna that can receive four normal radiation modes, corresponding to the four radiating element of the antenna, over a broadband frequency range. These modes define four possible detection quadrants and can be controlled to detect multiple polarisations and different radiation modes using mode transformer networks. These networks are normally composed of tapered-line magic-T's, phase difference circuits, isolated power dividers and quadrature hybrid couplers [85]. These networks are also known as Butler matrices. In most cases, these networks generally limit the versatility of the system, restricting the antenna to specific modes and not providing individual control of the normal modes of the antenna. Further more, instantaneous measurements using these networks are only possible if multiple receivers are employed, or high frequency microwave switches select from one mode to another. These approaches increase weight, volume and complexity, and make the latency of the system dependent on the rapid response of the switches.

It is here where Microwave Photonics represent an opportunity over traditional microwave mode transformer networks. Instantaneous measurement of the normal modes of the antenna can be done over a broadband range of frequency using Microwave Photonics, provided that each radiating element of the antenna is broadband matched to impedance of electro-optical modulators. Once the modulator converts the electrical signals onto the optical domain, multiple microwave signal processing techniques, normally realised by a complex microwave Butler matrix can be reproduced using photonic signal processing techniques.

The following Sections will introduce these Microwave Phonic techniques, proposed to implement a Microwave Photonic Mode Transformer that will control the multiple radiation modes and polarisations of the sinuous antenna. First, a Microwave Photonic quadrature hybrid coupler implementation based on photonic transversal filtering techniques will be introduced. This implementation will be adjusted to cover the frequency bandwidth of the sinuous antenna shown in Section 5.5. Then, this $90\,^{\circ}$ Microwave Photonic hybrid coupler will be combined with the previous demonstration of a $180\,^{\circ}$ Microwave Photonic hybrid coupler presented in Chapter 4 in order to form the Microwave Photonic Mode Transformer proposed to replace the Butler matrix shown in Figure 5.18. This network is characterised in terms of amplitude and phase response of each port. Finally, this Mode Transformer will be connected to the sinuous antenna presented in Section 5.5 and the complete system is characterised. This characterisation will be compared with the RF characterisation of the sinuous antenna conducted in Section 5.5, so it can be demonstrated that this implementation improves and extends the mode transformation performance of the microwave Butler matrix shown in Figure 5.18 over a broadband frequency range with minimum phase and amplitude variations.

5.6.1 Photonic Quadrature Hybrid Coupler Concept

A method that creates a quadrature phase signal and could substitute the 90° hybrid coupler in Figure 5.18 is the Hilbert Transformation. A Hilbert Transformer is a type of filter that changes only the phase of the spectral components of a signal, depending on the sign of their frequency. Appendix B presents an overview and mathematical treatment of the Hilbert transform. In particular, Appendix B shows that the Hilbert transform can be realised as an finite impulse response or transversal filter which may be realised photonically.

This section aims to show that a broadband 90° phase shift can be achieved in the optical domain and substitute the hybrid coupler shown in Figure 5.18 using the Hilbert Transformation and photonic transversal filtering techniques.

Photonic Transversal Filtering

Photonic transversal filtering [91, 95], is a technique where the RF signal is modulated onto several optical carriers (or taps) and each tap is delayed by a different amount of time before summation and detection.

The frequency response of the summation of these delayed taps will be the Fourier Transformation of the impulse response as shown in Figure 5.22. Figure 5.23 shows the basic scheme of the transversal filter concept.

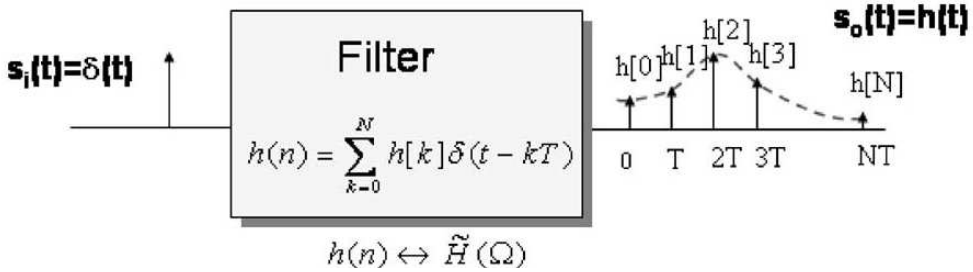

Figure 5.22: Transversal Filter Response

It can be seen that by adjusting the tap weights to positive or negative values a any time domain response can be achieved. The filter function, which is the Fourier Transformation of this time domain response is thus highly flexible.

Photonic Quadrature Hybrid Coupler

Appendix B shows that convolving any given signal g(t) with the function $\frac{1}{\pi}\,t$ can provide a relative phase shift of 90° to the signal. The Fourier Transformation of the impulse response $\frac{1}{\pi}\,t$ is a signum function (sgn(t)) and defines the Hilbert Transformation. This function extends infinitely and exhibits negative coefficients in the time domain.

By controlling the relative weights and delays of each sample of the signal, a convolution of the signal with the $\frac{1}{\pi}\,t$ function can be generated. For practical implementations of this function it is necessary to truncate this response by a finite number of samples and create positive and negative coefficients. These samples must be shifted in time. Using

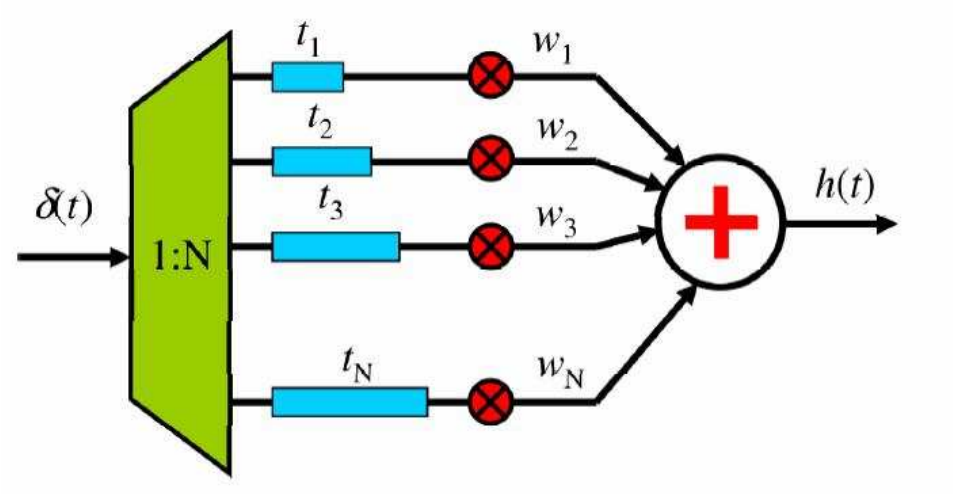

Figure 5.23: Block Diagram of a Transversal Filter

transversal filtering techniques in the optical domain, one could reproduce this convolution, in order to achieve a $90\,^{\circ}$ phase shift of the signal, using Microwave Photonics.

A recent implementation of a photonic quadrature hybrid coupler using transversal techniques has been demonstrated [96]. Figure 5.24 shows a reduced number of taps of an RF signal that reproduce the impulse response ($\frac{1}{\pi}\,t$). This response corresponds to the Hilbert Transformation of the signal. Each tap is generated by modulating the RF signal using single input electro-optic modulators. These modulated signals are delayed in time passing them through a determined length of dispersive fibre and including extra length of transmission line to reproduce the impulse response ($\frac{1}{\pi}\,t$). This implementation relies on the counter phase modulation of Mach-Zehnder external modulators [90] to create the negative coefficients of the Fourier response of the $\frac{1}{\pi}\,t$ function. Figure 5.25 shows the amplitude response of the photonic quadrature coupler when the impulse response ($\frac{1}{\pi}\,t$) is truncated to a discrete number of taps (2, 4 and 6) and the time delay ($\tau = 50\rho$) between the samples is such that the transversal filter response covers a frequency bandwidth from 2–18 GHz.

Figure 5.25 shows that the amplitude ripple of the band-pass of the realised filter is related to the number of taps used to define the convolution of the signal with the $\frac{1}{\pi}\,t$ function.

From Figure 5.25 it is evident that two taps can provide a 3 dB bandwidth of 5-15 GHz. This is close to the bandwidth of the sinuous antenna characterised in Section 5.5. Thus, for the remainder of this section it was considered that two taps could provide an acceptable performance for the quadrature hybrid function of the Butler matrix, shown in Figure 5.18.

5.6.2 Photonic Quadrature Hybrid Coupler Implementation

This section describes the configuration of a two tap photonic quadrature hybrid coupler [97], where the performance of the transversal filter is designed to match the frequency of operation of the sinuous antenna (4-10 GHz), shown in Section 5.5.

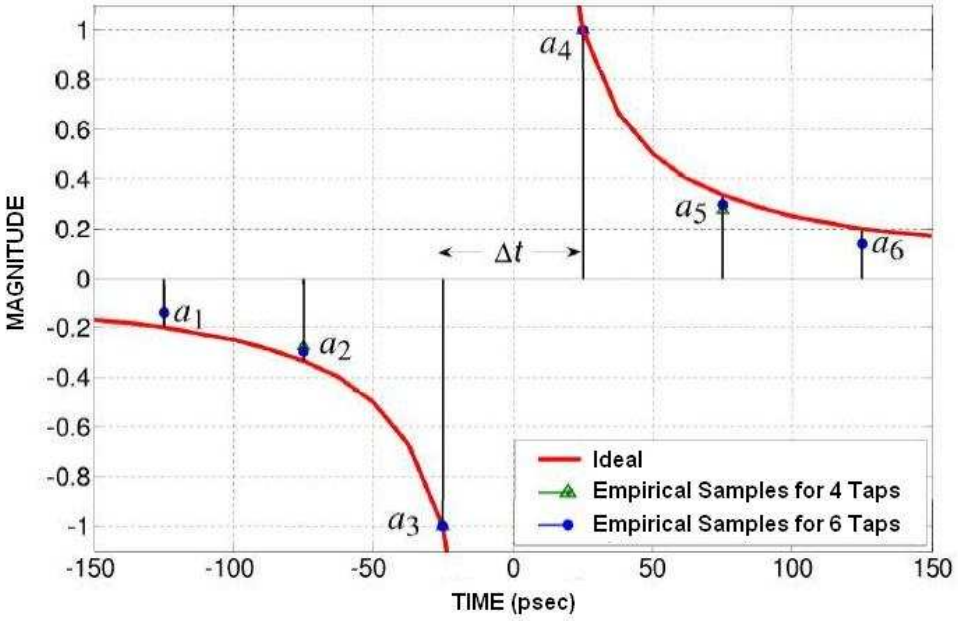

Figure 5.24: Taps of the Impulse Response $\frac{1}{\pi}\,t$ [97]

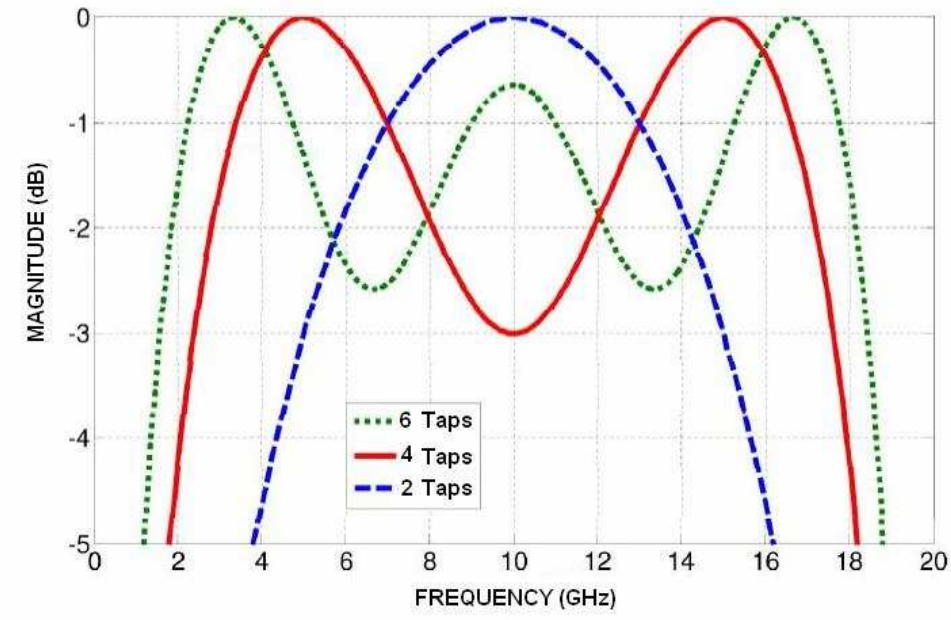

Figure 5.25: Hilbert Transform Response of the Truncated Impulse Response ($\frac{1}{\pi}\,t$) [97]

Figure 5.26 shows the block diagram of the photonic hybrid implementation. Three different wavelength and three single electro-optic modulators are used. One of the wavelengths carries the reference signal ($0\,^{\circ}$) while the other two form the taps of the impulse response.

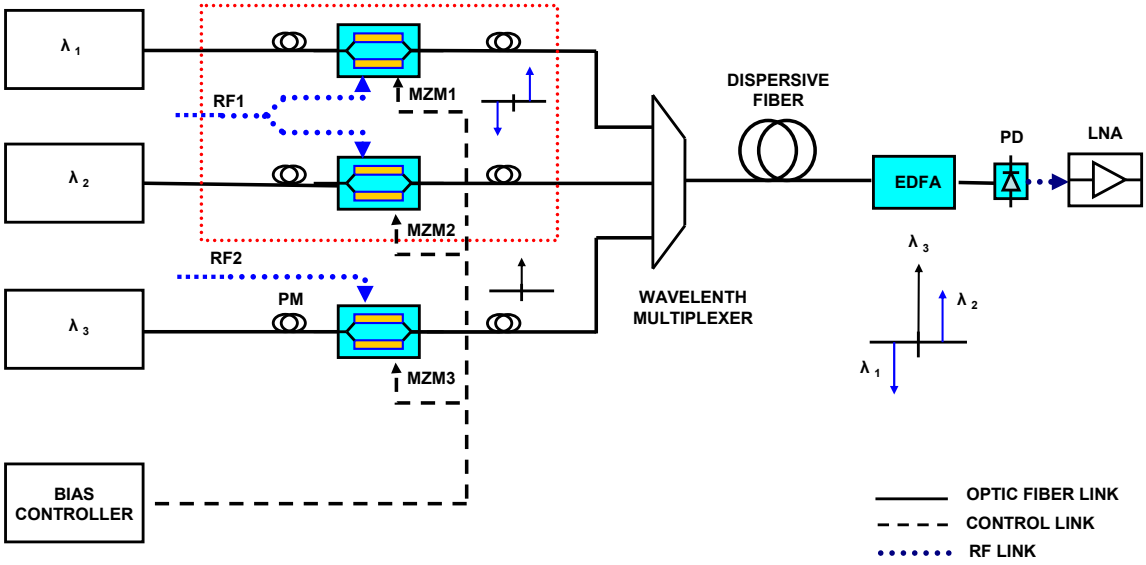

Figure 5.26: Photonic Quadrature Hybrid Coupler

Figure 5.26 shows three different wavelengths connected to three single input electro-optic modulators (MZM1-MZM3). The outputs of the modulators are then combined using another arrayed waveguide grating (AWG2) into a single optical link. The combined wavelengths are then connected to a length of dispersive fibre and amplified by an Erbium Doped Fibre Amplifier (EDFA) before being converted back into the RF domain by an AC coupled Photo Detector. A 3 dB microwave power divider is connected to the RF inputs of MZM1 and MZM2. Table 5.3 summarises the required configuration of the electro-optic modulators.

Table 5.3: Photonic Quadrature Hybrid Coupler Configuration

Laser	λ(nm)	MZM	Bias	Taps
λ_1	1542	MZM1	$V_{q+2\pi}$	$90\,^{\circ}$ 1^{st}
λ_2	1543.42	MZM2	V_q	$90\,^{\circ}$ 2^{nd}
λ_3	1545.06	MZM3	$V_{q+2\pi}$	$0\,^{\circ}$

It is evident from Figure 5.26 that each wavelength passing through the length of dispersive fibre will experience different time delays. These delays must be equalised and adjusted, modifying the path length of the links of the system so the reference signal (MZM3) can be located between the two taps (MZM1 and MZM2). This will enable the coherent detection of the two links by the photo detector, achieving a relative phase difference of $90\,^{\circ}$ according to the Hilbert Transformation concept.

Path Length Equalisation

The path lengths of the links shown in Figure 5.26 can be modified by including variable optical lines or variable microwave phase shifters, so all the modulated signals arrive at the photo detector at the same time for their coherent detection. This extra length can be calculated using $\Delta L=\tau(c/\epsilon_r)$, where τ is the time delay required to shift the taps to the required position in time, c is the speed of light in free space ($3x10^8$ m/s) and ϵ_r is the relative permittivity of the dielectric of the transmission line. τ correspond to $\tau = D\Delta\lambda L$, where D is the dispersion constant of the fibre and L is the length of dispersive fibre.

Equalising the path lengths of the links was done using as a reference the time delay between λ_1 and λ_2, which defines the 1^{st} and 2^{nd} taps of the impulse response and are the last ones to arrive at the photo detector. This time delay is approximately 64.028ρs. Semi-rigid coaxial cables with polytetrafluoroethylene (PTFE) dielectric (ϵ_r=2.1) were trimmed to provide the required extra length of transmission line. The extra length of RF cable was calculated considering a dispersive fibre with D = 17ps/nm.km and L = 2.354 km. In-line DC – 20 GHz phase shifters, manufactured by Aeroflux® (model PV-18), were connected to the input of the modulator for a fine tuning adjustment.

The extra length of semi-rigid coaxial cable required to delay the tap modulated by MZM3 by 96.042ρs resulted in a 9.94mm extra length. Locating the MZM3 tap between the taps modulated by MZM1 and MZM2 should result in two RF signals detected at the photo detector with a relative phase difference of 90° [96]

Potential Simplifications

It is worth noting that replacing the two oppositely biased modulator with a single balanced output modulator with complementary outputs, could eliminate the need for a RF power divider as well as simplify path length equalisation, reduce components and splitting losses [91, 98]. However, it is beyond the scope of this dissertation.

Photonic Quadrature Hybrid Coupler Characterisation

This section presents the characterisation of the two taps photonic hybrid coupler explained in Section 5.6.1. This Microwave Photonic implementation was tested using a 20 GHz Anritsu vector network analyser, model 33473. The output of the EDFA in Figure 5.26 was split into two portions by a 10% optical coupler for monitoring purposes. The 10% portion was input to an optical spectrum analyser (OSA) to monitor the amplitude of each tap and the 90% portion was input to the broadband Photo Detector (PD) which is connected to the Port II of the vector network analyser. Port I of the vector network analyser generated the testing signal which was used to feed the RF inputs, the reference link (RF1) and the quadrature link (RF2).

Figure 5.27 shows the relative phase response of the links of this implementation referenced to RF2. It is evident that RF1 exhibits a 90° phase shift with respect to RF2 over the desired frequency bandwidth.

Figure 5.28 shows the gain comparison of the links of the photonic hybrid coupler referenced to RF2. It shows that the gain difference between RF1 and RF2 exhibits a si-

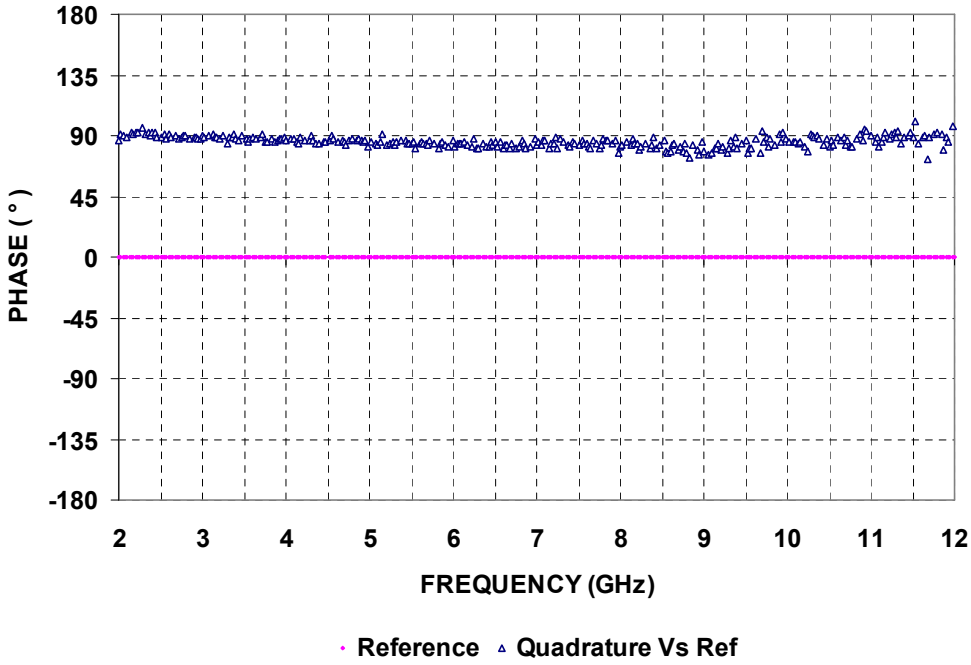

Figure 5.27: Relative Phase Difference of the Photonic Quadrature Hybrid Coupler Links

nusoidal response with a 3 dB gain bandwidth from 4–10 GHz. The maximum gain value of RF1 equals the gain level of the reference link (RF2) at the middle of the operational frequency bandwidth designed for this photonic hybrid coupler.

The relative phase and gain response of the photonic hybrid coupler in Figure 5.27 and Figure 5.28 shows excellent results. The two RF inputs of the photonic hybrid coupler are effectively shifted by a relative phase of $90\,^{\circ}$ respect to the reference link (RF2, $0\,^{\circ}$) and can be measured using a single optical link.

Having demonstrated that the photonic hybrid coupler presented in [97] provides a relative phase shift $90\,^{\circ}$ over the desired bandwidth, it should be possible to combine this photonic quadrature hybrid with the $180\,^{\circ}$ photonic hybrid presented in Chapter 4, in order to reproduce the butler matrix shown in Figure 5.18, using Microwave Photonics and a single optical fibre link. The frequency bandwidth of this implementation should only be limited by the bandwidth of the modulators and the operational bandwidth selected for the $90\,^{\circ}$ photonic hybrid coupler, which in this application has been designed to operate with a 3 dB bandwidth from 4–10 GHz. This bandwidth matches the operational bandwidth of the sinuous antenna shown in Section 5.5.

5.7 Photonic Mode Transformer

Having demonstrated in Chapter 4 that a $180\,^{\circ}$ hybrid coupler can be implemented using two electro-optic modulators biased at opposite quadrature, and also having demonstrated in Section 5.6.2 that a quadrature hybrid coupler can be achieved using photonic transversal techniques these implementations can be combined together using photonic multiplexing techniques to replace the Butler matrix shown in Figure 5.18. The following

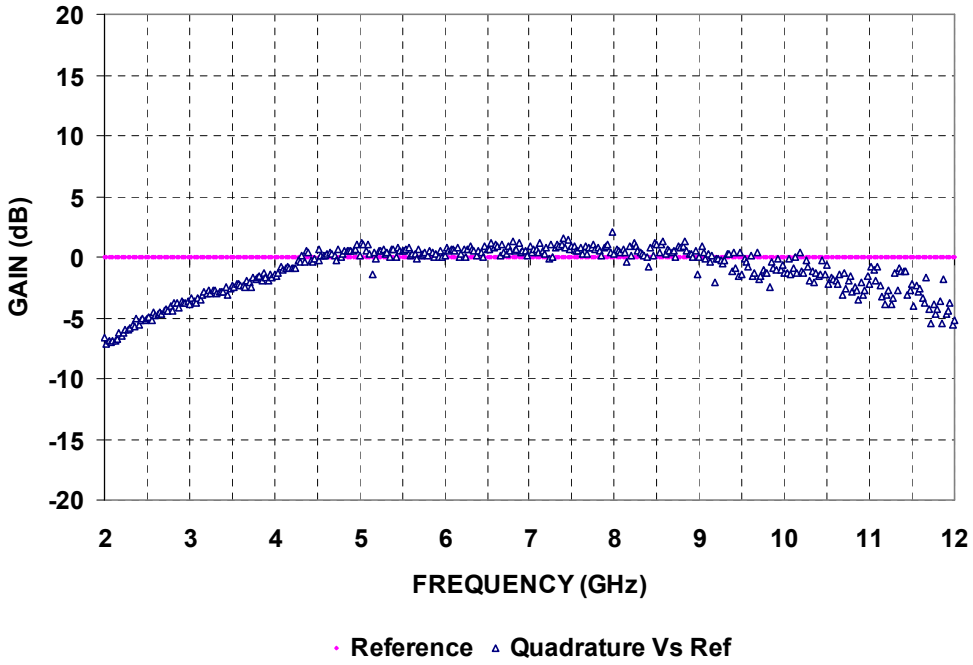

Figure 5.28: Relative Gain Difference of the Photonic Quadrature Hybrid Coupler Links

section presents a photonic version of the Butler matrix which is not only able to configure a four-arm sinuous antenna to receive right and left hand circular polarisation but also to receive several other radiation modes using a single fibre optical link.

Figure 5.29 shows the schematic of the Microwave Photonic configuration designed to receive the multiple polarisations and radiation modes of a four-arm sinuous antenna. Two photonic quadrature hybrid couplers and two single modulators biased in opposite quadrature were employed. A laser array provides the six different wavelengths multiplexed into a single optical fibre required for this implementation. These wavelengths are de-multiplexed using an arrayed waveguide grating (AWG1) [55, 56] and connected to six single input electro-optic modulators (MZM1-MZM6). The outputs of the modulators are combined using another arrayed waveguide grating (AWG2) into a single optical link. The combined wavelengths are then connected to a length of dispersive fibre and amplified by an Erbium Doped Fibre Amplifier (EDFA) before being converted back into the RF domain by an AC coupled Photo Detector (PD). Two 3 dB microwave power dividers are connected to the RF inputs of MZM1 and MZM2; and MZM4 and MZM5, respectively.

The six electro-optic Mach-Zehnder Modulators, were in-house made modulators electro-packaged by Micreo Limited, Australia, model number 592-BPH02 and were part of an array of modulators shown in Figure 5.33. The photo detector was manufactured by U^{2}T®, model XPDV2120R (PD). The AWGs of the system were two 8-channel 100 GHz Gaussian Wavelength Division Multiplexers by ANDevices®, model APMMUX1100. The 3 dB microwave power dividers were two Wilkinson 2-18 GHz power dividers manufactured by Norsal Industries®, model 8121.

The modulated signals travelling through the links of the photonic mode transformer shown in Figure 5.29 experience different time delays as they pass through the dispersive

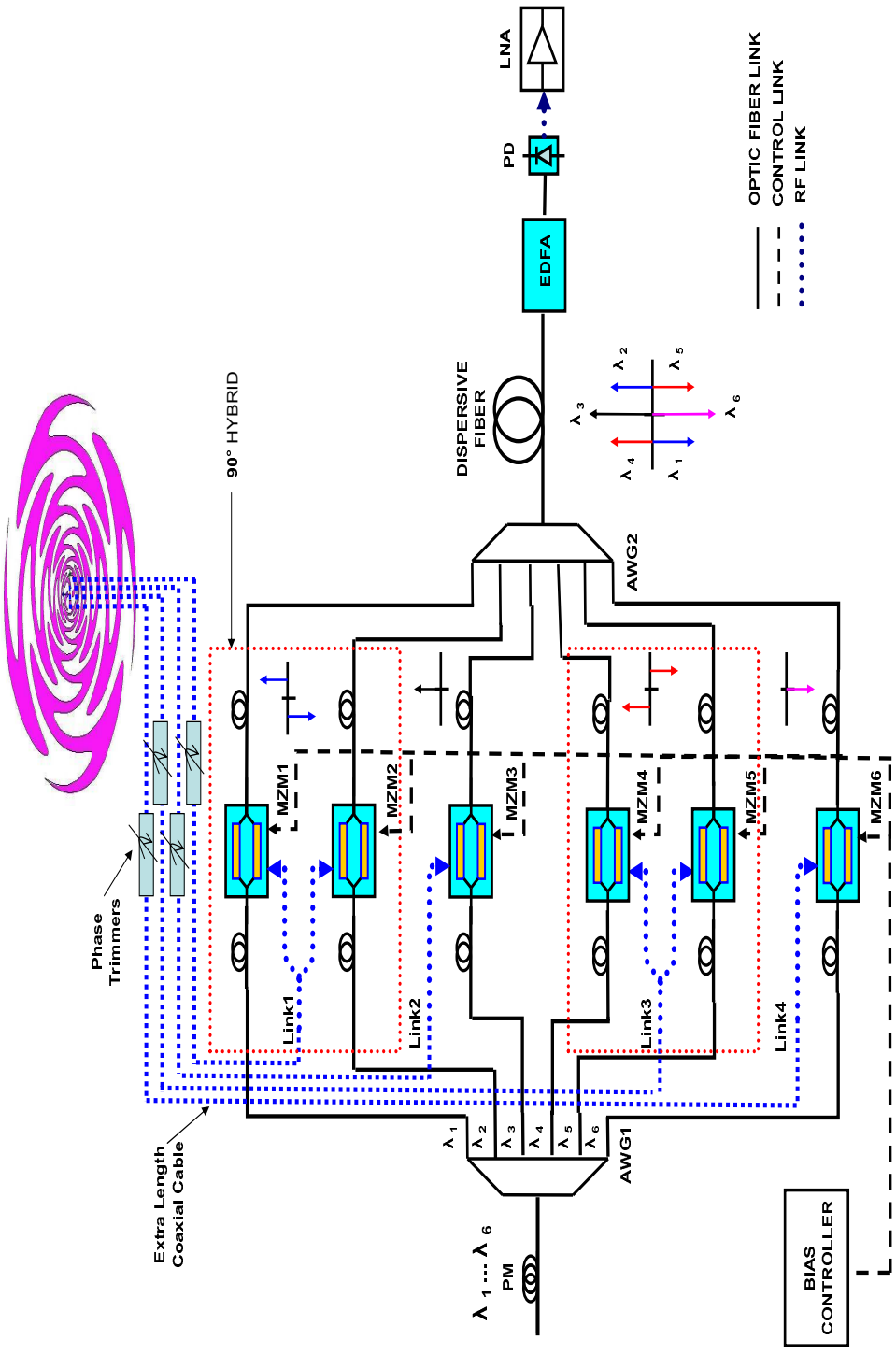

Figure 5.29: Reconfigurable Photonic Mode Transformer Configuration

fibre. In order to enable the coherent summation and detection of these modulated signals at the photo detector, the path length of the links must be equalised as it described in Section 5.6.2.

Considering that the order of arrival of the different wavelengths at the photo detector is as follows, λ_6, λ_5, λ_4, λ_3, λ_2 and λ_1 and that the time delay between the six wavelengths is the same ($\tau = 64.028\,\rho$s), the path lengths can be equalised as was done in Section 5.6.2. Section 5.6.2 showed that an extra length of 9.94mm of semi-rigid coaxial cable provides a delay of $\tau \times 1.5$ for the wavelength corresponding to the reference signal (MZM3), locating it between the two wavelengths (taps) forming the photonic quadrature coupler (MZM1 and MZM2). The same procedure can be applied in order to delay the other three wavelengths in such a way that they can be located in time as shown in the inset of Figure 5.29. The negatives coefficients of these modulated signals can be obtained by biasing the electro-optic modulator at opposite quadrature.

Table 5.4 presents calculations of the extra length of cable required considering a dispersive fibre with D = 17ps/nm.km and L = 2.354 Km. Broadband microwave phase shifters were connected to the input of the modulator for a fine tuning adjustment.

Table 5.4: Extra Length of RF cable

Laser	λ(nm)	MZM	RFL (mm)
λ_1	1542	MZM1	0.0
λ_2	1543.42	MZM2	0.0
λ_3	1545.06	MZM3	9.94
λ_4	1546.66	MZM4	19.98
λ_5	1548.26	MZM5	19.98
λ_6	1549.86	MZM6	29.92

At this point the hardware configuration of the photonic Butler matrix is complete. It is possible to reconfigure this network in a number of ways in order to receive radiation of several different polarisations and angles of incidence by changing only bias voltages and without any adjustment of this physical hardware. The following Sections demonstrate a number of these different configurations.

5.7.1 Phasing for Receiving Right Hand Circular Polarisation

The network can be configured to emulate the phasing behaviour of the Butler matrix shown in Figure 5.18 for receiving circularly polarised signals with the sinuous antenna. This requires a phase progression from Link1 to Link4 of $90\,^\circ$, $0\,^\circ$, $270\,^\circ$, $180\,^\circ$, respectively.

System Configuration

Table 5.5 summarises the required configuration of the electro-optic modulators to produce this phase progression.

Table 5.5: Photonic Mode Transformer Right Hand Circular Polarisation Configuration

Laser	λ(nm)	MZM	Bias	Taps
λ_1	1542	MZM1	$V_{q+2\pi}$	$90\,^\circ$ 1^{st}
λ_2	1543.42	MZM2	V_q	$90\,^\circ$ 2^{nd}
λ_3	1545.06	MZM3	$V_{q+2\pi}$	$0\,^\circ$
λ_4	1546.66	MZM4	V_q	$270\,^\circ$ 1^{st}
λ_5	1548.26	MZM5	$V_{q+2\pi}$	$270\,^\circ$ 2^{nd}
λ_6	1549.86	MZM6	V_q	$180\,^\circ$

Photonic Mode Transformer Characterisation

In order to verify that the RF signals received by each link will be effectively phase shifted according to Section 5.7, the system was characterised using a 20 GHz Anritsu vector network analyser, model 33473. The output of the EDFA was split into two portions by a 10% optical coupler for monitoring purposes. The 10% portion was input to an optical spectrum analyser (OSA) to monitor the amplitude of each tap and the 90% portion was input to the broadband Photo Detector (PD) which was connected to the Port II of the vector network analyser. Port I of the vector network analyser generated the testing signal which will be used to feed the RF inputs of the modulators shown in Figure 5.29.

Figure 5.30 shows the relative phase response of the links of the photonic mode transformer referenced to Link2. It shows that Link1 exhibits a $90\,^\circ$ phase shift respect to Link2, that Link3 a phase shift of $270\,^\circ$ and, that Link4 exhibit a phase shift of $180\,^\circ$.

Figure 5.31 shows the gain comparison of the links of the reconfigurable photonic mode transformer referenced to Link2. It shows that the gain difference between Link2 and Link4 is approximately 0dB, while the difference between Link2 and Link1, as well as Link2 and Link3, is the form of a single lobe of a sinusoid with a 3 dB gain bandwidth from 4–10 GHz. This is as expected for the two tap photonic Hilbert Transformer introduced in Section 5.6.1. The maximum gain value of Link1 and Link3 equals the gain level of the reference link (Link2) at the middle of the operational frequency bandwidth designed for this photonic mode transformer (7 GHz).

The relative phase and gain response of the photonic mode transformer are stable and uniform. The four inputs of the photonic mode transformer are effectively shifted by a relative phase of $90\,^\circ$, $180\,^\circ$ and $270\,^\circ$ respect to the reference link (Link2, $0\,^\circ$) and can be measured using a single optical link and thus can be used to receive right hand circularly polarised (RHCP) signals.

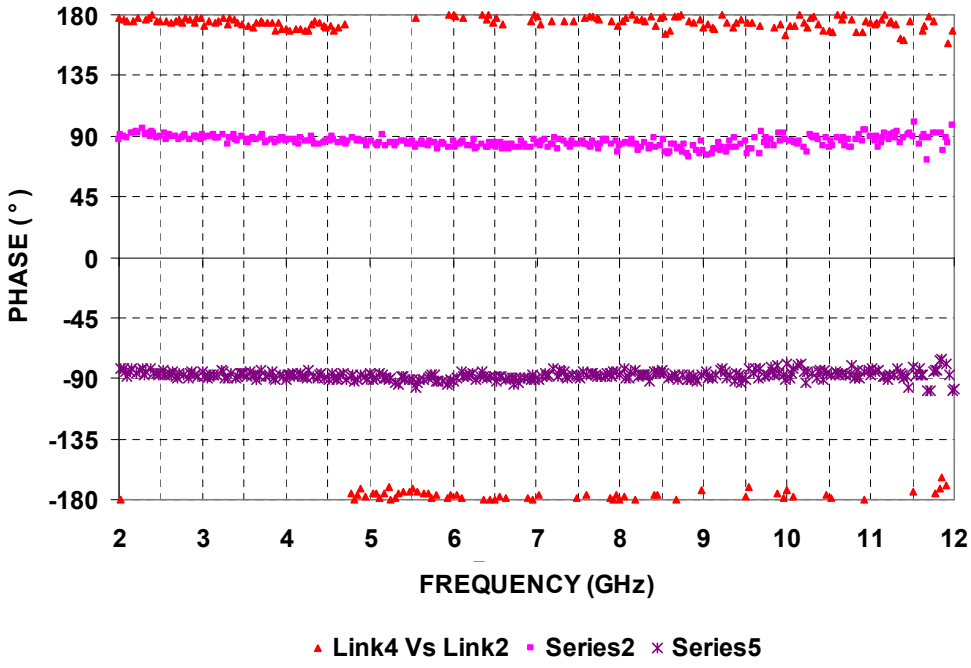

Figure 5.30: Reconfigurable Photonic Mode Transformer Phase Response

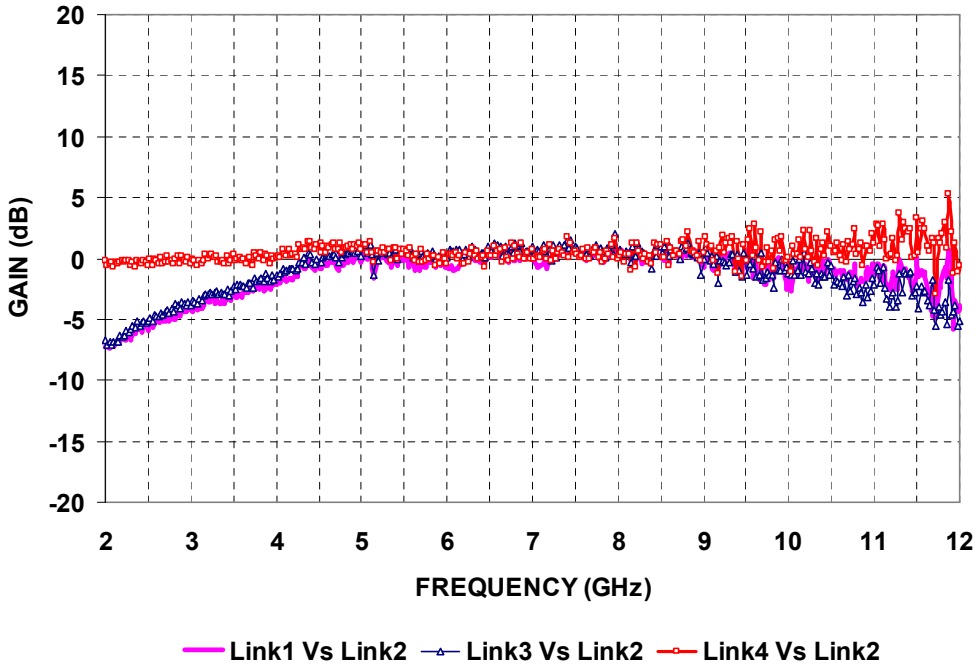

Figure 5.31: Reconfigurable Photonic Mode Transformer Gain Response

5.7.2 Reconfiguring the Mode Transformer

As discussed in Section 5.5 the sinuous antenna can receive multiple polarisation orientations, both linear and circular and various radiation modes. Section 5.7.1 has shown that the photonic mode transformer of Section 5.7 can be configured to receive right hand circular polarisation. This section will discuss how the network can be reconfigured to receive a selection of these other polarisations and radiation modes.

The relative phase difference of the signals received by the ports of the sinuous antenna is determined by the geometry of the sinuous antenna and the polarisation of the transmitting source. Opposite ports of the sinuous antenna exhibit an intrinsic relative phase difference of $180\,^{\circ}$

Phasing for Left Hand Circular Polarisation

One could imagine reconfiguring the photonic mode transformer to receive either right or left hand circular polarisations by changing the relative phase difference of the signals received by the ports of the sinuous antenna. This can be done swapping the bias voltage of two opposite links of the photonic mode controller simultaneously so the relative phase progression among the links can be either $0\,^{\circ}$, $90\,^{\circ}$, $180\,^{\circ}$ and $270\,^{\circ}$ for right hand circular polarisation, or $0\,^{\circ}$, $270\,^{\circ}$, $180\,^{\circ}$ or $90\,^{\circ}$ for left hand circular polarisation. Table 5.5 presented the configuration for right hand circular polarisation. One possible configuration for receiving left hand circular polarisation is presented in Table 5.6.

Table 5.6: Photonic Mode Transformer Left Hand Circular Polarisation Configuration

Laser	λ(nm)	MZM	Bias	Taps
λ_1	1542	MZM1	V_q	$270\,^{\circ}$ 1^{st}
λ_2	1543.42	MZM2	$V_{q+2\pi}$	$270\,^{\circ}$ 2^{nd}
λ_3	1545.06	MZM3	$V_{q+2\pi}$	$0\,^{\circ}$
λ_4	1546.66	MZM4	$V_{q+2\pi}$	$90\,^{\circ}$ 1^{st}
λ_5	1548.26	MZM5	V_q	$90\,^{\circ}$ 2^{nd}
λ_6	1549.86	MZM6	V_q	$180\,^{\circ}$

Phasing for Dipole Polarisations

If the sinuous antenna is operated with pairs of either North and South ports or East and West ports combined with a $180\,^{\circ}$ phase shift, then it will receive linear polarisation. The photonic mode converter of Section 5.7 can be configured to receive linear polarisations by simply switching off the lasers λ_3 and λ_6, or switching off all but these two wavelengths.

Phasing for Monopole Radiation

It may be desirable to operate the sinuous antenna a single element at a time as a monopole. This would provide radiation into beams facing at approximately 22.5° from bore-sight in one of four different directions. This could be useful for basic direction finding as discussed in Section 5.1.

One could imagine switching only one link of the photonic mode transformer at a time to measure the four normal modes of the sinuous antenna demonstrated in Section 5.5.2 without having to physically modify the phasing network and disconnect the antenna as was done in Section 5.5.2 to measure the RF characteristics of each element. This could be achieved by switching off all lasers and then only activating the wavelength or wavelengths corresponding to Link1, Link2, Link3 or Link4.

Phasing for Higher Order Mode Radiation

It may also be desirable to operate the sinuous antenna as a basic dipole, polarised in either the horizontal (West-East) or the vertical (North-South) directions, but operating in the higher order mode. As discussed in Section 5.5.4 this provides a null at bore-sight and a pair of linearly polarised beams that are angled at 35° off bore-sight. Access to this radiation pattern could refine the basic direction finding achievable by using single elements.

By switching on the two links controlling opposite ports of the antenna simultaneously, two orthogonal polarisations defined by the two orthogonal dipoles of the antenna shown in Section 5.5.4 can be received at a time. Further, these dipoles can be controlled to radiate their fundamental radiation mode (M=1) or their second radiation mode (M=2) by modifying the relative phase difference between opposite ports from 0° for M=1 to 180° for M=2. This can be done by only changing the bias voltage of one of the modulators in the case of Link2 and Link4 from $V_{q+2\pi}$ to V_q, or by changing the bias voltage of the two modulators generating the quadrature hybrid couplers in the case of Link1 and Link3 from $V_{q+2\pi}$ to V_q or from V_q to $V_{q+2\pi}$.

The ability of the sinuous antenna to receive multiple polarisations and different radiation modes with the photonic mode transformer shown in Figure 5.29 will be determined by the way that the four links of the photonic mode transformer are reconfigured as explained in this Section.

The frequency bandwidth of this implementation should only be limited by the bandwidth of the modulators and the operational bandwidth selected for the photonic quadrature hybrid couplers. This bandwidth has been designed to operate with a 3 dB bandwidth from 4–10 GHz, which matches the operational bandwidth of the sinuous antenna presented in Section 5.5.

5.7.3 Photonic Mode Transformer Summary

This section has demonstrated that a flexible reconfigurable phasing network can be achieved by using photonic transversal techniques, electro-optic modulator bias control

and wavelength division multiplexing techniques. This reconfigurable phasing network can be used to control and measure the multiple polarisation and radiation modes of a four-arm sinuous antenna.

Contrary to the Butler matrix shown in Figure 5.18 which is unable to measure the two linear polarisation that define the circular polarisation performance of the sinuous antenna, or the four normal radiation modes that defines these linear polarisations, the photonic mode transformer presented in this section can be reconfigured and controlled to measure all these other radiation modes of the antenna The following Sections demonstrates how the photonic mode transformer can measure a selection of radiation modes of this sinuous antenna.

5.8 Sinuous Antenna Radiation Characteristics with Photonic Mode Control

Having demonstrated in section 5.7.2 that it is possible to create a reconfigurable photonic mode transformer using Microwave Photonics, it is now possible to connect this photonic mode transformer to the four-arm sinuous antenna of Section 5.5 and measure the radiation characteristics of the multiple modes in which it can operate.

5.8.1 Method for Measuring Radiation Characteristics

The characterisation of the multiple polarisation and radiation modes of the antenna was conducted using the gain transfer antenna characterisation method described in Section 2.2.1. However, the vector network analyser used for the RF characterisation was substituted by a computer controlled antenna measurement network shown in Figure 5.32. This network divides the function of the vector network analyser into a signal generator, which provides the testing signal for the transmitting antenna, and a spectrum analyser which monitors the power received by the photonic mode transformer and the sinuous antenna. Using a signal generator and a spectrum analyser allows an increase in the power transmitted by the antenna, enables the received signal to be averaged and avoids the transmission losses of long coaxial cables.

Two different sets of known standard antennas were employed, such that different polarisations could be tested. One of these sets of antennas consisted of two right hand circularly polarised spiral antennas, model LS24 by RFSpin®. The other set consisted of two double ridged pyramidal horn antennas, model 3115 by ETS-Lindgren®.

The known standard antennas were used to measure the transmission link gain of the antenna measurement system using a single photonic link as was described in Section 2.4.1. This was done by mounting the reconfigurable photonic mode transformer implementation on a rotating platform inside the anechoic chamber, connecting one of the standard antennas to the input of MZM1 and activating only carrier, λ_1, in Figure 5.29. This response was used as a reference for all subsequent measurements.

Once the link gain had been characterised, the sinuous antenna was connected to the photonic mode transformer as shown in Figure 5.33 for characterisation purposes.

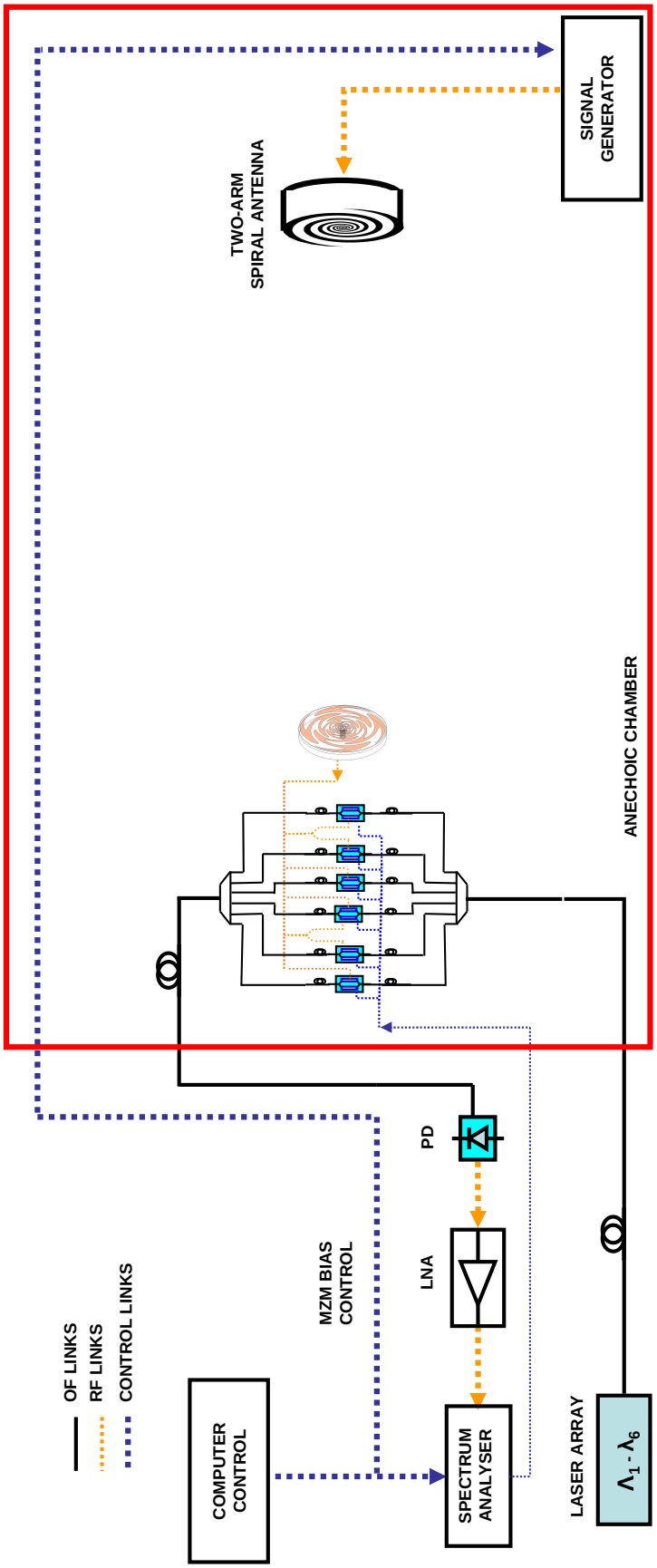

Figure 5.32: Antenna Measurement Network Setup

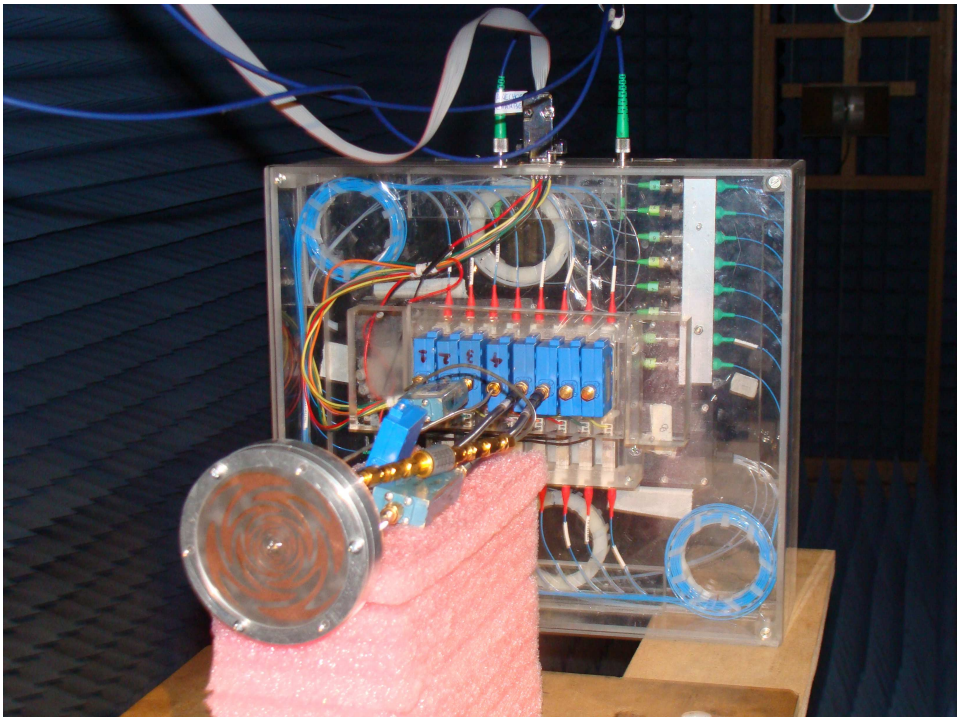

Figure 5.33: Reconfigurable Photonic Mode Transformer. Anechoic Chamber

5.8.2 Interfacing the Sinuous Antenna to the Photonic Mode Transformer

As discussed in Section 5.7.2 it is possible to configure the photonic mode transformer in order to achieve a phase progression among the ports of the sinuous antenna of $90\,^{\circ}$ clockwise. This configuration corresponds to a right hand circularly polarised signal generated by four individual monopoles aligned orthogonally.

Table 5.7 shows the connection selected to measure the multiple polarisations and radiation modes of the antenna using the photonic mode transformer.

Table 5.7: Initial Configuration of the Reconfigurable Photonic Mode Transformer

Links	Antenna Ports	Modulators	Axis Components
L1	North	MZM1-MZM2	Vertical
L2	East	MZM3	Horizontal
L3	South	MZM4-MZM5	Vertical
L4	West	MZM6	Horizontal

The following Sections will progressively demonstrate how the photonic mode transformer can control individually the normal radiation mode of the four orthogonally oriented “monopoles” of the sinuous antenna to receive two orthogonal linear polarisations, and then finally right and left hand circular polarisations.

5.8.3 Monopole Radiation Patterns Characterisation

The RF characterisation of the sinuous antenna in Section 5.5.2 demonstrated that the four normal modes of the antenna are symmetric around the central axis of the antenna. Therefore, measuring only one port (North, South, East or West) of the sinuous antenna, should determine whether or not the photonic mode transformer is able to receive each of the four normal modes of the sinuous antenna. It is predicted that the radiation characteristics of a single monopole will not change simply due to the photonic feeding as previous investigation has demonstrated [22]. However, the results will enable comparison of the RF measurement system and the Microwave Photonic measurement system of Figure 5.32.

Having connected the sinuous antenna according to the configuration described in Table 5.7, Link2 of the photonic mode transformer was activated independently by switching on λ_3 in order to measure the radiation response of Port-E. The radiation patterns of Port-E was done by rotating the photonic mode transformer and the antenna, using the antenna measurement network setup shown in Figure 5.32. This network rotated the antenna around its azimuth angle (ϕ) and measured its response averaging the power received from the antenna three times every $2\,^\circ$.

Figure 5.34 shows the E-plane and H-plane radiation pattern response of Port-E when only one link of the photonic mode transformer is activated. It shows that the E-plane pattern of Port-E exhibits a single broad beam with a 3 dB beam-width of approximately $50\,^\circ$ tilted $-25\,^\circ$ off bore-sight. The H-plane pattern of Port-E exhibits a single beam with a 3 dB beam-width of approximately $50\,^\circ$ centered at bore-sight. Although both planes' radiation patterns exhibit the same 3 dB beam-width, Figure 5.34 shows that the H-plane pattern is narrower than the E-plane pattern.

Comparing Figures 5.34 and Figure 5.11, it is evident that the response of the antenna using the reconfigurable photonic mode transformer obtains similar results to the RF characterisation. Both Figures show similar tilted beams facing at $-25\,^\circ$ off bore-sight and similar 3 dB beam-width (approximately $50\,^\circ$). Figure 5.34 shows that the noise floor of the system shown in Figure 5.32 is higher than the RF measurement system. This was expected due to the insertion loss of the optical fibre link which is approximately -27 dB.

Differences in the shape of the radiation patterns could be attributed to differences in the alignments of the antenna from one setup to the other. Slight misalignments of the main polarisation axes of the antenna at the frequency under test (5 GHz) provide different cuts of the radiation performance of the antenna. These differences could also be attributed to the presence of the array of modulators, cables and variable microwave phase shifters shown in Figure 5.33, elements not present in the RF characterisation that interfere with the free space measurements, reflecting and refracting the test signal received from the antenna using the photonic mode transformer.

Comparing the photonic results obtained in this section with the photonic results obtained for the double fed two-arm spiral antenna in Section 4.7, it is evident that the sampling function and the step size selected for the rotation of the antenna using the setup shown in Figure 5.32 provided less detailed radiation patterns of the sinuous antenna. The loop response of the antenna measurement system was extremely long compared to the measurement system using the vector network analyser, if the sampling was increased or

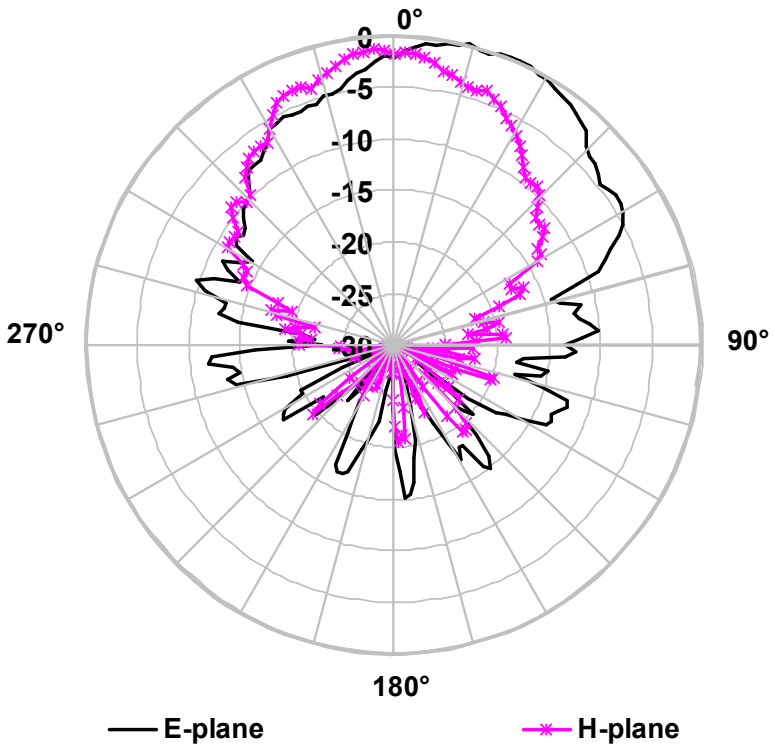

Figure 5.34: E-plane and H-plane Radiation Patterns of Port-E @ 5 GHz

the step size of rotation refined. Since the results obtained in this section are similar to the RF results presented in Section 5.5.2, the sampling and step size were not modified.

The analysis of the individual performance of the ports matches the RF characterisation presented in Section 5.5.2, confirming that the photonic mode transformer is able to receive the four normal modes of the sinuous antenna independently, by activating one link of the photonic configuration at a time. Differences between the results obtained by the photonic mode transformer and the RF measurements presented in Section 5.5.2 are mostly attributable to the gain amplification process of the antenna measurement network that compensates the insertion loss of the optical fibre link, the discrete sampling function of the antenna measurement network, the presence of the phonic mode transformer components on the back of the antenna, and differences in the alignments of the antenna in the RF and the Photonic characterisations.

5.8.4 Dipole Radiation Patterns Characterisation

Activating the links of the photonic mode transformer corresponding to opposite ports of the sinuous antenna as explained in Section 5.7.2 can generate the patterns of two orthogonal "dipole" antennas. It should be possible to control these dipoles so as to exhibit their first order mode or their second order mode, by switching the relative phase difference between the activated links of the photonic mode transformer from $180\,^{\circ}$ to $0\,^{\circ}$. Since Section 5.5 has demonstrated the symmetry of the antenna, this section presents only the characterisation of one "dipole" on the H-plane as proof of concept.

Table 5.7 shows that Port-E and Port-W form the horizontal dipole, while Port-N and Port-S from the vertical dipole of the sinuous antenna. By activating Link2 and Link4 of the photonic mode transformer in Figure 5.29 or Link1 and Link3 simultaneously, the horizontal or vertical dipoles, respectively, can be measured. The horizontal dipole was selected in order to simplify the comparison with the individual radiation patterns of Port-E presented in Section 5.8.3. By switching off all the wavelengths of the photonic mode transformer except λ_3 and λ_6, and by biasing MZM3 and MZM6, first to V_q and V_q and then to $V_{q+2\pi}$ and V_q, the first order and second order radiation mode of the horizontal dipole, was measured. Figure 5.35 shows the combined response of Port-E and Port-W added coherently when both modulators are biased at the same quadrature points ($0\,^\circ$ relative phase difference, M=1), and when the modulator is biased at opposite quadrature points ($180\,^\circ$ relative phase difference, M=2).

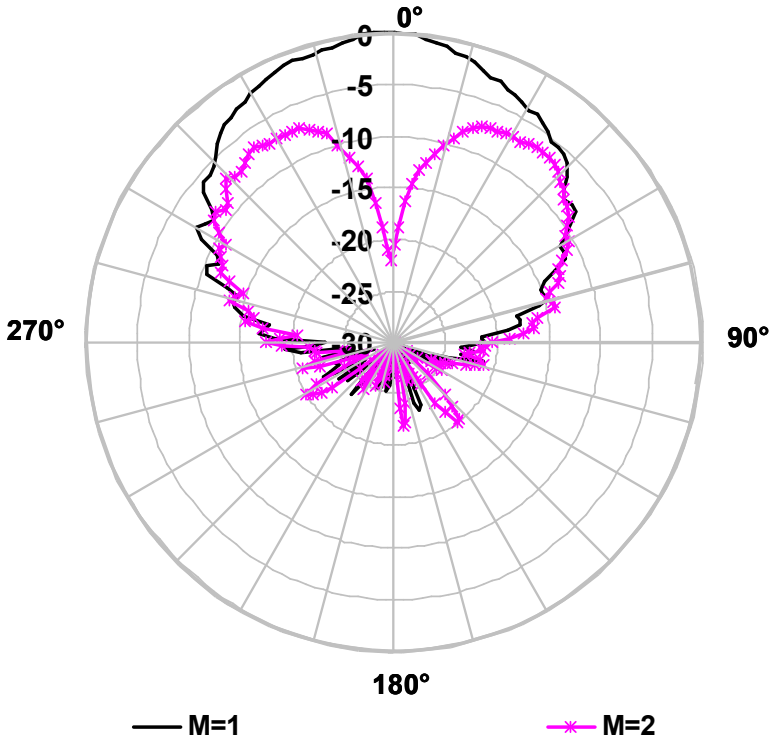

Figure 5.35: Mode M=1 and M=2 of the Combined Response of Port-E and Port-W @ 5 GHz

Figure 5.35 shows that the radiation pattern of the horizontal dipole, when the modulators are biased at the same quadrature points, exhibits a broad single beam pattern (M=1). This radiation pattern exhibits a 3 dB beam-width of approximately $70\,^\circ$ and it is centered along bore-sight. Although the radiation patterns in this section have been normalised to zero, the power received from the antenna, operating in mode M=1, is almost 6 dB higher than the individual response shown in Figure 5.34 at bore-sight.

Figure 5.35 also shows that biasing the modulators at opposite quadrature points, generates a characteristic null at bore-sight direction and two side-lobes facing approximately at $35\,^\circ$ off bore-sight (M=2). The received power of these two side-lobes is around 7 dB lower than the radiation pattern for mode M=1 at bore-sight.

Comparing Figures 5.35 and 5.16, it is evident that the response of the antenna using the reconfigurable photonic mode transformer obtains similar results to the RF measurements presented in Section 5.5.4.

The main difference is the asymmetric radiation patterns obtained for mode M=1, which exhibits a slight gain reduction over its right side. This difference can be attributed to physical change in the characteristics of the antenna, caused by connecting and disconnecting the antenna in order to measure the RF patterns using the $180\,^{\circ}$ microwave hybrid coupler in Section 5.5. It is worth noting that the gain and time delay of each link of each photonic link was equalised as described in section 5.7.1. It would be possible to finely adjust both the laser power and the static optical delay using variable optical delay lines to compensate for this observed non-ideal behaviour of the antenna or its coaxial interface.

The differences between the RF radiation pattern of the antenna operating in mode M=2, shown in Figure 5.16, and the photonic mode transformer radiation pattern shown in Figure 5.35 make evident that the presence of the components of the photonic mode transformer affected the radiation pattern characteristics of the sinuous antenna, as this was rotated around its azimuth angle ϕ. These effects are observed by the characteristic ripple or "scallop" effect on the radiation pattern response of mode M=2, which is clearly appreciated in Figure 5.35 after $\phi = 30\,^{\circ}$.

In summary, although the presence of the components of the photonic mode transformer disturb the radiation pattern performance of the antenna, the photonic mode transformer is able to change from the radiation response of the dipoles of the antenna from mode M=1 to M=2 by simply changing the bias voltage of the modulators of the system. Extending the ground plane of the sinuous antenna to shield both the RF and the photonic mode transformer measurement systems, as would be done in a real application, would provide closer results to the RF results presented in Section 5.5.4

5.8.5 Circular Polarisation Performance Characterisation

The polarisation ellipse of a circularly polarised antenna shown in Figure 4.10a) is tangent to the polarisation pattern, and can be used to measure how circularly polarised an antenna is [52]. The axial ratio is the difference between the main axes of the polarisation ellipse and defines whether an antenna is circularly or elliptically polarised. A practical method for measuring the axial ratio of an antenna consists of rotating a linearly polarised transmitting antenna, while the antenna under test rotates along its main axes: vertical and horizontal for a circularly polarised antenna, E-plane and H-plane for a linearly polarised antenna. The difference between the inner and outer envelopes of the radiation patterns exhibited by the antenna defines the axial ratio. A minimum variation between these envelopes is expected of a pure circularly polarised antenna.

Table 5.7 shows that the individual components of the horizontal and vertical dipoles of the sinuous antenna are connected to the photonic mode transformer in such a way that Link1 and Link3, corresponding to the photonic quadrature couplers, control the components of the vertical dipole, and Link2 and Link4, corresponding to the $180\,^{\circ}$ photonic hybrid coupler, control the horizontal components of the horizontal dipole. Provided that the main axes of the antenna are aligned with the axes of the polarisation ellipse, a

qualitative approximation of the circular polarisation characteristic of the antenna can be obtained by comparing the radiation pattern response of the orthogonal dipoles operating in mode M=1, instead of defining the axial ratio of the antenna by rotating the transmitting antenna.

These measurements were conducted using a linearly polarised pyramidal horn antenna for normalising purposes. First the horizontal axis of the sinuous antenna was aligned with the polarisation of the horn for measuring its E-plane response and then the vertical axis, by rotating the sinuous antenna $90\,^{\circ}$ along its central axis (bore-sight) for measuring its H-plane response. These measurements correspond to the E-plane response of both dipoles (Port-E and Port-W, Port-N and Port-S), which corresponds to the axes of the polarisation ellipse as it was shown in Section 5.5.4.

Figure 5.36 shows the E-plane measurements of the vertical and horizontal axes of the sinuous antenna. The radiation patterns in both the vertical and horizontal plane exhibit broad beams with a 3 dB beam-width of approximately $75\,^{\circ}$, centered at bore-sight direction. The horizontal response and the vertical response present a notorious difference around $\phi = 40\,^{\circ}$. As explained in Section 5.8.4, this difference can be attributed to the a gain link difference between the ports of the antenna which is unbalancing the performance of the horizontal dipole. The difference between the radiation patterns presented in Figure 5.36, inside the 3 dB beam-width region, represents an approximation of the axial ratio of the antenna. Differences outside this region can be attributed to the interference caused by the components of the photonic mode transformer which influence in the radiation patterns of the antenna becomes evident after $\phi = 30\,^{\circ}$, as explained in Section 5.8.4.

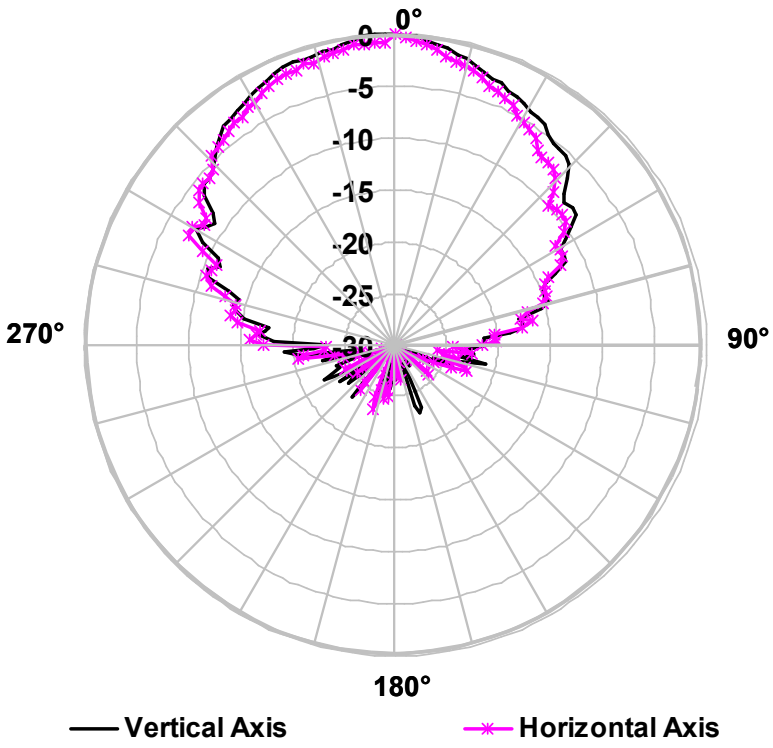

Figure 5.36: Vertical and Horizontal E-plane Radiation Response @ 5 GHz

A comparison of the radiation pattern response of the horizontal and vertical dipoles confirms that Port-E exhibits a gain link difference compared to Port-W that unbalances the response of the horizontal dipole. It is here that the photonic mode transformer represents another significant advantage over traditional microwave butler matrix. These link gain differences can be easily controlled by finely adjusting both the laser power and the static optical delay, using variable optical delay lines, so what seems to be a tilting of the main beam of the dipole can be rectified. Adjusting any unbalanced response of the ports of the sinuous antenna within their 3 dB beam-width, can control the overall response of the antenna so it can be considered fairly circularly polarised.

5.8.6 Circularly Polarised Radiation Patterns. Discrete Frequency Performance

The broadband circular polarisation performance of a sinuous antenna has been previously demonstrated [71, 73]. This antenna can exhibit uniform radiation characteristics across its operational bandwidth. In order to match its uniform radiation response across the frequency, a microwave butler matrix should also present uniform and stable amplitude and phase response across the entire bandwidth of the antenna, so the circular polarisation performance of the antenna remains uniform. This is normally very difficult to achieve over a large frequency range using traditional microwave components.

As shown in Section 5.7 the amplitude and phase response of the photonic Hilbert transform is fairly stable across the operational bandwidth of the antenna. Therefore, the radiation patterns should also be fairly stable across the entire bandwidth.

Having adjusted the link gain response of Port-E to balance the response of the horizontal dipole, reducing with this the differences among the horizontal and vertical dipoles shown in Figure 5.36, the uniformity of the radiation characteristics of the antenna was investigated across its operational bandwidth. A discrete frequency analysis of the circularly polarised radiation pattern response of the antenna was conducted. This was done by activating all the links of the photonic mode transformer shown in Figure 5.29, simultaneously. The bias quadrature points of the modulators were adjusted as shown in Table 5.5, so the ports of the sinuous antenna were configured to receive a phase progression of 90° clockwise, corresponding to a right hand circularly polarised configuration. A right hand circularly polarised spiral antenna transmitted the test signal.

Figure 5.37 to Figure 5.39 shows the radiation pattern response of the horizontal axis of the antenna when the photonic mode transformer is configured as shown in Table 5.7 to receive a right hand circularly polarised signal at 4, 5, 6, 7, 8, 9 GHz. The radiation patterns were normalised to the maximum power received by the antenna at these frequencies. The results show that a broad beam pattern is maintained from 4–8 GHz. The radiation pattern gets narrower at 9 GHz.

These patterns confirm that the balanced mode M=1 of the sinuous antenna is successfully generated by the photonic mode transformer across the entire frequency bandwidth. Narrowing of the beam pattern at 9 GHz has nothing to do with photonics and can be attributed to the separation of the elements of the sinuous antenna and the size of the feeding point of the sinuous antenna, which operates as phase antenna array beyond

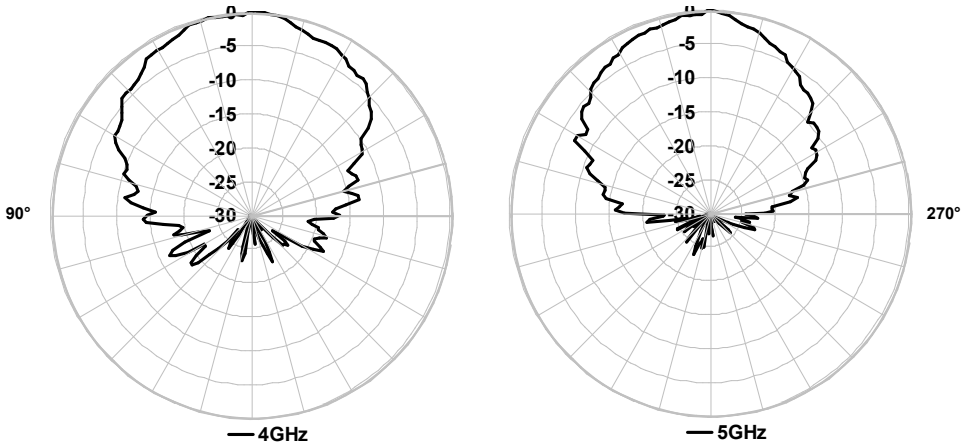

Figure 5.37: Radiation Pattern Response @4 GHz and 5 GHz

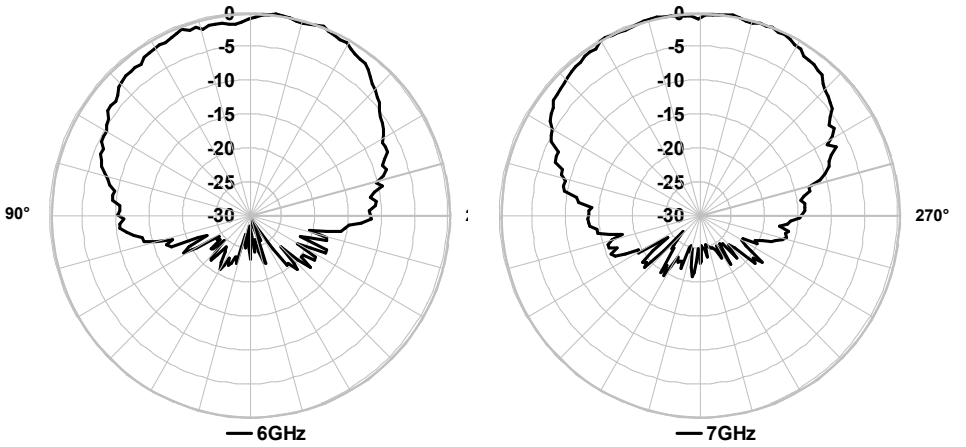

Figure 5.38: Radiation Pattern Response @6 GHz and 7 GHz

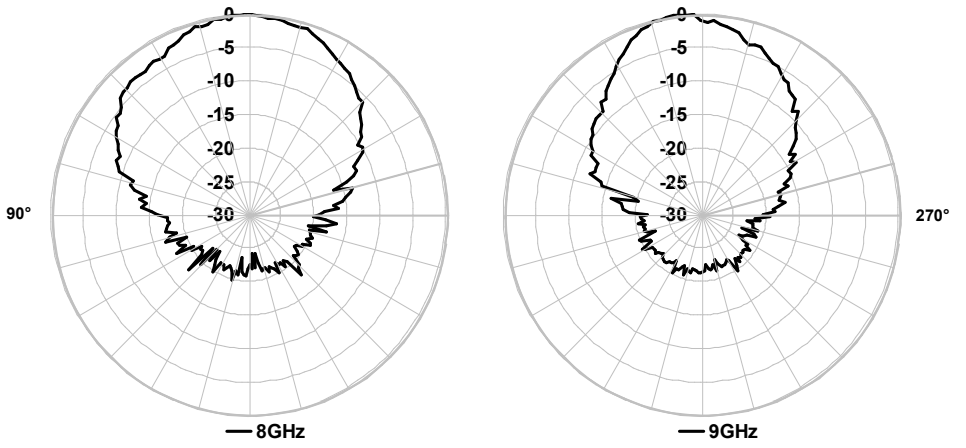

Figure 5.39: Radiation Pattern Response @8 GHz and 9 GHz

this frequency. This feeding point was selected to enable interfacing the coaxial bundle which has been demonstrated in previous investigations [92] being a limiting factor for the impedance bandwidth of the sinuous antenna, as shown in Section 5.5.1. Smaller coaxial cables, will result in smaller coaxial bundles and therefore smaller feeding points, which should broaden the radiation pattern bandwidth of the sinuous antenna. It is worth noting that these measurements could not be conducted before in the RF domain with a single $180\,^{\circ}$ microwave hybrid coupler.

By changing the configuration of the modulators as explained in Section 5.7.2, the relative phase of the ports of the antenna can be reconfigured to measure left hand circularly polarised signals. Since at the moment of conducting this investigation a left hand circularly polarised antenna was not available, the radiation patterns of the antenna for left hand circular polarisation could not be measured. It was possible however to measure the response of the photonic sinuous antenna configured for receiving left hand circular polarisation but excited with right hand circular polarisation radiation. This represents the cross polarisation response. Since the sinuous antenna is considered unable to filter polarisations [87], a radiation pattern of the cross circular polarisation by itself does not provide significant information. Instead, the cross polarisation gain response will be presented in the following Sections.

In summary, the analysis of the radiation patterns that the reconfigurable photonic mode transformer is able to receive from the sinuous antenna, demonstrated that it is possible to adjust the relative phase of each normal mode of the antenna independently in order to generate multiple radiation modes. It demonstrated that simultaneously operating the links of the photonic mode transformer can generate two orthogonal linear polarisations with a relative phase difference of $90\,^{\circ}$. The orthogonality of these linear polarisations defines the axes of the polarisation ellipse which enabled the photonic mode transformer to receive circularly polarised signals by activating all the links simultaneously.

The results obtained with the photonic mode transformer reproduced almost exactly the measurements done on the RF domain using a $180\,^{\circ}$ microwave hybrid coupler, demonstrating that the photonic mode transformer does not disturb the performance of the sinuous antenna considerably. The broadband bandwidth of sinuous antenna and the reconfigurable photonic mode transformer proved to be limited only by the performance of the bundle of coaxial cables.

Reconfiguring the photonic mode transformer by changing the bias voltage of the modulators showed that it is possible to control the relative phase of the taps of the photonic mode transformer. Adjusting the relative phase of one tap individually by changing the bias voltage of the modulator showed that M modes (M=2) can also be generated, showing radiation patterns with a characteristic null along the central axis of the antenna.

This section has demonstrated that the major advantage of the photonic mode transformer over traditional microwave systems is that each link gain can be finely adjusted to compensate any unbalanced response among the ports by adjusting the power of the laser controlling each link. Adjusting any unbalanced response of the ports of the sinuous antenna within their 3 dB beam-width, can control and configure the response of the antenna to be fairly circularly polarised over its entire frequency bandwidth.

5.9 Sinuous Antenna Gain Characterisation using the Photonic Mode Transformer

The key advantage that Photonics offers over traditional RF components is its invariant behaviour with frequency. Hybrid coupler implementations using traditional microwave techniques have been reported with moderate bandwidths (2-18 GHz). However, these implementations exhibit amplitude imbalances greater than 3 dB and impedance matching procedures that represent a continuous challenge, normally overcome using multi-resonant structures. In order to complement the radiation pattern measurements of the sinuous antenna presented in Section 5.8 and demonstrate that the performance of the photonic mode transformer exhibit a frequency invariant response across the entire operational bandwidth (4–10 GHz) of the sinuous antenna, the relative gain response of the system was characterised.

The radiation analysis in Section 5.8 showed that the photonic mode transformer can receive four normal modes of the sinuous antenna independently, combine these normal modes to generate two linear polarisations (vertical and horizontal) which can exhibit two different M radiation modes (M=1 and M=2), or configure the antenna to receive right and left hand circular polarisations.

It is worth remembering from Section 5.6.2 that the gain response of any component of the sinuous antenna attached to the photonic quadrature hybrid couplers shown in Figure 5.29, will be affected by the gain response of these photonic quadrature hybrid couplers. Having demonstrated in Section 5.5 the symmetry of the sinuous antenna, this section presents only a selection of these multiple polarisations and radiation modes. It focuses on the results related to Port-N and Port-S, which are the components of the antenna attached to the photonic quadrature hybrid couplers, instead of Port-E and Port-W. First, it presents the response of the individual gain response of Port-N. Then it presents a comparison of the gain response of the system when Port-N and Port-S (vertical dipole) are combined together to operate in its radiation modes M=1 and M=2, followed by, its co-polar and cross-polarisation characterisation. Finally, it presents the gain response of the system when the photonic mode transformer configures the sinuous antenna to receive right or left hand circular polarisations.

The sinuous antenna was connected to the microwave photonic transformer according to the configuration described in Table 5.7. All the measurements were conducted using the antenna measurement technique used in Section 5.8.1. The individual gain response of the normal mode corresponding to Port-N, and the gain response of the vertical dipole operating in modes M=1 and M=2 were normalised using the link gain characterisation obtained from the pyramidal horn antenna. The right and left hand circular polarisation gain response were normalised using the link gain characterisation obtained from the circularly polarised known spiral antenna.

5.9.1 Single Element Gain Response

Having connected the sinuous antenna according to the configuration described in Table 5.7, the wavelengths of the photonic mode transformer shown in Figure 5.29 were switched on and off as was shown in Section 5.8. First, λ_1 and λ_2 were switched on, with all other wavelengths off so the response of Port-N could be measured in isolation.

Figure 5.40 shows the individual response of Port-N, when the antenna is aligned at bore-sight direction. It shows that the individual gain response of Port-N raises from 4–6 GHz, exhibits an average power level of 0 dBi which varies around ± 2 dB from 6–10 GHz and decreases from 10-12 GHz.

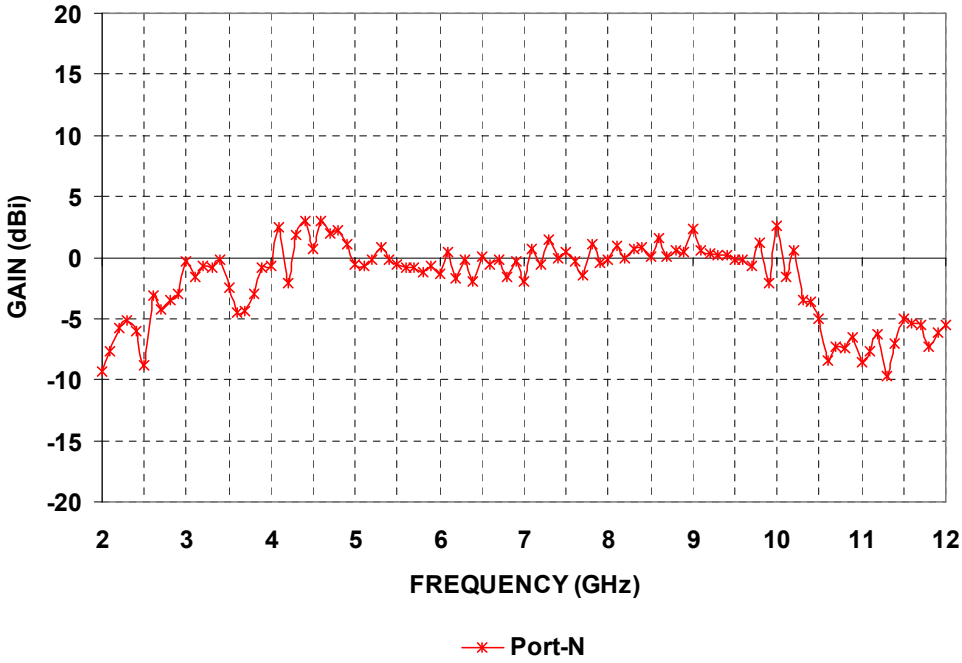

Figure 5.40: Sinuous Antenna Ports Gain Response

Comparing Figures 5.40 and 5.19 it is clear that the gain response of the photonic hybrid coupler presented in Figure 5.28 has affected the RF response of Port-N. The gain response of Port-N has been reduced so the lumps present at the edges of its gain bandwidth (4-10 GHz) decreased, flattening the overall response of the gain. The gain response presented in Figure 5.40 exhibit similar performance to is RF counterpart, despite it exhibits a higher amplitude variation which can be attributed to the signal sampling, averaging and amplification stages of the measuring network shown in Figure 5.32.

5.9.2 Dipole Gain Response

Having shown that the photonic link provides broadband remoting of a single element, even when configured as a transversal photonic hybrid, a further investigation should demonstrate that the photonic mode transformer can combine opposite elements of the antenna maintaining either a 180° or a 0° relative phase difference, as demonstrated in Subsection 5.8.4 over the full frequency range.

To do this, the carriers, λ_1, λ_2, λ_4 and λ_5 were switched on to measure the combined response of Port-N and Port-S operating as a vertical dipole. To measure the response of the M=1 mode (with a single lobe centered at bore-sight as depicted in Figure 5.35) MZM1 was biased at V_q, MZM2 at $V_{q+2\pi}$, MZM4 at $V_{q+2\pi}$ and MZM5 at V_q. To measure the response of the M=2 mode (with a pair of lobes and a null at bore-sight as depicted in Figure 5.35), the modulators MZM1 and MZM2 were again biased at V_q and $V_{q+2\pi}$ respectively, but the bias of MZM4 and MZM5 were inverted to V_q and $V_{q+2\pi}$ respectively.

Figure 5.41 shows the gain response of the dipole formed by Port-N and Port-S operating in the M=1 mode. The average gain is around 6 dBi and varies approximately ± 3 dB. Figure 5.41 also shows the power received by the antenna operating in mode M=2 (Δ) at bore-sight. Referring to Figure 5.35, this should be a null. The received power remains below -5 dBi for all the operational frequency bandwidth of the sinuous antenna. This indicates that a phase of $180\,^\circ$ is maintained across the band.

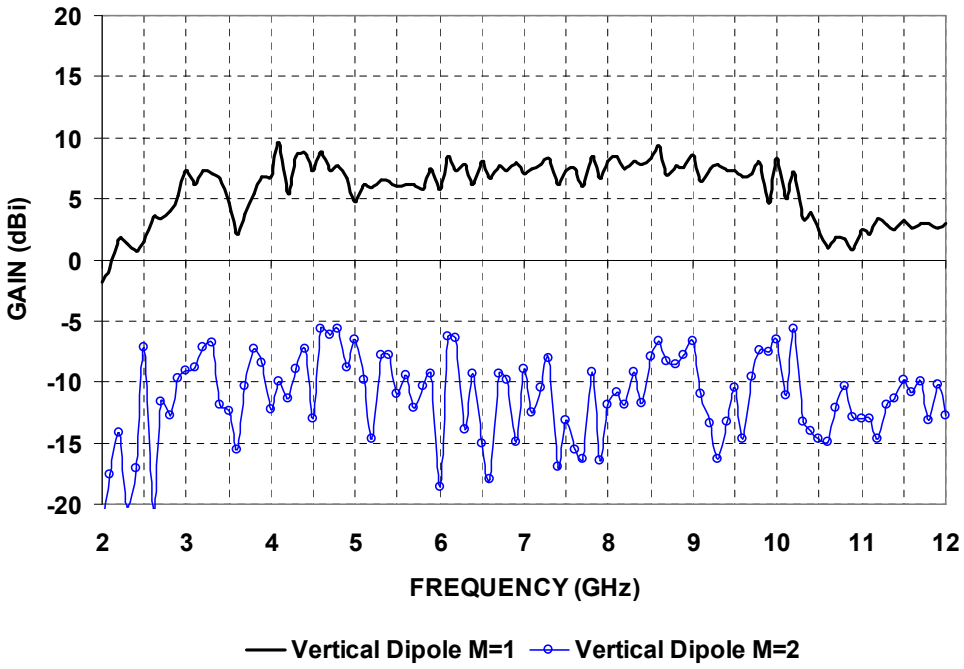

Figure 5.41: Sinuous Antenna Ports Gain Response

Comparing Figures 5.41 and 5.40, it is evident that the peak gain of two elements operating as a dipole is increased by 6 dB over the single element radiation. This indicates that the elements are being combined coherently. These results are well in agreement the analysis of the radiation patterns in Section 5.8 and with the RF results presented in Section 5.5.7. It should be noted that the photonic mode transformer reduces the gain response of the vertical dipole at the lower and upper edge of the operational bandwidth of the sinuous antenna, compared with the RF results. This gain reduction corresponds with the gain response of the photonic hybrid coupler as presented in Figure 5.28. As explained in Section 5.6.2 this could be improved by including more taps to the system or by increasing the 3 dB bandwidth of the photonic hybrid coupler.

5.9.3 Dipoles Co-polarisation and Cross-polarisation Performance

Measuring the co-polarisation and cross-polarisation performance of the dipoles of the sinuous antenna across the entire bandwidth can provide information about how the photonic mode transformer could disturb the linear polarisation characteristic of the two dipoles forming the sinuous antenna.

The co-polarisation and cross-polarisation response of the vertical axis were characterised by using the link gain characteristics of two linearly polarised standard horn antennas as a reference. The sinuous antenna was connected to the photonic mode transformer to measure the mode M=1 of the vertical dipole as was done in Section 5.9.2 by switching on λ_1, λ_2, λ_4 and λ_5, and by biasing MZM1 at V_q, MZM2 at $V_{q+2\pi}$, MZM4 at $V_{q+2\pi}$ and MZM5 at V_q.

Figure 5.42 shows the comparison of the co-polarisation and cross-polarisation characteristics of two opposite ports (Port-N and Port-S) added coherently by the photonic mode transformer in the M=1 mode.

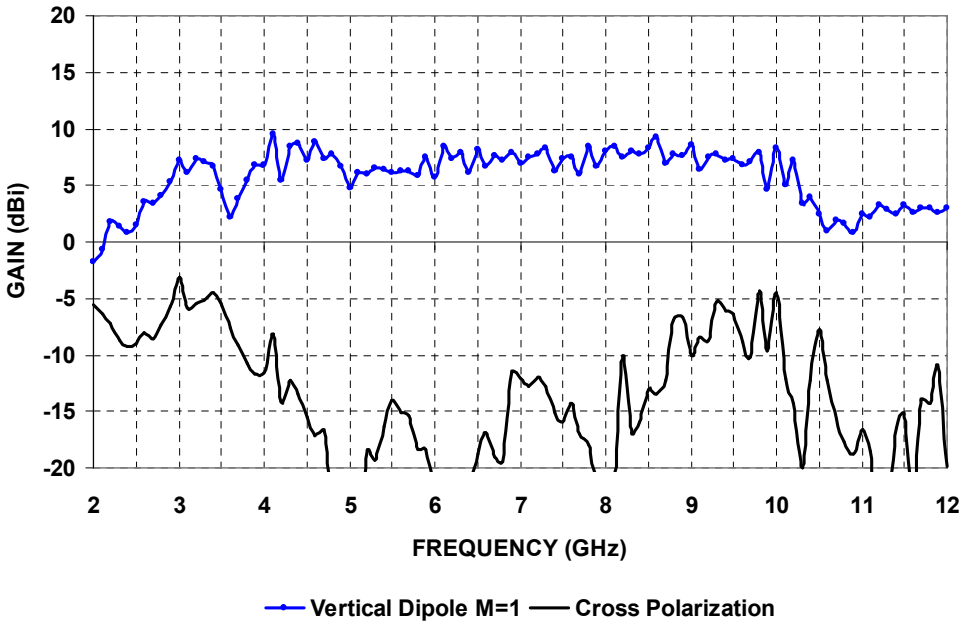

Figure 5.42: Sinuous Antenna Gain Polarisation Response

Figure 5.42 shows that the cross-polarisation of the vertical dipole exhibits an inverted sinusoid response from 4–10 GHz, which peaks at the centre of the band and ranges between -5 dBi and -20 dBi across the band. These results are in agreement with the RF results presented in Section 5.5.7.

Comparing Figures 5.42 and 5.21 demonstrates that the photonic mode transformer is able to receive two linear polarisation exhibited by the two dipoles of the antenna, and does not disturb their co-polarisation and cross polarisation performance.

5.9.4 Circular Polarisation Performance

As explained in Section 5.8.5, a circular polarisation wave can be decomposed into two linear polarisations. Variations on the received power of these two linear polarisations produces elliptically polarised antennas. As discussed in Section 5.7.1 configuring the sinuous antenna using the photonic mode transformer to receiving a 90° relative phase progression among its ports should exhibit circular polarisation characteristics. Provided that the gain response of the polarisation axes (dipoles) of the antenna is not the same, as was demonstrated in Section 5.9.3, the circular polarisation characteristic of the system are expected to be diminished at the lower and upper edge of the 3 dB bandwidth of the photonic hybrid couplers shown in Figure 5.29.

The sinuous antenna was measured using the photonic mode transformer in Figure 5.29 configured first to measure right hand circular polarisation (Table 5.5) and then left hand circular polarisation by changing the bias voltage of the modulators as shown in Table 5.6. This was done by connecting the antenna as shown in Table 5.7 and activating all six wavelengths of the photonic mode transformer. These configurations were characterised using the gain response of the right hand circularly polarised known spiral antennas as a reference, when a similar spiral antenna transmitted the test signal. The gain response of the vertical and the horizontal dipoles it is included in this section for comparison purposes.

Figure 5.43 shows a comparison of the gain response of the vertical and horizontal dipoles of the sinuous antenna (North-South, East-West), as well as the gain response of the photonic mode transformer configures the sinuous antenna to receive a circularly polarised signal.

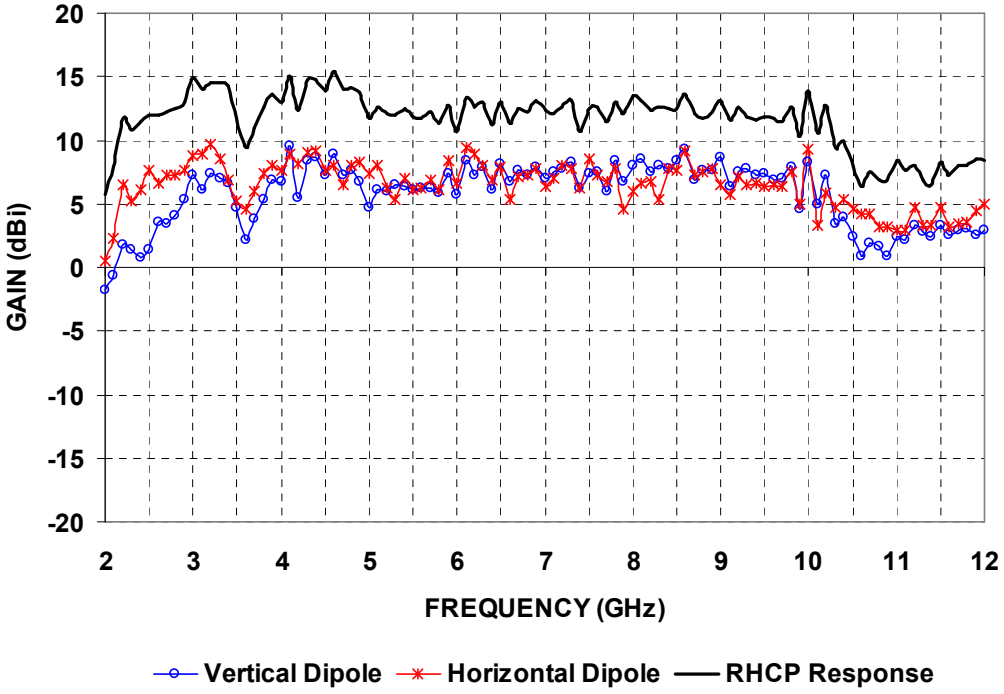

Figure 5.43: Sinuous Antenna Gain. Axes Comparison

Figure 5.43 shows that the combined gain of Port-N and Port-S, exhibits a sinusoidal gain response which increases between 2–5 GHz and decreases between 10–12 GHz as expected due to the response of the photonic hybrid (Section 5.7.1). The combined response of Port-E and Port-W shows a flatter response compared to Port-E and Port-W. The combination of the four ports of the antenna exhibits an average gain level of 12dBi that varies approximately $\pm$ 3 dB.

The difference between the both orthogonal dipole responses (Port-N and Port-S, and Port-E and Port-W) matches the gain difference exhibited between the links of the reconfigurable photonic mode transformer presented in Figure 5.31.

Although an RF characterisation of the circular polarisation performance of the sinuous antenna was not presented in Section 5.5, the results presented in Figure 5.43 confirm that the two orthogonal dipoles measured in Section 5.7.2 and Section 5.8.4 can be orthogonally combined with a relative phase difference of $90\,^{\circ}$ in order to receive a circularly polarised signal over the entire operational bandwidth of sinuous antenna.

As mentioned in Section 5.7.2, by changing the configuration of the modulators, the relative phase of the ports of the antenna can be reconfigured to measure left hand circularly polarised signals. However, not having a set of left hand circularly polarised antennas makes it difficult measuring the effectiveness of the photonic mode transformer to configure the sinuous antenna to receive right hand or left hand circular polarisation. However, using a right hand circularly polarised antenna to transmit the test signal can demonstrate the rejection ratio of cross-polarisation of the antenna using the photonic mode transformer.

Figure 5.44 shows a comparison of the gain response of the sinuous antenna when a right hand circularly polarised antenna transmits the test signal, and the photonic mode transformer is configured first, to receive a right hand circularly polarised (RHCP) signal and then, to receive a left hand circularly polarised (LHCP) signal.

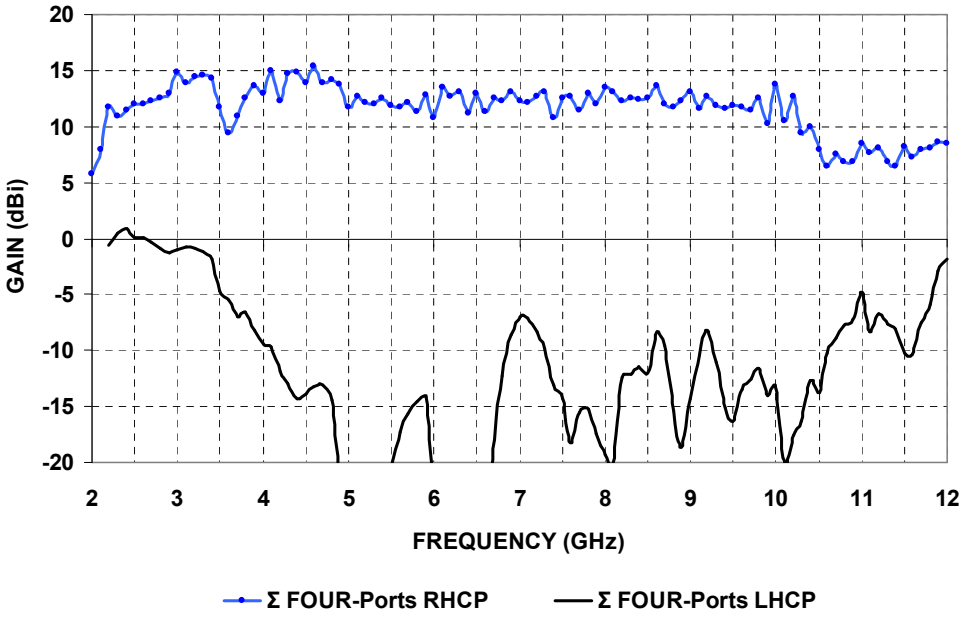

Figure 5.44: Sinuous Antenna Gain. Left Hand Circular Polarisation Rejection

Figure 5.44 shows that the configuring the four ports to measure a left hand circularly polarised signal exhibits an inverted sinusoidal gain response with a peak value of -7 dB in the centre of the band. This inverted sinusoid represents the ability of the system to reject opposite circular polarisations. The system exhibits the lowest gain response centered around 7 GHz, which corresponds with the frequency range where the two orthogonal dipoles exhibits similar gain responses (Figure 5.43)

Comparing Figures 5.44 and 5.42 suggests that the rejection ratio could be an inherent characteristic of the sinuous antenna. However, although there is not sufficient evidence to confirm this, the ability of the photonic implementation to reject opposite circular polarisation might also be defined by the characteristic response of the photonic quadrature hybrid couplers. The results shown in Figure 5.44 suggest that the different gain responses of the orthogonal dipoles affects the polarisation rejection ratio of the sinuous antenna at the edges of the frequency bandwidth. This difference corresponds to the gain difference exhibited between the gain response of the photonic quadrature hybrid coupler and the gain response of the $180\,^{\circ}$ photonic hybrid couplers shown in Figure 5.31.

If the polarisation rejection ratio of the sinuous antenna were defined by photonic hybrid couplers of the photonic mode transformer, different amplitude ripple responses of these photonic quadrature hybrid couplers (Figure 5.24) could provide different rejection performances. Note that the gain of the photonic quadrature hybrid taps (MZM1, MZM2, MZM4 and MZM5) has been adjusted so that the peak gain response is equal to the single tap gain of MZM3 and MZM6. This is not necessarily optimal. It would be quite easy, for example, to decrease the gain of MZM3 and MZM6 by simply attenuating the optical power on λ_3 and λ_6 such that gain balance between the four links of the photonic mode transformer can be achieved at two points across the edges of the operational bandwidth of the antenna, exhibiting a gain imbalance at the centre of this bandwidth. By carefully adjusting this gain balance it may be possible to trim the rejection response to increase the bandwidth.

The analysis of the circular polarisation of the sinuous antenna shown in Figure 5.43 and Figure 5.44 provides enough evidence to confirm that the photonic mode transformer is able to configure the sinuous antenna to receive circularly polarised signals. It also demonstrates that combining the two dipole polarisation axes together provides a 12 dB gain improvement over the individual radiation characteristics of the single element gain response of the sinuous antenna at bore-sight.

In summary, the gain analysis of sinuous antenna has demonstrated that the reconfigurable photonic mode transformer is able to control and measure the radiation characteristics of a four-arm sinuous antenna across the frequency bandwidth defined by the 3 dB bandwidth of the photonic hybrid couplers (4–10 GHz), with a uniform and constant phase and gain response. The major difference to the performance of the antenna caused by the reconfigurable photonic mode transformer is the gain difference between the orthogonal axes. This difference corresponds to the sinusoid response of the photonic quadrature hybrid couplers presented in Figure 5.31. This response can be improved by including more taps or by compromising the gain response of the $180\,^{\circ}$ photonic hybrid coupler so the gain difference with the photonic quadrature hybrid coupler can be reduced, increasing the overall frequency bandwidth.

5.10 Summary and Conclusions

A reconfigurable photonic mode transformer network, able to monitor and control the four normal modes of a four-arm sinuous antenna individually, has been implemented and demonstrated. This implementation substitutes and improves the mode controlling function of a Butler Matrix formed by $180\,^\circ$ and $90\,^\circ$ microwave hybrid couplers traditionally used for phasing dual circularly polarised antennas.

This implementation provides phasing for the multiple polarisations and radiation modes of a four-arm sinuous antenna using a single optical fibre. Two orthogonal linear polarisations, right and left hand circular polarisations directed at bore-sight and also the normal radiation modes of dipole pairs or individual elements of the sinuous antenna which are directed at an angle from bore-sight can be controlled. It is possible to switch between these modes rapidly by simply adjusting a modulator bias or using laser attenuation.

Measurements over a wide range of frequencies and multiple polarisations over different quadrants can represent an advantage for warning receiver systems. This single element can achieve coarse polarisation and direction finding as an initial step in threat identification. This will help guide more specialised systems to complete threat location and classification.

This investigation demonstrated microwave signal conditioning and processing techniques can be implemented on the optical domain. At the same time, it confirms that photonic techniques can be employed to extend the operational bandwidth of traditional microwave hybrid couplers with some bandwidth limitations, mostly determined by the interfacing between the modulator and the device under test, rather than the broadband frequency response of the modulator and the photonic configuration.

The amplitude variation of the photonic mode transformer is mostly determined by the photonic quadrature hybrid coupler employed in this investigation and can be significantly improved by using more taps to define the impulse response of the transversal filter response. This configuration could also be greatly simplified using balanced output modulators (with complementary outputs), in order to substitute the two single output modulators biased in opposite quadrature that were employed to create the two taps of the $90\,^\circ$ photonic hybrid couplers.

The most important advantage of the demonstrated system is its flexibility. Gain balancing can be achieved with high resolution by remotely adjusting the laser powers fed to the photonic mode converter and this can be used to subtly adjust the frequency response of the system. This reconfigurability would be very difficult to achieve with a traditional RF system.

Chapter 6

Conclusions

The aim of this dissertation was to improve electromagnetic sensors (antennas) and signal processing techniques for military front-end receiver. The main motivation of this dissertation was to use Microwave Photonics signal processing techniques to improve the characteristics of front-end receivers used in Electronic Warfare and navigation systems, particularly in military aircrafts where weight, volume, instantaneous detection and high latency response are critical design specifications.

Two main interfaces were implemented and demonstrated. The first interface extended the operational bandwidth of single antenna front-end receivers by photonically multiplexing multiple radiating elements with adjacent bandwidths into an ultra-broadband radiating shared aperture that exhibited uniform radiation characteristics across its entire bandwidth. The second interface controlled the multiple-beam pattern radiation characteristics of multi-mode single aperture antennas by implementing a reconfigurable Microwave Photonic version of traditional Butler matrix mode transformers used for phasing single aperture antennas with multiple radiating elements. The overall goal of the dissertation has been met. The specific accomplishments in each chapter are summarised in the following.

6.1 Outcomes of this work

The primary outcomes of this dissertation are several photonic signal processing techniques that could improve the volume, weight and reduce complexity of front-end device design and fabrication, using a cost-effective Microwave Photonic configurations.

In Chapter 2, an implementation of a two octave bandwidth antenna was demonstrated using microwave photonic links antenna and optical multiplexing techniques. Two aperture stacked patch antennas were combined into a single radiating shared aperture element by modulating the signals from each antenna onto optical carriers and then multiplexing them using polarisation diversity. A single laser source was used to drive both optical channels of the system.

The resulting system made use of a single photonic channel input and provided a single photonic channel at the output with the photonic combination of the two adjacent frequency bandwidths of the antennas. The key elements of this implementation were

the polarisation controller and the polarisation beam splitters used to split the optical carrier into two parallel carriers and combine them after being modulated, with the RF signal received by each antenna, with orthogonally polarised propagation modes. The Microwave Photonic implementation demonstrated the ability to combine the response of both antennas into a single larger bandwidth element while retaining the broadband characteristics of the original patch antennas, and without exhibiting coherent interference in the optical domain.

The measured results showed that the response of each antenna element can be effectively isolated in the optical domain avoiding the impedance loading effects occurred in the RF domain. An ultra-broadband ASP antenna with a broadband gain bandwidth of 1.1–3.8 GHz was demonstrated showing modest gain uniformity. The gain response of this antenna showed a variation on gain of approximately 3.5 dB. This variation was attributed to the interaction between the antennas at the overlapping zones where both antennas radiate simultaneously with similar levels. Therefore, it was concluded that trimming the gain bandwidth of each antenna was still necessary in order to achieve a flatter overall gain response. It was also noted that using polarisation diversity for this implementation, would only be effective for combining two antennas.

Chapter 3 investigated the use of more than two antennas and filtering techniques in order to improve and extend the multiplexing implementation shown in Chapter 2. This implementation used a wavelength division multiplexing approach employing an Array Waveguide Gratings (AWG) to combine, split and recombine three different wavelength carriers into a single optical fibre link. Each of the three carriers was modulated using the RF signal received from a different antenna. Each patch antenna was designed to have an adjacent octave bandwidth, with ASP1, ASP2 and ASP3 operating from 1-2, 2-4 and 4-8 GHz respectively. The frequency response of each antennas was trimmed using microwave filtering techniques to ensure that the coherent interference between each band at the cross-over frequencies did not cause undesirable gain ripple.

The measured results demonstrated that the individual characteristics of each antenna were maintained. The three adjacent bandwidths were successfully combined to create an ultra-broadband antenna element with uniform characteristics. The overall response exhibited an operational bandwidth from 1.1 GHz to 7.6 GHz and an amplitude gain response variation of approximately 2 dB. Unlike to the amplitude variation presented by the implementation demonstrated in Chapter 2 where the amplitude variation correspond to the interaction of the antennas at their intersection frequencies, the variation exhibited by this investigation was attributed to the individual gain response of each ASP antenna.

Chapter 3 also presented an investigation on frequency response stability of the beam pattern performance of the combined elements over the multi-octave bandwidth. The results of this radiation pattern investigation showed that the relative placement of the antennas was critical for achieving uniform radiation characteristics at all frequencies. At the overlapping frequencies, two elements radiate simultaneously and thus, if the spacing between the two elements is bigger than half a wavelength, then considerable grating lobes were observed. Since the wavelength was frequency dependant, the onset of grating lobes was highly frequency dependent. To counter the appearance of grating lobes, the separation between the antennas must remain as small as possible. This is true for both, vertical and horizontal antenna separation. It was demonstrated that a diagonal arrange-

ment between antennas of adjacent bandwidths was the optimum placement to minimise the separation in both vertical and horizontal planes.

Chapter 2 and Chapter 3 demonstrated that multiple broadband antennas can be combined together in order to extend the operational bandwidth of single antenna front-end receivers. The flexibility of incorporating antennas into front-end receivers without interfering with the response of the existing elements makes this implementation particularly suitable for current and future applications where platforms with multiple protocols or multiple services providers share the same hardware ("Antenna Kiosk").

Although, multiple photonic multiplexing techniques have been demonstrated to be useful for extending the bandwidth of front-end receivers by combining multiple single antenna elements, photonic signal processing techniques can be used for many other applications. These applications include beam-steering, null steering or channelisation to mention only a few. Chapter 4 investigated how to use photonic signal processing techniques such as phase shifting, multiplexing and amplitude weighting in order to control the multi-beam pattern characteristics of a two-arm spiral antenna.

Chapter 4 has demonstrated that a Microwave Photonic 180° hybrid coupler can be implemented using photonic techniques in order to control the dual mode operation of a two-arm spiral antenna. This implementation was demonstrated using the same principle employed in Chapter 2 used to combine two ASP antennas. A cavity backed two-arm spiral antenna was modified for testing purposes in order to access both balanced radiation modes of the antenna. The traditional balanced to unbalanced transition (Balun) of the spiral antenna that limits its operation to only the fundamental radiation mode was replaced by a multi-port mode transformer. The developed transformer was bandwidth limited, exhibiting an impedance bandwidth of 2–12 GHz. The impedance bandwidth of this RF mode transformer was considered to be enough to test the Microwave Photonic 180° hybrid coupler controller.

The counter phase modulation characteristics of the Mach-Zehnder modulators included in this implementation was exploited in order to use the bias of the modulators to modify the phase of the RF signal received by each port of the spiral antenna by 180°. Changing the relative phase received from the ports of the antenna using this Microwave Photonic implementation configures the two-arm spiral antenna to receive either its fundamental mode, characterised by a single beam pattern, or its second radiation mode, characterised by two main tilted beams which location and orientation varies with frequency.

The measured results demonstrated that the balanced operation of the antenna can be easily adjusted by simply modifying the splitting ratio of the optical source with the polarisation controller.

The splitting ratio of the optical source can also be controlled to direct the full optical power into one channel at the time, enabling this implementation to receive only the signal from one port of the antenna at the time and create single tilted radiation beam patterns.

Traditional RF 180° hybrid couplers does not enable individual access to the ports of this customised two-arm spiral antennas, making Microwave Photonics hybrid coupler even more attractive for controlling the multiple radiation patterns of this two-arm spiral antenna and use them to implement a crude version of direction finding applications.

Measured results demonstrated however that the single radiation beams received from each port of the spiral antenna are frequency dependent and rotates around broadside direction across the entire operational bandwidth. Therefore special software considerations might need to be implemented to achieve a reliable direction finding application.

Finally, Chapter 5 investigated the multiple-beam radiation pattern control of a four-arm sinuous antenna so multi-mode single aperture antenna applications can also benefit from using photonic signal processing techniques. A reduced cavity backed four-arm sinuous antenna with individual access to its radiating element was developed. The limited impedance bandwidth response achieved for the multi-port sinuous antenna (4–10 GHz) was considered sufficient for a proof of concept demonstration. The Microwave Photonic mode transformer was implemented using the 180° photonic hybrid coupler concept demonstrated in Chapter 4 and a 90° photonic hybrid coupler based on photonic transversal techniques. The key components of this configuration were the AWGs that combined individual laser sources into a single fibre and split them into individual channels connected to Mach-Zehnder modulators.

This implementation could substitute a complex Butler matrix composed of two 180° hybrid couplers and a 90° hybrid coupler with an elegant reconfigurable Microwave Photonic implementation that improves weight, volume and flexibility of a front-end receiver for navigation systems in military aircrafts.

Measured results demonstrated that the Microwave Photonic transformer was not only able to configure the four-arm sinuous antenna to receive right and left hand circular polarisation (as with the RF Butler matrix) but also to receive several other radiation modes using a single optical fibre link. Two linearly polarised - orthogonally oriented "dipole" like antenna response were demonstrated. These "dipoles" could be operated either in their fundamental radiation mode or their second radiation mode characterised by a dual beam radiation pattern that exhibited a null at broadside direction.

Four individual beam patterns were also achieved by switching on and off the power of the optical source, so the signals received by the arms of the sinuous antenna were controlled individually. These radiation patterns proved to exhibit better radiation pattern stability, compared with the spiral antenna demonstrated in Chapter 4, which patterns are constantly changing. The alternating winding of the radiating elements of the sinuous antenna stop the patterns to wobble more than 4%, confirming that this single aperture sinuous antenna can be used for coarse polarisation and direction finding purposes.

Chapter 2 through Chapter 5 have progressively demonstrated that Microwave Photonic techniques can be used to enable sophisticated solutions that can integrate multiple applications into compact, light weight, robust and flexible front-end receivers for Electronic Warfare applications, particularly for airborne platforms.

The developed antennas and the photonic multiplexing and polarisation diversity techniques presented in Chapter 3 have demonstrated two main points. The first one is that Microwave Photonics enables to control multiple electromagnetic sensors and reduces the overall weight and space requirements of front-end receivers by using optical fibre technologies. The second point is that implementing a broadband platform where multiple antennas can be integrated as they emerge, facilitate flexible and efficient deployment, maintenance, revision, upgrade and retirement of Electronic Warfare applications.

The Microwave Photonic hybrids implemented in Chapter 4 and Chapter 5 have demonstrated that controlling multifunctional broadband antennas it is possible without deploying complex RF mode converters such a Butler matrix. Both front-end receivers developed in these Chapters have demonstrated to be able to adapt to multiple scenarios by only changing the polarisation bias of the electro-optic modulators, by adjusting the weight function of the optical power and by using photonic transversal techniques.

6.2 Suggestions for future work

The concept of a front-end device able to receive arbitrary combinations of frequencies bands, able to control multiple antenna diversity schemes of multifunctional single aperture antennas, and significantly flexible so it can adapt to future scenarios without deploying expensive hardware modifications has been demonstrated in this dissertation. These Microwave Photonic implementations have demonstrated to optimise weight and spatial requirements for airborne Electronic Warfare applications. However, all of them can be potentially monolithically fabricated, which would result in smaller size, lighter weight and lower cost devices. Further investigation on this area is recommended so other aspects of the systems mentioned in this dissertation can be explored. Below, there is a summary of areas that hold potential for future work.

Monolithic integration techniques could improve the flexibility of the system so the antennas can be easily positioned in different locations. Chapter 2 and 3 demonstrated that rearranging the relative position of the ASP antennas was necessary. Rearrangement was somewhat cumbersome due to the bulk of the optical modulator/filter/antenna combination. Using a diagonal arrangement, both radiation planes of the antenna are approximately affected in the same proportion. However, this "optimum" results must be reconsidered on individual bases according to the application. Integration of these components would results in a far more compact and robust module, enabling flexible rearrangement of the various antenna elements.

Polarisation and bias drift of various components within the Microwave Photonic implementations significantly impacted the reliable operation of the system. If these implementations are to be used in practical applications, it is recommended that electronic monitoring and control of the bias of the modulators should be implemented. Further, polarisation maintaining components should be used throughout the system.

The current latency response of these implementations has not been fully investigated due the fact that electronic bias controllers were not employed. Automated polarisation controllers and DC voltage sources could improve the latency of the weighting function achieved in Chapter 2 and 4 and the multiple-beam pattern time selection of the sinuous antenna demonstrated in Chapter 5.

It is recommended that the sinuous antenna design should be further investigated and optimised in order to achieve a larger impedance bandwidth response suitable for current military applications. The Microwave Photonic implementation of the 90° photonic hybrid coupler was implemented with two taps and RF delay lines in order to meet the impedance bandwidth of the sinuous antenna. However, a broadband 90° photonic hybrid coupler can be implemented using multiple taps and optical delay lines [96].

The circular polarisation performance of the sinuous antenna investigated in Section 5.9.4 was only characterised radiating in the broadside direction due the lack of equipment and proper antenna testing facilities. It is suggested that this investigation should be expanded in order to fully characterise the dual polarised response of the sinuous antenna [85] and the multiple-beam pattern control of the Microwave Photonic mode transformer.

Appendix A

Self-complementary Frequency Independent Antennas

A.1 Self-complementary Sinuous Antenna

A self-complementary sinuous antenna may consist of N-arms and N slots with a rotational symmetry such that a rotation of $360\,^{\circ}$/N around the perpendicular axis to the surface of the antenna leaves the antenna unchanged for a viewer located at bore-sight direction.

As shown in Figure A.1, the sinuous antenna geometry is fully defined by angles α or angular span, δ or rotation angle, as well as the log-periodic growth rate of τ. The curve which defines each arm of the sinuous antenna is a series of cells starting with cell1 at the outer radius R_1. R_p defines the outer radius of the $cell_p$; α, its angular width, and τ_p defines ratio of the inside-to-outside radius for each cell R_p/R_{p-1}. The equation for the p^{th} cell is given by

$$\phi = (-1)^p \alpha_p sin\left[\frac{180ln(\frac{r}{R_p})}{ln\,\tau_p}\right] \qquad R_{p+1} \leq r \leq R_p \tag{A.1}$$

where r and ϕ are the polar coordinates of the curve.

The radii R_p are related by

$$R_p = \tau_{p-1} R_{p-1} \tag{A.2}$$

One sinuous arm is formed by rotating the curve of Eq. A.1 by $\pm\,\delta$ around the origin (ϕ), as shown in Figure A.1. A complete sinuous antenna is developed by the angular rotation on ϕ of the single arm through 360/N degree increments to form an N-arm structure. The amount of interleaving between the arms, defined by α_p and δ should be adjusted so that $\alpha + \delta\ < 70\,^{\circ}$ to ensure good efficiency, gain response and frequency response of the antenna [85].

Also, Figure A.1 shows that δ defines the self-complementary condition for the N-arm sinuous antenna. It is believed that δ is important in providing the capacitance necessary to tune out the sharp inductive corners of the sinuous antenna. Figure A.2 shows a picture of a four-arm sinuous antenna.

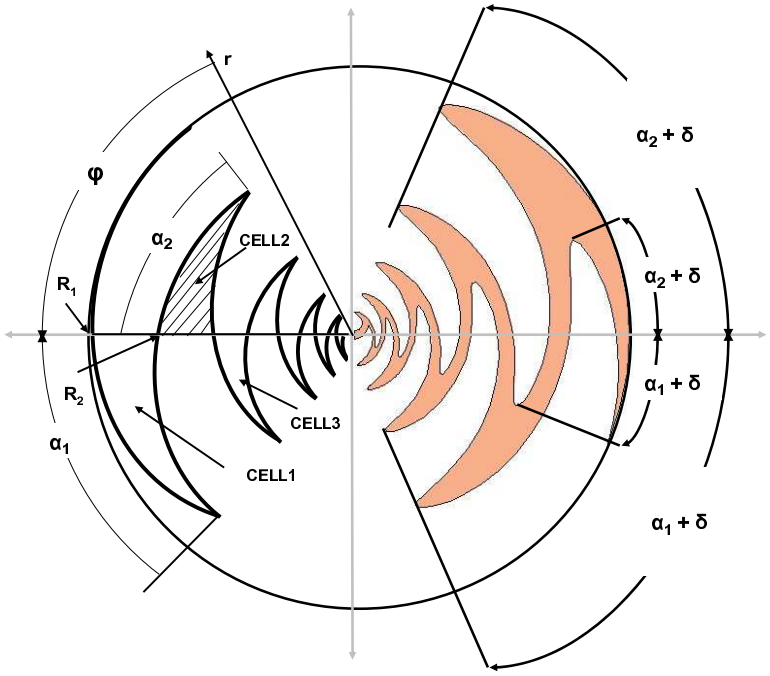

Figure A.1: Sinuous Arm Parameterisation

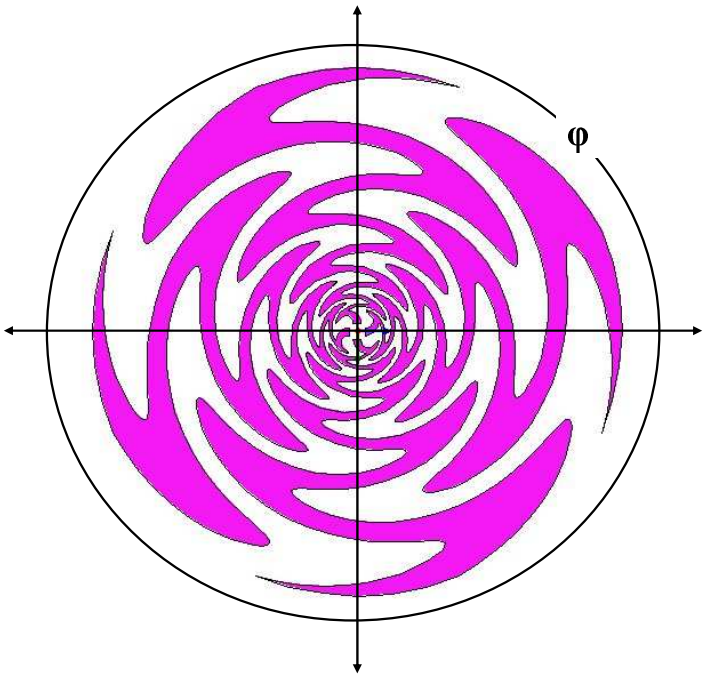

Figure A.2: Sinuous Antenna

Analysis of the geometry of the sinuous antenna structure demonstrated that this antenna can exhibit rotational symmetry around its central axis, provided that the right parameters are chosen. This particular property makes the antenna a self-complementary structure with printed arms and slots identical around its origin. Thus, this antenna can be analysed using the self-complementary antenna principle presented by [74].

A.1.1 Sinuous Antenna Modes

According to the analysis on self-complementary structures presented in [74], each arm of the sinuous antenna can be excited individually generating a characteristic beam pattern tilted off bore-sight with broadband frequency response. This individual form of excitation is defined as a normal mode. There are N normal modes for an N-arm sinuous structure.

Exciting one or more normal modes simultaneously produces a variety of useful radiation patterns. A combination of normal modes is defined as an "M-mode". For any M-mode, the normal modes are often fed with equal magnitudes and with progressive phases as given by $2\,\pi\,M/N$, where N is the number of arms and M is an integer that defines desired M-mode.

A sinuous antenna with sufficient interleaving between its arms has approximately the same frequency limits as a spiral antenna. In order for the sinuous antenna to support efficient normal modes, the antenna needs to be N wavelengths in circumference. According to [92], if M modes of operation with the same polarisation are desired, an N=2M+1 arm sinuous antenna is needed.

Figure A.3 shows some of the M-modes that can be generated by an N-arm sinuous antenna using a combination of its normal modes. Only one mode has a broadside radiating component (M=1) and all other modes have a null on broadside, with each higher-order mode peaking further from the null.

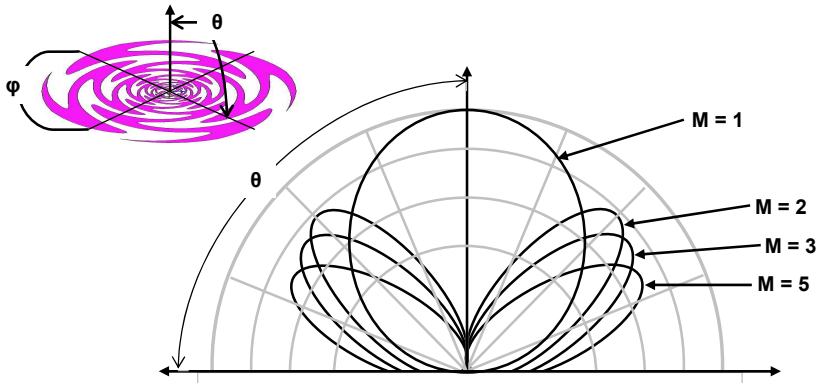

Figure A.3: Sinuous Antenna M-modes Radiation Patterns

Each arm of the self-complementary sinuous antenna can be considered as a travelling wave monopole antenna which maintains an impedance match over multiple octaves. As long as the feeding network provides a broadband impedance matching for the normal modes, phasing these modes can generate M-modes with the same broadband characteristics.

A.1.2 Free Space Antenna Characteristic Impedance

Broadband performance of the sinuous antennas can only be achieved if each of the characteristic input impedance of the antenna for the desired M-mode is matched by its feeding network. Effectively, only one of the M-modes can be matched at the time by the same feeding network.

The input impedance to the ground for a self-complementary N-arm structure in the free space is derived by [74] and is given as

$$Z_M = \frac{\frac{\eta_0}{4}}{sin\left(\frac{M\pi}{N}\right)} \tag{A.3}$$

where $\eta_0 = 120\pi\Omega$ is the impedance of the free space and M is the integer that defines the M mode. N is the number of arms on the structure. Table A.1 shows some calculated values corresponding to the input impedance of different multi-arm self-complementary structures for different modes of excitation.

Table A.1: Input Impedance for Self-Complementary Structures in Free Space

	Self-complementary Modes				
#Arms	1	2	3	4	5
2	94.2				
3	108.8	108.8			
4	133.3	94.2	133.3		
5	160.3	99.1	99.1	160.3	
6	188.5	108.8	94.2	108.8	188.5

Practical implementations of a four-arm sinuous antenna using 140Ω balanced feed lines for M=1 radiation mode have resulted in VSWR values on the average of 1.7:1 bandwidths [85]. Similar to this, various investigations [71, 73] have demonstrated that operating a multi-arm sinuous antenna in mode M=1 with a balanced feed line, whose impedance approximates the values presented in Table A.1, obtains broadband radiation characteristics.

A.1.3 Multi-mode Operation

As discussed in Section 5.1, it would be desirable to operate an antenna in more than one mode for direction finding purposes. Effectively, only one of the M-modes of the sinuous antenna can be matched at the time by the same feeding network. However, Chapter 4 has demonstrated that two unbalanced transmission lines can be driven with a relative phase difference of 0° or 180° in order to generate the M-modes M=1 and M=2 of a two-arm cavity backed spiral antenna, respectively.

From Table A.1 it can be observed that a sinuous antenna operating over multiple modes needs to balance the performance of the antenna between the input charac-

teristic impedance of these N number of M-modes. For example: selecting an average input impedance of 112Ω for a four-arm sinuous antenna operating in mode M=1 ($Z_0 = 133.3\Omega$) and M=2 ($Z_0 = 94.2\Omega$). This has been shown to limit the inherent mismatch of the feeding network to less than 1.19 for both modes [85].

Multi-mode operation of sinuous antenna is only possible by designing feeding networks able to control the relative phase between the arms of the antenna and also able to provide with an equivalent impedance to that which compromises the performance of antenna operating in N number of M-modes based on Eq. A.3.

Appendix B

Hilbert Transform

B.1 Hilbert Transform Properties

The properties of the Hilbert Transformation are of relevant interest for multiple applications such as digital communication systems [99], radar systems [100], time difference of arrival processing in direction finding systems [101] and single sideband modulators [102], where a phase shift of 90° provides an additional degree of flexibility and versatility for signal processing. Chapter 5 introduces another application where implementing the Hilbert Transformation in the optical domain could be used to substitute a microwave Butler matrix designed for controlling and phasing a four-arm sinuous antenna.

An ideal Hilbert Transformer is a type of filter that changes only the phase of the spectral components of a signal, depending on the sign of their frequency, leaving intact the amplitude of the signal.

Using a cosine and a sine signal as an example, this appendix illustrates the properties of the Hilbert Transformation, which are the fundamentals of a photonic quadrature hybrid implementation introduced in Chapter 5 of this dissertation.

B.1.1 Fourier Series

Jean Baptiste Joseph Fourier demonstrated that any periodic signal can be considered as a composition of multiple sine waves. The Fourier Series of these signals can be written as

$$f(t) = \sum_{n=-\infty}^{\infty} C_n e^{jnwt} \tag{B.1}$$

where

$$C_n = A_n + jB_n \tag{B.2}$$

and

$$C_{-n} = A_n - jB_n \tag{B.3}$$

and An and Bn are the spectral amplitudes of cosine and sine waves. The phase spectrum of this signal is computed by

$$\varphi = tan^{-1}\frac{B_n}{A_n} \tag{B.4}$$

Cosine Fourier Components

Figure B.1 shows the amplitude and the phase spectrum of a cosine wave. Cosine wave has no sine spectral content, so B_n is zero in Eq. B.2. The phase calculated is $0\,^\circ$ for both positive and negative frequency. The wave has two spectral components, each of magnitude $1/2$ A, both positive and lying in the real plane.

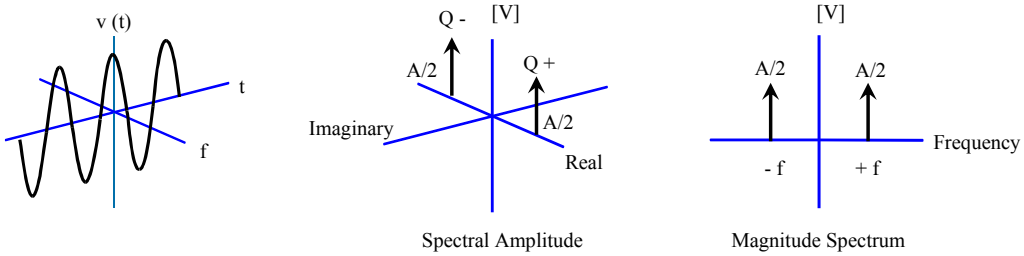

Figure B.1: Cosine Wave Properties

Sine Fourier Components

Figure B.2 shows the amplitude and the phase spectrum of a sine wave. The sine wave phase is not symmetric because the amplitude spectrum is not symmetric. The quantity A_n is zero and B_n in Eq. B.1 has either a positive or negative value. The phase is $90\,^\circ$ for the positive frequency and $-90\,^\circ$ for the negative frequency.

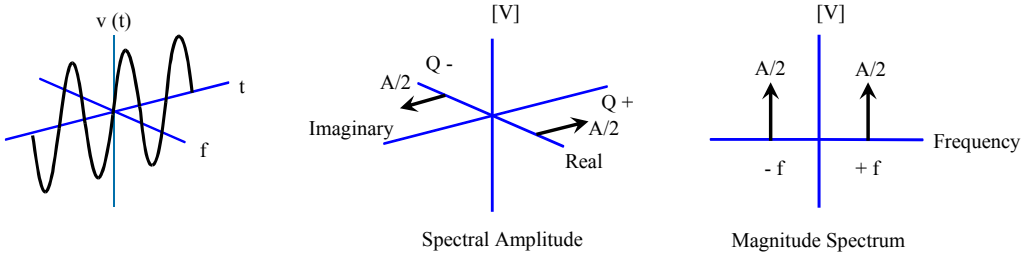

Figure B.2: Sine Wave Properties

The relative phase difference between a Cosine and Sine is $\pm\,90\,^\circ$. Therefore, using a spectral transformer to change from one to another will demonstrate a phase shifting effect equal to a quadrature hybrid coupler effect.

B.1.2 Hilbert Transformation in Frequency Domain

Comparing Figure B.1 and Figure B.2 it is clear that in order to change the cosine function to a sine function, the spectral amplitude of the signal needs to be rotated as shown in

Figure B.3. The negative frequency component of the cosine must be rotated by +90 and the positive frequency component, by -90 . The Hilbert Transform can be summarised as a function that shifts all the negative frequencies of a signal by $90\,^{\circ}$ and all the positive frequencies by $-90\,^{\circ}$.

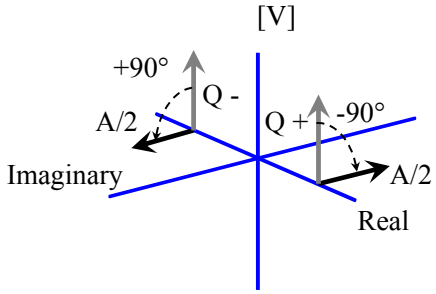

Figure B.3: Phasor Rotation

For any signal $g(t)$, its Hilbert Transform has the following property

$$\overset{\wedge}{G(f)} = \begin{matrix} -j\ for\ f > 0 \\ \\ +j\ for\ f < 0 \end{matrix} \tag{B.5}$$

For this reason a Hilbert Transformer is also called a "quadrature filter". This filter can be drawn as shown in Figure B.4.

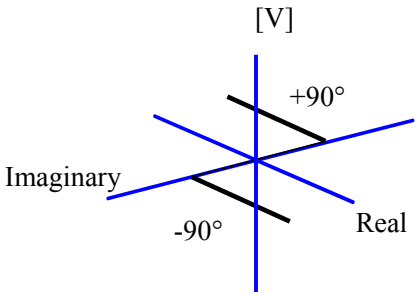

Figure B.4: Filter Response of the Hilbert Transform

B.1.3 Hilbert Transformation in Time Domain

A Hilbert Transformation of the signal $g(t)$ in time domain can be defined as:

$$\overset{\wedge}{g(t)} = \frac{1}{\pi}\int_{-\infty}^{+\infty}\frac{g(\tau)}{t-\tau}d\tau \tag{B.6}$$

which is also the convolution of function $\frac{1}{\pi}\,t$ with the signal $g(t)$. Therefore, Eq. B.6 can be rewritten as:

$$\overset{\wedge}{g(t)} = \frac{1}{\pi\,t} * g(t) \tag{B.7}$$

This illustrates that achieving a Hilbert Transformation of the signal $g(t)$ in time domain means convolving the signal $g(t)$ with the function $\frac{1}{\pi}\,t$. The Fourier Transform of $\frac{1}{\pi}\,t$ function is defined as.

$$F\left(\frac{1}{\pi\,t}\right) = -jsgn(f) \tag{B.8}$$

where sgn(f) is called the signum function and can be rewritten as follows:

$$F\left(\frac{1}{\pi\,t}\right) = -jsgn(f) \begin{array}{l} -j\;for\;f > 0 \\ \\ +j\;for\;f < 0 \end{array} \tag{B.9}$$

Figure B.5 shows that although $\frac{1}{\pi}\,t$ is a real function, it has a Fourier transform that lies strictly in the imaginary plane and has no real components.

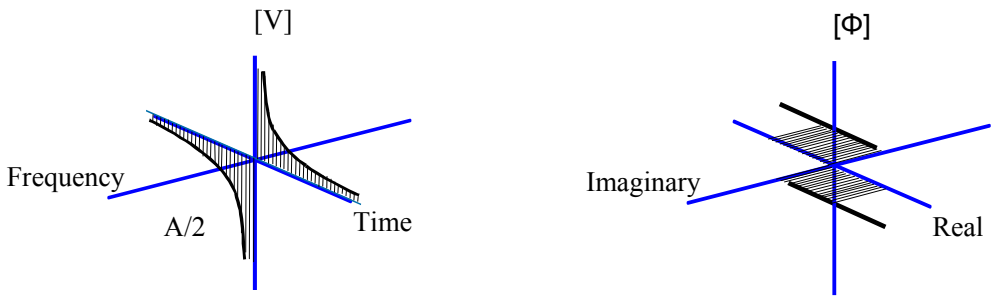

Figure B.5: Function f(t)=$\frac{1}{\pi}\,t$ and its Fourier Transformation

It is evident that convolving the signal $g(t)$ with the function $\frac{1}{\pi}\,t$ could provide a relative phase shift of $90\,^{\circ}$ to the signal. Function $\frac{1}{\pi}\,t$ can be approximated by using discrete samples of the signal $g(t)$ that are weighted (apodised) according to the impulse response of the function $\frac{1}{\pi}\,t$.

Convolving a signal in time can be practically achieved using a technique called transversal filtering [103, 104, 105], and specifically photonic transversal filtering [90, 95]. A description of transversal and photonic transversal filters can be found in Section 5.6.1.

Bibliography

[1] T. Ojanpera, "Perspectives on 3g system development [mobile communications]," in *IEEE International Symposium on Personal, Indoor and Mobile Radio Communications*, vol. 1, pp. 405–409, Sep 1998.

[2] E. D. Kaplan and C. J. Hegarty, *Understanding GPS Principles and Applications*, pp. 1–4. Norwood, MA:Artech House, Inc., second ed., 2006.

[3] Z. Lizhong and C. Xiuwan, "The application of satellite positioning technology and its industrialization in china," in *IEEE International Conference on Communications, Circuits and Systems and West Sino Expositions*, vol. 2, pp. 1561–1565, Jul 2002.

[4] H.-R. Chuang, L.-C. Kuo, C.-C. Lin, and W.-T. Chen, "A 2.4 ghz polarization-diversity planar printed antenna for wlan and wireless communication systems," in *IEEE Antennas and Propagation Society International Symposium*, vol. 4, pp. 76–79, 2002.

[5] H. Ma and X. Shen, "The performances of the antennas in active/passive compounded guidance part ii: Compounded antennas schemes and performances of active/passive guidance," *Journal International Journal of Infrared and Millimeter Waves*, vol. 19, pp. 119–128, Nov 2004.

[6] P. Grant and J. Collins, "Introduction to electronic warfare," *IEE Proceedings For Communications, Radar and Signal Processing*, vol. 129, pp. 113–132, Jun 1982.

[7] A. Spezio, "Electronic warfare systems," *IEEE Transactions on Microwave Theory and Techniques*, vol. 50, pp. 633–644, Mar 2002.

[8] D. Horwitz, "Cots fiber optic applications in military and aerospace," in *Optical Fiber Communication Conference*, vol. 4, pp. 12–14, 2000.

[9] S. Koehler, "Advances in hybrid optical packaging enable high-bandwidth photonic rf transmission," *Military and Aerospace Electronics Magazine*, Oct 2005.

[10] R. Erickson, R. Gunnarsson, T. Martin, L.-G. Huss, L. Pettersson, P. Andersson, and A. Ouacha, "Wideband and wide scan phased array microstrip patch antennas for small platforms," in *The Second European Conference on Antennas and Propagation*, pp. 1–6, Nov 2007.

[11] A. Dokuchaev, *Encyclopedia of Naval Radio-Electronic Warfare. From Port Arthur to the Present*, ch. 1, pp. 1–4. Arms and Technologies Publishing House, 2004.

[12] G. Lewis and T. Postol, "Future challenges to ballistic missile defense," *IEEE Spectrum Magazine*, vol. 34, pp. 60–68, Sep 1997.

[13] E. Greneker, "Technology for the detection of airborne intruders approaching the high-security, high-value asset," in *Proceedings of the IEEE International Carnahan Conference on Security Technology*, pp. 159–162, Oct 1995.

[14] D. Forrai and J. Maier, "Generic models in the advanced ircm assessment model," in *Proceedings of the Winter Simulation Conference*, vol. 1, pp. 789–796, 2001.

[15] F. Leferink, "Emc for maritime systems, workshop part2," in *EMC Europe*, Sep 2008.

[16] G. Tavik, C. Hilterbrick, J. Evins, J. Alter, J. Crnkovich, J.G., J. de Graaf, I. Habicht, W., G. Hrin, S. Lessin, D. Wu, and S. Hagewood, "The advanced multifunction rf concept," *IEEE Transactions on Microwave Theory and Techniques*, vol. 53, pp. 1009–1020, Mar 2005.

[17] R. G. Corzine and J. A. Mosko, *Four-arm Spiral Antennas*. Artech House, 1990.

[18] M. Kim, H. Choo, and I. Park, "Two-arm microstrip spiral antenna for multi-beam pattern control," *Electronics Letters*, vol. 41, pp. 627–629, May 2005.

[19] J. Wang, G. Hopkins, and V. Tripp, "A new class of wideband low-profile, conformal antennas-its impact to wireless telecommunications," in *IEEE International Conference on Selected Topics in Wireless Communications*, pp. 115–117, Jun 1992.

[20] J. Blau, "Supermarket's futuristic outlet," *IEEE Spectrum Magazine*, vol. 41, no. 4, pp. 21–22, 25, 2004. TY - JOUR.

[21] K. Ghorbani and R. B. Waterhouse, "Ultrabroadband printed (ubp) antenna," *IEEE Transaction on Antennas and Propagation*, vol. 50, pp. 1697–1705, 2002.

[22] E. Lopez, L. Bui, K. Ghorbani, W. Rowe, and A. Mitchell, "Ultra-broadband photonic patch antenna," in *Microwave Symposium Digest, 2006. IEEE MTT-S International*, pp. 1939–1942, June 2006.

[23] A. Margulies and I. Mitola, J., "Software defined radios: a technical challenge and a migration strategy," in *IEEE 5th International Symposium on Spread Spectrum Techniques and Applications*, vol. 2, pp. 551–556, Sep 1998.

[24] I. Mitola, J., "Software radios-survey, critical evaluation and future directions," in *National Telesystems Conference*, vol. 13, pp. 15–23, May 1992.

[25] J. Mitola, "Software radio architecture evolution: Foundations, technology tradeoffs and architecture implications," *IEICE Trans*, vol. E83-B, no. 6, 2000.

[26] K. Raghu, "Overcoming effects of electromagnetic interference in warships through multi-sensor data fusion," in *International Conference on Electromagnetic Interference and Compatibility*, pp. 152–156, 2002.

[27] K. Yazdandoost and R. Kohno, "Bow-tie antenna for uwb communication frequency," in *IEEE Antennas and Propagation Society International Symposium* (R. Kohno, ed.), vol. 3, pp. 2520–2523, 2004.

[28] C. Ying and Y. Zhang, "A planar antenna in ltcc for single-package ultrawide-band radio," *Antennas and Propagation, IEEE Transactions on*, vol. 53, no. 9, pp. 3089–3093, 2005.

[29] P.-L. Chi, S.-S. Wu, and Y.-D. Lin, "Integrated antennas and diplexers for dual-band wireless local area network (wlan) system," in *Asia-Pacific Microwave Conference*, vol. 4, p. 4, 2005.

[30] R. B. Dybdal and S. J. Curry, "Arraying large antennas," in *IEEE Antennas and Propagation International Symposium* (S. J. Curry, ed.), pp. 5973–5976, 2007. TY - CONF.

[31] J. Powell, "Antenna design for ultra wideband radio," Master's thesis, Massachusetts Institute of Technology, 2004.

[32] A. Lestari, A. Yarovoy, L. Ligthart, and E. Rahardjo, "A uwb antenna for impulse radio," in *IEEE Vehicular Technology Conference*, vol. 6, pp. 2630–2634, May 2006.

[33] P. Eyring, "Compact df antenna delivers high aoa accuracy," *Microwaves and RF Magazine*, vol. 36, p. 61, Jun 1997.

[34] B. Galwas, "Photonic technology for microwave engineering," in *12th International Conference on Microwaves and Radar*, vol. 4, pp. 117–134, May 1998.

[35] L. Johnson, G. Betts, P. Schulz, P. Juodawlkis, and W. Lyons, "Photonics for agile-beam wideband antenna systems," in *Digest of the LEOS Summer Topical Meetings Electronic-Enhanced Optics, Optical Sensing in Semiconductor Manufacturing, Electro-Optics in Space, Broadband Optical Networks*, pp. III9–II10, 2000.

[36] S. Targonski, R. Waterhouse, and D. Pozar, "Design of wide-band aperture-stacked patch microstrip antennas," *Antennas and Propagation, IEEE Transactions on*, vol. 46, no. 9, pp. 1245–1251, 1998.

[37] W. S. C. Chang and G. E. Betts, *RF Photonic Technology in Optical Fiber Links*. Cambridge, 2002.

[38] C. H. Cox, *Analog optical links: theory and practice*. Cambridge, 2004.

[39] S. Mathai, F. Cappelluti, T. Jung, D. Novak, R. Waterhouse, D. Sivco, A. Cho, G. Ghione, and M. Wu, "Experimental demonstration of a balanced electroabsorption modulated microwave photonic link," *IEEE Transactions on Microwave Theory and Techniques*, vol. 49, pp. 1956–1961, Oct 2001.

[40] C. Cox, "Gain and noise figure in analogue fibre-optic links," *Optoelectronics, IEE Proceedings J*, vol. 139, pp. 238 –242, aug 1992.

[41] X. Zhang and A. Mitchell, "A simple black box model for erbium-doped fiber amplifiers," *IEEE Photonics Technology Letters*, vol. 12, pp. 28–30, Jan 2000.

[42] D. Sabido and L. Kazovsky, "Dynamic range of optically amplified rf optical links," *IEEE Transactions on Microwave Theory and Techniques*, vol. 49, pp. 1950–1955, Oct 2001.

[43] J. C. Palais, *Fiber Optic Communications*. Prentice-Hall, 1988.

[44] K. Thyagarajan and A. K. Ghatak, *Fiber Optic Essentials*. Wiley-IEEE, 2007.

[45] H. C. Kandpal, S. Anand, and J. S. Vaishya, "Experimental observation of the phenomenon of spectral switching for a class of partially coherent light," *IEEE Journal of Quantum Electronics*, vol. 38, pp. 336–339, 2002.

[46] I. Yokohama, K. Okamato, and J. Noda, "Fiber-optic polarising beam splitter employing birefringent-fiber coupler," *IEEE Photonics Technology Letters*, vol. 21, pp. 415–416, 1985.

[47] T. Oguchi, A. Sugita, and J. Noda, "Integrated polarization diversity front end optics," *IEEE Photonics Technology Letters*, vol. 2, pp. 830–831, Nov 1990.

[48] J. Pan and Y. Shi, "Dense WDM multiplexer and demultiplexer with 0.4 nm channel spacing," *Electronics Letters*, vol. 34, no. 1, pp. 74–75, 1998. TY - JOUR.

[49] IEEE, "Ieee standard test procedures for antennas," *ANSI/IEEE Std 149-1979*, 1979.

[50] M. Phillips and M. Regan, "Enhancement of microwave optical link gain by self-phase modulation in a fiber interferometer," *IEEE Photonics Technology Letters*, vol. 20, pp. 2174–2176, Dec 2008.

[51] E. R. Lopez, W. Fu, K. Ghorbani, W. S. T. Rowe, and A. Mitchell, "Reconfigurable two-arm spiral antenna microwave photonic polarization diversity technique," *IEEE Photonic Technology Letters*, 2009. Accepted for future publication.

[52] C. A. Balanis, *Antenna Theory. Analysis and Design*. Wiley, second ed., 1997.

[53] R. Levy, R. Snyder, and G. Matthaei, "Design of microwave filters," *IEEE Transactions on Microwave Theory and Techniques*, vol. 50, pp. 783–793, Mar 2002.

[54] S. Melvin, M. Goldy, and J. Ilow, "Antenna load mismatch effects in eer-based transmitters for digital audio broadcasting," in *Fifth Annual Conference on Communication Networks and Services Research*, pp. 41–46, May 2007.

[55] K. McGreer, "Arrayed waveguide gratings for wavelength routing," *IEEE Communications Magazine*, vol. 36, no. 12, pp. 62–68, 1998. TY - JOUR.

[56] H. Takahashi, S. Suzuki, K. Kato, and I. Nishi, "Arrayed-waveguide grating for wavelength division multi/demultiplexer with nanometre resolution," *Electronics Letters*, vol. 26, no. 2, pp. 87–88, 1990. TY - JOUR.

[57] R. Yoshimura, Y. Sakai, H. Sanjoh, M. Kohtoku, M. A4 Kohtoku, H. Tanobe, H. A5 Tanobe, and Y. Yoshikuni, Y. A6 Yoshikuni, "A 16-channel simultaneous detection of gigabit signals with a compact wdm receiver containing a monolithically integrated awg-pd," in *Optical Fiber Communication Conference and Exhibit* (Y. Sakai, ed.), pp. 277–279, 2002. TY - CONF.

[58] D. Shively and W. Stutzman, "Wideband arrays with variable element sizes," *Microwaves, Antennas and Propagation*, vol. 137, no. 4, pp. 238–240, 1990. TY - JOUR.

[59] E. Lopez, T. Lunn, W. Fu, K. Ghorbani, W. Rowe, and A. Mitchell, "Ultra-broadband photonic antenna system with microwave photonic combination," in *Microwave Conference, 2007. APMC 2007. Asia-Pacific*, pp. 1–4, Dec. 2007.

[60] C. Dolph, "A current distribution for broadside arrays which optimizes the relationship between beam width and side-lobe level," *Proceedings of the IRE*, vol. 34, pp. 335–348, June 1946.

[61] R. Taylor and S. Forrest, "Steering of an optically driven true-time delay phased-array antenna based on a broad-band coherent wdm architecture," *IEEE Photonics Technology Letters*, vol. 10, pp. 144–146, Jan 1998.

[62] T. A. Milligan, *Modern antenna design*, ch. 4. Wiley, second ed., 2005.

[63] National, Telecommunications, and I. A. (NTIA), *Manual of Regulations and Procedures For Federal Radio Frequency Management*, Jan 1993.

[64] L. J. Volakis, *Antenna Engineering Handbook: Direction Finding Antennas and Systems*, ch. 47. Mc GrawHill, fourth ed., 2007.

[65] L. J. Volakis, *Antenna Engineering Handbook: ESM and ECM Antennas*, ch. 48. Mc GrawHill, fourth ed., 2007.

[66] R. Penno and K. Pasala, "Angle estimation with a multi-arm spiral antenna," in *IEEE Aerospace Conference*, vol. 3, pp. 195–207, 1999. TY - CONF.

[67] P. Mayes, "Frequency-independent antennas and broad-band derivatives thereof," *Proceedings of the IEEE*, vol. 80, pp. 103–112, Jan 1992.

[68] A. W. Rudge, *The Handbook of antenna design*. IEE Electromagnetic Wave Series, second ed., 1986.

[69] V. Rumsey, "Frequency independent antennas," in *IRE International Convention Record*, vol. 5, pp. 114–118, Mar 1957.

[70] J. Kaiser, "The archimedean two-wire spiral antenna," *IRE Transactions on Antennas and Propagation*, vol. 8, pp. 312–323, May 1960.

[71] R. H. DuHamel, "Dual polarized sinuous antennas," tech. rep., Mountain View, CA, Feb 1985. USPTO.

[72] P. Gonnet, A. Sharaiha, C. Terret, and A. Skrivervik, "Feeding network for sinuous antennas," *Microwave and Optical Letters*, vol. 20, pp. 195–200, Feb 1999.

[73] P. Salem, C. Wu, and M. Yagoub, "Four arm dual circular polarized sinuous antennas design for 2-18ghz operation," *Antennas, Radar and Propagation*, 2005.

[74] G. Deschamps, "Impedance properties of complementary multiterminal planar structures," *IEEE Transactions on Antennas and Propagation*, vol. 7, pp. 371–378, Dec 1959.

[75] L. Becker, J. Cloete, and H. Reader, "Radio frequency coupling between an antenna and two unshielded parallel wires above a metal sheet-measurement precautions," *IEEE Transactions on Electromagnetic Compatibility*, vol. 43, pp. 85–88, Feb 2001.

[76] J. P. Helton, "Four arm spiral direction finding system," *Private communication Radiation Systems*, Dec 1960.

[77] H. Johnson and M. Graham, *High Speed digital design: A handbook of Black Magic*. Prentice Hall, 1993.

[78] R. Araneo, "Propagation characteristics of differential lines: the odd-mode impedance," in *International Symposium on Electromagnetic Compatibility*, vol. 1, pp. 34–38, Aug. 2005.

[79] P. Piksa and M. Mazank, "A self-complementary 1.2 to 40 ghz spiral antenna with impedance matching," tech. rep., RFspin S. R. O., 2005. Broadband Log-Spiral Antenna LS24.

[80] T. Rutkowski, W. Zieniutycz, and K. Joachimowski, "Wideband coaxial balun for antenna application," in *12th International Conference on Microwaves and Radar*, vol. 2, pp. 389–392, May 1998.

[81] G. Engargiola, "Tapared microstrip balun for ata feed development," tech. rep., Astro Berkeley, 2001.

[82] L. J. Volakis, *Antenna Engineering Handbook: ESM and ECM Antennas*, ch. 52. Mc GrawHill, fourth ed., 2007.

[83] R. Sivan-Sussman, "Various modes of the equiangular spiral antenna," *IEEE Transactions on Antennas and Propagation*, vol. 11, pp. 533–539, Sep 1963.

[84] N. Stutzke and D. Filipovic, "Broadband two-arm dual-mode dual-polarized spiral antenna," in *IEEE Antennas and Propagation Society International Symposium*, vol. 1B, pp. 414–417, July 2005.

[85] R. C. Johnson and H. Jasik, *Antenna Engineering Handbook*, ch. 14. McGraw-Hill Book Co., second ed., 1993.

[86] C. A. Balanis, *Antenna Theory: Analysis and Design*, ch. 1, p. 878. Wiley, second ed., 1997.

[87] L. J. Volakis, *Antenna Engineering Handbook: Direction Finding Antennas and Systems*, ch. 13. Mc GrawHill, fourth ed., 2007.

[88] F. Ferrero, C. Luxey, G. Jacquemod, R. Staraj, and V. Fusco, "A reconfiguralbe hybrid coupler circuit for agile polarisation antenna," in *First European Conference on Antennas and Propagation*, pp. 1–5, Nov 2006.

[89] A. J. Seeds and K. J. Williams, "Microwave photonics," *Journal of Lightwave Technology*, vol. 24, pp. 4628–4641, Dec. 2006.

[90] J. Capmany, D. Pastor, B. Ortega, and S. Sales, "Microwave photonic filters with negative coefficients based on phase inversion in an electro-optic modulator," *Optics Letters*, pp. 1415–1417, 2003.

[91] J. Capmany, B. Ortega, and D. Pastor, "A tutorial on microwave photonic filters," *Journal of Lightwave Technology*, vol. 24, pp. 201–229, Jan 2006.

[92] L. J. Volakis, *Antenna Engineering Handbook: ESM and ECM Antennas*, ch. 13. Mc GrawHill, fourth ed., 2007.

[93] U. Kraft, "Optimisation of circular polarisation performance for 4-arm planar spiral antenna with non perfect excitation networks," *Microwaves, Antennas and Propagation*, vol. 137, pp. 45–50, Feb 1990.

[94] M. Buck and D. Filipovic, "Unidirectional spiral antenna with improved gain and wow," in *Antennas and Propagation Society International Symposium, 2005 IEEE*, vol. 3A, pp. 541–544, July 2005.

[95] S. Mansoori, L. A. Bui, and A. Mitchell, "A novel rf photonics band-pass filter," in *International Topical Meeting on Microwave Photonics*, pp. 93–96, Sept. 2003.

[96] H. Emami, N. Sarkhosh, L. A. Bui, and A. Mitchell, "Wideband rf photonic in-phase and quadrature-phase generation," *Optics Letters*, vol. 33, no. 2, pp. 98–100, 2008.

[97] H. Emami, L. Bui, S. Mansoori, and A. Mitchell, "Quadrature hybrid coupler using photonic transversal approach," in *Australian Conference on Optical Fibre Technology/Australian Optical Society*, pp. 1–3, July 2006.

[98] R. Minasian, "Photonic signal processing of microwave signals," *IEEE Transactions on Microwave Theory and Techniques*, vol. 54, pp. 832–846, Feb. 2006.

[99] R. Hui, B. Zhu, R. Huang, C. Allen, K. Demarest, and D. Richards, "Subcarrier multiplexing for high-speed optical transmission," *Journal of Lightwave Technology*, vol. 20, pp. 417–427, Mar 2002.

[100] M. Otten, "Alternative solutions for hilbert filtering in a pulse compression radar," in *Radar Conference, 1990., Record of the IEEE 1990 International*, pp. 86–89, May 1990.

[101] C. Eggen and R. Goddard, "Bottom mounted active sonar for detection, localization, and tracking," in *OCEANS '02 MTS/IEEE*, vol. 3, pp. 1291–1298, Oct 2002.

[102] K. Tanaka, K. Takano, K. Kondo, and K. Nakagawa, "Improved sideband suppression of optical ssb modulation using all-optical hilbert transformer," *Electronics Letters*, vol. 38, pp. 133–134, Jan 2002.

[103] E. Hafner and P. Leuthold, "Transversal filters with continuously tapped delay lines (ctt filters)," *Proceedings of the IEEE*, vol. 57, pp. 2114–2122, Dec. 1969.

[104] K. Feher and R. De Cristofaro, "Transversal filter design and application in satellite communications," *IEEE Transactions on Communications*, vol. 24, pp. 1262–1268, Nov 1976.

[105] N. Maeda, "Transversal filters with nonuniform tap spacings," *Circuits and Systems, IEEE Transactions on*, vol. 27, pp. 1–11, Jan 1980.

Publications

A. Mitchell, L.A. Bui, K. Ghorbani, S. Mansoori, W. Rowe, E. Lopez, T.H. Chio, "Demonstration of a wideband photonic phased array using integrated optical RF phase shifter based on the vector sum approach," *IEEE International Symposium on Phased Array Systems and Technology*, pp. 199-204, Oct. 2003.

L.A. Bui, A. Mitchell, K. Ghorbani, T.H. Chio, S. Mansoori, E.R. Lopez, "Wide-band photonically phased array antenna using vector sum phase shifting approach," *IEEE Transactions on Antennas and Propagation*, vol.53, no.11, pp. 3589-3596, Nov. 2005.

E.R. Lopez, L.A. Bui, K. Ghorbani, W.S.T. Rowe, A. Mitchell, "Ultra-broadband Photonic Patch Antenna," *IEEE MTT-S International Microwave Symposium*, pp.1939-1942, June 2006.

E.R. Lopez, T. Lunn, W. Fu, K. Ghorbani, W.S.T. Rowe, A. Mitchell, "Ultra-broadband Photonic Antenna System with Microwave Photonic Combination," *Asia-Pacific Microwave Conference*, pp.1-4, Dec. 2007.

W. Fu, E.R. Lopez, J. Scott, W.S.T. Rowe, K. Ghorbani, "Broadband Equiangular Spiral Antenna with Embedded Chip Resistors," *Asia-Pacific Microwave Conference*, pp.1-4, Dec. 2007.

W. Fu, E.R. Lopez, W.S.T. Rowe, K. Ghorbani, "A compact broadband spiral antenna," *Asia-Pacific Microwave Conference*, pp.1-4, Dec. 2008.

E.R. Lopez, T. Lunn, W. Fu, K. Ghorbani, W.S.T. Rowe, A. Mitchell "Multiple Frequency Band Microwave Photonic Receiver," *IEEE Transactions on Antennas and Propagation*, vol.57, no.11, pp.3688-3692, Nov. 2009.

E.R. Lopez, W. Fu, K. Ghorbani, W.S.T. Rowe, A. Mitchell "Reconfigurable Two-arm Spiral Antenna Microwave Photonic Polarization Diversity Technique," *IEEE Photonics Technology Letters*, vol.21, no.22, pp.1668-1670 , Nov.15, 2009.

W. Fu, E.R. Lopez, W.S.T. Rowe, K. Ghorbani, "A Planar Dual-arm Equiangular Spiral Antenna," *IEEE Transactions on Antennas and Propagation*. In press.